



National Library
of Canada

Bibliothèque nationale
du Canada

Canadian Theses Service

Service des thèses canadiennes

Ottawa, Canada
K1A 0N4

NOTICE

The quality of this microform is heavily dependent upon the quality of the original thesis submitted for microfilming. Every effort has been made to ensure the highest quality of reproduction possible.

If pages are missing, contact the university which granted the degree.

Some pages may have indistinct print especially if the original pages were typed with a poor typewriter ribbon or if the university sent us an inferior photocopy.

Reproduction in full or in part of this microform is governed by the Canadian Copyright Act, R.S.C. 1970, c. C-30, and subsequent amendments.

AVIS

La qualité de cette microforme dépend grandement de la qualité de la thèse soumise au microfilmage. Nous avons tout fait pour assurer une qualité supérieure de reproduction.

S'il manque des pages, veuillez communiquer avec l'université qui a conféré le grade.

La qualité d'impression de certaines pages peut laisser à désirer, surtout si les pages originales ont été dactylographiées à l'aide d'un ruban usé ou si l'université nous a fait parvenir une photocopie de qualité inférieure.

La reproduction, même partielle, de cette microforme est soumise à la Loi canadienne sur le droit d'auteur, SRC 1970, c. C-30, et ses amendements subséquents.

**DEVELOPMENT OF AN IN-LINE RHEOMETER
FOR CONTROL OF REACTIVE EXTRUSION**

by

Taras Oscar Broadhead, M.Eng.

Department of Chemical Engineering
McGill University, Montreal

February 1992

A Thesis submitted to the Faculty of Graduate Studies and
Research in partial fulfilment of the requirements of the
degree of Doctor of Philosophy.

© 1992, Taras Oscar Broadhead



National Library
of Canada

Bibliothèque nationale
du Canada

Canadian Theses Service Service des thèses canadiennes

Ottawa, Canada
K1A 0N4

The author has granted an irrevocable non-exclusive licence allowing the National Library of Canada to reproduce, loan, distribute or sell copies of his/her thesis by any means and in any form or format, making this thesis available to interested persons.

The author retains ownership of the copyright in his/her thesis. Neither the thesis nor substantial extracts from it may be printed or otherwise reproduced without his/her permission.

L'auteur a accordé une licence irrévocable et non exclusive permettant à la Bibliothèque nationale du Canada de reproduire, prêter, distribuer ou vendre des copies de sa thèse de quelque manière et sous quelque forme que ce soit pour mettre des exemplaires de cette thèse à la disposition des personnes intéressées.

L'auteur conserve la propriété du droit d'auteur qui protège sa thèse. Ni la thèse ni des extraits substantiels de celle-ci ne doivent être imprimés ou autrement reproduits sans son autorisation.

ISBN 0-315-74613-0

Canada

ABSTRACT

This study involves the development and evaluation of an in-line melt rheometer (ILR) for use in process control. The ILR consists of a rotating drum, which is positioned directly in the main process flow channel. The drum creates a shear deformation in a zone formed between the drum and the channel wall. A method to correct for the effects of pressure flow superposed on the shear deformation was developed. The problems associated with sample renewal and temperature control in the shearing zone were explored with the help of simulations. The ILR's sensitivity to processing conditions was documented, and its accuracy and repeatability were demonstrated.

The ILR was used as a viscosity sensor to control ionomer neutralisation by reactive extrusion. Proportional-integral and minimum variance control algorithms were successfully implemented. The quality of control was good but could be improved by reducing ILR signal noise and by decreasing the ILR's measurement delay, which is governed primarily by the sample renewal rate.

RESUME

Cette étude présente le développement et l'évaluation d'un rhéomètre en lingé (REL) utilisé en contrôle. Le REL consiste en un tambour tournant, qui est positionné directement dans le canal de l'écoulement. Le tambour crée une déformation de cisaillement dans un pincement formé entre le tambour et la paroi du canal. Une méthode pour corriger les effets de pression d'écoulement superposés à la déformation de cisaillement a été développée. Les problèmes dus au remplacement de l'échantillon et dus au contrôle de température dans la zone de cisaillement furent explorés à l'aide de simulations. La sensibilité du REL aux conditions de mise en oeuvre a été documentée et sa fiabilité et répétitivité furent démontrées.

Le REL fut utilisé comme capteur de viscosité pour contrôler la neutralisation d'ionomère lors d'une extrusion réactive. Des algorithmes de contrôle basés sur les méthodes proportionnelle-intégrale et sur les minimum des variances furent utilisés avec succès. La qualité du contrôle était bonne mais pourrait être améliorée en réduisant le rapport signal/bruit du REL et en diminuant le retard de la mesure du REL, qui est dominé principalement par le renouvellement de l'échantillon.

To Laria and Bud

ACKNOWLEDGEMENTS

This project continues Professor J.M.Dealy's pioneering research in the field of rheometry. Professor Dealy conceived the idea of a process rheometer using a shear stress transducer and contributed significantly to the design of the instrument used in this work. He co-ordinated the considerable funds needed for the project and supervised every stage of the instrument's development and use. Professor W.I.Patterson co-supervised this research. He contributed many ideas to the development of the rheometer and provided principal guidance during the modelling and control stage of the project.

Burke Nelson explored a related research topic, using the same rheometer and extrusion facility, during the period of my own work. He co-operated with me and contributed at every stage of my project. In particular, he contributed ideas to the rheometer design, installed and wrote the controlling software for the MACO 8000 extruder controller, wrote excellent software to communicate with the MACO 8000 and the data acquisition board and helped with every crisis that arose with the equipment.

Mr. Frank Bubic designed the rheometer from ideas contributed by Dr.J.M.Dealy, Burke Nelson and me.

Alain Gagnon machined, built and made many refinements to the in-line rheometer. Charles Dolan, Walter Greenland and Andy Krish helped to build the extrusion facility and made many emergency repairs to our equipment.

Luciano Cusmich designed and built a number of electronic components for our equipment and diagnosed and repaired many elusive electronic problems.

Jean Dumont helped source, order and expedite the many components that were needed to build and maintain our extrusion facility and new rheometer.

Dr.A.Eisenberg advised me regarding the chemistry,

processing and analysis of ionomers.

Colleagues Tony Samurkas, Dr.Günter Lohfink, Mark Weber, Philip Bates, Joe McDermid, Dr.Savvas Hatzikiriakos and Dr.Daniel St-Cyr contributed solutions to problems, ideas on the design and implementation of experiments and computer software suggestions.

Rob Latosinsky, Dr. Michel Perrier and Dr. Vincent Gomez offered invaluable advice on process control techniques.

The DuPont Company and Werner and Pfleiderer Corp. supported this work with materials, funds and invaluable advice. In particular, J.E.Curry of Werner and Pfleiderer Corporation and Dr.K.Ogunde of the DuPont Company offered invaluable technical advice.

The Natural Sciences and Engineering Research Council of Canada and McGill University supported this work financially.

TABLE OF CONTENTS

ACKNOWLEDGEMENTS	i
TABLE OF CONTENTS	iii
LIST OF TABLES	viii
LIST OF FIGURES	x
NOMENCLATURE	xvii
CHAPTER 1	
PROCESS RHEOMETRY FOR REACTIVE EXTRUSION CONTROL	1
1.1 The Need for Rheological Process Sensors	1
1.2 Process Rheometers for Molten Polymers	3
1.2.1 Fundamental Challenges of Process Rheometry	3
1.2.2 Capillary and Slit Flow Process Rheometers	5
1.2.3 Rotational Process Rheometers	15
1.3 Process Control of Reactive Extrusion	19
1.4 Research Objectives	26
CHAPTER 2	
FUNDAMENTALS OF THE MCGILL IN-LINE MELT RHEOMETER DESIGN	27
2.1 Principle of Operation	27
2.2 Superposition of Pressure Flow on Drag Flow	30
2.2.1 Visualisation of Pressure Plus Drag Flow	30
2.2.2 Pressure Flow Correction Concept	32
2.2.3 Pressure Flow Correction Equations	34
2.2.4 Pressure Flow Correction Parameter Sensitivity	40
2.3 Sample Renewal in the McGill In-Line Rheometer	45
2.3.1 Description of the Sample Renewal Problem	45
2.3.2 Simulation of Polymer Flow in the McGill ILR	46
2.3.3 Interpretation of ILR Flow Simulations	53

2.4	Temperature Uniformity in the ILR Shearing Zone and the Effect of Temperature Disturbances	53
2.4.1	Simulation of the Temperature Distribution in the ILR Shearing Zone	53
2.4.2	Implications of the ILR Shearing Zone Temperature Distribution Simulations	57
2.4.3	Viscosity Measurement Compensation for Temperature Changes	58

CHAPTER 3

	IMPLEMENTATION OF THE MCGILL IN-LINE MELT RHEOMETER DESIGN	59
3.1	In-Line Rheometer Component Descriptions	59
3.1.1	The Shear Stress Transducer	59
3.1.2	Rotating Drum, Rheometer Motor and Rheometer Speed Tachometer	63
3.1.3	Pressure Sensors	66
3.1.4	Temperature Sensors	68
3.1.5	Rheometer Body Heaters	70
3.1.6	Rheometer Computer Control and Data Acquisition	71
3.2	Factors Influencing the Shear Stress Transducer's Performance	74
3.2.1	The Effect of Pressure on Shear Stress Transducer Performance	74
3.2.2	The Effect of Through-Flow on Shear Stress Transducer Performance	76
3.2.3	The Effect of Vibration on SST Performance	78
3.2.4	A Model for the In-Situ Behaviour of the SST	78
3.2.5	The Effect of Temperature on SST Performance	81
3.2.6	Dynamic Response of the SST Beam	82
3.2.7	Unexplained SST Dynamics	83
3.3	Shear Stress Transducer Calibration	87
3.3.1	External Calibration	87

3.3.2	In-Situ Calibration	88
3.3.3	Pressure Effect	90
3.3.4	Temperature Effect	91
CHAPTER 4		
IN-LINE RHEOMETER VISCOSITY MEASUREMENTS		92
4.1	Viscosity Measurement Procedure	92
4.2	Rheometer Discrimination	96
4.3	Rheometer Accuracy	97
4.4	Rheometer Repeatability and Reproducibility	107
CHAPTER 5		
REACTIVE EXTRUSION OF ETHYLENE METHACRYLIC ACID IONOMERS		111
5.1	Motivation for Studying the EMAA Ionomer System	111
5.2	Model Reactive Extrusion Process	112
5.3	EMAA Ionomer System Characterisation Experiments	114
5.4	Degree of Neutralisation versus Ionomer Blend Composition	115
5.5	Viscosity versus Degree of Neutralisation	117
5.6	Viscosity versus Temperature	124
CHAPTER 6		
CONTROL OF ETHYLENE-METHACRYLIC ACID NEUTRALISATION		126
6.1	The Challenges of Ethylene-Methacrylic Acid Neutralisation Control	126
6.2	Dynamic Characterisation of the Extruder plus ILR System	127
6.2.1	Viscosity Step Change Test Experiment Design	127
6.2.2	First Order plus Dead Time Model Fitting Procedure	129
6.2.3	Dead Time	134
6.2.4	Process Gains	135
6.2.5	First Order Time Constants	139

6.2.6	Identification of Rheometer Measurement Dynamics	141
6.3	Proportional-Integral Control of EMAA Neutralisation	147
6.3.1	Description of Control System and Control Algorithm	147
6.3.2	Selection of Controller Parameters	149
6.3.3	Set Point Tracking Experiments	150
6.3.4	Disturbance Rejection Experiments	154
6.3.5	Comments on PI Control Effectiveness	160
6.4	Minimum Variance Control of EMAA Neutralisation	162
6.4.1	Minimum Variance Controller Structure and Parameters	162
6.4.2	Set Point Tracking Experiments	167
6.4.3	Disturbance Rejection Experiments	173
6.4.4	Comments on MV Control Effectiveness	178
6.5	ILR Performance as a Viscosity Sensor	180
CHAPTER 7		
EVALUATION OF THE MCGILL IN-LINE MELT RHEOMETER		182
7.1	In-Line Rheometer Design	182
7.1.1	Principle of Operation	182
7.1.2	In-Line Rheometer Instrumentation	184
7.1.3	In-Line Rheometer Temperature Control	185
7.1.4	The Disk-Spring Shear Stress Transducer	186
7.2	In-Line Rheometer Performance	187
7.2.1	ILR Accuracy and Repeatability	187
7.2.2	Dynamic Modelling of EMAA Neutralisation by Reactive Extrusion	189
7.2.3	Control of EMAA Neutralisation	190
CHAPTER 8		
CONTRIBUTIONS TO KNOWLEDGE		192
REFERENCES		194

A1	APPENDIX OF EXPERIMENTAL PROCEDURES	198
A1-1	Typical Extrusion Conditions used to Prepare Ionomer Blends	198
A1-2	Summary of Ionomer Blend Compositions used in the Composition-Degree of Neutralisation-Viscosity Study	199
A1-3	Ionomer Titration Procedure	200
A2	APPENDIX OF SOFTWARE LISTINGS	203
A2-1	BASIC Program Simulating the Heat Balance in the ILR Shearing Zone	203
A2-2	Example of Rheometer Control Software	208
A3	APPENDIX OF MECHANICAL DRAWINGS	220
A3-1	Process Rheometer Model 3.45 - Assembly Drawing	220
A3-2	Side and Front View Cross-Sections of the Rheometer	221
A3-3	Side and Front View Cross-Sections of the Rheometer: Detailed Dimensions	222
A3-4	Top View Cross-Section of the Rheometer	223
A3-5	Top View of the Rheometer Body: Detailed Dimensions	224
A3-6	Drive Shaft Dimensions	225
A3-7	Shear Stress Transducer: Assembly Drawing	226
A3-8	Shear Stress Transducer: Disk Spring Detail	227
A3-9	Shear Stress Transducer: Probe Target Detail	228
A3-10	Shear Stress Transducer: Active Face /Head	229
A3-11	Summary of CAD Analysis for SST Model 3.45F by F.R.Bubic	230

LIST OF TABLES

Table 13-1:	Data of Pabedinskas et al. (1989) -- "Discrete and Continuous Model Parameters for Various Concentration Step Changes".	24
Table 22-1:	Summary of Power-Law Parameters and Experimentally Determined Pressure Drops in the Shearing Zone	41
Table 22-2:	Newtonian-Power-Law Fluid Strain Rate Profile Crossover Point for Three Polymers over a Range of Strain Rates	41
Table 22-3:	Percent Error Introduced into Strain Rate Estimate as a Result of Assuming a Constant $\dot{\gamma}$.	42
Table 43-1:	Summary of Commodity Polyolefins Tested	97
Table 43-2:	Summary of Activation Energies for Flow for the Polymers Studied.	98
Table 44-1:	Summary of ILR Signal Reproducibility for the Materials Tested.	108
Table 44-2:	Peak to Peak Variation of ILR Measurements Made Over a Three Week Period.	110
Table 55-1:	95% Confidence Intervals Expressed in Units of Viscosity and as a Percent of the Mean for the Data Presented in Figure 55-1.	119
Table 62-1:	Summary of the Expected Change in Viscosity and the Mean ILR Signal Noise as a function of Strain Rate.	134
Table 62-2:	Summary of Dead Times fit to Viscosity Step Change Data.	135
Table 62-3:	Summary of Statistics describing some Residence Time Distributions measured by Chen (1992)	144
Table 63-1:	Digital Proportional-Integral Controller Settings using ITAE Criteria	149
Table 63-2:	Summary of Observed Process Response Times with PI Control.	150
Table 64-1:	Summary of Moving Average Noise Model Parameters	165
Table 64-2:	Summary of Observed Process Response Times with MV Control.	171

Table A11-1:	Summary of Typical Operating Temperatures Used for Ionomer Blend Preparation and Control Experiments	198
Table A11-2:	Summary of Typical Extruder Settings Used for Ionomer Blend Preparation and Control Experiments.	198
Table A12-1:	Table of Ionomer Blend Compositions Described in Section 5.3.	199

LIST OF FIGURES

Figure 12-1a:	Cross-section of a Capillary Rheometer	6
Figure 12-1b:	Cross-section of a Slit Rheometer	6
Figure 12-2:	Schematic Diagram of the Göttfert By-Pass Rheograph	9
Figure 12-3:	Schematic Diagram of the Rheometrics Melt Flow Monitor	10
Figure 12-4:	Schematic Diagram of a Rotational Rheometer	16
Figure 12-5:	Schematic Diagram of the Rheometrics On-Line Rheometer from Orwoll (1983).	17
Figure 13-1:	Schematic Diagram of the Reactive Extrusion Process Studied by Fritz and Stöhrer (1986)	20
Figure 13-2:	Schematic Diagram of the Reactive Extrusion Process Studied by Pabedinskas et al. (1989)	23
Figure 21-1:	Cross-sectional Diagram of the McGill In-Line Rheometer, Side View	27
Figure 21-2:	Cross-sectional Diagram of the McGill In-Line Rheometer, Front View.	29
Figure 22-1a:	Velocity and Strain Rate as a Function of Position in the Shearing Zone for a Simple Shear Flow.	31
Figure 22-1b:	Velocity and Strain Rate as a Function of Position in the Shearing Zone for a Small Pressure Flow Superposed on a Simple Shear Flow.	31
Figure 22-1c:	Velocity and Strain Rate as a Function of Position in the Shearing Zone for a Large Pressure Flow Superposed on a Simple Shear Flow.	31
Figure 22-2:	Strain Rate as a Function of Position in the Shearing Zone.	34
Figure 22-3:	Cartesian Representation of the ILR's Shearing Zone	35
Figure 22-4a:	Viscosity versus Strain Rate for Polymer C -- Correct Power-law Model Fit.	43
Figure 22-4b:	Viscosity versus Strain Rate for Polymer C -- Approximate Power-law Model Fit.	44

Figure 23-1:	Computational Grid used to Model Flow Through the ILR.	46
Figure 23-2:	FIDAP Simulation of the Flow through the ILR with the Rotating Drum Stationary	47
Figure 23-3:	FIDAP Simulation of a High Throughput (15 kg/h) through the ILR with the Drum Rotating at a Low (5 s^{-1}) Rate.	48
Figure 23-4:	FIDAP Simulation of a Low Throughput (5 kg/h) through the ILR with the Drum Rotating at a Low (5 s^{-1}) Rate.	49
Figure 23-5:	FIDAP Simulation of a Low Throughput (5 kg/h) with the Drum Rotating at a High (30 s^{-1}) Rate.	50
Figure 23-6:	FIDAP Simulation of the ILR with the Drum Rotating in the Counter-clockwise Direction.	51
Figure 24-1:	Simulation of Temperature Profile in the Shearing Zone: Strain Rate of 5 s^{-1}	55
Figure 24-2:	Simulation of Temperature Profile in the Shearing Zone: Strain Rate of 20 s^{-1}	56
Figure 31-1:	Cross-sectional Diagram of the Disk Spring SST	60
Figure 31-2:	SST Clamping Device	63
Figure 31-3:	Illustration of Poor Capacitance Probe-SST Target Alignment.	62
Figure 31-4:	Front View of the ILR Showing the Rheometer Motor Assembly.	64
Figure 31-5:	Typical Process Follower-Strain Rate Calibration Curve.	65
Figure 31-6:	Top View of the ILR Showing the Positions of the Pressure Transducers.	67
Figure 31-7a:	Side View of the ILR Showing Temperature Sensor Positions.	69
Figure 31-7b:	Top View of the ILR Showing Temperature Sensor Positions.	69
Figure 31-8:	Positions of ILR Heaters.	70
Figure 31-9:	Schematic Diagram of the Communication Pathways between the ILR and Its Controlling Computer.	73
Figure 32-1:	SST Signal Response to Pressure	75

Figure 32-2:	Cross-sectional View of ILR Shearing Zone Illustrating the Flow Through the Lower SST Housing.	76
Figure 32-3:	Top View of the ILR Flow Channel Illustrating the Disruption of the Flow Profile in the Shearing Zone due to Through-Flow.	77
Figure 32-4a:	Baseline SST Signal versus Time.	79
Figure 32-4b:	SST Signal during Typical Operating Conditions.	79
Figure 32-5:	Typical Pressure Fluctuations Observed During Extruder Operation.	80
Figure 32-6:	Coded SST and Pressure Signals versus Time.	80
Figure 32-7:	SST Signal as a Function of Temperature.	83
Figure 32-8:	Illustration of Unexplained SST Signal Change with Time.	84
Figure 32-9:	Illustration of Unexplained SST Signal Change with Time.	84
Figure 33-1:	Illustration of the External Beam Calibration Method.	88
Figure 33-2:	Illustration of the In-Situ Beam Calibration Apparatus.	89
Figure 33-3:	SST Signal as a Function of Calibration Weight. Illustration of the Effect of Pressure on the SST Beam Constant.	91
Figure 41-1a:	Typical SST Signal During a Viscosity Measurement.	94
Figure 41-1b:	Typical Tachometer Signal During a Viscosity Measurement.	94
Figure 43-1:	Viscosity of Profax 6631 at 200°C	99
Figure 43-2:	Viscosity of Profax 6501 at 200°C.	99
Figure 43-3:	Viscosity of Sclair 2907 at 206°C.	100
Figure 43-4:	Viscosity of Sclair 11L1 at 223°C.	100
Figure 43-5:	Illustration of the Problem Encountered in Measuring Low Viscosity Ionomer Blends.	102
Figure 43-6:	Viscosity of a 15 % Neutralised EMAA Ionomer Blend at 185°C.	105
Figure 43-7:	Viscosity of a 22 % Neutralised EMAA Ionomer Blend at 187°C.	105

Figure 43-8:	Viscosity of a 29 % Neutralised EMAA Ionomer Blend at 187°C.	106
Figure 44-1:	Comparison of Viscosity Data at Various Degrees of Rates Measured over a Three Week Period to a Reference Viscosity Curve Measured at the Start of the Experimental Period.	109
Figure 52-1:	Reactive Extrusion Process used to Neutralise EMAA Ionomer.	114
Figure 54-1:	Degree of Neutralisation as a Function of Ionomer Blend Composition.	116
Figure 55-1:	Viscosity of the 29.3 % Neutralised Ionomer Blend at 175 °C: three repeats.	119
Figure 55-2:	Moisture Content versus Melt Flow Index for SURLYN [®] Ionomer Resins. From DuPont Company Product Literature (1986).	120
Figure 55-3:	Illustration of the Effect of the "Drying" Procedure. Viscosity of a 22 % Neutralised Ionomer Blend at 180 °C.	120
Figure 55-4:	EMAA Ionomer Blend Viscosity for Five Blend Compositions at 180 °C.	122
Figure 55-5a:	Viscosity versus Degree of Neutralisation at 5, 15 and 30 s ⁻¹ at 180 °C.	123
Figure 55-5b:	Viscosity versus Degree of Neutralisation at 5, 15 and 30 s ⁻¹ : Selected Composition Range	123
Figure 56-1:	Activation Energy for Flow Calculated at Three Degrees of Neutralisation.	124
Figure 62-1a:	Nominal Viscosity at 186°C and 5 s ⁻¹ versus Time: 3% Neutralisation Steps.	131
Figure 62-1b:	Nominal Viscosity at 186 °C and 5 s ⁻¹ versus Time: 6% Neutralisation Steps.	131
Figure 62-1c:	Nominal Viscosity at 186°C and 5 s ⁻¹ versus Time: 12% Neutralisation Steps.	132
Figure 62-2a:	Nominal Viscosity at 186°C and 30 s ⁻¹ versus Time: 3% Neutralisation Steps.	132
Figure 62-2b:	Nominal Viscosity at 186°C and 30 s ⁻¹ versus Time: 6% Neutralisation Steps.	133
Figure 62-2c:	Nominal Viscosity at 186°C and 30 s ⁻¹ versus Time: 12% Neutralisation Steps.	133

Figure 62-3:	Process Gain as a Function of Degree of Neutralisation for 5 s ⁻¹ Viscosity Measurements.	136
Figure 62-4:	Process gain as a function of degree of neutralisation for 30 s ⁻¹ measurements	137
Figure 62-5:	First Order Time Constants Determined from Step Tests at 186°C and 5 s ⁻¹ .	139
Figure 62-6:	First Order Time Constants Determined from Steps Tests at 186°C and 30 s ⁻¹ .	140
Figure 62-7:	Residence Time Distributions for the Twin Screw Extruder with and without the ILR.	143
Figure 63-1a:	Nominal Viscosity at 186°C and 30 s ⁻¹ : 60 Pa s Viscosity Set Point Changes.	151
Figure 63-1b:	Neutralising Agent Feed Rate versus Time: Controller Response to Program of 60 Pa s Viscosity Set Point Changes.	151
Figure 63-2:	Nominal Viscosity @ 186°C and 30 s ⁻¹ : 120 Pa s Viscosity Set Point Changes.	152
Figure 63-3:	Nominal Viscosity at 186°C and 30 s ⁻¹ : 200 Pa s Viscosity Set Point Changes.	152
Figure 63-4:	Simulated PI Controlled Process Response to a 60 Pa s Viscosity Set Point Change.	153
Figure 63-5:	Nominal Viscosity @ 186°C and 30 s ⁻¹ : Open Loop Response to a Neutralising Agent Concentration Disturbance.	155
Figure 63-6a:	Nominal Viscosity at 186°C and 30 s ⁻¹ : Controlled Response to a Neutralising Agent Distrubance. 15% Neutralisation Set Point.	157
Figure 63-6b:	Neutralising Agent Feed Rate in Response to the Neutralising Agent Concentration Disturbance. 15% Neutralisation Set Point.	157
Figure 64-7a:	Nominal Viscosity at 186°C and 30 s ⁻¹ : Controlled Response to two Neutralising Agent Disturbances. 22% Neutralisation Set Point.	158
Figure 63-7b:	Neutralising Agent Feed Rate in Response to the Neutralising Agent Concentration Disturbance. 22% Neutralisation Set Point.	158

Figure 63-8a:	Nominal Viscosity at 186°C and 30 s ⁻¹ : Controlled Response to Subtle Neutralising Agent Concentration and Copolymer Molecular Weight Disturbances. 22% Neutralisation Set Point.	159
Figure 63-8b:	Neutralising Agent Feed Rate in Response to the Small Neutralising Agent Concentration and Copolymer Molecular Weight Disturbances.	159
Figure 63-9a:	Nominal Viscosity at 186°C and 30 s ⁻¹ : Controlled Response to Impulse Disturbances Introduced Before and After a Throughput Change.	161
Figure 63-9b:	Neutralising Agent Feed Rate in Response to Impulse Disturbances Introduced Before and After a Throughput Change.	161
Figure 64-1a:	Differenced Nominal Viscosity Signal Illustrating the Underlying Noise	164
Figure 64-1b:	Autocorrelations of Differenced Nominal Viscosity Signal.	164
Figure 64-2:	Nominal Viscosity at 186°C and 30 s ⁻¹ : MV Controlled, 60 Pa s Viscosity Set Point Changes.	168
Figure 64-3:	Nominal Viscosity at 186°C and 30 s ⁻¹ : MV Controlled, 120 Pa s Viscosity Set Point Changes.	168
Figure 64-4a:	Nominal Viscosity at 186°C and 30 s ⁻¹ : MV Controlled, 200 Pa s Viscosity Set Point Changes.	169
Figure 64-4b:	Neutralising Agent Feed Rate Response to 200 Pa s Viscosity Set Point Changes	169
Figure 64-5a:	Histogram of Standard Deviations Computed during Open Loop Operation.	170
Figure 64-5b:	Histogram of Standard Deviations Computed during PI Controlled Operation.	170
Figure 64-5c:	Histogram of Standard Deviations Computed during MV Controlled Operation.	170
Figure 64-6:	Simulated MV Controlled Response to a 60 Pa s Viscosity Set Point Change.	172

Figure 64-7a:	Nominal Viscosity at 186°C and 30 s ⁻¹ : MV Controlled Response to a Neutralising Agent Concentration Disturbance. 15% Neutralisation Set Point.	174
Figure 64-7b:	Neutralising Agent Feed Rate in Response to Neutralising Agent Concentration Disturbance.	174
Figure 64-8a:	Nominal Viscosity at 186°C and 30 s ⁻¹ : MV Controlled Response to a Neutralising Agent Concentration Disturbance. 22% Neutralisation Set Point.	175
Figure 64-8b:	Neutralising Agent Feed Rate in Response to Neutralising Agent Concentration Disturbance.	175
Figure 64-9:	MV Controller Simulation Illustrating the Effect of Signal Noise on Controller Performance.	177
Figure 64-10a:	Nominal Viscosity at 186°C and 30 s ⁻¹ : MV Controlled Response to Two Impulse Disturbances Introduced After a Throughput Change.	179
Figure 64-10b:	Neutralising Agent Feed Rate in Response to Impulse Disturbances Introduced After a Throughput Change.	179

NOMENCLATURE

a_t \equiv discrete random number sequence,
ASTM \equiv American Society for Testing and Materials,
BPR \equiv Götffert By-Pass Rheograph,
 C_p \equiv heat capacity,
CP \equiv capacitance probe,
 d \equiv number of sampling periods per dead time,
 $D, D_{of}N$ \equiv percent degree of neutralisation,
 e_t \equiv process deviation from set point at time "t",
 E_a \equiv activation energy for flow,
EMAA \equiv Ethylene-Methacrylic Acid,
 g \equiv shearing zone gap dimension,
 H \equiv shear stress transducer beam calibration constant,
ILR \equiv In-Line Rheometer,
 k \equiv power-law pre-exponential factor or thermal conductivity, as indicated,
 K_c \equiv PI controller gain,
 L \equiv length of the shearing zone,
 m \equiv mass fraction,
 M \equiv torque or mass percent, as indicated,
MI, MFI \equiv Melt Index or Melt Flow Index, ASTM 1238
MFM \equiv Rheometrics Melt Flow Monitor,
MV \equiv minimum variance control,
 n \equiv power-law exponent,
NA \equiv neutralising agent,
 p' \equiv pressure gradient along the shearing zone,
PC \equiv personal computer,
PI \equiv proportional-integral control,
 P_L, P_0 \equiv pressure at the exit and entrance to the shearing zone,
 ΔP \equiv pressure drop,
 $r(k)$ \equiv autocorrelation function at lag "k",
ROR \equiv Rheometrics On-Line Rheometer,
RTD \equiv Residence Time Distribution or Resistance Temperature Device, as indicated,

RTR = Göttfert Real Time Rheometer,
 s = slope of the SST beam deflection versus calibration weight data plot,
 SPR = Sliding Plate melt Rheometer,
 SST = Shear Stress Transducer,
 T = temperature,
 T_i = controller integral time,
 ΔT_s = sampling period,
 u = fluid velocity in the x-direction,
 Δu = change in manipulated variable,
 V = shearing velocity or voltage, as indicated,
 x, y = cartesian co-ordinates
 y^* = Newtonian fluid, shear thinning fluid strain rate profile cross-over point,
 z^{-1} = backward shift operator,

α = pressure correction parameter (Equation 32-1),
 β = parameter for power-law, drag plus pressure flow strain rate profile (Equations 22-7c and 22-8d),
 $\dot{\gamma}$ = strain rate,
 η = viscosity,
 θ = moving average noise model parameter,
 ρ = melt density,
 σ = shear stress,
 ω = angular frequency,
 ω_o = discrete process gain.

CHAPTER 1

PROCESS RHEOMETRY FOR REACTIVE EXTRUSION CONTROL

1.1 The Need for Rheological Process Sensors

Effective monitoring and control of polymerisation reactors and polymer processing operations is limited by the lack of suitable process instrumentation (MacGregor et al. (1984), Elicabe and Meira (1988)). In particular, sensors are needed to measure polymer qualities such as molecular or bulk composition, molecular size and structure, rheology and processability, morphology, the distribution of multiple phases, and end use properties such as electrical conductivity. Recent trends in the polymer industry have increased the need for a high level of quality control and therefore the need for dependable polymer quality process sensors. For example, many polymer products are made in small, "tailor-made" lots to meet very specific customer needs. These specialty products demand a high level of consistency; production of off-spec product cannot be tolerated. The environmental necessity of recycling polymers poses another challenge. The properties of re-claimed polymers can vary dramatically. In order to properly process reclaimed materials, these variations in quality must be measured.

Rheological process sensors are ideal for many polymerisation reactions and processing applications. Rheological properties are directly related to processing behaviour and, for many polymer products, this is the key concern. Furthermore, rheological properties are fundamentally related to molecular composition, size, and structure as well as to bulk composition and, though their functional relationships are usually complex or unknown, strong correlations exist between rheological properties and these fundamental quality parameters. Control systems employing rheological measurements can, therefore, address many of the current polymer control needs.

This thesis documents the development of a novel process rheometer and its application as a viscosity sensor in a closed loop reactive extrusion process. The balance of this chapter surveys both the state of the art of process rheometry and the application of rheological sensors to reactive extrusion control. It identifies the challenges of rheological process sensor design and reactive extrusion control and presents the objectives of this study. Chapter 2 introduces the McGill in-line melt rheometer (ILR) and discusses fundamental aspects of its design and operation. Chapter 3 presents mechanical details of the ILR design, documents the rheometer's sensitivity to operating conditions, and describes the rheometer's calibration procedures. Experimental evidence documenting the accuracy and repeatability of ILR measurements is presented and discussed in Chapter 4. Chapter 5 gives a brief introduction to the ethylene-methacrylic acid (EMAA) neutralisation process used to make ionomers and gives details of the reactive extrusion process studied in this work. It also presents ionomer viscosity versus composition and temperature data which are critical for the design of the rheometer, the operation of the extrusion process and the identification of the neutralisation control problem. Chapter 6 describes the objectives of EMAA neutralisation control, presents an empirical model for the neutralisation process and describes the implementation of PI (proportional-integral) and minimum variance algorithms to control ionomer viscosity. Chapter 7 assembles the observations and conclusions of this study into a detailed evaluation of the ILR design and performance and proposes directions for future work. Chapter 8 summarises the contributions to knowledge made by this thesis.

1.2 Process Rheometers for Molten Polymers

Commercially available process rheometers for molten polymers have been adapted from successful laboratory rheometer designs. Their use is limited primarily by the long times they require to perform a rheological test. A number of experimental process rheometers have also been reported, but they too suffer significant deficiencies. The objective of this section is to survey the state of the art of process rheometry with the ultimate purpose of defining the requirements of a better rheological sensor.

1.2.1 Fundamental Challenges of Process Rheometry

Rheological properties are difficult to measure in manufacturing or processing environments. The problems posed by vibration, electrical noise, dust and chemical hazards are obvious. But there are some difficulties that stem from the fundamentals of rheological measurement.

A rheological property quantifies a material's state of stress in response to a specific deformation or, conversely, a material's deformation in response to an applied stress. Rheological measurements are, as a result, active measurements. Rheometers must deform the samples they test. To ensure an unambiguous rheological property measurement, the deformation must be known precisely and accurately. This requires a certain mechanical sophistication and reliability. Also, the active nature of rheological measurements can introduce time as a factor in the measurement.

The complex nature of the rheological properties of polymers increases the difficulty of process rheometer measurements. Polymer melts are typically very viscous, non-Newtonian, shear-thinning, and usually exhibit marked elastic properties. Polymer rheological properties can also be time dependent. All of these features can complicate the execution of measurements, confound the analysis of data or, if ignored, seriously obscure the results. For example, because of high

polymer viscosities, polymer processes run at high pressures. As a result, melt rheometer components must be very sturdy, and moving parts must be dynamically sealed to prevent the incursion of melt. Furthermore, these high pressures can superpose unwanted flows (deformations) on the intended rheometrical deformation. The non-Newtonian nature of the polymer complicates the strain rate profiles of non-uniform viscometric flows such as pressure driven flows. Such rheological measurements must be corrected by a material dependent procedure. The elastic nature of polymers introduces complications when the rheometer employs a non-viscometric flow. Then, some combination of material properties controls the state of stress in the sample.

Temperature control also poses a significant challenge for rheometer designers. Rheological properties are very temperature sensitive. Because of their high viscosities, polymer melts can increase in temperature due to viscous dissipation. Coupled with this is the fact that polymers conduct heat poorly. Consequently, it can be difficult to ensure the uniform sample temperature needed for an unambiguous rheological measurement.

Finally, the difficulties of sampling the process in an efficient and representative fashion must be discussed. Ideally, a polymer sample should be taken from the fastest moving region of the process and then transported to the rheometer and tested instantaneously. It is important that each successive rheological test be performed on a completely new, compositionally homogeneous sample of material. Because of the high viscosity of polymer melts, polymer flows are low Reynolds number, laminar flows. This fact influences the way in which the main process flow stream is sampled and the way in which the sample in the rheometer is refreshed. If the sample is withdrawn from the wall of the process stream, a slower moving and thus "older" polymer will be tested. Furthermore, before a truly new sample can be tested, the

transfer line to the rheometer and the rheometer itself must be completely purged of the previous sample. Again, because most polymers flow in a laminar fashion, the process of sample renewal can be very slow and can introduce a significant time delay to the measurement. If one tests before the sample is completely renewed, the rheological property of a material of intermediate composition will be measured. The change in rheometer signal over this time will be representative of the sample renewal process rather than the underlying material change dynamics. In other words, the viscosity measurement will have its own dynamics.

The term "sample renewal" will be used throughout this work when referring to the process of sampling to emphasize the importance of completely refreshing the sample between tests.

1.2.2 Capillary and Slit Flow Process Rheometers

Capillary and slit flow process rheometers are popular because of their simplicity and because of the success of capillary and slit laboratory instruments. Both types rely on a pressure driven flow for sample deformation. Figure 12-1a illustrates a capillary rheometer while Figure 12-1b illustrates a slit rheometer. Polymer is pumped through the conduit, and pressures are measured at one, two or more locations along the length of the flow path. The equations needed to analyze slit and capillary data are straightforward and are summarized by Dealy (1982a). Because viscosity is a function of strain rate for non-Newtonian fluids, a special correction to the data must be made. This stems from the fact that the strain rate is not uniform over the cross-section of pressure driven flows. The correction is widely known as the Rabinowitsch correction and is described in detail by Walters (1975).

Figure 12-1a: Cross-section of a Capillary Rheometer

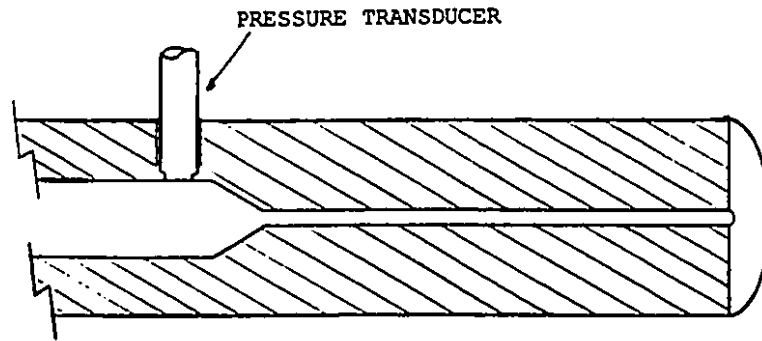
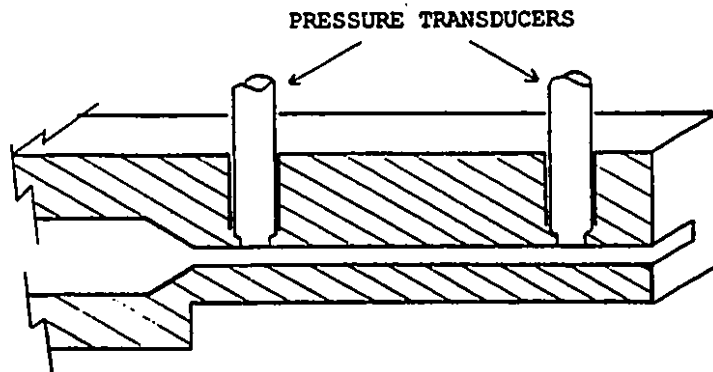


Figure 12-1b: Cross-section of a Slit Rheometer



The significance of this is that for capillary rheometers, true viscosity versus strain rate data are obtained by a two-step iterative procedure that makes use of the slope of the pressure drop versus shear rate curve. Thus, a single data point cannot be corrected. An alternative is to use a constitutive equation (or model) that gives the general form of the strain rate profile. This limits the use of the rheometer to materials of the type modelled. Schümmer and Worthoff (1979) have proposed an alternative to the Rabinowitsch correction. It is described in Section 2.2. Another correction, known as the Bagley correction (see Dealy (1982a)), must be made to capillary rheometer data if the pressure drop used in the stress calculation is measured over regions of non-viscometric flow, such as the entrance region to the capillary itself.

Because of industrial demand, commercial melt rheometer manufacturers often design their instruments to simulate the Melt Index (MI) test described in ASTM Test Method 1238. Briefly, the MI test consists of loading a small sample of polymer into a vertical, heated barrel. A plunger supporting a specified weight forces the melted polymer through a die of specified dimensions. The mass of polymer extruded in 10 minutes is reported as the Melt Index (MI). While the Melt Index is a useful indicator of melt consistency, it is not a true rheological property and can be somewhat ambiguous. In addition, in order to measure MIs accurately, the ASTM test method geometry must be matched closely, and this is not always practical in a process rheometer. Dealy and Wissbrun (1990) summarize the procedure of simulating the Melt Index test using capillary dimensions and an imposed pressure consistent with ASTM 1238.

All commercially available capillary melt rheometers are "on-line" instruments. This means they are located next to the process and rely on a gear pump and transfer line to sample the main process stream. The conventional reasoning

for this is that the rheometer must be isolated from process temperature and pressure fluctuations to be accurate. The practical reason is that in order to have control over capillary throughput, and therefore strain rate, a separate pump is needed. This requires space and precludes in-line implementation.

One of the inherent disadvantages of pressure-driven flow rheometers is that the sample renewal rate in the capillary (or the slit) is directly related to the desired test strain rate. For low strain rate measurements, the sample in the capillary is displaced slowly while at high strain rate the sample is renewed somewhat more quickly. This problem is compounded for on-line capillary rheometers, because the sample in the transfer line as well as in the capillary are renewed at a rate dependent on the test strain rate.

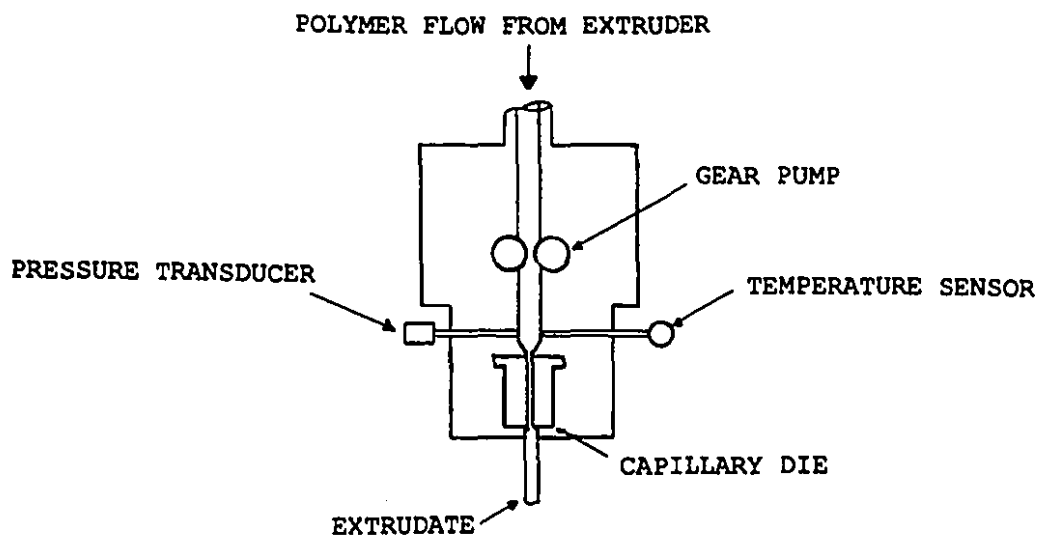
The Göttfert By-Pass Rheograph (Göttfert (1986)) illustrated in Figure 12-2, is an example of a conventional on-line capillary rheometer. It employs a single gear pump to sample the process stream and to control the flow rate through the capillary. Material passing through the capillary is discarded, typically at a rate of 0.5 to 1 kg/h. Viscosities in the range of 10 to 10^6 Pa s can be measured at strain rates in the range of 2 to 10^4 s⁻¹. Göttfert (1986) reported By-Pass Rheograph data that were in excellent agreement with a laboratory capillary rheometer. However, no detailed accuracy or repeatability estimates were published.

Göttfert (1991) presented data describing the dynamic performance of the By-Pass Rheograph (BPR) in response to a composition transition. The BPR reacted 13.5 minutes after the initiation of the transition and required 80 minutes to track the transition completely. In contrast, another instrument, described later, responded within one minute and tracked the same composition transition in 10 minutes. The difference in performance of these two rheometers is directly related to the sample renewal problem. In the case of the

BPR, sample renewal is restricted to the flow rates corresponding to the test strain rate and is complicated by the fact that the sampling line and then the capillary must be purged before a change in viscosity can be measured.

Curry et al. (1988) also identified the measurement delay of the By-Pass Rheograph. In empirically modelling their reactive extrusion process, they attributed most of the observed 4.8 minute process dead time to the rheometer measurement delay.

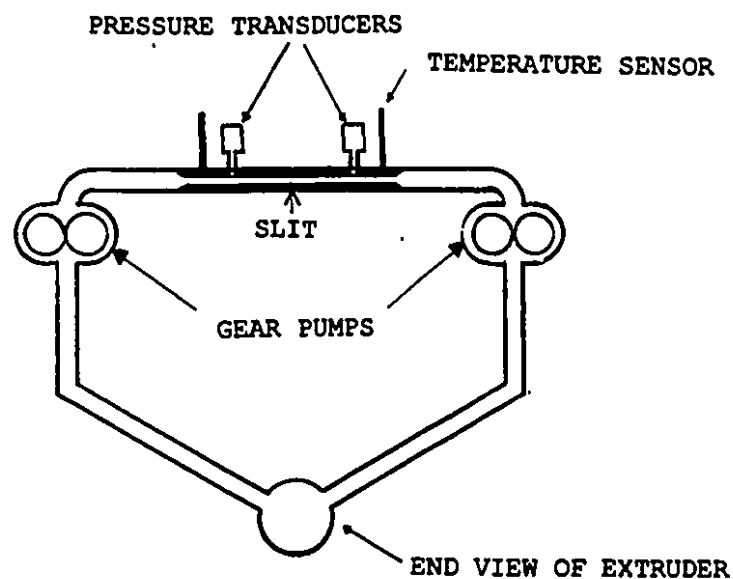
Figure 12-2: Schematic Diagram of the Göttfert By-Pass Rheograph



The limitations posed by long measurement delays have motivated rheometer manufacturers to shorten the sampling path of on-line capillary rheometers. The Rheometrics Melt Flow Monitor (MFM), described in the patent of Blanch et al. (1989), pumps polymer from an extruder through a slit located immediately on top the extruder. A second gear pump returns

the sample to the extruder. Blanch et al. (1989) claim that their design, illustrated schematically in Figure 12-3, greatly reduces measurement delay and eliminates the need to discard the tested sample. However, they point out that because of the rheometer's close proximity to the process, controlled thermal conditioning of the melt sample is impossible. The MFM corrects measured stresses to a reference temperature using an Arrhenius form equation.

Figure 12-3: Schematic Diagram of the Rheometrics Melt Flow Monitor



The MFM can be run in either constant strain rate (constant pump speed) mode or in constant stress mode. In the constant stress mode, the flow through the capillary is controlled to keep the pressure drop constant. The constant stress mode is used to simulate the Melt Index test. A single viscosity can be measured in 1 or 2 minutes in constant strain

rate mode (Samurkas (1990)) while a Melt Index can be measured in approximately 4 minutes (Lacey (1991)) in constant stress mode. These times refer only to the duration of the rheological tests themselves. Lacey (1991) reported that the MFM responded to step transitions in viscosity in times ranging from 20 to 45 minutes. He attributed this slow performance to the problems associated with withdrawing a polymer sample from the extruder barrel and to the long transportation and flushing time required to provide a fresh sample to the rheometer. A viscosity versus strain rate curve covering the range from 0.25 to 200 s⁻¹ can be measured in approximately 30 minutes.

Lacey (1991) reported that the repeatability of MFM measurements was outstanding. However, for process related reasons and in order to verify corrections for the entrance and exit losses, the instrument's signal had to be fine-tuned with laboratory measurements on a regular basis.

The Göttfert Real Time Rheometer (RTR) (Göttfert (1991)) addresses the problem of sample renewal in a slightly different way. The RTR employs three gear pumps. One pump provides a continuous stream of polymer to the rheometer and back into the extruder. Two gear pumps positioned at either end of the capillary itself control the flow, and, consequently, the strain rate in the capillary. By maintaining a high recirculation rate of polymer in the sampling loop, a much shorter measurement delay is incurred. Evidence of the advantage of the sampling loop has already been presented. It was the RTR that was compared earlier with the By-Pass Rheograph by Göttfert (1991). He showed that the RTR responded within one minute of a composition transition and tracked the transition within 10 minutes.

In an attempt to substantially reduce measurement delay, a number of research groups have designed in-line capillary and slit rheometers. Ross et al. (1990) incorporated a well-instrumented capillary rheometer in the nozzle of an injection

moulding machine. They correlated injection moulder ram speed with strain rate at six speeds. They then estimated empirical pressure and temperature correction expressions using apparent viscosity versus apparent strain rate data at 3 pressures, many temperatures and at six strain rates. Finally, they used the Cross and Carreau models (see Dealy and Wissbrun (1990)) to summarize the viscosity data. This last step was done to "normalize" the data and allow them compute percent deviations from the model, facilitating comparison of real time data. They also computed a "statistical master viscosity band" (confidence region) for the measurements in terms of percent deviation from the model. A deviation from the model greater than approximately $\pm 8 \%$ was considered a significant change.

Ross et al. (1990) compared their in-line rheometer data with laboratory capillary rheometer measurements. The in-line measurements were consistently low. Ross et al. felt that the observed differences were due, in large part, to the fact that the laboratory instrument tested virgin material, while the in-line instrument measured the properties of once processed polymer. The in-line rheometer was used successfully to monitor the decrease in viscosity due to an increase in moisture in a PBT moulding resin.

Once a process is in steady state operation, an in-line rheometer of the design of Ross et al. (1990) can measure viscosities only at the strain rate corresponding to the process throughput. Springer et al. (1975) addressed this problem with their twin slit rheometer design. This rheometer consisted of two slits in parallel. The flow through each slit was controlled by a valve. The measurement slit was instrumented with 4 pressure and 4 temperature transducers. The other slit had only temperature sensors. By adjusting the valve at the entrance to the measurement slit, a range of strain rates could be tested. The valve at the entrance to the other slit could be adjusted to keep the extruder back pressure, and therefore the polymer processing history,

constant. In this way viscosities could be measured over a strain rate range of approximately 10 to 1000 s⁻¹. The actual apparent strain rate was measured by collecting and weighing extrudate samples from the measuring slit at each valve setting. The strain rate was not controlled and was susceptible to all of the typical process disturbances affecting throughput.

Springer et al. (1975) compared data from their rheometer with literature data. Their apparent viscosity values were consistently low. They attributed this to the fact that the literature data were for a virgin polymer sample while the in-line rheometer tested once-processed polymer.

Pabedinskas et al. (1991) took a different approach to permit the measurement of viscosities at several strain rates. Their slit rheometer has a wedge profile. The strain rate experienced by the polymer increases as it flows down the length of the wedge. This is an innovative idea for a difficult problem, but it does have a fundamental drawback. Flow in a wedge is not a viscometric flow. The pressure differences measured in the wedge will reflect both viscous and elastic stresses. For some polymers, the elastic stress contribution may be dominating. Consequently, the wedge rheometer could be in considerable error. Also, their rheometer has no strict control on strain rate. The whole process stream flows through the rheometer; samples are collected and weighed periodically to determine the strain rate. Disturbances in throughput cannot be monitored or controlled in this manner.

The goal of the Pabedinskas et al. (1991) work was to monitor the molecular weight (M_w) and molecular weight distribution (MWD) of peroxide-degraded polypropylene. Based on the extensive background work of Tzogonakis (1988) and on their own analytical expertise, they felt that M_w and MWD could be monitored effectively using power-law parameters: n , the power-law exponent and k , the pre-exponential factor.

They derived a method of calculating n and k from three pressure measurements along the wedge. Viscosities are computed using the model and the current parameters.

The wedge rheometer can measure viscosities over a broad range of strain rates (10 to 1000 s^{-1}). In actual operation, a single throughput, calibrated ahead of time, would be used. Pabedinskas et al. (1991) were satisfied with the wedge rheometer performance. Agreement with a laboratory capillary rheometer was very good for low viscosity materials. For higher viscosity samples, the wedge rheometer measurements were consistently lower than the lab results. However, the slopes of the lab viscosity curves were well matched, satisfying the application requirements.

In summary, capillary and slit rheometers are popular choices for process applications because of their simplicity and respected performance in the laboratory. To enable precise control over test strain rates (capillary throughputs) conventional capillary process rheometers require gear pumps. This necessitates the on-line location of the rheometer. On-line rheometers have the advantage of being able to thermally condition samples prior to testing as well as being able to isolate the rheometer from process pressure disturbances. One criticism of on-line rheometers is that by being pumped through the sampling lines by a gear pump, the tested polymer sample does not have a processing history representative of the polymer in the main process stream. Furthermore, the long delay in transporting polymer melt samples to on-line instruments is recognized as a critical problem. Some commercial on-line rheometer designs have addressed this problem, but with limited success.

In-line slit and capillary rheometers have been designed in order to reduce the signal delay of on-line instruments. Quantifying the capillary throughput and thus the apparent test strain rate must be done off-line. This is undesirable because the typical upsets in throughput encountered in most

extrusion processes will not be detected and will represent a source of noise. Also, only a single test strain rate, corresponding to the throughput, can be studied. Consequently, the Rabinowitsch correction cannot be made and only apparent viscosities can be measured. Apparent viscosities can be corrected to true viscosities using a constitutive equation, but this will restrict the range of applicability of the rheometer. Corrections for the pressure and temperature dependence of viscosity must also be made. Empirical expressions are generally used for this purpose.

1.2.3 Rotational Process Rheometers

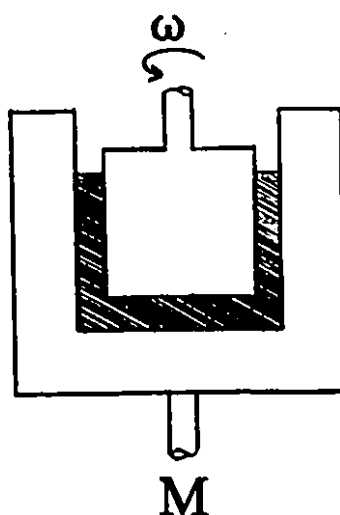
Rotational rheometers have also been developed for polymer process applications. An appealing attribute of the rotational rheometer geometry is that, when designed correctly, the strain rate profile in the shearing gap is uniform. Consequently, true rheological properties can be measured directly, without corrections. Also, rotational rheometers can be designed to measure rheological properties at very low strain rate. Such properties are particularly sensitive to molecular structure and are excellent indicators of a polymer's processability in film blowing or blow moulding applications. Rotational rheometers can also be used to measure linear viscoelastic (LVE) properties.

Wu (1985) has outlined a procedure for relating M_w and MWD to LVE data. Starita and Rohn (1987) applied this procedure to a polystyrene melt using an on-line rotational rheometer. Zeichner and Patel (1981) correlated MWDs of polypropylene with key features of the dynamic modulus plot to give a sensitive molecular structure index.

Rotational process rheometers designed for polymer melts generally use a concentric cylinder geometry. One of the cylinders is driven, while the torque on one of the cylinders is measured. This torque is proportional to the shear stress. This is illustrated in Figure 12-4. When one of the cylinders

is driven at a constant speed, the viscosity can be measured. Linear viscoelastic properties, such as the storage and loss moduli (G' and G'' respectively), and the complex viscosity $|\eta^*|$, can be determined when one cylinder is oscillated to create sinusoidal deformations of small amplitude. Dealy (1982a) outlines the equations needed to analyze rotational rheometer data.

Figure 12-4: Schematic Diagram of a Rotational Rheometer

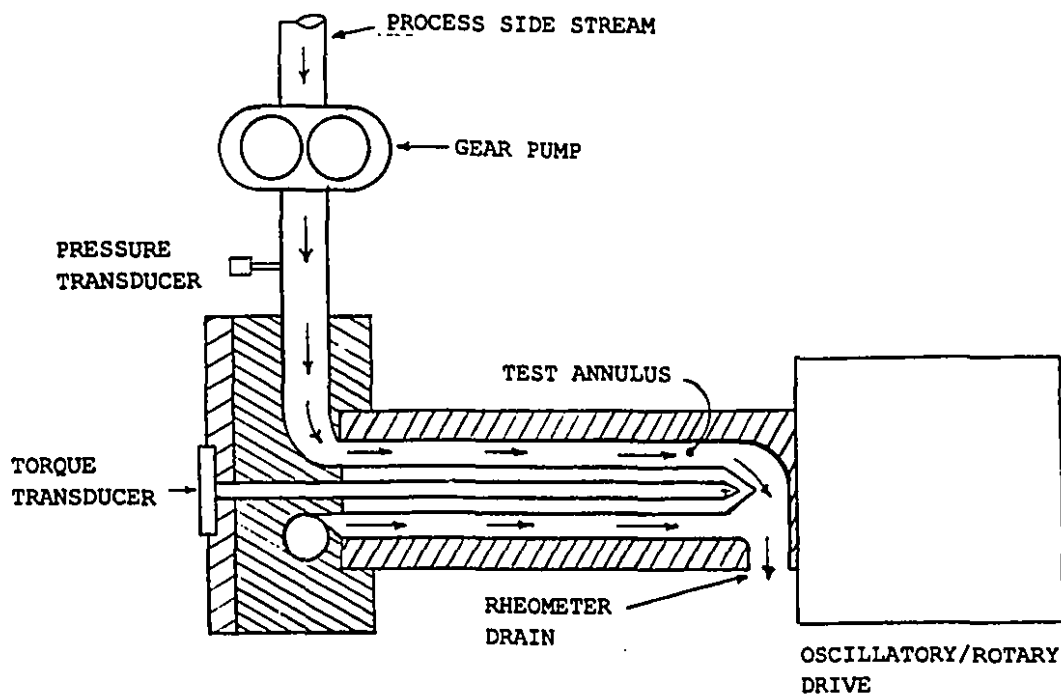


Legend: M = torque, ω = angular velocity.

Orwoll (1983) describes the Rheometrics On-Line Rheometer (ROR), which has been used as a rheological sensor in reactive extrusion studies by Zeichner and Macosko (1982), Fritz and Stöhrer (1986), Starita and Rohn (1987), and Hertlein and Fritz (1990). The ROR pumps polymer from the main flow stream through a transfer line and then axially through the annulus between the concentric cylinders. The outer cylinder is oscillated, while the torque on the inner cylinder is sensed with a torque tube transducer. Complex viscosity and dynamic moduli can be measured over a frequency range of 0.1 to 500 s^{-1} . The ROR is illustrated in Figure 12-5. Orwoll has shown excellent agreement between the ROR and a laboratory

dynamic rheometer for polyurethane, high density polyethylene and polypropylene. In fact, all of the aforementioned researchers have noted the instrument's accuracy.

Figure 12-5: Schematic Diagram of the Rheometrics On-Line Rheometer from Orwoll (1983).



However, the ROR's accuracy is affected by the axial polymer flow in the rheometer's measurement annulus ("through-flow"). Orwoll (1983) and Fritz and Stöhrer (1986) have documented this measurement bias as a function of through-flow. The undesirable effect of this phenomenon is to make the rheology-property correlations process specific. The only solution to the problem is to stop the through-flow during measurements.

Fritz and Stöhrer (1986) have employed a correlation

linking complex viscosity data to melt index, relying on the Cox 'erz rule. While this procedure is attractive because it puts the data in a commonly used form, it introduces further complexity in the data analysis.

The Rheometrics On-Line Rheometer suffers from the same measurement delays incurred by all on-line capillary rheometers. Fritz and Stöhrer (1986) modelled a reactive extrusion process empirically and reported a 3-minute process delay, which they attributed largely to measurement delay. In order to achieve even this level of performance, Fritz and Stöhrer had to restrict their rheometer's operation to high frequency tests with high sample through-flow rates. Stopping the flow through the rheometer during tests introduced too much delay; low frequency tests could not be completed in an acceptable period of time. Hertlein and Fritz (1990) reported a 5 to 6 minute measurement delay. Zeichner and Macosko (1982) reported a 10 minute process response time. This represents a marginal improvement over the responses reported by the other workers when process dynamics are taken into consideration.

In-line rotational rheometers have also been reported. Heinz (1984) describes the Dynvimeter; a design consisting of three concentric cylinders. The middle cylinder is oscillated and is also used to measure shear stress related torque. The purpose of making both inner and outer cylinders stationary is to minimize the effects of non-viscometric flow at the edges of the cylinders. Axial slots on the outer cylinder allow for passive sample refreshment. Heinz claims that the inaccuracy due to the influence of the slots on the viscometric flow is less than 5%.

The Dynvimeter measures linear viscoelastic properties over a frequency range of 0.01 to 10 Hz. It can measure a maximum complex viscosity of 10^4 Pa s and a maximum storage modulus of 3000 Pa. Dynvimeter results looked reasonable but were not verified in the 1984 paper. Heinz estimated that the

material sample could be renewed in 5 to 10 minutes. He reported no bias error due to pressure flow in the measurement gap. The Dynvimeter is sold by Brabender Messtechnik KG (Duisberg, Germany).

Khachatryan et al. (1983) reported an in-line concentric cylinder steady shear rheometer. In their design, the inside cylinder rotates at a steady 10 rpm and the torque on the outer cylinder is measured. The cylinders are located in a cell in the main flow stream. Khachatryan et al. estimate that only a small proportion of the total melt flow enters the rheometer gap. They claim good agreement with another instrument but do not quantify their rheometer's response. They also imply that changing the flow rate through the rheometer has no effect on the measurements.

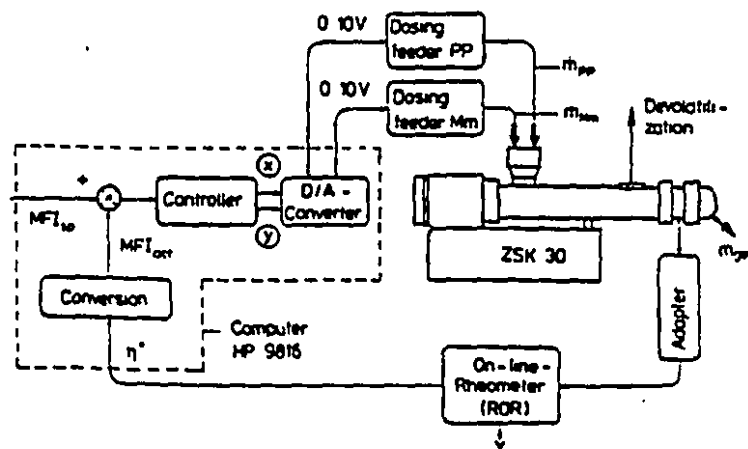
To summarize, rotational rheometers make sensitive and accurate process rheometers. A complication evident from extensive experience with the Rheometrics On-Line Rheometer is that pressure flow superposed on the oscillating drag flow in the measurement gap introduces a significant, process-dependent error. Also, like other on-line rheometers, the measurement delay incurred with the ROR is long. In-line rotational rheometers have also been reported though little information regarding their performance is available.

1.3 Process Control of Reactive Extrusion

Fritz and Stöhrer (1986), Curry et al. (1988) and Pabedinskas et al. (1989) studied the control of reactive extrusion using rheological measurements. All three groups studied the reactive "visc-breaking" process for polypropylene. This process involves the reaction of polypropylene melt with peroxide radicals to achieve an overall decrease in polymer molecular weight coupled with a narrowing of the molecular weight distribution. This imparts flow properties favourable to fibre spinning and injection moulding operations.

A schematic of the model polypropylene visc-breaking process used by Fritz and Stöhrer (1986) is shown in Figure 13-1. Two gravimetrically controlled feeders metered two constant mass flow rate streams to a 30 mm Werner and Pfleiderer ZSK-30 twin screw extruder. These feed streams consisted of a polypropylene pellet stream and a peroxide masterbatch stream (0.2 mass % peroxide dispersed on polypropylene pellets). An adapter on the end of the extruder facilitated sampling of the melt stream by a gear pump. This sample stream was pumped to a Rheometrics On-Line Rheometer (ROR) where an oscillatory shear test was performed. Complex viscosity data were converted to Melt Flow Index (MFI) values using a rather complicated correlation. Control actions were computed using a digital, velocity-form PI algorithm. Control actions consisted of complementary changes to the two feed rates, keeping the total feedrate constant, but increasing or decreasing the relative proportion of peroxide.

Figure 13-1: Schematic Diagram of the Reactive Extrusion Process Studied by Fritz and Stöhrer (1986)



The goal of the control system was to track set point changes and to reject disturbances in the polypropylene feed molecular weight, in the peroxide masterbatch activity, and in peroxide masterbatch homogeneity. Also, because of their effect on the peroxide reaction rate, temperature disturbances due to temperature controller malfunction or due to changes in shear heating had to be controlled.

From laboratory tests, Fritz and Stöhrer (1986) determined that the relationship between MFI and % peroxide was linear. Fritz and Stöhrer modelled their process with a first order plus dead time model fitted to step change test data. They identified a 3 minute (180 s) dead time and a step direction dependent time constant. Steps from high to low viscosity (low to high MFI) had a first order time constant of 3.3 minutes (198 s), while steps from low to high viscosity (high to low MFI) had a time constant of 2.6 minutes (156s). Fritz and Stöhrer explained the time constant direction dependence by noting that extruders are more efficient in pumping viscous rather than non-viscous materials. Consequently, low viscosity melts are "swept out" more quickly by more viscous melts.

Fritz and Stöhrer reported controlled process responses in terms of settling times. MFI set point changes were sluggish. Steps to high MFI (low viscosity) were damped and had settling times of 13.5 and 14 minutes (810 and 840 s). The reported response to a step to lower MFI (high viscosity) was oscillatory and had a settling time of 12.5 minutes (750 s). A masterbatch activity disturbance was simulated by instantaneously changing the masterbatch feed from a 0.2 % peroxide concentration to a 0.15 % concentration. The resultant deviation from set point lasted 25 minutes. Fritz and Stöhrer also created a process temperature disturbance by dramatically increasing the extruder screw speed. The resultant increase in shear heating and consequent increase in peroxide reaction rate caused an increase in MFI (decrease in

viscosity). The control system's response was a damped oscillation that attained the desired set point value in 10 minutes (600 s).

Fritz and Stöhrer (1986) discussed their process control performance in terms of a "controllability ratio". This is the ratio of process dead time to process time constant. PI control is ineffective if the controllability ratio is greater than 1.2. Fritz and Stöhrer found controllability ratios of 0.86 to 1.10 and concluded that the process dead time was so large that the process was at the limit of controllability. They felt that the most important goal of future work would be to decrease the controllability ratio.

Unfortunately, Fritz and Stöhrer do not comment on the magnitude or potential sources of measurement noise. As explained in Section 1.2, the ROR's accuracy is compromised by the flow of material through the measurement annulus.

Curry et al. (1988) studied the visc-breaking of polypropylene using a process identical to that of Fritz and Stöhrer with the exception that they employed an on-line capillary rheometer; the Göttfert By-Pass Rheograph. Using composition step change tests, they identified a first order plus dead time model for their process consisting of a 4.8 minute (288 s) dead time and a 4.0 minute (240 s) time constant. These parameters are significantly different from those of Fritz and Stöhrer. This could be due to a difference in process throughput or to differences in the on-line rheometer performance. Curry et al. confirmed Fritz and Stöhrer's observation of a linear melt flow index versus ξ peroxide relationship (constant process gain) and the observation of step direction dependent time constants.

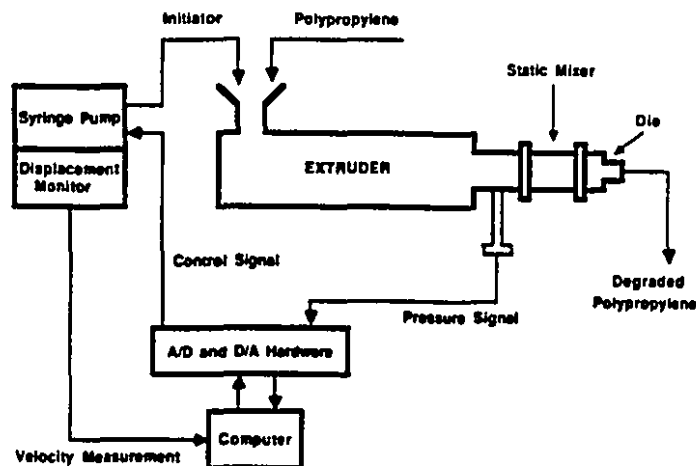
Curry et al. (1988) also implemented a PI control algorithm based on a measure of the melt flow index (MFI). Interestingly, they commented that a derivative term was not included in the controller because the measurement signal was too noisy. With fixed parameters, their process responses to

MFI set point changes were very sluggish. Settling times of 18 to 20 minutes (1080 to 1200 s) were observed. However, by using controller gains and integral times "optimized" for each MFI operating point, the response times were greatly reduced. Rise times of 4.3 to 7.8 minutes (258 to 468 s) are apparent in plots of their data. It should be noted that the "optimized" parameters resulted in oscillatory responses.

The fact that a program of optimized parameters (a technique known as "gain scheduling") improved performance implies that the process dynamics and the process gains were nonlinear. This was not stated explicitly by Curry et al.

Pabedinskas et al. (1989) were motivated by the long measurement delays experienced by Fritz and Stöhrer to search for a faster responding viscosity indicator. They chose to measure the process pressure because of its strong, though complex, relationship to viscosity. The objective of their study was to control the reactive visc-breaking of polypropylene in a single screw extruder. A schematic diagram of their process is given in Figure 13-2.

Figure 13-2: Schematic Diagram of the Reactive Extrusion Process Studied by Pabedinskas et al. (1989)



Polypropylene pellets were fed to the feed hopper, while the peroxide was injected directly into the melt using a syringe pump. A 9-element static mixer was mounted on the end of the extruder to ensure complete mixing and reaction. The melt pressure was monitored at the entrance to the static mixers.

The most significant source of pressure measurement noise encountered by Pabedinskas et al. was due to fluctuations in the peroxide injection rate. This caused a relatively high frequency, composition-related fluctuation. They alleviated this problem by implementing a control loop on the injection pump speed. They also attributed some the measurement noise to the pressure fluctuations typically observed during single screw extrusion. Tadmor and Klein (1970) discuss these fluctuations in detail.

Pabedinskas et al. used step change data to fit the parameters of a first order plus dead time model. A dead time of 160 s was identified. They found that both the gain and the process time constants were nonlinear functions of peroxide concentration. These are reproduced in Table 13-1.

Table 13-1: Data of Pabedinskas et al. (1989) -- "Discrete and Continuous Model Parameters for Various Concentration Step Changes".

Initiator Conc'n Change [wt%]	Process Gain [MPa/wt%]	Time Constant [s]
0.01-0.02	-110.6	146
0.02-0.01	-117.7	154
0.02-0.03	-78.1	95
0.03-0.02	-90.0	112
0.03-0.04	-62.3	118
0.04-0.03	-58.5	165

The gain decreases with increasing peroxide concentration while the time constant seems to pass through a minimum. In addition, Table 13-1 shows that smaller time constants are consistently observed for steps of increasing peroxide concentration which corresponds to a decrease in molecular weight and viscosity. This is opposite to the effect observed by Fritz and Stöhrer and suggests that an explanation other than the one based on extruder pumping efficiency is needed to explain the time constant asymmetry.

It is important to note that the process dead time observed by Pabedinskas et al. was smaller than those observed by Fritz and Stöhrer (1986) and Curry et al (1988). Yet, because their process time constants were also smaller in magnitude, Pabedinskas et al. did not achieve an improvement in the controllability ratio. This is reflected in the performance of their digital, velocity-form PI control algorithm. The response time of a set point change was 15 minutes (900 s). A peroxide feed disturbance, created by suddenly decreasing the pumping capacity of the syringe pump by one third, was rejected only after 32 minutes (1920 s). Recognizing the nonlinear process gain, Pabedinskas et al. implemented a gain scheduling algorithm. With gain scheduling, the controller still took 15 minutes to track a set point change. Pabedinskas et al. also implemented a Smith Predictor algorithm to address the problems posed by the process dead time. With the Smith Predictor, a set point change was tracked in 12 minutes (720 s).

The evidence presented by the above studies documents a difficult control problem. The relationship between melt flow index and peroxide concentration is linear, and Fritz and Stöhrer (1986) and Curry et al. (1988) report no operating point dependence of process dynamics. Yet, Curry et al. demonstrated that programmed adaptation of controller parameters improved control quality considerably. Using pressure as a rheological measure, Pabedinskas et al. (1989)

clearly observed nonlinear gains and time constants.

Another puzzling fact is the contradiction of time constant direction dependence. This suggests that factors other than a viscosity-dependent extruder pumping efficiency are responsible for reactive extrusion dynamics.

Finally, it is disappointing that Pabedinskas et al. (1989) did not see a significant controller performance improvement, considering that they had a dependable in-line measurement. It appears that the advantage gained by the in-line measurement was offset by the contribution of the static mixing elements to the process dynamics.

In conclusion, it is clear that a faster responding viscosity sensor is needed to improve the performance of reactive extrusion control. However, there are many other factors, including the reactive extrusion system dynamics and, perhaps, process design, that also pose considerable barriers to successful control.

1.4 Research Objectives

The primary objective of this research was to develop a new viscosity sensor for applications in reactive extrusion monitoring and control. Two guiding principles were observed in the design of the rheometer. First of all, the instrument had to be located "in-line" in order to measure viscosity with a minimum of delay. Secondly, the rheometer had to have a sound rheological basis in order that it be accurate and reliable.

A further objective of this study was to demonstrate the rheometer for use in a closed loop viscosity control application. To this end, a process for the manufacture of ethylene-methacrylic acid ionomers by reactive extrusion was assembled. The process was modelled empirically using step test data and two closed loop control schemes were implemented.

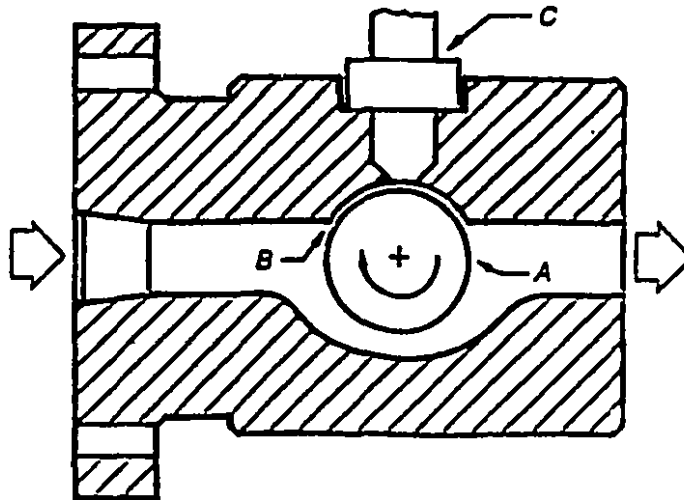
CHAPTER 2

FUNDAMENTALS OF THE MCGILL IN-LINE MELT RHEOMETER DESIGN

2.1 Principle of Operation

The McGill in-line melt rheometer (ILR) is shown in cross-section in Figure 21-1. It is designed to fit on the end of a twin screw extruder, before the forming die. In this way the entire polymer melt stream flows through the rheometer. In concept, the ILR is a "partial" Couette flow rheometer. The rotating drum, labelled "A" in Figure 21-1, forms a shearing zone (B) with a portion of the flow channel wall. The shear stress generated in the shearing zone is sensed by the shear stress transducer (SST), labelled "C" in Figure 21-1.

Figure 21-1: Cross-sectional Diagram of the McGill In-Line Rheometer, Side View



The SST was conceived by Dealy (1982b) in order to measure shear stresses over a small wall area. With this ability, it is only necessary to provide a small region of fully developed, viscometric flow, in order to make a rheological measurement. Complex flows outside of this small region do not affect the measurement. It is this fact that

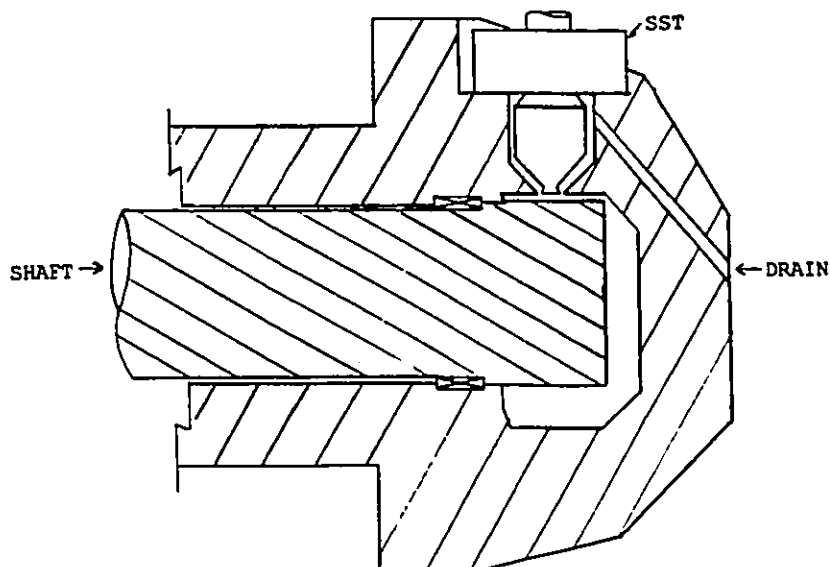
makes possible the design of a rheometer that can be positioned in the main process flow stream.

Several criteria guide the selection of the rheometer shearing zone dimensions. First, the ratio of the shearing zone gap to rotating drum radius must be small to ensure that the deformation in the shearing zone is uniform (Dealy, 1982a). Second, because polymers have high viscosity and low thermal conductivity, one must be concerned about viscous heating. A small shearing zone gap minimizes this problem. Also, pressure-driven flow in the shearing zone is undesirable because it complicates data interpretation. Minimizing the gap also reduces this effect. On the other hand, it is crucial that the rheometer be capable of generating the range of shear rates that are most useful for a given polymer system. The rotating drum's angular velocity is one of the variables governing the shear rate; the shearing zone gap dimension is the other. Finally, the rate at which the shearing zone can be replenished with new material is directly related to its length to width ratio. This will be discussed further in Section 2.3. A large shearing zone gap or short shearing zone length will promote sample renewal.

With these criteria in mind, a shearing zone gap of 1 mm was selected. The rotating drum's radius was 25 mm. The shearing zone length was approximately one third of the drum's circumference. The combination of rotating drum velocity and shearing zone gap size enabled the rheometer to operate over the shear rate range from 3 to 33 s⁻¹. Chapter 3 gives details of the rheometer design.

To ensure that the pressure flow through the shearing zone was small, the flow channel in the vicinity of the rotating drum was widened. This is illustrated in Figure 21-2, which shows a vertical section through the axis of the rotating drum. It was estimated that only 1/600 th of the total polymer mass would flow through the shearing zone due to the pressure gradient.

Figure 21-2: Cross-sectional Diagram of the McGill In-Line Rheometer, Front View.



The rheometer described above was designed to offer the following advantages:

- 1) flow kinematics in the shearing zone approximating steady simple shear, which would allow the viscosity to be determined solely from a measurement of the shear stress and the rotating drum's angular velocity,
- 2) a shear rate independent of the process throughput,
- 3) a small measurement delay because: i) the rheometer is located immediately in the process stream, ii) the shearing zone volume is small and iii) the rotating drum, fully exposed to the main melt stream will drag fresh material continuously into the gap.

The following sections of this chapter discuss important fundamental questions about the rheometer's design. A method to deal with the effects of pressure flow superposed on the drag flow in the ILR is presented in Section 2.2. Section 2.3 presents simulations of the flow of polymer in the ILR and discusses the problems of sample renewal. The last section of

the chapter investigates the constraints imposed on measurements by virtue of the rheometer's in-line placement and the consequent inability to control temperature precisely.

2.2 Superposition of Pressure Flow on Drag Flow

2.2.1 Visualisation of Pressure Plus Drag Flow

Early experiments with the ILR indicated that pressure flow in the shearing zone could not be ignored. The way in which pressure flow effects drag flow in the shearing zone is illustrated in Figure 22-1. The right hand axis in each figure represents the rotating drum surface. In each case, the drum is in motion at velocity V . The left hand axis represents the rheometer body which is stationary. Figure 22-1a shows the velocity and strain rate profiles in the ILR gap when there is no pressure flow. The velocity profile is a straight, sloped line. The strain rate is the derivative of the velocity with respect to the shearing zone gap dimension at each point. It is a constant in this case.

The velocity and strain rate profiles resulting from a drag plus small pressure flow in the shearing zone are illustrated in Figure 22-1b. The velocity profile is now curved. The shape of this curve is governed by the material's rheological behaviour. A Newtonian fluid will have a quadratic velocity profile and a straight, sloping strain rate profile. A shear thinning fluid's velocity and strain rate profiles will be higher order curves. Figure 22-1c shows the velocity and strain rate profiles for the situation where the pressure drop across the shearing zone is large and/or the fluid viscosity is low. In this case,

Figure 22-1a: Velocity and Strain Rate as a Function of Position in the Shearing Zone for a Simple Shear Flow.

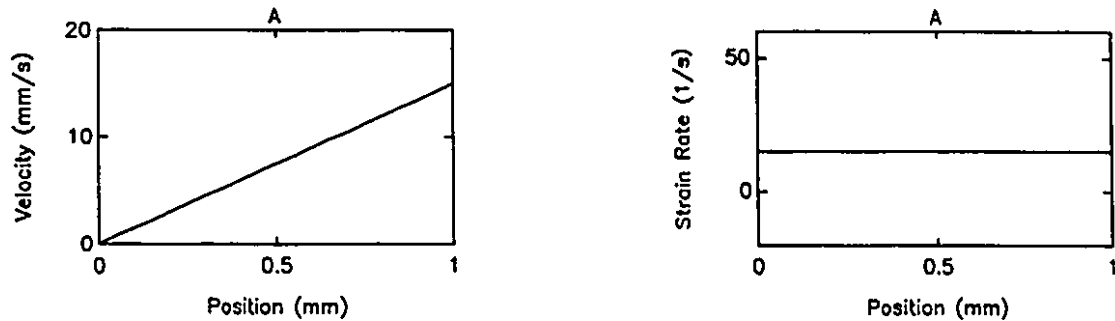


Figure 22-1b: Velocity and Strain Rate as a Function of Position in the Shearing Zone for a Small Pressure Flow Superposed on a Simple Shear Flow.

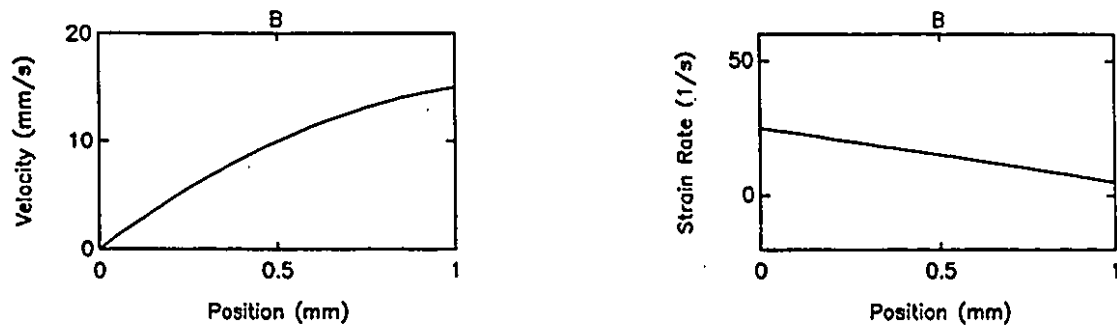
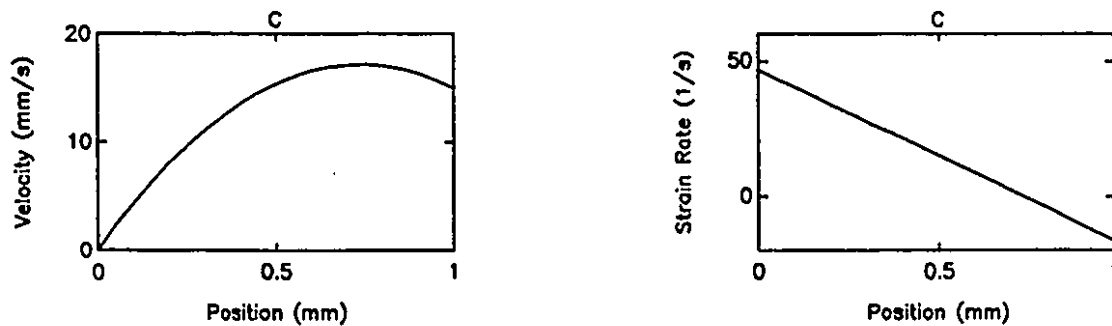


Figure 22-1c: Velocity and Strain Rate as a Function of Position in the Shearing Zone for a Large Pressure Flow Superposed on a Simple Shear Flow.



the velocity profile exhibits a maximum, and again the strain rate can be non-uniform.

In conclusion, the addition of pressure flow to drag flow results in a non-uniform strain rate in the shearing zone that cannot be easily specified.

2.2.2 Pressure Flow Correction Concept

Capillary and slit rheometers employ pressure driven flows to generate a shearing deformation. To take into account the non-uniformity of the shear rate in these pressure-driven flows, a technique known as the Rabinowitsch correction is generally used. An explanation of this technique is given by Walters (1975). It involves correcting the apparent strain rate using the slope of a log-log plot of the apparent stress versus the apparent shear rate. An analogous approach cannot be taken in this case due to the lack of symmetry in the ILR shearing zone.

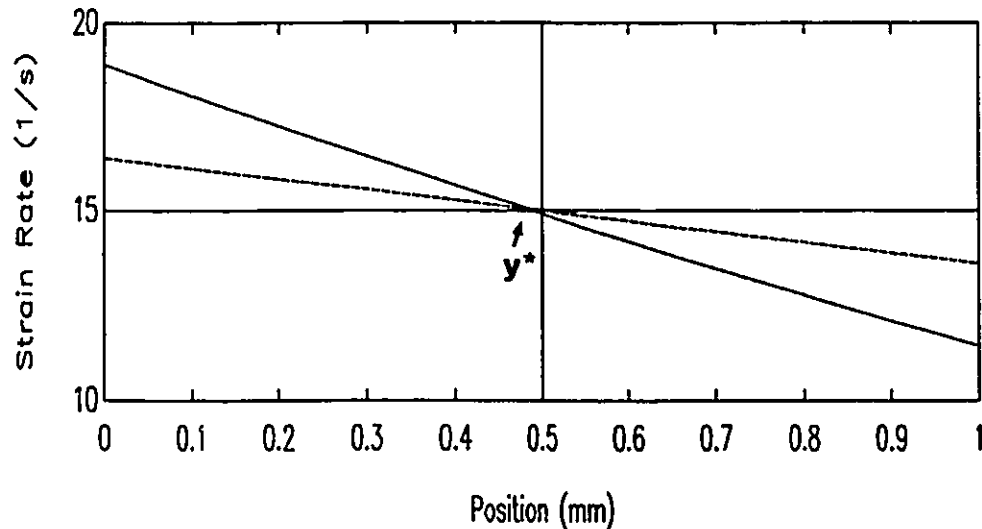
An alternative procedure is to use an expression for the strain rate derived from an assumed viscosity model. Flummerfelt et al. (1969) described such an expression for a pressure plus drag flow geometry based on a power-law model. The obvious problem with this approach is that the model parameters for the material being tested must be known ahead of time. Errors in the model parameters would lead to measurement errors. An iterative technique could be used to adjust the parameters, but this would be time consuming.

The approach followed in this work is patterned after the method described by Schümmer and Worthoff (1979). Their method is based on two important facts about the deformation of samples in a rheometer gap. These facts are: 1) the shear stress profile in the gap is independent of the type of fluid, and 2) the strain rate profiles of Newtonian and shear thinning fluids of approximately the same viscosity will cross at some point in the gap. It follows that at the point of intersection of the Newtonian and shear thinning fluid strain

rate profiles, the apparent (Newtonian) viscosity is equal to the true (shear thinning) fluid viscosity. Schümmer and Worthoff (1979) and Laun (1983) show that very little error is incurred when a constant value is assumed for this intersection point for a range of materials. In other words, the apparent viscosity can be scaled to give a reliable estimate of the true viscosity.

A pressure-flow correction for the drag plus pressure flow geometry, using the ideas of Schümmer and Worthoff (1979), can be explained with the aid of Figure 22-2. The strain rate is constant for steady simple shear, regardless of the material. This is marked by a solid line in Figure 22-2. The strain rate of a Newtonian fluid experiencing steady simple shear and a pressure gradient is a linear function of position and has the value of the shearing velocity divided by the shearing zone gap at the gap midpoint. This is illustrated by the dashed line in Figure 22-2. This reflects the facts that for Newtonian fluids: i) pressure flow and drag flow deformations are additive and ii) at the midpoint of the shearing zone gap, there is no deformation due to pressure flow. (Newtonian pressure flow velocity profiles are parabolic; the parabola maximum occurs at the midpoint of the gap, and the maximum is a point of zero strain rate.) For shear-thinning fluids, the pressure and drag flow deformation components are not strictly additive, but the point at which the pressure flow makes no contribution to the deformation is still in the vicinity of the shearing zone gap mid-point. This is illustrated by the dashed-dotted line in Figure 22-2. Clearly, at the stationary wall ($y = 0$ mm) the strain rates for a Newtonian and a shear thinning-fluid can be very different and would, consequently, lead to very different viscosity measurements. However, near the centre of the shearing zone, the two shear rate profiles cross, i.e., the shear rates are equal. Consequently, at this point near the

Figure 22-2: Strain Rate as a Function of Position in the Shearing Zone.



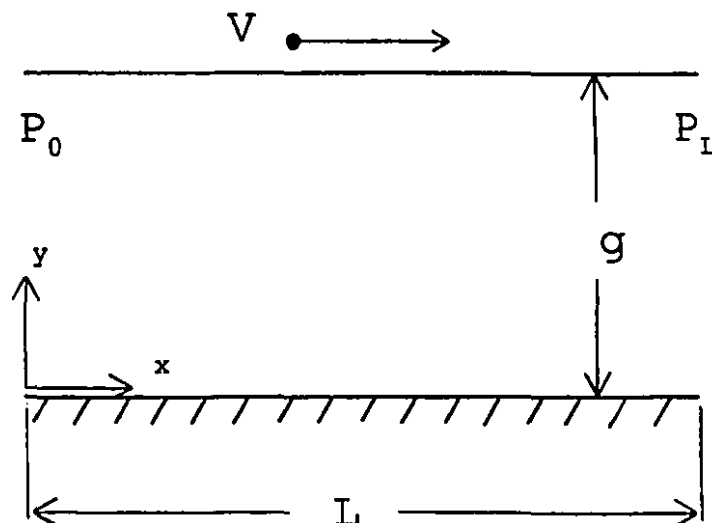
Legend: (-) a simple shear flow. (- -) simple shear flow with a small superposed pressure flow.
(-·) simple shear flow with a large superposed pressure flow.

centre of the gap, the viscosity computed using an analysis for Newtonian fluids will give an accurate estimate of the viscosity of a shear thinning fluid.

2.2.3 Pressure Flow Correction Equations

The method of Schümmer and Worthoff (1979) was derived for the drag plus pressure flow case using the geometry and symbols shown in Figure 22-3. A cartesian approximation of the cylindrical geometry is justified because the shearing zone gap is small compared to the radius of the rotating cylinder. [The gap is only 4% of the rotating drum radius.]

Figure 22-3: Cartesian Representation of the ILR's Shearing Zone



The shear stress at any point in the shearing zone can be derived directly from Cauchy's equation in 2 dimensions:

$$0 = -\frac{\delta P}{\delta x} + \frac{\delta \tau_{yx}}{\delta y} \quad (22-1)$$

defining, $\sigma \equiv \tau_{yx}$, integrating and applying the boundary condition $\sigma = \sigma_w$ at $y = 0$ gives,

$$\sigma = \sigma_w - p'xy \quad (22-2)$$

where

$$p' = \frac{(P_0 - P_L)}{L} > 0$$

For a Newtonian fluid, the expression for the strain rate profile in the shearing zone is:

$$\dot{\gamma}_N(y) = \frac{V}{g} - \frac{p'}{\eta_N} \times (y - \frac{g}{2}) \quad (22-3)$$

Since the shear stress at the wall is a measured quantity, a more useful expression is obtained by eliminating the viscosity by use of the definition $\eta_N = \sigma/\dot{\gamma}$ and substituting equation 22-1 for σ to give,

$$\dot{\gamma}_N(y) = \frac{V}{g} \times \left(\frac{\sigma_N - p' \times y}{\sigma_N - p' \times \frac{g}{2}} \right) \quad (22-4)$$

Schümmer and Worthoff's shear-thinning / Newtonian fluid viscosity equality can be expressed mathematically as:

$$\eta_{ST}[\sigma(y^*), \dot{\gamma}_{ST}(y^*)] = \eta_N[\sigma(y^*), \dot{\gamma}_N(y^*)] \quad (22-5)$$

where y^* is the point of intersection of the Newtonian (subscript N) and shear-thinning (subscript ST) fluid strain rate profiles. Substituting equation 22-2 and 22-4 into the Newtonian fluid definition, $\eta_N = \sigma(y)/\dot{\gamma}_N(y)$, gives

$$\eta_N = \frac{\sigma_N - p' \times \frac{g}{2}}{\frac{V}{g}} \quad (22-6a)$$

and

$$\dot{\gamma}_N(y^*) = \frac{V}{g} \times \left(\frac{\sigma_N - p'xy^*}{\sigma_N - p'x \frac{g}{2}} \right) \quad (22-6b)$$

Thus using the pressure correction, one computes the Newtonian viscosity from the measured stress, drum velocity and pressure signals and then adjusts the Newtonian (or apparent) strain rate by a constant factor to find the shear rate at which this equals the viscosity of the shear-thinning fluid. This effectively shifts the apparent viscosity curve horizontally to obtain the true viscosity curve.

An estimate of y^* is needed to be able to use equations 22-6a and 6b. This requires an expression that summarizes the shear thinning fluid's strain rate profile in the shearing zone. In the present work, a power-law expression ($\sigma = k\dot{\gamma}^n$) was used. It should be stressed however, that this assumption does not limit the applicability of the method to power-law fluids. It will be shown that in fact y^* is not very sensitive to the power-law parameters and can therefore give a valid estimate of the true viscosity even for fluids deviating somewhat from power-law behaviour.

Strain rate profiles for drag plus pressure flow between parallel plates based on the power-law model were obtained by differentiating the velocity profile expressions of Flummerfelt et al. (1969). Flummerfelt et al. classified the possible velocity profiles into two cases. In Case I profiles, illustrated in Figure 22-1b, drag flow dominates. Typically, the pressure drop across the gap is low or the viscosity is high. Case I profiles can be identified using the inequality given in Equation 22-7a:

$$\Lambda = \frac{p' \times g}{k} \times \left(\frac{g}{V}\right)^n \leq \left(\frac{n+1}{n}\right)^n \quad (22-7a)$$

The variables used above are explained in Figure 22-3. The strain rate profile is given by:

$$\dot{\gamma}_{PL} = \left(\frac{n+1}{n}\right) \left(\frac{V}{g}\right) \left(\frac{(\beta - \frac{y}{g})^{\frac{1}{n}}}{\beta^{\left(\frac{n+1}{n}\right)} - (\beta-1)^{\left(\frac{n+1}{n}\right)}} \right) \quad (22-7b)$$

where the parameter β can be obtained by numerically solving Equation 22-7c.

$$\Lambda - \left(\frac{\left(\frac{n+1}{n}\right)}{\beta^{\left(\frac{n+1}{n}\right)} - (\beta-1)^{\left(\frac{n+1}{n}\right)}} \right)^n = 0 \quad (22-7c)$$

Case II profiles are illustrated in Figure 22-1c. In this case, pressure flow in the shearing zone is significant enough to cause the velocity profile to have a maximum. Generally, this can occur when the pressure drop is large and the viscosity is relatively low. Case II behaviour will occur when the inequality given in Equation 22-8a is satisfied.

$$\Lambda \geq \left(\frac{n+1}{n}\right)^n \quad (22-8a)$$

For Case II flows, the strain rate profile is defined over two separate regions, delineated by β . Here, β has the significance of being the point of the velocity profile maximum. Consequently, the strain rate profile is given by:

$$\dot{\gamma}_{PL} = \frac{-\left(\frac{V}{g}\right) \left(\frac{n+1}{n}\right) \left(\beta - \frac{y}{g}\right)^{\frac{1}{n}}}{\beta^{\left(\frac{n+1}{n}\right)} - (1-\beta)^{\left(\frac{n+1}{n}\right)}} \quad (22-8b)$$

over the region $0 < y/g < \beta$, and

$$\dot{\gamma}_{PL} = \frac{-\left(\frac{V}{g}\right) \left(\frac{n+1}{n}\right) \left(\frac{y}{g} - \beta\right)^{\frac{1}{n}}}{\beta^{\left(\frac{n+1}{n}\right)} - (1-\beta)^{\left(\frac{n+1}{n}\right)}} \quad (22-8c)$$

for $\beta < y/g < 1$. β is obtained by solving the following equation.

$$\left(\frac{n+1}{n}\right) - \Lambda^n \times \left[\beta^{\left(\frac{n+1}{n}\right)} - (1-\beta)^{\left(\frac{n+1}{n}\right)} \right] = 0 \quad (22-8d)$$

Again, β must be solved numerically. The power-law parameters can be determined from viscosity versus strain rate data obtained either in the laboratory or using the ILR. The pressure drop along the shearing zone must be measured experimentally. Values in the range of 0.04 MPa to 0.37 MPa were typical and values as high as 0.5 MPa were observed.

To find y^* , the following equation must be solved:

$$f(y^*) = \dot{\gamma}_N - \dot{\gamma}_{PL} = 0 \quad (22-9)$$

$\dot{\gamma}_N$ is given by Equation 22-4; $\dot{\gamma}_{PL}$ is given by either Equation 22-7b, 22-8b or 22-8c, whichever is appropriate. For the materials studied in this work, y^* was found to fall in the range 0.45 to 0.50. A good overall compromise value was $y^* = 0.465$.

2.2.4 Pressure Flow Correction Parameter Sensitivity

Clearly, y^* , and therefore the pressure flow correction, is a function of the power-law parameters, k and n and the operating conditions ΔP and V . In their applications of this method, Schümmer and Worthoff (1979) and Laun (1983) proved that y^* was independent of the power-law pre-exponential factor, k , and insensitive to changes in the power-law exponent, n , over a fairly broad range. Unfortunately, the asymmetry of the drag plus pressure flow geometry prevents this degree of algebraic simplification.

Luckily, there are two mitigating factors that ensure that the value of y^* does not vary widely. First, the combination of shearing zone gap and rheometer flow channel dimensions ensure that the pressure flow in the shearing zone is small. Secondly, except for the lowest shearing velocities, the deformation due to pressure flow is small compared to the deformation due to shearing. It is only the deformation due to pressure flow that is sensitive to fluid type.

The range of variation of y^* in response to the power-law and deformation parameters is illustrated in Tables 22-1 and 22-2. Table 22-1 summarises the power-law parameters and experimentally observed pressure drops for three different polymers. These polymers exhibit the range of properties that the current ILR was design for. Polymer A is a low viscosity polymer, exhibiting only a moderate degree of shear-thinning. Polymer B is a higher viscosity, much more shear thinning polymer. Polymer C is of comparable viscosity to Polymer B but is less shear-thinning. Table 22-2 presents values of y^* calculated for each polymer, over a range of shear rates.

Table 22-1: Summary of Power-Law Parameters and Experimentally Determined Pressure Drops along the Shearing Zone

Polymer	A	B	C
n	0.840	0.485	0.663
k	1368.4	7360.6	6092.9
ΔP (Pa)	57550	339800	365000

Table 22-2: Newtonian-Power-Law Fluid Strain Rate Profile Crossover Point for Three Polymers over a Range of Strain Rates

Straining Velocity (mm/s)	Newtonian-Power Law Cross-over point, y^* (mm)		
3	0.5139	0.4569	0.4289
5	0.4688	0.4700	0.4719
10	0.4931	0.4795	0.4841
15	0.4954	0.4829	0.4877
20	0.4961	0.4853	0.4893
25	0.4967	0.4866	0.4904
30	0.4965	0.4875	0.4907

Table 22-2 shows that y^* is relatively insensitive to the power-law parameters. The pressure drop along the shearing zone increases with viscosity. Its effect could not be studied independently. y^* does exhibit a dependence on the shearing velocity, V . This can be explained as follows. At low straining velocities, a larger proportion of the deformation is due to pressure flow. Because the pressure

flow shear rate is not uniform, its description is subject to the complications imposed by shear-thinning behaviour. Consequently, a larger correction to the apparent shear rate (smaller value $\dot{\gamma}^*$) is needed. At higher straining velocities, most of the deformation is due to drag flow. Consequently, a smaller shear thinning correction is needed.

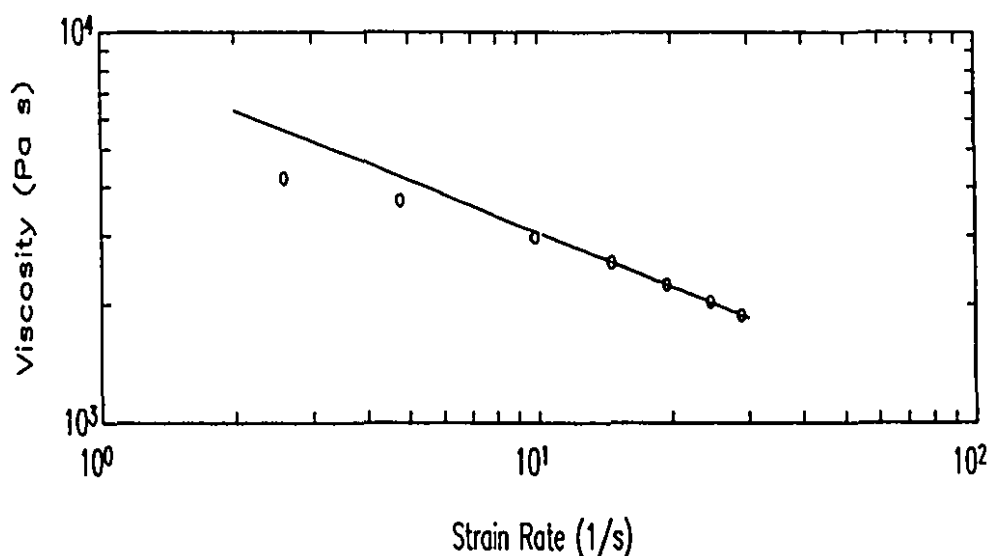
Table 22-3: Percent Error Introduced into Strain Rate Estimate as a Result of Assuming a Constant $\dot{\gamma}^*$.

Straining Velocity (mm/s)	Percent Error Incurred by assuming a constant value of $\dot{\gamma}^* = 0.47$ [%]		
	Polymer A	Polymer B	Polymer C
3	2.0	4.33	1.05
5	0.03	0.19	0
10	0.28	0.28	0.341
15	0.22	0.31	0.37
20	0.18	0.30	0.38
25	0.15	0.28	0.38
30	0.13	0.27	0.37

Table 22-3 presents the percent error in strain rate incurred by assuming a constant value of $\dot{\gamma}^*$ for all three polymers. For most of the strain rate range, very little error is incurred by assuming a single value of $\dot{\gamma}^*$. The only significant error occurs at the lowest strain rate. One reason for this has already been discussed. In addition, this error may reflect the inadequacy of the power-law model in representing the true viscosity behaviour at low shear rates. The power-law model is valid only at higher strain rates and

does not portray the zero-shear viscosity plateau or the transition region of the viscosity-shear rate curve. This is illustrated in Figure 22-4a. Clearly, at low strain rates, the measured shear stress is lower than the stress predicted by the model. The effect of this in the y^* fitting routine is to produce a lower value of y^* , in other words, to overestimate the contribution of pressure flow. A value of y^* closer to 0.5 might be better.

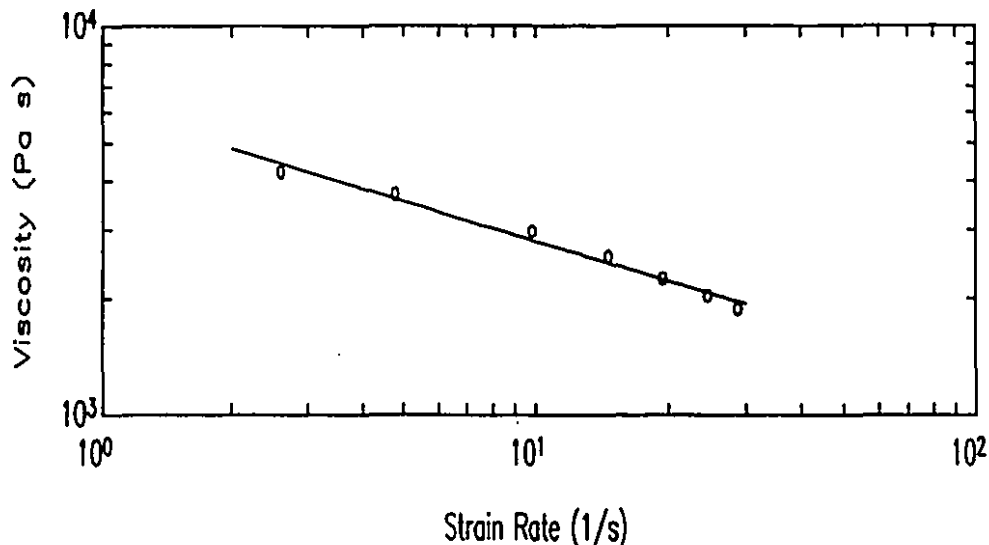
Figure 22-4a: Viscosity versus Strain Rate for Polymer C -- Correct Power-law Model Fit.



Legend: (o) viscosity data; (-) power-law model fit to data in power-law region.

One way of reducing the effect of this error is to fit the power-law model to all of the data, as shown in Figure 22-4b, rather than just those in the true power-law region. This will introduce error over the whole range of applicability, but because the ILR measures viscosity over a limited range, only a small amount of error will be incurred at any particular strain rate.

Figure 22-4b: Viscosity versus Strain Rate for Polymer C -- Approximate Power-law Model Fit.



Legend: (o) viscosity data; (-) power-law model fit to all data.

There is another potential difficulty in estimating γ^* at low strain rates. This arises from the use of experimentally determined pressure drops and shear stresses. Because the relative contributions of pressure and shear stresses govern whether the shear stress profile is of Case I or Case II type, an error in either stress or pressure measurement may incorrectly suggest a Case II strain rate profile where in truth a Case I profile exists. This will result in a γ^* greater than 0.5. This phenomenon is suspected in the case of the γ^* computed at 3 s^{-1} for Polymer A of Table 22-1. It is likely that a value closer to 0.47, as indicated for the other strain rates, would be closer to the truth.

In summary, the pressure flow correction method presented in this section is a useful and accurate technique for converting stress, pressure and shearing velocity measurements into true viscosities. It is relatively insensitive to the model parameters used in its development.

2.3 Sample Renewal in the McGill In-Line Rheometer

2.3.1 Description of the Sample Renewal Problem

Ideally, a process rheometer should perform an instantaneous measurement on a compositionally homogeneous sample of polymer that is representative of the material exiting the extruder at that instant in time. In practice, the mechanism of renewing the sample in the rheometer's shearing zone is a time consuming process that contributes both a time delay and dynamics to the measurement process.

The mechanism of sample renewal in the McGill ILR is best described by following the progress of a step change in composition of material leaving the extruder. The flow in the rheometer's main channel is always laminar. Consequently, new material entering the rheometer displaces old material slowly. The polymer near the centre of the channel is displaced more quickly than the polymer near the channel walls. The time it takes to displace the old polymer in the main flow channel, up to the position of the rotating drum, represents a pure measurement time delay. Once fresh material reaches the rotating drum, it is dragged by the drum into the shearing zone. Again, the flow of fresh material into the shearing zone is a slow laminar flow because the rotating drum velocities are low. The time it takes the new polymer to reach the zone under the shear stress transducer represents an additional, pure time delay. During the time that the old fluid in the vicinity of the shear stress transducer is being displaced, the SST will register a change in signal. However, this signal will not be representative of the new fluid until the sample is homogeneous. During this time, the ILR will display a transient (or dynamics) that is related strictly to the process of sample renewal and not to an extrusion process dynamics.

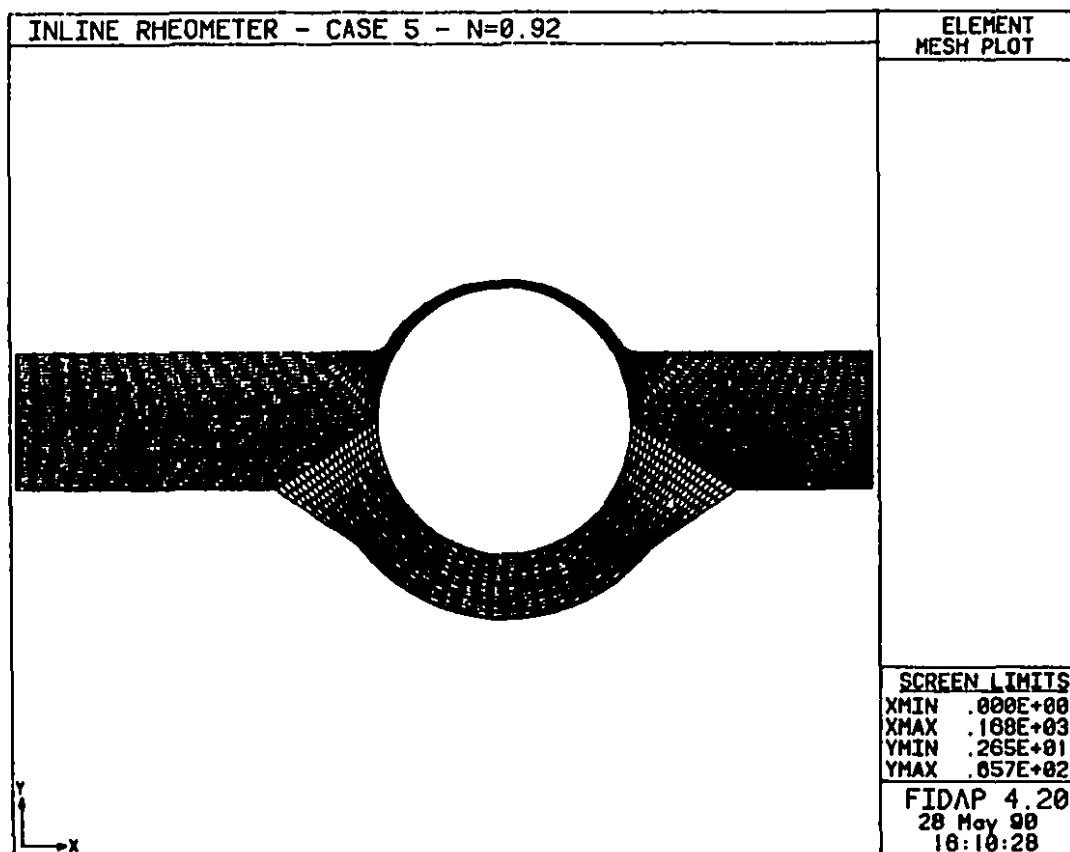
The visualisation of flow through the ILR presented above is only qualitative. The detailed flow patterns in the ILR need to be studied in order to better understand the processes

of sample renewal.

2.3.2 Simulation of Polymer Flow in the McGill ILR

The flow of polymer through the rheometer and into the rheometer shearing zone was studied using a finite element simulation package. The flow geometry shown in Figure 21-1 was modelled. FIDAP, a commercially available fluid dynamics simulation package, sold by Fluid Dynamics International Inc. (reference, FIDAP (1987)), was used. FIDAP requires that a computational grid, or mesh, be defined for the flow geometry. The mesh used in this study is shown in Figure 23-1.

Figure 23-1: Computational Grid used to Model Flow Through the ILR.



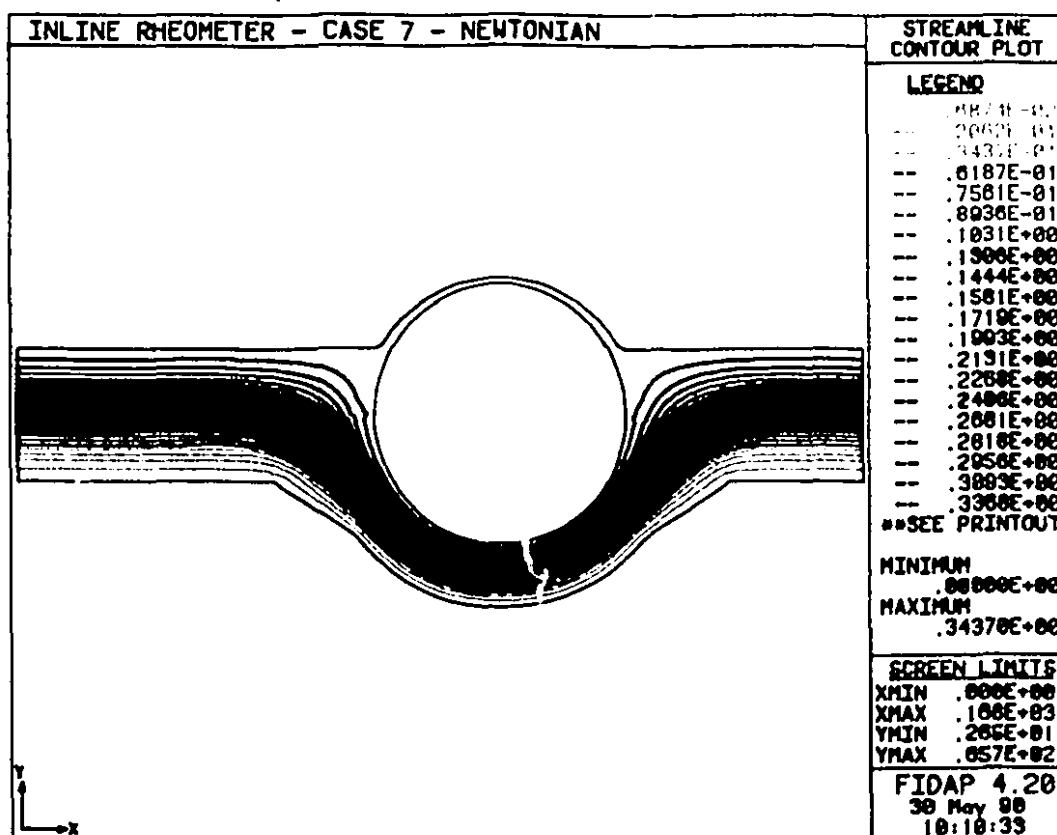
The following assumptions were made in simulating the ILR:

- 1) Two-dimensional flow,
- 2) Creeping (zero inertia) flow,
- 3) Isothermal flow,
- 4) A parabolic velocity profile at the entrance to the rheometer.

The effects of shearing velocity (or nominal strain rate), rheometer throughput and viscosity model were examined in a series of case studies. The Newtonian fluid model and power-law fluid models with exponents of 0.92 and 0.45 were used.

Figure 23-2 presents the simulated streamlines for a Newtonian fluid flowing through the ILR with the shearing

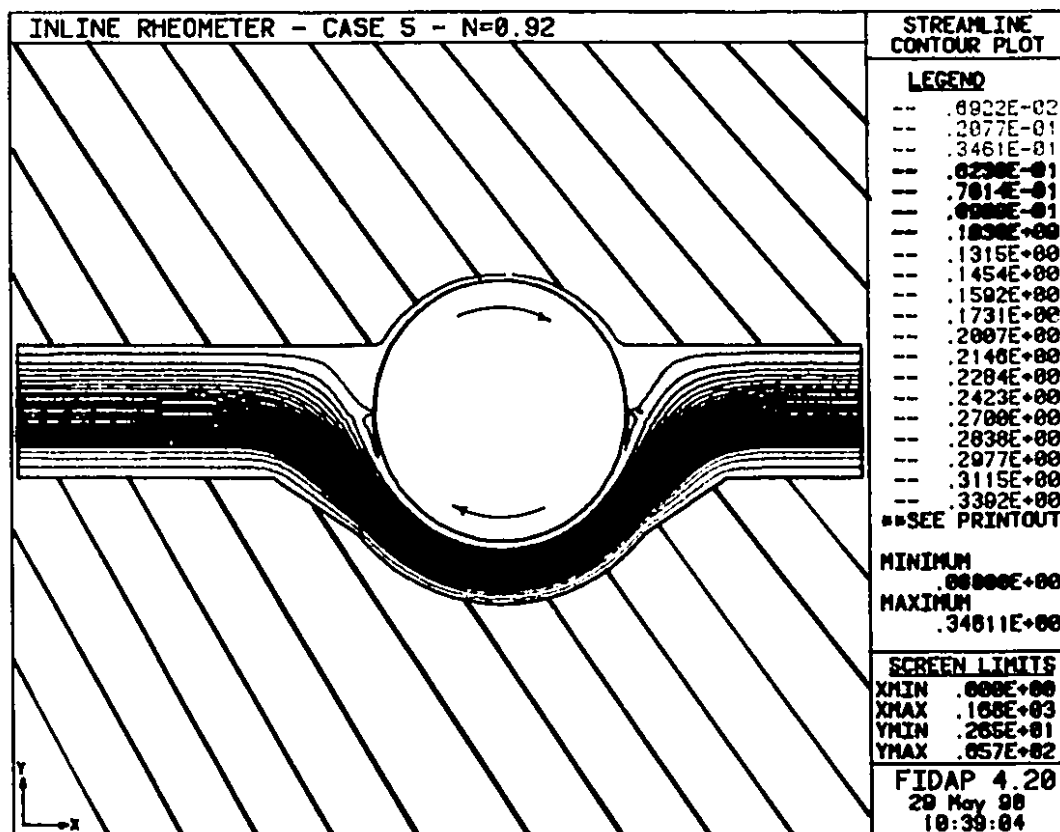
Figure 23-2: FIDAP Simulation of the Flow through the ILR with the Rotating Drum Stationary



cylinder stationary. This figure shows no streamlines entering the shearing zone. This suggests that very little polymer flows through the shearing zone due to the pressure gradient. It further suggests that the material at the shearing zone entrance and exit is moving very slowly.

Figure 23-3 shows the flow streamlines of a mildly shear-thinning fluid ($n=0.92$) flowing through the ILR at a high rate with the drum turning at a low angular velocity. This simulation shows that the streamline of material flowing along the top ILR channel wall eventually flows into the shearing zone. Furthermore, it indicates that this slow moving material flows around a fairly large stagnation zone at the

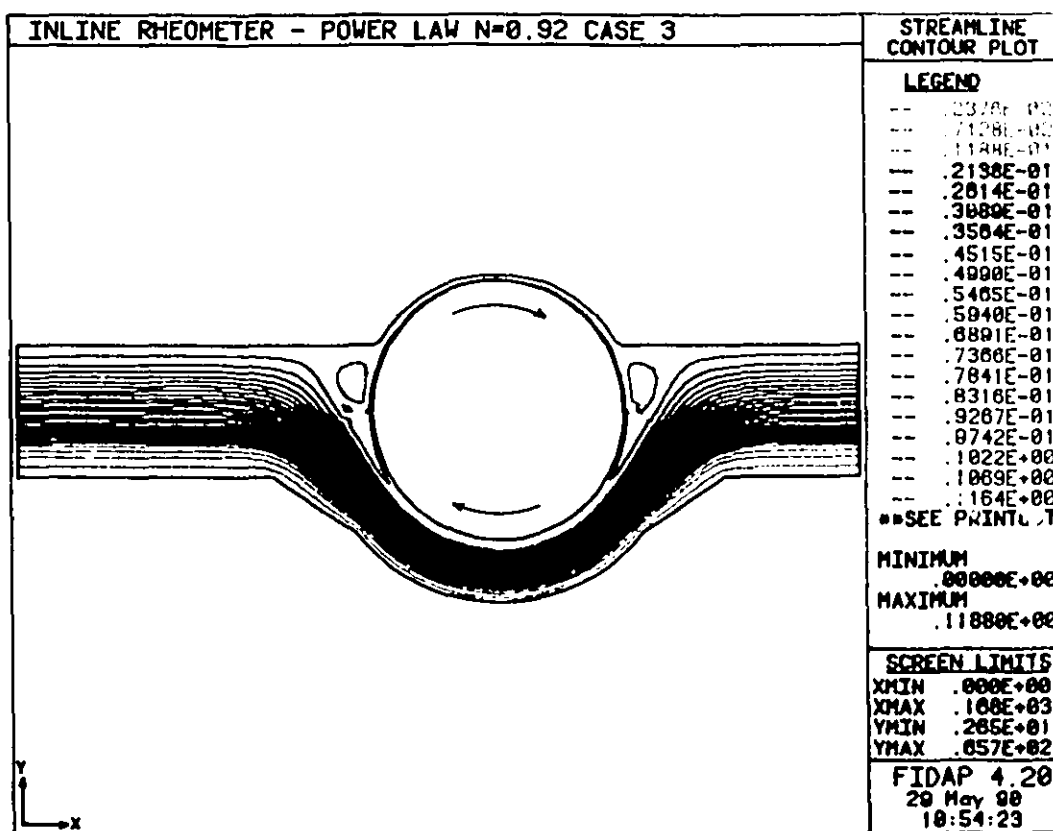
Figure 23-3: FIDAP Simulation of a High Throughput (15 kg/h) through the ILR with the Drum Rotating at a Low (5 s^{-1}) Rate.



shearing zone entrance. [The tear drop shaped loop on the end of the stagnation zone is an artifact of the mesh.]

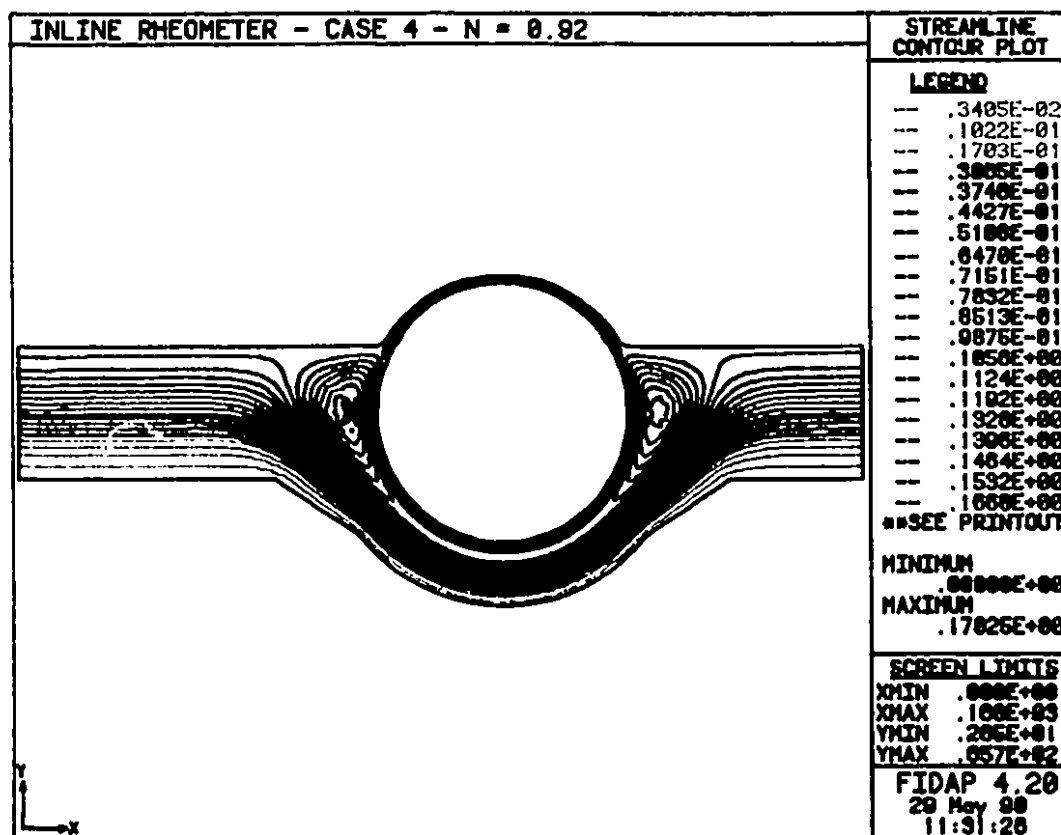
If the flow of polymer through the ILR is decreased, keeping all other variables constant, the stagnation zones at the shearing zone entrance and exit increase in size and become recirculation eddys. This is shown in Figure 23-4. Again, this figure suggests that only slow moving polymer from the rheometer wall flows into the shearing zone, after following a circuitous route around the recirculation eddys.

Figure 23-4: FIDAP Simulation of a Low Throughput (5 kg/h) through the ILR with the Drum Rotating at a Low (5 s^{-1}) Rate.



Increasing the shearing velocity worsens the situation. Figure 23-5 shows the most severe case studied, where a low volumetric throughput and high shearing velocity were simulated. The recirculation flows at the shearing zone entrance and exit apparently merge, forming one large, complex recirculation eddy which severely limits the flow of new material into the shearing zone. This latter conclusion was prompted by the observation that streamlines of material in the shearing zone form unbroken circles around the rotating drum. [The jaggedness of the streamlines in the recirculation flows is an artifact of the mesh design.] Increasing the throughput at high shearing velocity was observed to decrease the size of this huge recirculation flow, but it did not eliminate it.

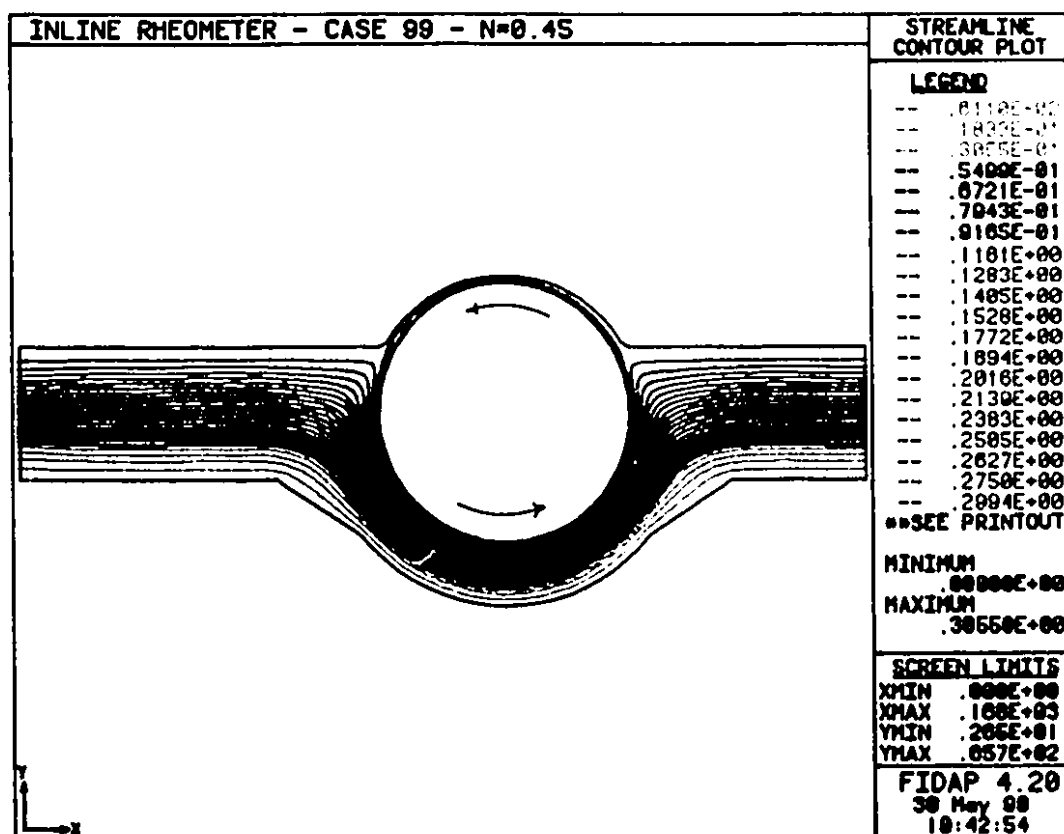
Figure 23-5: FIDAP Simulation of a Low Throughput (5 kg/h) with the Drum Rotating at a High (30 s^{-1}) Rate.



Simulations of a strongly shear-thinning material ($n=0.45$) showed that the flow patterns in the rheometer do not change dramatically with fluid type. The recirculation flows at the shearing zone entrance and exit become thinner and longer, but the general nature of the flow does not change.

The rheometer was also simulated with the drum turning in the counterclockwise direction. Surprisingly, though no stagnation zones or recirculation flows were observed at the shearing zone entrance or exit, the streamlines in the shearing zone formed unbroken circles around the rotating drum. This is illustrated in Figure 23-6. This suggests that there is very little sample renewal in the shearing zone.

Figure 23-6: FIDAP Simulation of the ILR with the Drum Rotating in the Counter-clockwise Direction.



In summary, two-dimensional, finite element simulations of the flow in the ILR suggest that sample renewal in the shearing zone is poor. The only material that is predicted to flow into the shearing zone is the slow moving material from the wall region of the main flow channel. Furthermore, large stagnation zones and recirculation eddys are predicted at the entrance and exit to the shearing zone, which increases the flow path of material into the shearing zone. The recirculation flows envelop the rotating drum at high shearing velocities, limiting the flow of fresh polymer into the shearing zone.

2.3.3 Interpretation of ILR Flow Simulations

The most extreme of the simulation's predictions, the complete inability of the rheometer to refresh its sample at high strain rates, was never observed in practice. It is hypothesized that flow in the lateral direction affects the recirculation eddys predicted by the two-dimensional simulations and enhances sample renewal. Examination of Figures 21-1, 21-2 and 31-6 shows the flow path and suggests the nature of the lateral flow.

Though the consequences of the predicted flow behaviour may not be as severe as indicated, the simulations did highlight a number of important issues. First of all, the simulations show that only the slow moving polymer that flows along the rheometer channel wall refreshes the shearing zone. This suggests that a change in the viscosity of the polymer exiting the extruder will not be quickly detected by the rheometer. Furthermore, the potential for recirculation zones at the shearing zone entrance may retard sampling. Because the recirculation zones increase in size with shearing drum rotational speed, sampling may become slower with increasing test strain rate, contrary to intuition.

It should be noted that the assumption of isothermal flow in the rheometer also limits the simulation's validity. In

fact, the temperature in the rheometer flow channel varies strongly with position. However, it is believed that consideration of the non-isothermal nature of the flow through the rheometer would not affect the general conclusions drawn from the FIDAP simulations.

2.4 Temperature Uniformity in the ILR Shearing Zone and the Effect of Temperature Disturbances

Rheological properties depend strongly on temperature. To measure rheological properties with confidence, the sample temperature must be uniform and accurately known. Rheological measurements made in-line are particularly challenging because they are susceptible to process disturbances that can cause temperature fluctuations. There are techniques for compensating rheological measurements for temperature excursions, but the requirement for temperature uniformity must be satisfied in the rheometer's design.

2.4.1 Simulation of the Temperature Distribution in the ILR Shearing Zone

The shearing gap is 1 mm. It is difficult to measure the temperature distribution of a fluid within such a small gap accurately and precisely. Consequently, heat transfer in the shearing zone was simulated in order to understand the relative effects of operating parameters on the uniformity of temperature.

The shearing zone was again modelled using rectilinear co-ordinates. A time-steady, two-dimensional heat balance was written for the 1 mm by 52 mm long shearing zone. Figure 22-3 adequately describes the simulated geometry. The flow in the shearing zone was assumed to be fully developed. Both pressure and drag flow were considered. Conduction, convection and viscous dissipation were included in the heat balance. The resulting differential equation for $T(x,y)$ is shown in Equation 24-1.

$$u \cdot \frac{\delta T}{\delta x} = \frac{k}{\rho C_p} \cdot \left(\frac{\delta^2 T}{\delta x^2} + \frac{\delta^2 T}{\delta y^2} \right) + \frac{\eta}{\rho C_p} \cdot \left(\frac{\delta u}{\delta y} \right)^2 \quad (24-1)$$

where u is the velocity in the flow direction, k is the thermal conductivity (0.117 W/(m K)), C_p is the heat capacity (1924.6 J/(kg K)), and ρ is the melt density of the polymer (750 kg/m³). [Thermal conductivity and heat capacity data were taken from DuPont Company (1985) product literature.]

Equation 24-1 was cast in dimensionless form and solved using a finite difference method. The boundary conditions were specified in the following manner: i) wall temperatures were assumed to be constant but not necessarily equal, ii) a parabolic temperature profile was chosen arbitrarily for the input; a range of maximum temperatures was studied, and iii) the axial temperature gradient at the end of the shearing zone was assumed to be zero. The finite difference equations were solved by successive substitution. A weighted average of the current and past temperature estimates was used for the next iteration. A listing of the heat balance simulation program is given in Appendix A2-1.

An adjustable penetration depth thermocouple was used to determine the temperature profile in the rheometer's main flow channel. While temperatures at the flow channel centre-line could be as much as 40°C higher than the wall temperature, the temperatures within 3 mm of the wall were generally less than 4°C higher and usually only 1 or 2°C higher than the wall temperature. In the simulations, inlet temperature profile maxima were chosen to be 2, 4 and 20°C.

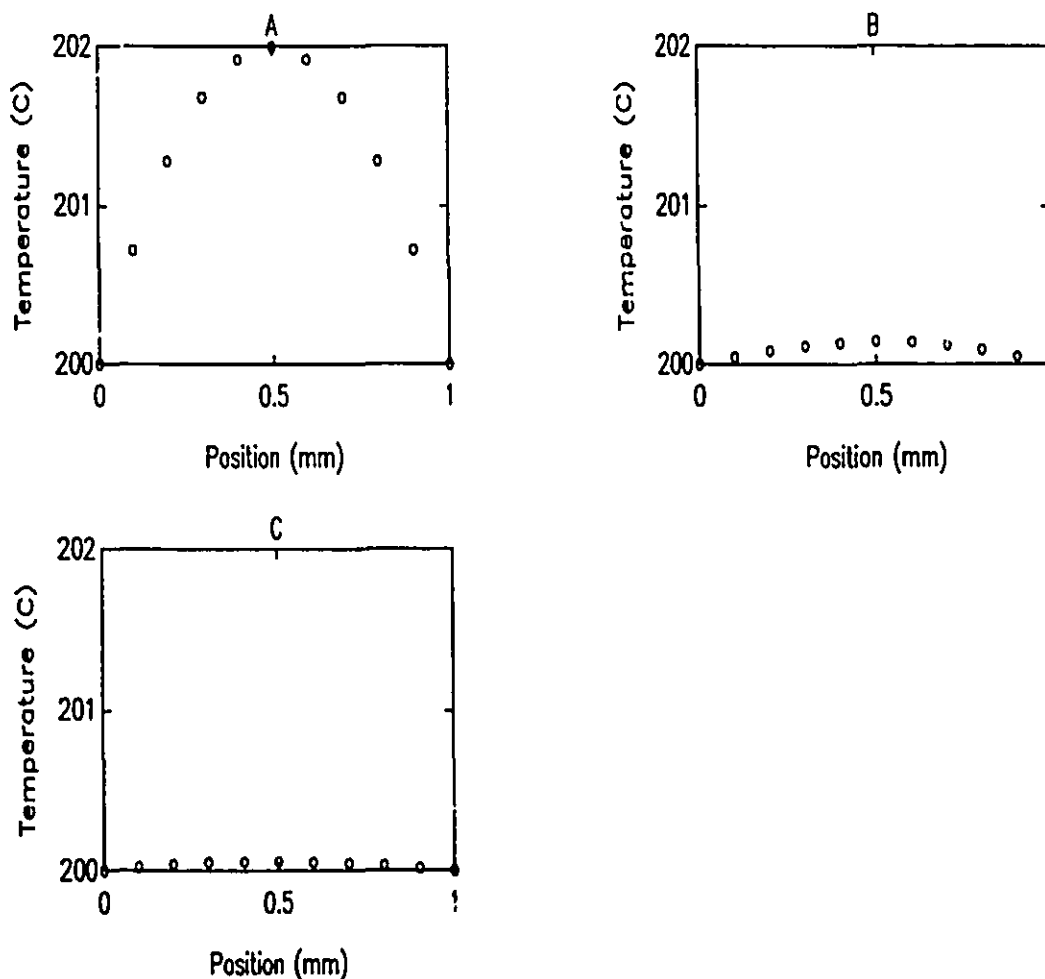
The following conclusions were drawn from the simulations:

- 1) At low strain rates, conduction to the walls ensured that the temperature of the polymer at the shear stress transducer was uniform. This is illustrated in Figure 24-1 which shows the temperature profile at the entrance, at

halfway to the SST, and at the SST, for a strain rate of 5 s^{-1} .

2) At strain rates greater than 15 s^{-1} , the convection of heat from the main flow channel dominated the heat balance in the gap. The temperature profile at the SST was not uniform. Figure 24-2 shows that at high strain

Figure 24-1: Simulation of Temperature Profile in the Shearing Zone at a Strain Rate of 5 s^{-1} .



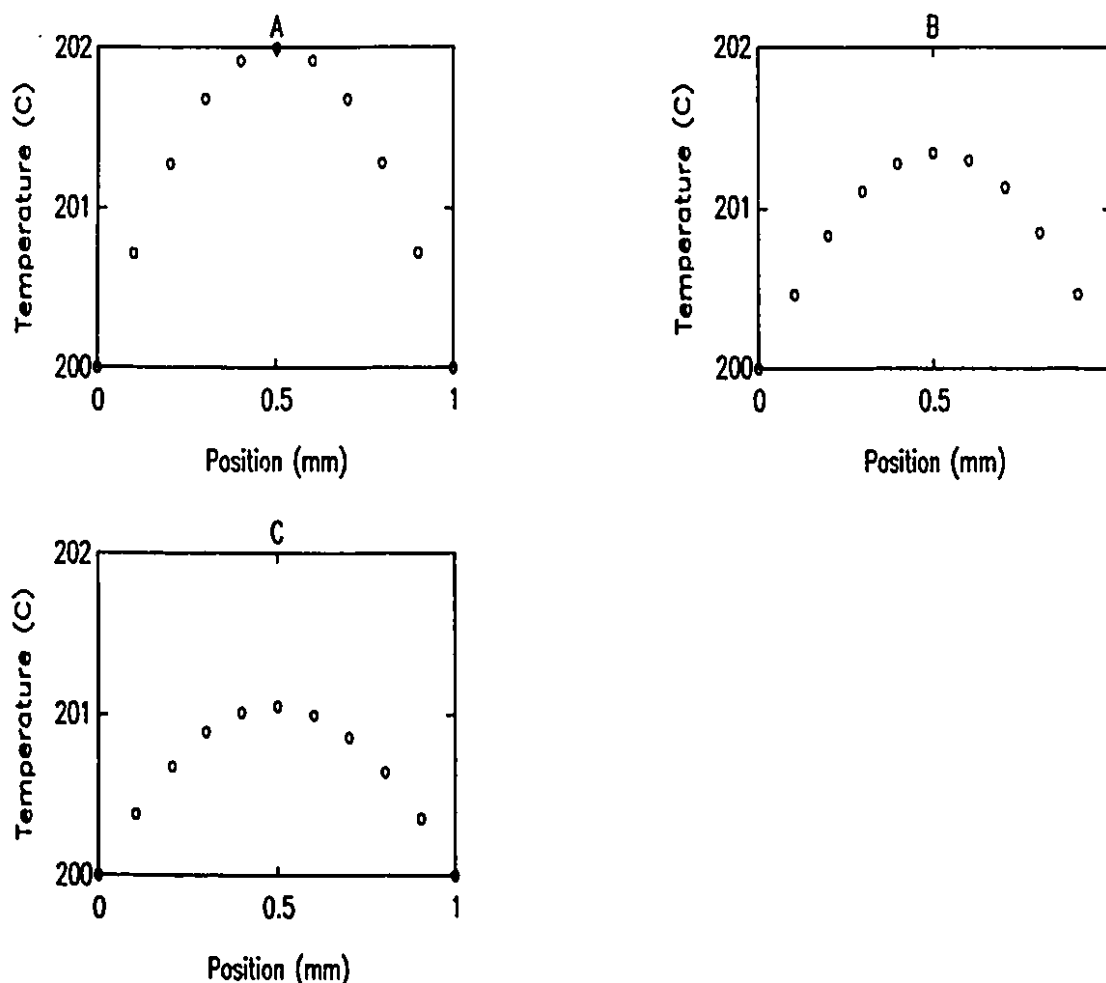
Legend: A) Temperature profile at the shearing zone entrance. Maximum melt temperature is $2 \text{ }^\circ\text{C}$ higher than ILR wall temperature.
 B) Temperature profile half-way to the SST.
 C) Temperature profile at the SST.

rate, the temperature non-uniformity of polymer entering the gap is moderated only marginally by the time it reaches the SST.

3) Pressure flow contributed in only a small way to the convection of heat from the main flow channel.

4) Viscous heating was never found to contribute significantly to the temperature profile in the gap.

Figure 24-2: Simulation of Temperature Profile in the Shearing Zone at a Strain Rate of 20 s^{-1} .



Legend: A) Temperature profile at the shearing zone entrance. Maximum melt temperature is 2 °C higher than ILR wall temperature. B) Temperature profile half-way to the SST. C) Temperature profile at the SST.

2.4.2 Implications of the ILR Shearing Zone Temperature Distribution Simulations

A non-uniform temperature distribution of the kind described above would lead to a decrease in the stress measured at the SST and an under-estimation of the true viscosity at a given rheometer body temperature. None of the experimental results of this study exhibited an obvious trend that could be attributed to temperature non-uniformity in the shearing zone. A reason for this is suggested by the ILR flow simulations of Section 2.3. They indicate that only the slow moving polymer that flows along the main ILR channel wall will eventually flow into the shearing zone. This material is conditioned to the rheometer wall temperature by virtue of its long residence time next to the wall and is, therefore, at the correct temperature when it enters the shearing zone.

The results of the heat balance simulations draw attention to a potential dilemma. They suggest that a high throughput of polymer through the shearing zone is undesirable from the point of view of maintaining a uniform temperature distribution. This conflicts with the goal of increasing polymer throughput in the shearing zone to minimize the sample renewal time. This is an important fact to consider in designing an ILR to improve the sample renewal rate.

While no concrete evidence of shearing zone temperature non-uniformity was observed, it is likely that there will be some contribution to measurement inaccuracy due to temperature non-uniformity. One approach to minimizing the temperature non-uniformity would be to operate the rheometer at a temperature closer to the main flow channel mid-stream melt temperature. However, this may not be desirable for other reasons; for example, the melt may be too hot for downstream processing, or it may be so hot that its viscosity is too low to be measured with the ILR.

2.4.3 Viscosity Measurement Compensation for Temperature Changes

Because the ILR is located directly in the process flow, it is expected that the temperature of the sample in the shearing zone will vary as a result of upsets in the process. To be useful, the ILR must provide viscosity values at a fixed reference temperature and specified strain rate so they can be compared over long time periods. A commonly used approach is to correct the viscosity value measured at one temperature to give a value at some reference temperature using an Arrhenius or other equation. The equation used here is given below.

$$\eta(T_{REF}) = \eta(T_c) \exp\left[\frac{E_A}{R} \times \left(\frac{1}{T_{REF}} - \frac{1}{T_c}\right)\right] \quad (24-2)$$

where T_{REF} is the reference temperature, T_c is the temperature in the shearing zone at the time of the test, and E_a is the activation energy, determined experimentally over a temperature range including T_{REF} , $\eta(T_{REF})$ is the viscosity at the reference temperature and $\eta(T_c)$ is the viscosity actually measured. The Rheometrics Melt Flow Monitor (Blanch et al. (1989)) and the in-line capillary rheometer described by Ross et al. (1990) use this method.

This is a strictly empirical procedure and is useful typically only where the polymer exhibits Newtonian (zero shear viscosity) behaviour or over narrow strain rate ranges. When applied to viscosity data in the transition zone of the viscosity-strain rate curve, the activation energy (E_a) will be a function of strain rate. Furthermore, E_a is often a function of temperature and can only be assumed to be constant over a narrow range of temperatures.

CHAPTER 3

IMPLEMENTATION OF THE MCGILL IN-LINE MELT RHEOMETER DESIGN

The McGill in-line rheometer (ILR) was conceived and developed by J.M.Dealy, B.I.Nelson and T.O.Broadhead with the help of F.R.Bubic. Detailed mechanical drawings of the instrument, prepared by F.R.Bubic, are presented in Appendix A3. This chapter summarizes the ILR design only briefly. Its purpose is to describe the rheometer's performance characteristics and to highlight improvements made to the original design over the course of this study.

3.1 In-Line Rheometer Component Descriptions

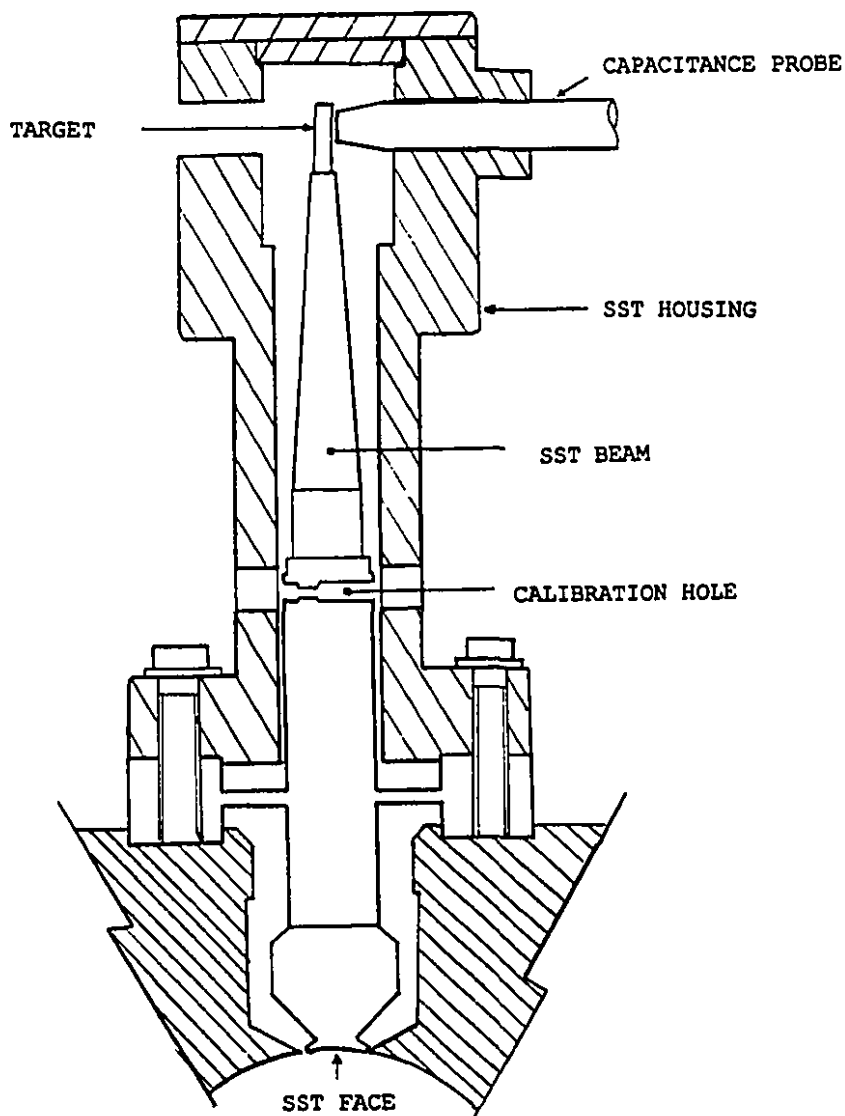
The ILR, shown in cross-section in Figure 21-1, fits on the last barrel section of a twin screw extruder, before the die. Polymer flows through the rheometer from left to right in Figure 21-1. The rotating drum, marked "A", drags material into the shearing zone "B". The stress imposed on the sample in the shearing zone is sensed by the SST, labelled "C".

3.1.1 The Shear Stress Transducer

The shear stress transducer (SST) used in the ILR is shown in Figure 31-1. This is a novel embodiment of an SST conceived by Dealy, Doshi and Bubic (1992). The active element of the transducer is a beam that is incorporated into a disk spring. A shear stress on the tip (or face) of the beam causes the disk to flex and the beam to pivot at the disk. The disk also forms a seal to prevent the flow of polymer into the upper housing cavity. Though polymer does flow into the lower SST housing, it has only a minimal damping effect on the motion of the beam. The polymer in the lower SST housing can be drained periodically by opening a valve.

For this study, the disk spring was designed so that a shear stress of 0.25 MPa would cause the face of the beam to be displaced by 0.00953 mm. This translates to a 0.0254 mm displacement of the probe target. The motion of the beam is

Figure 31-1: Cross-sectional Diagram of the Disk Spring SST



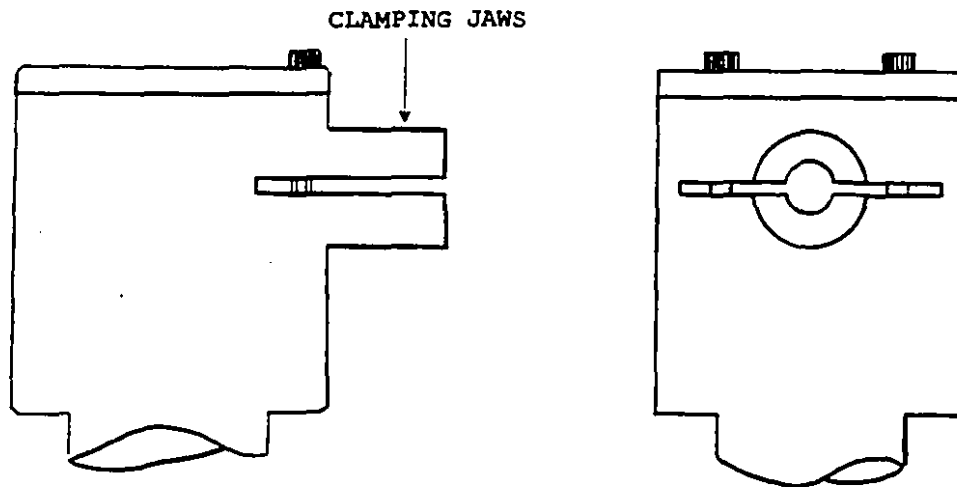
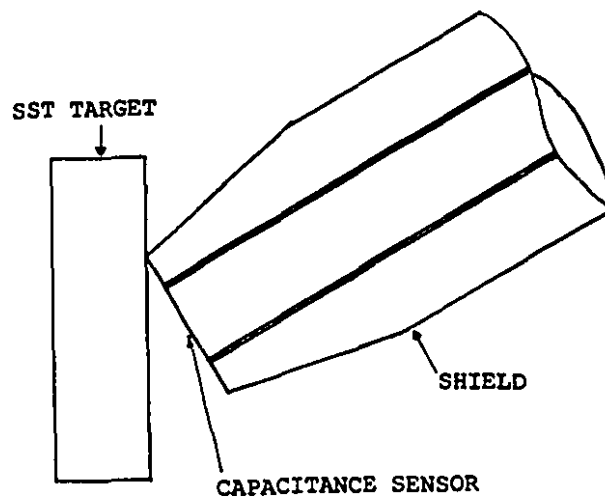
detected by a capacitance probe (MTI model ASP-1HT, Accumeasure™ System 1000 amplifier). It transmits a 0 to 10 V signal, proportional to a displacement in the range of 0 to 0.0254 mm. The displacement is proportional to shear stress.

The SST beam is very stiff and deflects very little. This is an essential feature of the design. Displacements of

the SST beam face must be small to minimize damping by the fluid in the housing. Also, small, purely elastic displacements are essential for a good frequency response. Finally, the disk spring must be rigid and strong to endure pressures typical of polymer processing operations. However, the measurement of the small beam deflections proved to be challenging.

Vibration was the major source of SST beam deflection measurement noise. Initially the levels of vibration encountered obscured most measurements. The problem was greatly reduced by an improvement to the capacitance probe clamping device. The mechanism shown in Figure 31-2, designed and built by Alain Gagnon of the McGill Department of Chemical Engineering machine shop, was the best of several designs. The probe is clamped between two, semi-cylindrical jaws. The jaws are in contact with a large portion of the probe surface area. The jaws are welded directly to the SST housing. A cut is made in the housing so that bolts, which span the split, can be adjusted to tighten the clamp. With this design, the vibration related noise was attenuated from 400 mV to less than 80 mV. The essential features of this clamp are its large clamp contact area and the fact that it is integral to the housing. Clamps that fitted over the housing and were tightened down but not welded on did not work well.

Measuring the small SST beam deflections required very precise alignment of the capacitance probe. To function over its full range, the probe must be perpendicular to its target. If the probe and target are not perpendicular, the outer probe casing can touch the target, grounding the probe before the actual capacitance sensing part of the tip comes in contact with the target. This is illustrated in Figure 31-3. This problem limited the effective range of the probe, sometimes by as much as 70 or 80 %. It was also found that the soft aluminium target could be scored by the stainless steel probe, compounding the displacement measurement problem.

Figure 31-2: SST Clamping Device**Figure 31-3: Exaggerated Illustration of Poor Capacitance Probe-SST Target Alignment.**

The solution to this problem was to polish a flat, perpendicular surface onto the target after the SST was assembled. A piece of dowel, of diameter equal to that of the probe, was inserted into the clamp. A piece of polishing

cloth was clipped to the tip of the dowel, from the inside of the housing. A dab of 2 to 7 μm diamond paste was placed on the polishing cloth. The dowel was turned gently on the target face until a smooth, shiny surface was obtained on the target. If the target was very rough, a small strip of fine emery cloth could be pinched between the dowel and the target, and withdrawn to remove gross features. Using this procedure, probe target alignment was improved to the point where 50 to 60% of the rated measuring range could be used.

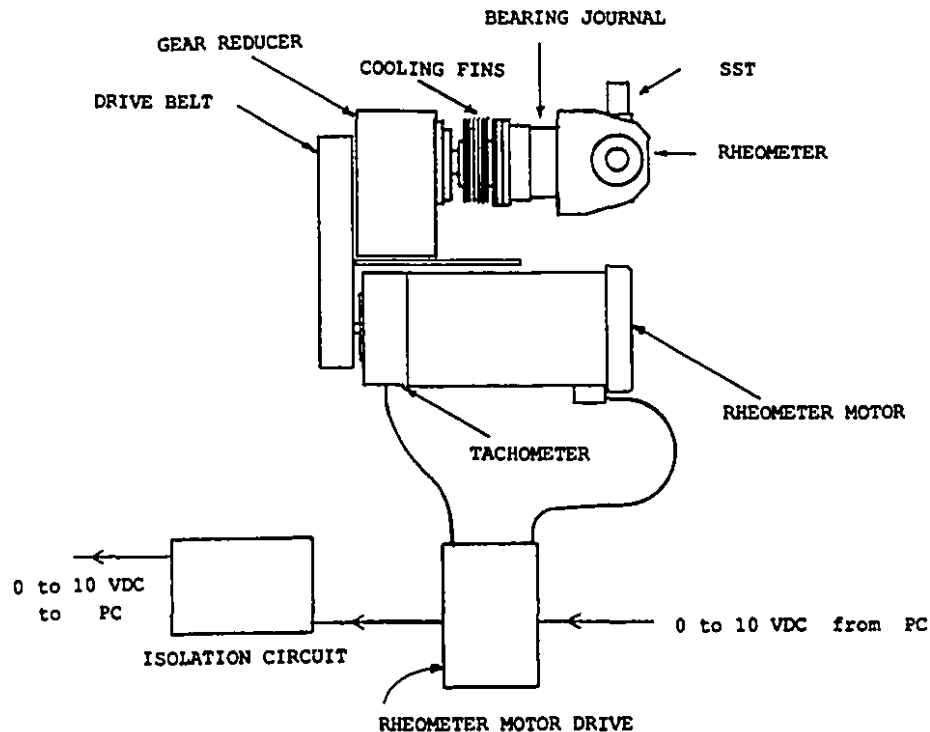
The capacitance probe was connected to an amplifier by a co-axial cable. Occasionally, the probe-cable joint became loose, and this introduced considerable noise. This joint could be tightened sufficiently to prevent loosening during operation.

3.1.2 Rotating Drum, Rheometer Motor and Rheometer Speed Tachometer

The rotating drum, labelled "A" in Figure 21-1, is 50 mm in diameter and 25.4 mm wide. It was machined as a keyed, annular insert that fits over the drive shaft. In this way, the drum diameter can be changed or an additional feature, such as a cleaning flight, can be incorporated simply by machining another insert. The drum diameter governs the rheometer gap width. A gap width of 1 mm was chosen for this work on the basis of the discussion given in Section 2.1. The geometrical integrity of the drum and gap were confirmed, once the rheometer was assembled, using a micrometer.

The rotating drum, drive shaft, transmission and motor assembly are illustrated in Figure 31-4. For this study, the ILR was required to measure only viscosity. Therefore, a constant speed motor was adequate. A 560 W (3/4 h.p.) motor, capable of 1750 rpm, was selected. The motor power was transmitted to the drum through a belt, a (150:1) gear reducer and a drive shaft. The motor speed was controlled to a nominal $\pm 0.5\%$ of set point by a tachometer feedback controller

Figure 31-4: Front View of the ILR Showing the Rheometer Motor Assembly.

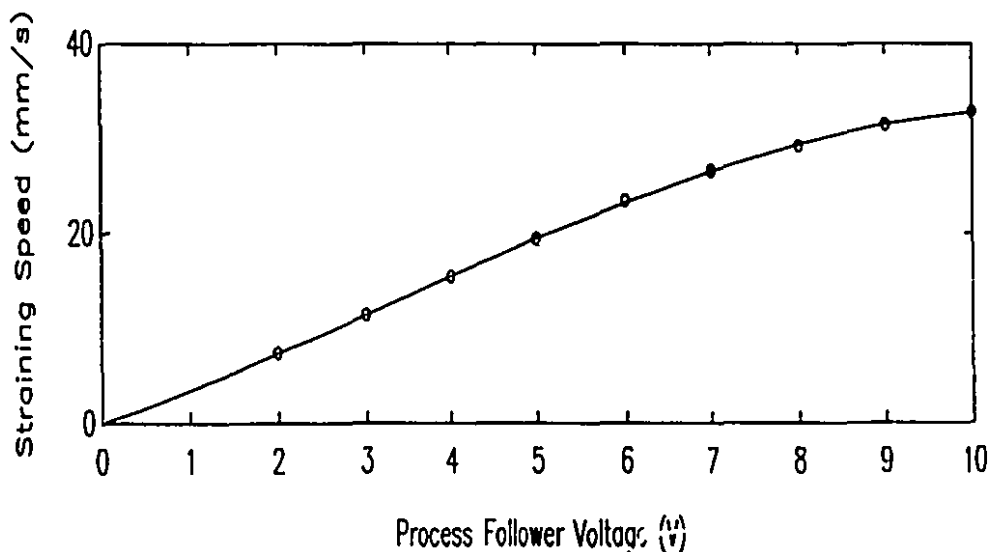


(Incom International Inc. (INCOM), Tach Fdbk 60223 1047365) using the 0 to 60 VDC tachometer signal as a measure of the actual motor speed. A follower card (INCOM # 104572501) in the motor drive (Boston Gear Ratiotrol™ VEL75) enabled the set point to be specified with a 0 to 10 VDC signal from a computer. The 0 to 60 VDC tachometer signal was routed through a voltage divider and isolation circuit to an analog-to-digital conversion board (Data Translation DT-2801A) in a personal computer (PC). The signal isolation circuit was essential because it removed a superimposed AC signal from the tachometer signal in the motor drive. (The isolation circuit was designed especially for this application by Lou Cusmich of the Chemical Engineering Department electronics shop.)

The 0 to 10 V motor speed set point (follower) signal from the computer and the true shaft speed had to be

calibrated from time to time. This was done by sending a known signal to the drive and measuring the drive shaft speed with a stop watch. A typical calibration curve is shown in Figure 31-5. A cubic polynomial was fitted to the calibration data. This polynomial was used in rheometer control software to translate a desired strain rate to a motor speed set point voltage. The relationship between the tachometer signal and the true shaft velocity was always linear and did not vary with time. It was re-calibrated routinely each time the set point-motor speed calibration was carried out. These calibration equations are presented below in equations 31-2 and 31-3.

Figure 31-5: Typical Process Follower-Strain Rate Calibration Curve.



Legend: (o) data, (-) cubic polynomial.

The rheometer motor did not run steadily at very low speeds because the motor could not develop enough torque to overcome the high friction in the seals of the drive shaft bearing journal. Consequently, the rheometer was restricted

to the strain rate range 3 to 33 s⁻¹.

The strain rate was calculated from the angular velocity of the drum using,

$$\dot{\gamma} = 2\pi r\omega/g \quad (31-1)$$

where r is the drum radius (25 mm), g is the shearing zone gap, (1 mm) and ω is the drum's angular velocity. The tachometer signal-strain rate correlation was,

$$\dot{\gamma} = (3.343 \pm 0.026) V_T - (0.357 \pm 0.035) \quad (31-2)$$

where V_T is the tachometer signal voltage. The strain rate-process follower voltage correlation was,

$$\begin{aligned} \dot{\gamma} = & (-0.0216 \pm 0.0019) V_P^3 + (0.1809 \pm 0.0403) V_P^2 \\ & + (3.5970 \pm 0.2001) V_P - (0.4002 \pm 0.2724) \end{aligned} \quad (31-3)$$

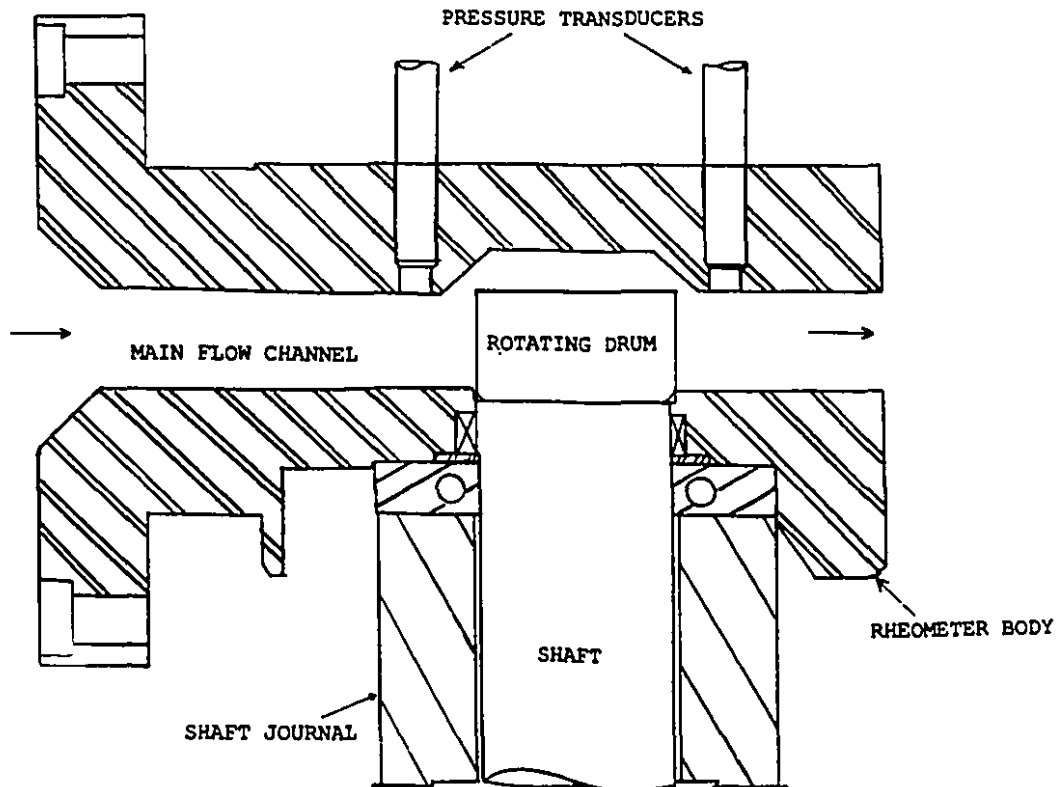
where V_P is the process follower voltage, that is, the 0 to 10 V signal from the computer to the rheometer motor drive.

3.1.3 Pressure Sensors

The absolute pressure in the rheometer and the pressure drop through the rheometer gap were measured using two Dynisco pressure transducers (one model PT-422A-1.5 and one model TPT 432A-1.5). They were positioned as shown in Figure 31-6. These are not the best positions to measure the pressure drop along the shearing zone; the best locations would be at the entrance and exit of the shearing zone. In their actual

positions the transducers measure the pressure drop across the whole rheometer section, which is greater than the shearing zone pressure drop. Entrance effects, including the recirculation zones suggested by the flow simulations presented in Section 2.2, will confuse the true shearing zone pressure drop.

Figure 31-6: Top View of the ILR Showing the Positions of the Pressure Transducers.



Initially, the signals from the pressure transducers were sampled by the Barber-Coleman MACO 8000 control system, which is described in more detail later. However, late in the course of this project, Nelson (1992) built separate pressure transducer amplifiers in order to sample the transducers

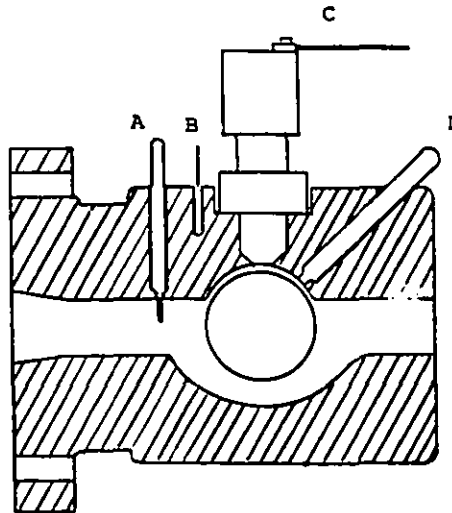
directly using the analog to digital conversion board of the PC. (This will also be described in more detail later.) This improvement made it possible to measure pressures simultaneously with the shear stress and the angular velocity of the drum.

3.1.4 Temperature Sensors

Temperature sensors were installed at the locations indicated in Figures 31-7a and b. A resistance temperature device (RTD) (labelled "F" in Figure 31-7b) on the end of a long, sheathed probe, was inserted in a hole that ran the length of the drive shaft and measured the temperature at the centre of the rotating drum. Sheathed, J-type thermocouples were installed to measure the rheometer body temperature (B) and the shaft bearing temperature (E). A sheathed J-type melt thermocouple was installed upstream of the rotating drum, protruding into the melt (A). This gave an estimate of the maximum temperature of the melt in the main flow channel. Two types of thermocouple were tried in the shearing zone. Initially, a special J-type ribbon thermocouple (Nanmac Extrud-o-couple C8-6) was installed in the shearing zone in the position marked "D" in Figure 31-7a. This thermocouple was mounted flush with the wall. It was thermally insulated to minimize conduction of heat from the metal of the rheometer body in order to measure an accurate melt temperature, and by virtue of its "ribbon" design it responded quickly to temperature changes. However, it was unreliable and required frequent maintenance. Conventional sheathed thermocouples were also used to measure the gap temperature. Unfortunately, they were not well designed for flush mounting. As a result, they had to be either recessed in the wall or allowed to protrude a little into the gap.

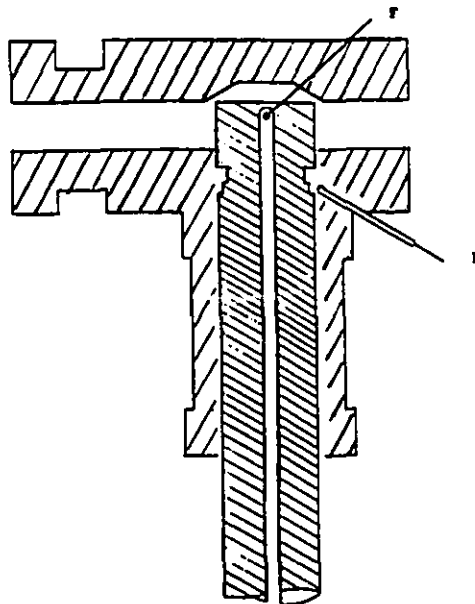
The SST temperature was measured by a "washer" thermocouple (C) that was held in place by an SST cap bolt.

Figure 31-7a: Side View of the ILR Showing Temperature Sensor Positions.



Legend: A Melt Thermocouple, B Rheometer Body Thermocouple, C SST Thermocouple, D Rheometer Shearing Zone Thermocouple.

Figure 31-7b: Top View of the ILR Showing Temperature Sensor Positions.



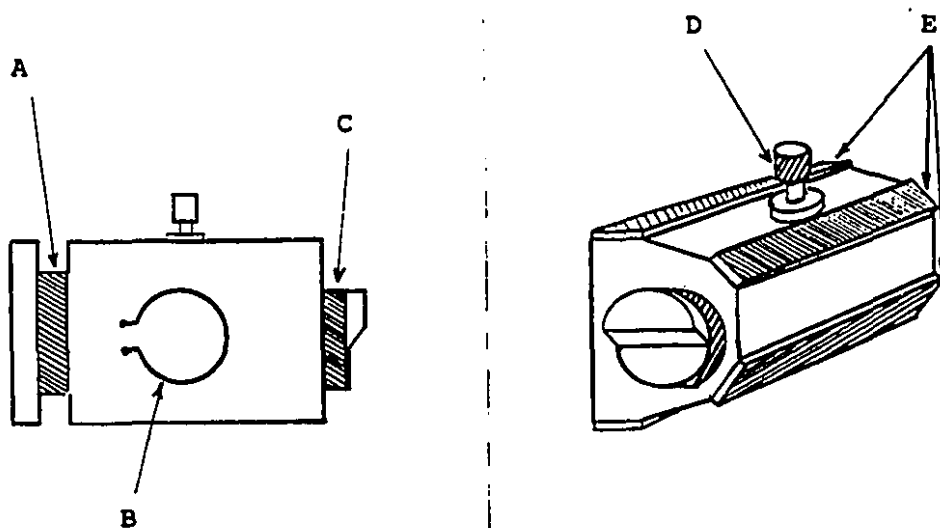
Legend: E Rheometer Shaft Bearing Thermocouple, F Rotating Drum RTD.

This was not an ideal choice but was necessitated by space restrictions. Care was taken in insulating the SST in order to minimize temperature gradients within it.

3.1.5 Rheometer Body Heaters

The locations of the rheometer body heaters are indicated in Figure 31-8. The 300 W band heater positioned immediately after the flange (A) connecting the rheometer to the extruder and the 4 400 W plate heaters (E) are controlled together, using the rheometer body (metal) temperature measured by thermocouple "B" shown in Figure 31-7a. The rotating drum's drive shaft is heated independently with a 400 W rod heater (B). The heat from the rod is transmitted by means of a brass bushing to the shaft. The shaft temperature is measured by the thermocouple marked "E" in Figure 31-7b. The SST is

Figure 31-8: Positions of ILR Heaters.



Legend: A ILR flow channel band heater, B Shaft bearing rod heater, C rheometer die heater band, D SST heater band, E Rheometer body plate heaters.

heated with a separate 50 W band heater (D) that fits over the SST housing. Two brass inserts fill in the contours of the SST housing and ensure that heat is transmitted uniformly. The SST temperature is measured with the thermocouple marked "C" in Figure 31-7a. SST temperature control is critical to its operation. This will be discussed in Section 3.2.5. The final temperature control zone maintains the rheometer die temperature. The melt temperature in the die is used to control the power to the 300 W heater band (C) on the die.

All temperatures are controlled by the Barber-Coleman MACO 8000 system described in the next section.

3.1.6 Rheometer Computer Control and Data Acquisition

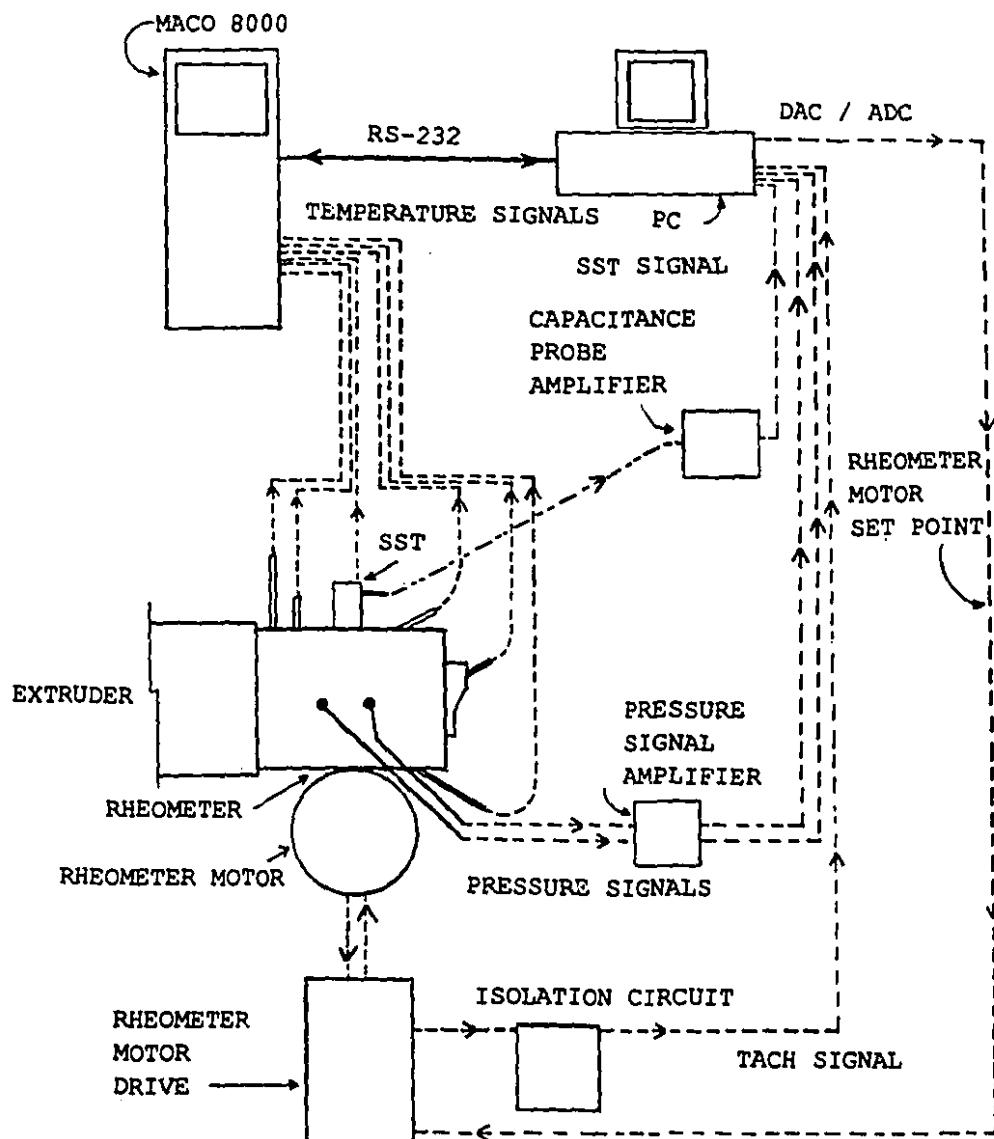
The McGill ILR's operation is controlled by two computers. The "low level" or sustaining functions of temperature control and temperature and pressure measurement are performed by the Barber-Coleman MACO 8000 modular, distributed control system. The MACO 8000 consists of 6, microprocessor controlled modules; two monitor and control temperatures, one monitors (and controls) pressure, another monitors and controls drive speeds, yet another controls the sequence of operations, and the last coordinates communication between the modules and other computers. The MACO modules function independently. Their primary function is to maintain control over the rheometer and extruder, but they also offer substantial capabilities for monitoring process operations and sounding alarms when dangerous conditions arise.

The higher level of control is performed by a personal computer (PC). Higher level functions include executing viscosity tests and, ultimately, controlling extrusion process operation using viscosity measurements. The PC is equipped with a Data Translation DT2801-A analog to digital conversion (ADC) board. This board enables sampling of the SST, rheometer motor tachometer and pressure signals at high sampling rates. It also is capable of digital to analog

conversion (DAC). The DAC is used to communicate the rheometer motor speed set point to the drive controller. The DT2801-A board functions are controlled by a comprehensive set of BASIC subroutines (drivers) written by Nelson (1992). Utilising the drivers, BASIC programs can be easily written to sample rheometer signals and control the strain rate for calibration or viscosity measurement purposes. Viscosity tests can be timed using both BASIC and DT 2801-A functions to enable the PC to monitor viscosity with time. A listing of a viscosity control program is given in Appendix A2-2. This program illustrates the use of all of the data sampling, manipulating and downloading steps. Listings of transducer calibration and other rheometer control programs along with B.I.Nelson's data acquisition board drivers are given in ASCII formatted files on the diskette provided with the thesis.

The PC also communicates with the MACO via an RS-232 communication line. The PC samples essential rheometer temperatures in this way. Equally important is the ability for the PC to "download" or impose set points on the MACO control loops. In addition to controlling the rheometer temperatures, the MACO controls all aspects of extruder operation. The details of the MACO's control of the extrusion process is described in Section 5.2, but it is important to point out here that the RS-232 communication between PC and MACO is the last important link in the control chain. The PC commands the rheometer operation, measures the stress, pressure and drum velocity signals, samples temperature via the MACO, calculates viscosity, computes control actions and then, using the RS-232 line, manipulates feed rate set points in order to control product viscosity. The communication network is summarised in Figure 31-9. (B.I.Nelson's MACO 8000 communication drivers are also listed on the data diskette provided with the thesis.)

Figure 31-9: Schematic Diagram of the Communication Pathways between the ILR and Its Controlling Computer.



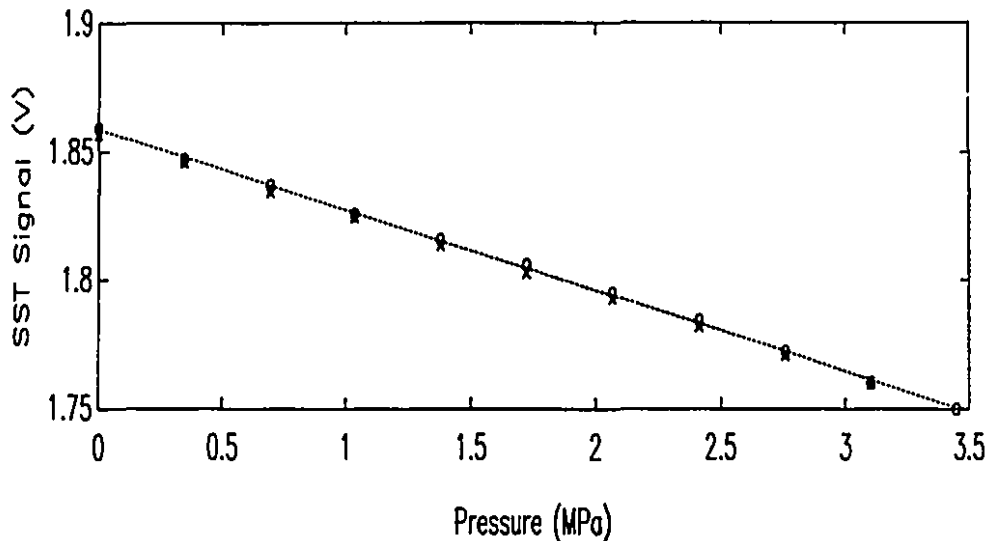
3.2 Factors Influencing the Shear Stress Transducer's Performance

Ideally, the SST should be sensitive only to the shear stress on the active face of the SST beam. In practice, the SST also responds to several other phenomena. These are sources of noise or error and must be identified and either compensated for or, at least, modelled empirically.

3.2.1 The Effect of Pressure on Shear Stress Transducer Performance

Pressure acting on the SST beam face and on the disk spring is the most important source of SST measurement error. If the disk spring were machined perfectly and the modulus of the disk spring material were perfectly homogeneous, pressure would cause the SST beam to be displaced only in the axial direction. Furthermore, if the SST beam target were perfectly flat one would not expect to see any effect due to pressure changes. In practice, however, pressure does affect the output signal.

The SST's response to pressure was measured using a "dead weight tester" (Chandler Engineering Co.), a device commonly used for calibrating pressure transducers. A special fixture with a threaded inlet was made, in order to connect the SST to the dead weight tester. The SST was bolted firmly to the fixture over a copper gasket. The bolt holes and the fixture-SST seam were sealed with a crosslinking silicone based rubber. The fixture formed a small fluid reservoir, equivalent to the lower SST housing of the ILR. Using the dead weight tester, hydraulic oil was pumped into the fixture at precise pressure increments. Experiments performed in this way revealed that the SST beam deflected, rather than just translating axially, under the influence of pressure. The results of such a static pressure test are shown in Figure 32-1. The slope of the observed line was found to be (-0.163 ± 0.012) V/MPa. The negative sign of the coefficient signifies

Figure 32-1: SST Signal Response to Pressure

Legend: (o) increasing pressure, (x) decreasing pressure, (***.) linear regression of data.

that in response to an increase in pressure the beam deflects in the opposite direction to that observed when the beam is responding to an increase in shear stress. A second series of experiments using another capacitance probe and a modified probe amplifier and filter produced a value of (-0.111 ± 0.007) V/MPa. The difference in the two values reflects the difference in sensitivity of the two probes.

Using the parameters shown above, the SST signal can be corrected using,

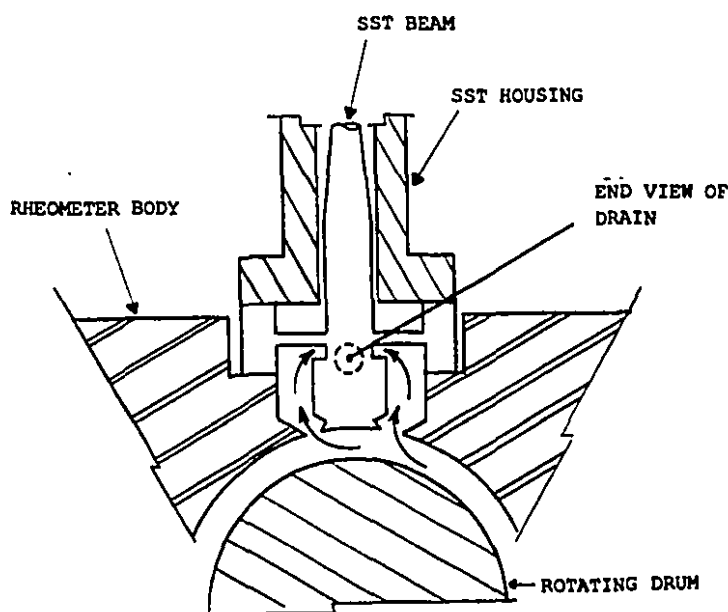
$$V_{SST}^{corr} = V_{SST} + \alpha \times \Delta P \quad (32-1)$$

where α is the pressure correction parameter in units of V/MPa.

3.2.2 The Effect of Through-Flow on Shear Stress Transducer Performance

The ILR was designed with a drain in order to purge polymer that collects in the lower SST housing. Originally the intention was to run the ILR with the drain open so that a small continuous flow would purge the material in the housing and prevent it from degrading. However, experiments with an earlier prototype of the disk spring SST showed that the transducer was sensitive to this purge or through-flow. It was hypothesized that the whole lower arm of the SST beam would be sensitive to the through-flow in the same way that the beam face (or tip) was sensitive to the viscometric flow in the shearing zone. This phenomenon is illustrated in Figure 32-2. A feature of this early prototype was that its drain could be moved and pointed in any direction. A study of the effect of drain orientation showed that when the drain is pointed in a direction perpendicular to the plane of deflection of the SST beam, the through-flow effect is at a minimum.

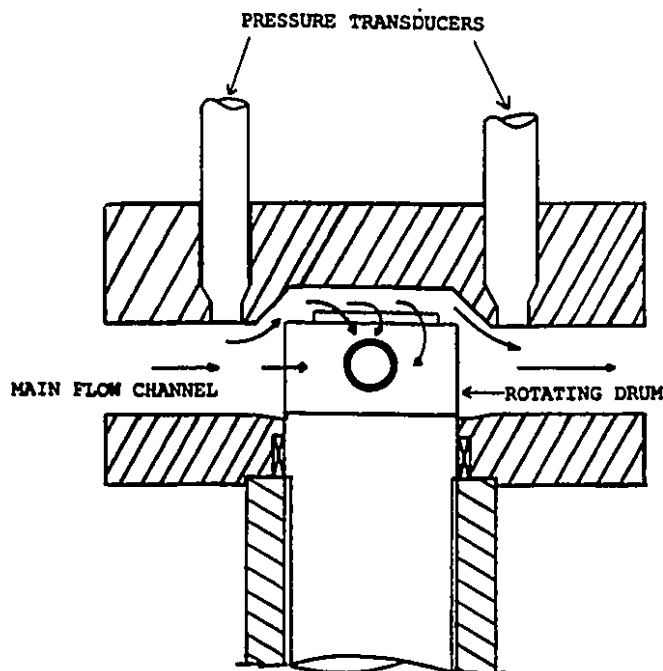
Figure 32-2: Cross-sectional View of ILR Shearing Zone Illustrating the Flow Through the Lower SST Housing.



Although the transducer drain was aligned perpendicularly to the SST deflection plane, the through-flow still had a significant effect on the SST signal. The magnitude of the effect ranged from 0.1 to more than 2 V and, as expected, was proportional to the volumetric through put and the viscosity of the polymer. This represented an unacceptably large proportion of the total SST signal.

The top view of the ILR flow channel shown in Figure 32-3 illustrates another effect of through-flow. The pressure gradient created by the open drain promotes flow over the edge of the shearing drum that complicates the flow in the shearing zone. Since it is essential that the flow in the shearing zone be well defined, through-flow could not be allowed. Consequently, the ILR was always operated with the drain closed.

Figure 32-3: Top View of the ILR Flow Channel Illustrating the Disruption of the Flow Profile in the Shearing Zone due to Through-Flow.



To ensure that the polymer in the lower SST housing did not degrade severely, the following procedure was followed. At the start of each day of experiments, the drain was left open and the SST was purged for 10 to 15 minutes. The drain was then closed for the balance of the day. At the end of the day, the drain was opened and the rheometer was purged again.

3.2.3 The Effect of Vibration on SST Performances

Figure 32-4a shows a "baseline" SST signal sampled at 256 Hz. In this case the rheometer was heated, but the extruder was not in operation. The peak to peak magnitude of the observed variation in the signal is only 20 mV. This represents approximately 0.4% of the effective full scale signal. An analysis of the frequency spectrum of the signal indicated several dominant frequency components. The only easily assignable component was clearly related to the 2-second temperature control cycle of the SST heater.

Figure 32-4b shows a sample of the SST signal produced while the extruder is compounding at 12 kg/h and the rheometer is performing a test at 30 s^{-1} . The stress signal is obviously noisier. The peak to peak magnitude of the higher frequency signal variation is in the range of 60 to 80 mV (representing 1.2 to 1.6% of the effective signal range). The frequency spectrum of this signal exhibits many distinct frequency components, which probably reflect the various modes of vibration.

There is also a low frequency (0.16 to 0.2 Hz) component obvious in Figure 32-4b. This is discussed in the next section.

3.2.4 A Model for the In-Situ Behaviour of the SST

Nelson (1992) instrumented the ILR to sample rheometer pressures simultaneously with shear stress. He observed that the pressures in the rheometer fluctuated in the manner

Figure 32-4a: Baseline SST Signal versus Time.

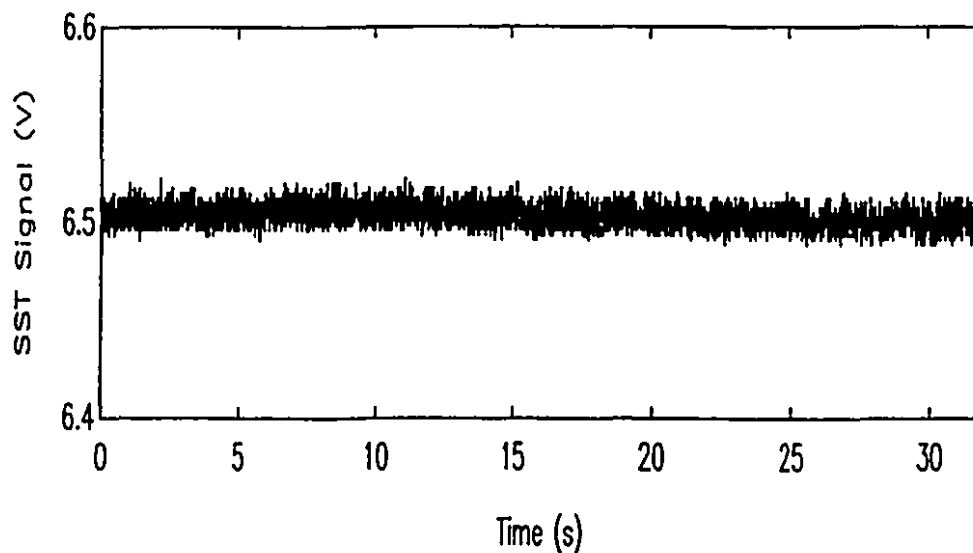
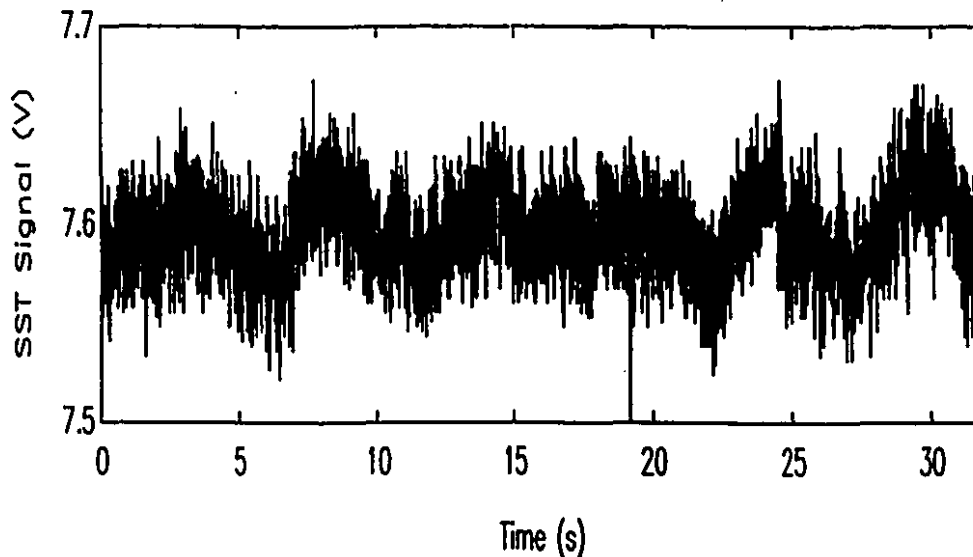


Figure 32-4b: SST Signal during Typical Operating Conditions.



illustrated in Figure 32-5 and recognized that these fluctuations could represent a considerable source of SST noise in light of the evidence presented in Sections 3.2.1 and 3.2.2. Figure 32-6 shows a plot of the shear stress signal sampled at the same time as the pressure signal of Figure

32-5. The two signals are transformed so that they can be compared on the same axes. This plot clearly demonstrates that there is a correlation between the two signals.

Figure 32-5: Typical Pressure Fluctuations Observed During Extruder Operation.

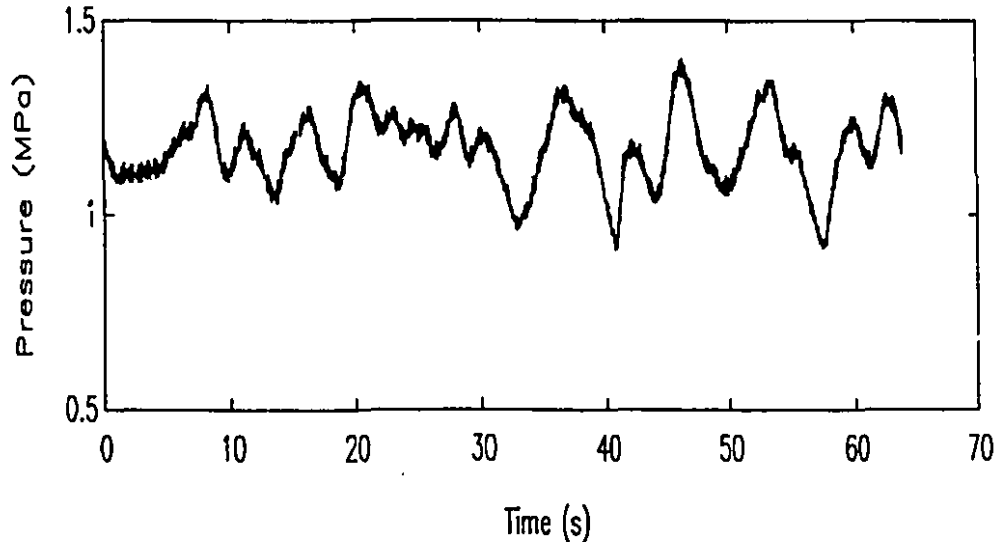
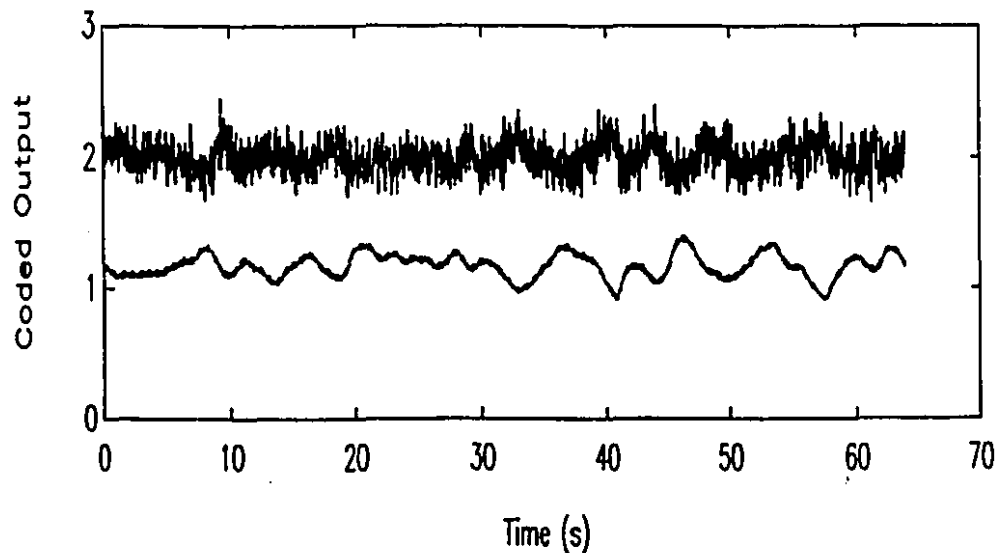


Figure 32-6: Transformed SST and Pressure Signals versus Time.



Legend: The upper line is the coded SST signal, the lower line is the coded pressure signal.

Nelson (1992) found that the relationship between the two signals was a complex one. He proposed that the SST signal would be influenced by the pressure fluctuations through the following phenomena: i) fluctuations in the pressure flow superposed on drag flow in the shearing zone would be sensed at the SST beam face, ii) fluctuations in pressure would cause the linear (elastic) beam deflections described in Section 3.2.1, and iii) fluctuations in pressure would compress or decompress the polymer in the lower SST housing causing a minute, time dependent pressure flow into and out of the housing.

Unfortunately, the ability to measure pressure quickly and the understanding of the consequences of the pressure fluctuations came too late to be of benefit in this study. It is believed that the SST noise due to pressure fluctuations represents the largest source of uncertainty in ILR viscosity measurements. The magnitude of this uncertainty is discussed in Section 4.4.

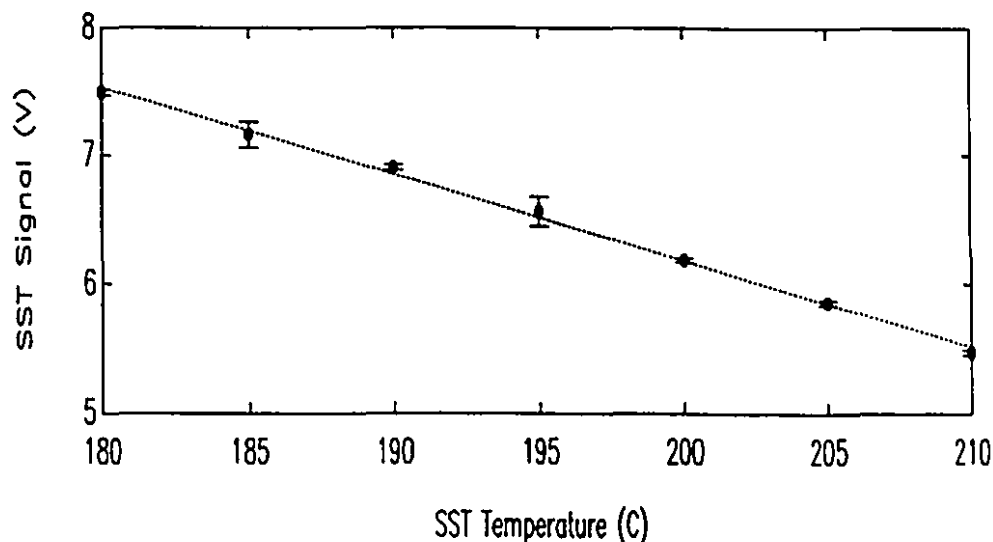
The pressure fluctuations are believed to be characteristic of the dynamics of melting and pumping in a twin screw extruder. They are dependent on the material type and the screw design but only to a small degree on the screw speed. For the materials studied in this work, pressure fluctuations as large as 1 MPa were observed, though typically they ranged from 0.1 to 0.4 MPa.

3.2.5 The Effect of Temperature on SST Performance

Thermal expansion and contraction of the transducer components can also interfere with shear stress measurement. This is another consequence of the attempt to measure a very small beam deflection. Figure 32-7 illustrates the magnitude of the potential temperature effect. It shows the SST signal as a function of the steady state temperature. (The rheometer was heated but the extruder was not running in this experiment.) A straight line was fitted to the data by linear

regression. The slope of this line is (-0.0669 ± 0.0002) V/°C. A 1°C temperature fluctuation could, consequently,

Figure 32-7: SST Signal as a Function of Temperature.



Legend: (o) data, (•••) linear regression of data.

introduce a fairly large uncertainty.

In practice, transducer temperature was well controlled. Careful insulation of the SST and fine-tuning of the SST heater controller minimized temperature fluctuations, although examination of an SST signal by spectral analysis will usually reveal a periodic component attributable to the SST heater cycle.

3.2.6 Dynamic Response of the SST Beam

An intrinsic limitation on the frequency response of the SST arises from damping due to the melt in the lower SST housing. This was not a source of error in this study since only steady state viscosities were of interest. As long as the beam's reaction to a change in shear stress is much faster than the mechanical transients involved in starting the rheometer motor and the rheological transients associated with

the start-up of shear, no error will result from this damping.

The beam reaction time was measured as follows. The extruder was run in order to fill the lower SST housing with polymer. A moderately viscous ionomer blend was used. The extruder was then shut down. The rheometer heaters maintained a constant temperature. A 200 g weight was hung from the SST beam using a steel wire guided by an air bearing. The experimental set-up was identical to that used in the in-situ calibration procedure explained in Section 3.3.2. The SST signal was sampled at 64 Hz. After 5 to 10 s of sampling the SST signal, the 200 g weight was suddenly lifted, relieving the stress on the beam. The beam reaction was recorded for approximately 2 minutes in total.

First order time constants were fitted to the reaction curves, and these ranged from 0.01 to 0.03 s. This is insignificant compared to the observed rheological and mechanical transients, which were in the range of 1 to 2 s.

3.2.7 Unexplained SST Dynamics

One feature of the SST's behaviour remains unresolved. Over long periods of time, without any perceived rheological change, the SST signal changes with time. Typically, the signal increases with time reaching a plateau value after 20 to 40 minutes. In total, the signal has been observed to increase by 0.1 to 0.3 V, though changes as large as 2 V have been observed as well as cases where there was no change or even a small decrease. Figure 32-8 illustrates a typical SST signal change. The SST signal was sampled while the drum was stationary over the duration of a long experiment. While this slow transition to an apparent steady-state level was typical, other types of behaviour were also observed, including sustained oscillations as illustrated in Figure 32-9.

Figure 32-8: Illustration of Unexplained SST Signal Change with Time.

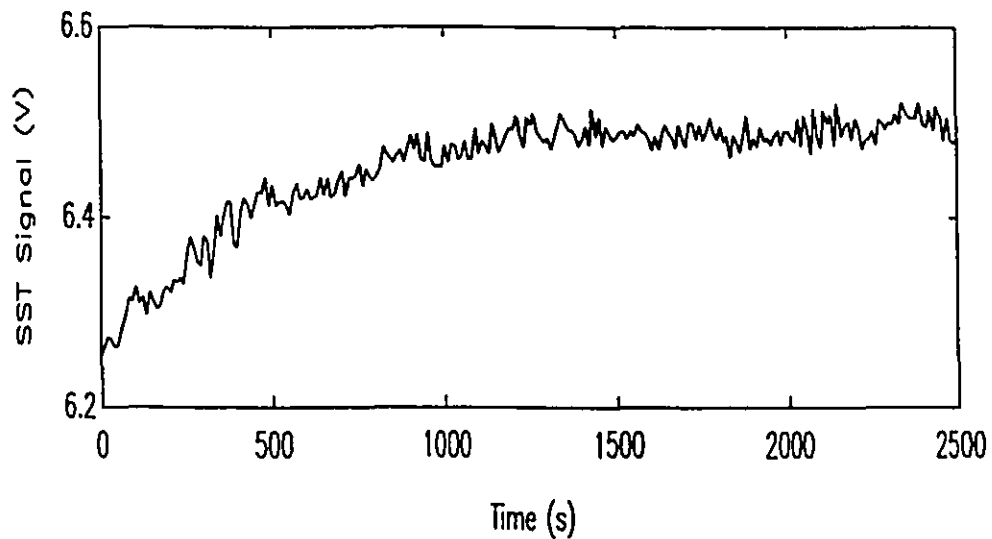
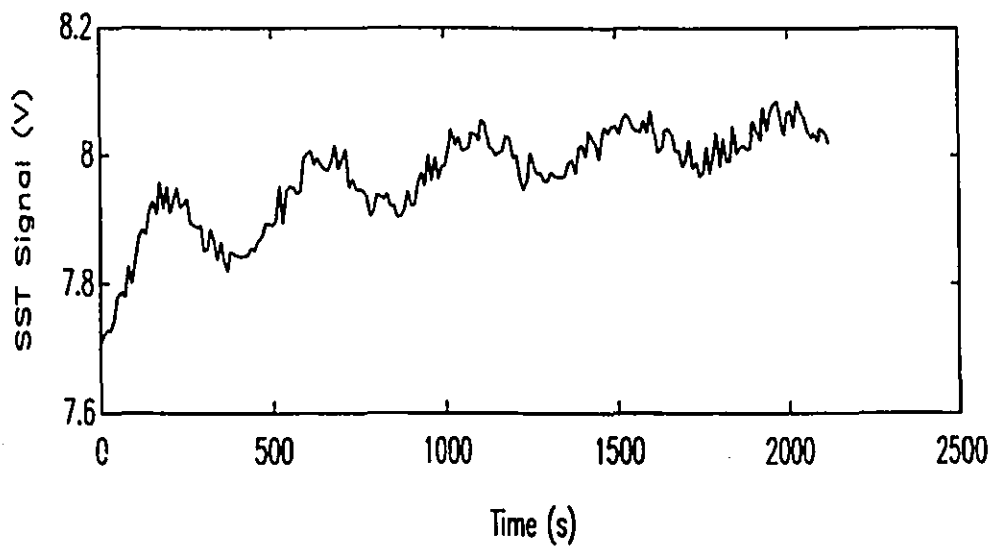


Figure 32-9: Illustration of Unexplained SST Signal Change with Time.



The characteristic times of the observed SST signal changes and oscillations were long. This suggests that the phenomenon may be related to a thermal change in the rheometer or extruder. However, there are other observations that seem to challenge this hypothesis. First, the SST signal was generally observed to increase with melt temperature, whether the temperature change was caused by electrical heater power or by shear heating. An increase in temperature would be expected to decrease polymer viscosity, decreasing the SST signal. Alternatively, an increase in temperature would be expected to cause the thermal expansion of the SST, which would also cause a decrease in SST signal (Section 3.2.5). Furthermore, this trend of increasing SST signal with melt temperature was not consistent in every case. In fact, SST signal changes have not been consistently correlated with any of the measured temperatures or heater duty cycles.

The fact that in many cases the SST signal seemed to approach a steady state suggested that the problem was related to a start-up or "warming-up" transient. Running the extruder for 20 or 30 minutes prior to initiating an experiment often minimized the changes observed in the SST signal, but it did not completely eliminate the problem.

The possibility of the SST signal change being related to the inflow and outflow of material in the lower SST housing was also investigated. The rheometer was run with its SST drain open, throttled, and closed and with different sized annular gaps around the SST face. This was done to vary the rate of exchange of material in the lower SST housing and to try to control its effect on the SST beam deflection. These measures had no effect on the SST signal change.

The unexplained SST dynamics has a serious consequence for the operation of the ILR. Ideally, the ILR would be run in the following manner. An SST signal "baseline" would be read, once the rheometer was at operating temperature but before the extrusion process was initiated. In this way, any

change in SST signal, once corrected for pressure changes as described in Section 3.2.1, would reflect the state of stress in the sample in the shearing zone. In particular, if the rotating drum were stationary, one would measure the stress due to the small pressure flow in the shearing zone and if the drum were rotating, a true measure of stresses due to both drag and pressure flow would be made. But, because the SST signal changes with time in an unpredictable fashion, a time dependent error is introduced into the measurement. The magnitude of this error can be large as explained at the beginning of this section.

As a result, the method of operation had to eliminate the effect of the unexplained SST dynamics. The following method of operation was adopted. The baseline stress signal was measured prior to the initiation of rotation of the drum, with polymer flowing through the rheometer. The output signal was then measured after the drum rotation was initiated and after any rheological transient had subsided. The total time between the two stress measurements was 4 to 6 s. Given the slow nature of the unexplained dynamics, little error is introduced over this short period. However, by not measuring the baseline prior to the initiation of flow through the ILR, the stress signal baseline includes a component due to pressure flow through the shearing zone. Consequently, the true state of stress is under-estimated by the stress measurement. In relative proportion, however, the error introduced in this way is small compared to the error that would be introduced by the unexplained dynamics. The stress signal due to pressure flow was observed to be in the range of 0.04 to 0.08 V, while the unexplained dynamics could introduce an uncertainty of as much as 2 V into the stress signal. As will be shown later, this procedure provided a stable and relatively accurate stress measurement.

3.3 Shear Stress Transducer Calibration

The sensitivity of the SST is governed by the disk spring thickness and diameter. For the range of strain rates and viscosities of interest in this project, a disk spring with a calibration constant of about 25,000 Pa/V was needed. This section outlines the SST calibration procedure and discusses factors that could affect the calibration constant.

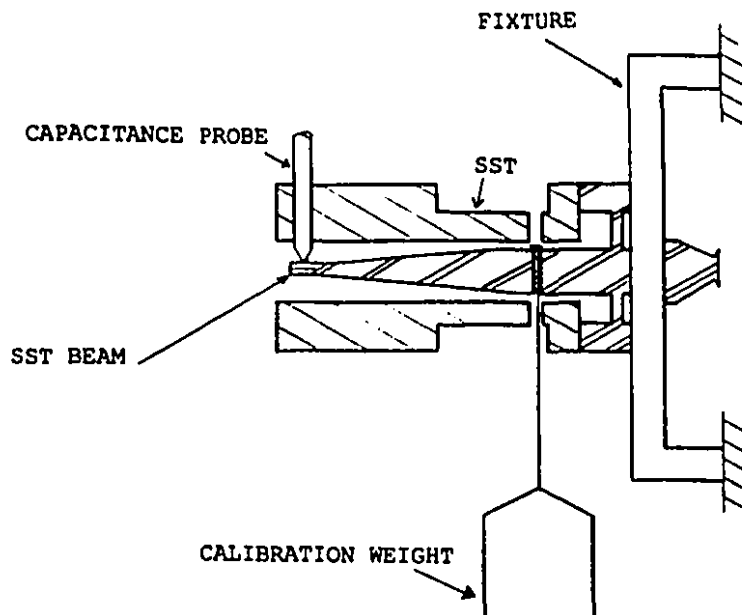
3.3.1 External Calibration

The first measurement of the calibration constant was made in the lab. The SST was fixed in a horizontal position, as indicated in Figure 33-1. A steel wire was fastened to the beam and passed through the calibration hole. Weights ranging from 0.051 to 0.5 kg were hung from the end of the wire. The deflection of the beam was measured using the capacitance probe, and output voltages plotted against weight gave a straight line. The calibration constant is proportional to the slope of this line and is calculated using the following formula,

$$H = \left(\frac{1}{s}\right) \left(\frac{g}{\pi r_s^2}\right) \left(\frac{25}{30}\right) \left(\frac{1}{dr}\right) \quad (33-1)$$

where H is the transducer calibration constant in (Pa/V), s is the slope of the calibration line in (V/kg), g is the acceleration due to gravity, 9.81 m/s^2 , r_s is the radius of the SST face, the factor $25/30$ represents the ratio of the distance from the calibration hole to the fulcrum over the distance from the SST face to the fulcrum, and dr is the deflection ratio that corrects for the bending of the beam between the disk spring and the calibration hole. For this beam, the deflection ratio is 1.094875.

Figure 33-1: Illustration of the External Beam Calibration Method.



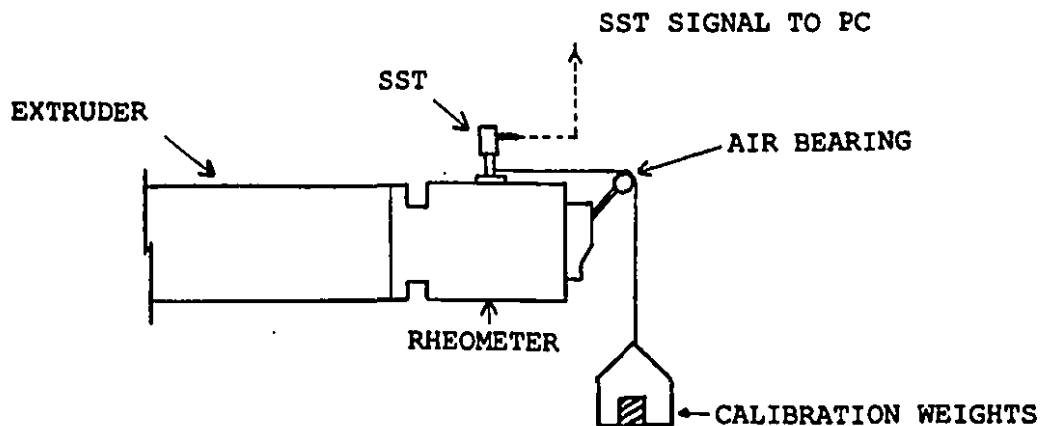
The calibration constant was found to be (17130 ± 60) Pa/V and to be independent of the direction of deflection of the beam. This value is less than the design value, but the difference is within the expected range of machining tolerances and the range of variation of modulus of the steel. In any event, the beam was amply sensitive for this study.

3.3.2 In-Situ Calibration

A procedure was also developed for calibrating the SST in-situ, fixed in the rheometer at operating temperature. An air bearing was mounted in the rheometer die face to guide the calibration wire over the end of the rheometer. This is illustrated in Figure 33-2. Because of friction in the air bearing, capacitance probe voltages were measured twice for each calibration mass. In the first test, the calibration mass was placed gently on the weight pan recognizing that the bearing friction would decrease the effective force due to the

weight. In the second test, the calibration weight and pan were pulled downward and released, assuming that bearing friction would prevent the SST beam from returning precisely to its equilibrium position for the given weight. The mean of the two tests performed in this way was taken as the correct value. This repetition of calibration tests was only necessary for calibration masses greater than 100 g, though it was performed routinely for all weights.

Figure 33-2: Illustration of the In-Situ Beam Calibration Apparatus.



(The software used to perform the SST calibration is listed on the data diskette provided with the thesis.)

There are many sources of variability in the in-situ calibration procedure. The most important one has to do with the way the SST is tightened into place in the rheometer. It was noted after many calibrations that the SST beam calibration constant varied, sometimes markedly, after the rheometer had been disassembled and reassembled. The SST is fixed to the rheometer by 4 bolts. Three of the bolts are easily accessible, but the fourth is difficult to tighten.

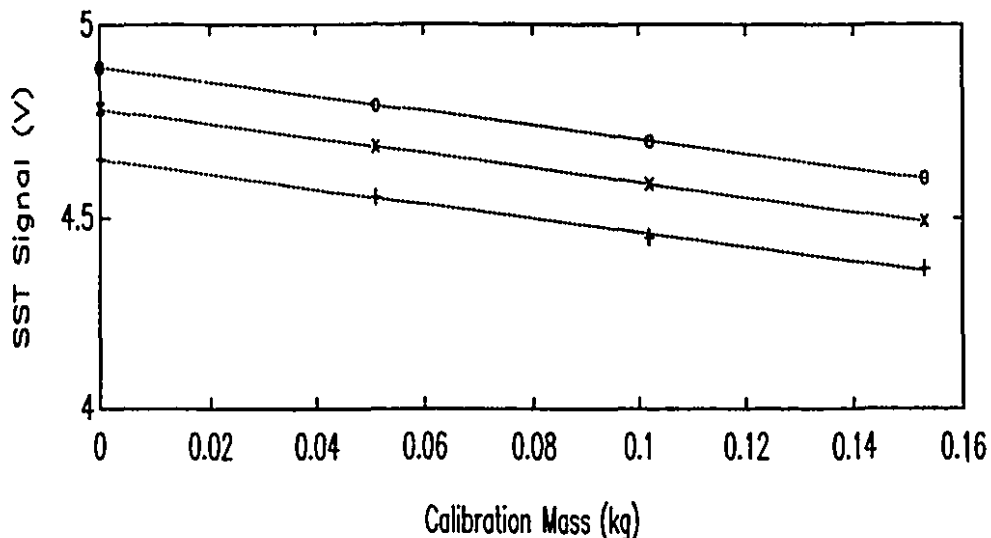
Depending on the installation of the transducer, calibration constants in the range of 15000 to 18500 Pa/V (with occasional values as high as 24000 Pa/V) were observed. With care in installation, values in the range of 15000 to 16500 Pa/v with confidence limits (based on a pooled variance) of ± 210 Pa/V could be attained.

Comparing the confidence limits of the external (60 Pa/V) and the in-situ (210 Pa/V) calibrations, it is clear that the in-situ procedure is considerably less precise. The most important source of variability in the in-situ calibration is the SST signal noise resulting from temperature control action. This phenomenon was described in Section 3.2.5. Nelson (1992) identified this problem and has significantly reduced the variability of the in-situ calibration procedure by performing the calibrations under carefully controlled conditions. Finally, some of the variability observed during in-situ calibrations is due the air bearing friction problem discussed in the previous section.

3.3.3 Pressure Effect

SST calibrations cannot be made while the extruder is operating for practical reasons. Calibrations were performed using the test fixture described in Section 3.2.1 at 0, 1.72 and 3.45 MPa to ensure that a calibration constant determined at atmospheric pressure was valid at the operating pressure of the extruder. The results of one such experiment are shown in Figure 33-3. The calibration constants calculated from this figure are 15949, 15717 and 15848 Pa/V for pressures of 0, 1.72 and 3.45 MPa respectively. These agree well within the 210 Pa/V confidence interval. The SST calibration constant is thus demonstrated to be independent of pressure.

Figure 33-3: SST Signal as a Function of Calibration Weight. Illustration of the Effect of Pressure on the SST Beam Constant.



Legend: (o) 0 MPa, (x) 1.72 MPa, (+) 3.45 MPa, (•••) linear regression lines fit to each data set.

3.3.4 Temperature Effect

It was expected that the modulus of the stainless steel SST beam would change with a change in temperature, thus affecting the calibration constant. However, it was found experimentally that the change in the calibration constant with temperature was very small. In fact, given the level of confidence of the in-situ calibrations, the change in the calibration constant with temperature was insignificant. A value of (-2.3 ± 2.4) Pa/V °C was determined. Clearly, the complications posed by thermal expansion and contraction of the SST, discussed in Section 3.2.5 are much more important.

CHAPTER 4
IN-LINE RHEOMETER VISCOSITY MEASUREMENTS

4.1 Viscosity Measurement Procedure

The practical constraints of operation of the ILR were discussed in sections 3.1 and 3.2. Of the identified constraints and non-idealities, the unexplained SST dynamics was found to have the dominant effect on the ILR's performance. This fact governed the measurement method and obviated the need for some of the other measurement corrections identified earlier. Unfortunately, the adopted method also introduced an inherent uncertainty.

Ideally, the SST signal sampled prior to operation of the extruder should be used as a reference value. (This signal will be referred to as the "baseline" in the following discussion.) In this way, any pressure flow in the gap would be correctly accounted for. The fact that the SST signal drifts for unknown reasons, requires that the stress signal baseline be measured immediately prior to a viscosity test. This approximation of the true stress measurement is justified because the unexplained SST signal dynamics can cause the SST baseline to change by an amount equal to or greater than that of the viscosity test itself. For example, at the low end of the ILR's range of operation, the SST signal would be typically in the range of 0.3 to 0.5 V. The unexplained SST dynamics has been observed to change the baseline signal by as much as 0.2 to 2 V. In contrast, the contribution of the pressure flow to the stress signal is less than 0.08 V for the materials studied.

Because the SST baseline was measured at the same absolute pressure as that used in the viscosity test itself, the SST pressure correction (Equation 32-1) was judged to be unnecessary. (It was later recognised that the pressure correction could have been used to partially correct for the pressure fluctuations described in Section 3.2.4.)

A summary of the viscosity measuring procedure is as follows:

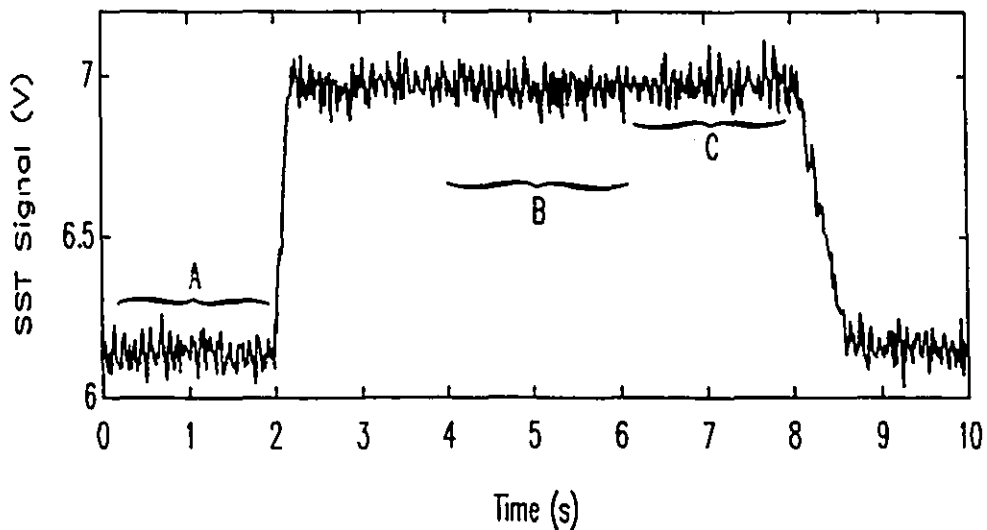
- 1) With the extruder running but the rheometer's shearing cylinder stationary, the SST signal baseline was sampled for 2 seconds at 64 Hz. This part of the SST signal is identified as region "A" in Figure 41-1a. These signal values were averaged.
- 2) The rheometer body, rheometer gap and rheometer melt temperatures were sampled along with the up- and down-stream rheometer pressures.
- 3) Drum rotation was then initiated.
- 4) The SST and tachometer feedback signals were sampled at 64 Hz for 5 or 6 seconds after the initiation of shearing. The relevant parts of the SST and tach signals are identified as region "B" in Figures 41-1a and b.
- 5) The shearing cylinder rotation was terminated.
- 6) Only the last 1 or 2 seconds of the SST and tachometer signal records were averaged. These parts of the signals are identified as regions "C" in Figures 41-1a and b.
- 7) The stress at the wall was calculated using,

$$\sigma_w = H \times (\bar{V}_{SST} - \bar{V}_{BASELINE}) \quad (41-1)$$

where σ_w is the shear stress at the wall, H is the SST beam calibration constant, \bar{V}_{SST} is the mean SST signal (voltage) during the viscosity test, $\bar{V}_{baseline}$ is the mean SST baseline signal.

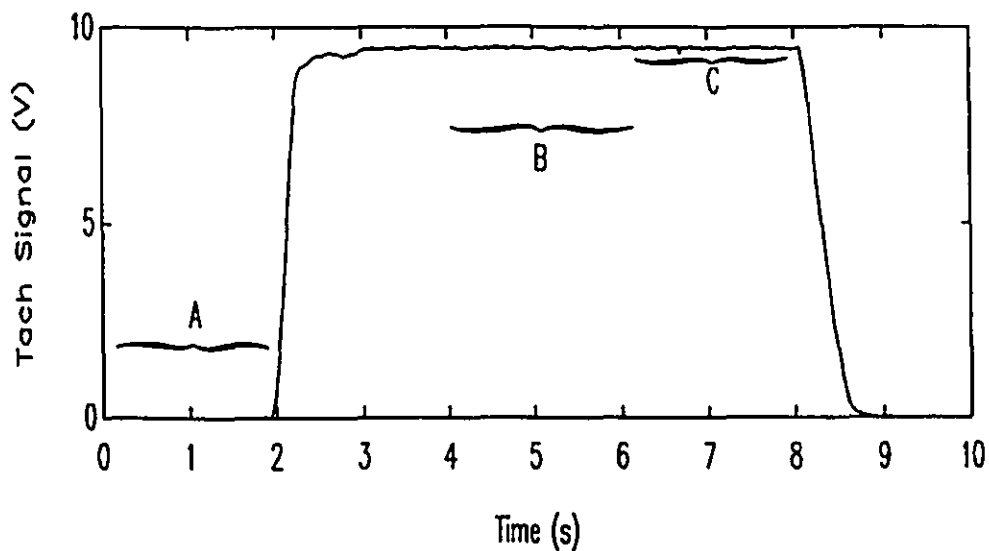
- 8) The shearing velocity, or nominal strain rate, was calculated using the tach voltage-strain rate calibration (Equation 31-3).
- 9) The apparent stress at position y^* in the gap (in the Schümmer approximation) was calculated from:

Figure 41-1a: Typical SST Signal During a Viscosity Measurement.



Legend: A \equiv Period of baseline signal sampling, B \equiv period of drum rotation, C \equiv period of signal averaged for viscosity measurement.

Figure 41-1b: Typical Tachometer Signal During a Viscosity Measurement.



Legend: same as above

$$\sigma_A(y^*) = \sigma_N - \frac{\Delta P \times y^*}{L} \quad (41-2)$$

10) The apparent strain rate at position y^* was calculated using:

$$\dot{\gamma}_A(y^*) = \frac{V}{g} \times \left(\frac{(\sigma_N \times L - \Delta P \times y^*)}{(\sigma_N \times L - \Delta P \times \frac{g}{2})} \right) \quad (41-3)$$

11) The true viscosity (Schummer approximation) was calculated using:

$$\eta = \frac{\sigma_A(y^*)}{\dot{\gamma}_A(y^*)} \quad (41-4)$$

The apparent viscosity was calculated using:

$$\eta_A = \frac{\left(\sigma_N - \frac{\Delta P \times \frac{g}{2}}{L} \right)}{V/g} \quad (41-5)$$

The nominal viscosity (assuming no pressure flow in the shearing zone) was calculated using:

$$\eta_N = \frac{\sigma_N}{(V/g)} \quad (41-6)$$

4.2 Rheometer Discrimination

In instrument performance terminology (Sydenham (1982)), the term "discrimination" denotes the smallest change of a measured property that will cause a sensor's signal to change. The ILR's discriminating ability is governed by the SST and tachometer discriminations.

The SST discrimination is limited by the following factors:

- 1) The inability to align the capacitance probe and the SST target limited the effective range of the capacitance probe (0.0127 mm instead of 0.0254 mm),
- 2) the SST beam calibration constant (16000 Pa/V) and
- 3) the number of bits used in the analog to digital conversion (4096 bits).

All of these factors are discussed in Chapter 3. The value of the SST discrimination is 39 Pa/bit.

The tachometer discrimination is limited by:

- 1) The effective strain rate range (3 to 36 s^{-1}),
- 2) the effective rheometer motor speed signal range (0.85 to 10 V),
- 3) the number of bits used in the analog to digital conversion (4096 bits).

The tachometer signal discrimination is 0.00881 s^{-1} /bit.

Clearly, the ILR's discrimination is limited by the stress measurement. To gain a better understanding of the ILR's discriminating ability, it is useful to express discrimination as a percent of the total viscosity measured. Over the range of materials tested, the ILR's discrimination ranged from a maximum of 7.5 % for the lower viscosity polymers tested at low shear rate to 0.17 % for the higher viscosity polymers tested at high shear rate.

4.3 Rheometer Accuracy

The in-line rheometer's accuracy was evaluated by collecting polymer that had had its viscosity measured in the ILR and remeasuring its viscosity using a sliding plate rheometer (SPR) (described by Giacomini (1987) and Dealy et al. (1989)). A total of 7 materials were tested; two polypropylenes, two polyethylenes and three ionomer blends. The commodity polyolefins, described briefly in Table 43-1, were high and intermediate viscosity grades. The ionomer blends ranged from intermediate to low viscosity.

Table 43-1: Summary of Commodity Polyolefins Tested

Polymer	Tradename	Melt Index ASTM-1238 (dg/min)	Density (kg/m ³)
PP	Profax ¹ 6631	2 ³	902
PP	Profax ¹ 6501	4 ³	902
HDPE	Sclair ² 2907	5 ⁴	960
LLDPE	Sclair ² 11L1	0.75 ⁴	919

1 Profax is a registered trademark of Himont Canada Inc.

2 Sclair is a registered trademark of DuPont Canada Inc.

3 ASTM-1238, Condition L. 4 ASTM-1238, Condition E.

The ILR viscosity measurements were corrected to the SPR's measurement temperature (or vice versa) using the Arrhenius expression given in section 2.4.3, and the data summarized in Table 43-2. The use of the temperature correction was necessary because the extrusion process, and therefore the ILR measurements, had to be run at temperatures beyond the range of operation of the SPR.

Table 43-2: Summary of Activation Energies for Flow for the Polymers Studied.

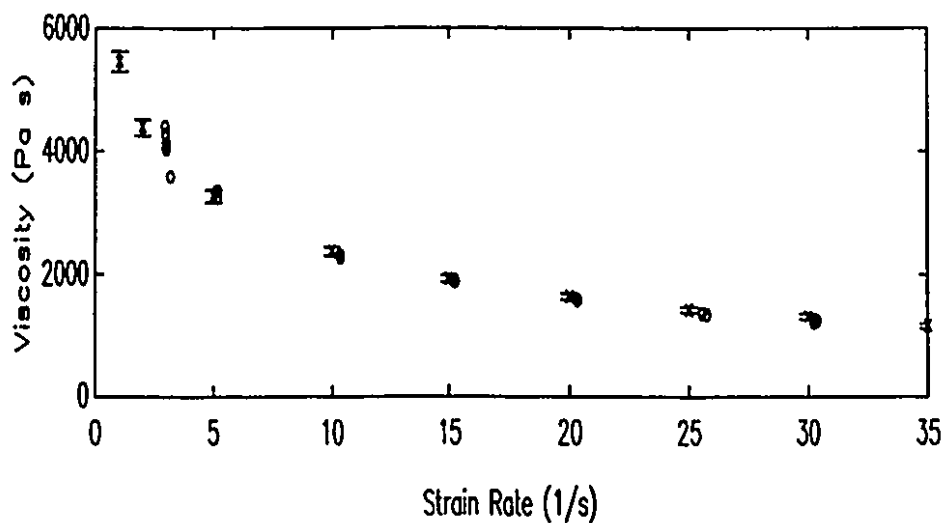
Polymer Tradename	Activation Energy for Flow [J/mol]	Source
Profax 6631	27,100	Determined experimentally
Profax 6501	27,100	Determined experimentally
Sclair 2907	23,300	Tanner (1985), HDPE pp 353
Sclair 11L1	56,900	Tanner (1985), LLDPE pp 353
15% Neutralised Ionomer Blend	51,000	Determined experimentally
22% Neutralised Ionomer Blend	51,000	Determined experimentally
29% Neutralised Ionomer Blend	51,000	Determined experimentally

SPR and ILR measurements for two polypropylene resins, Profax 6631¹ and Profax 6501¹ are presented in Figures 43-1 and 43-2. These materials were studied extensively with the SPR, and the viscosities and the activation energy used to correct ILR measurements for temperature differences are known with confidence. The agreement between the two instruments is excellent for these materials.

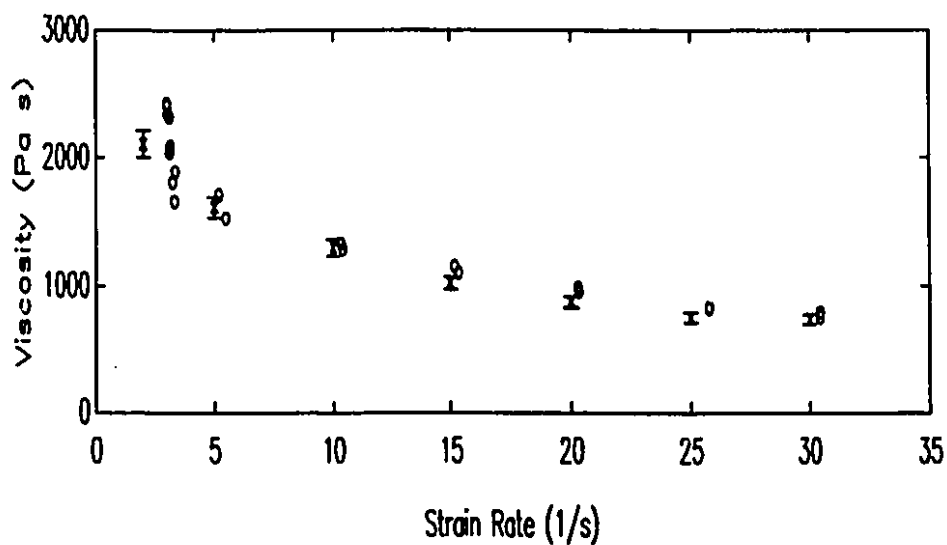
The viscosities of two polyethylene resins, Sclair 2907² and Sclair 11L1², were also measured using the two rheometers. The results are presented in Figures 43-3 and 43-4 respectively. This was a less rigorous test of the ILR

¹ Registered trademark of Himont Canada Inc.

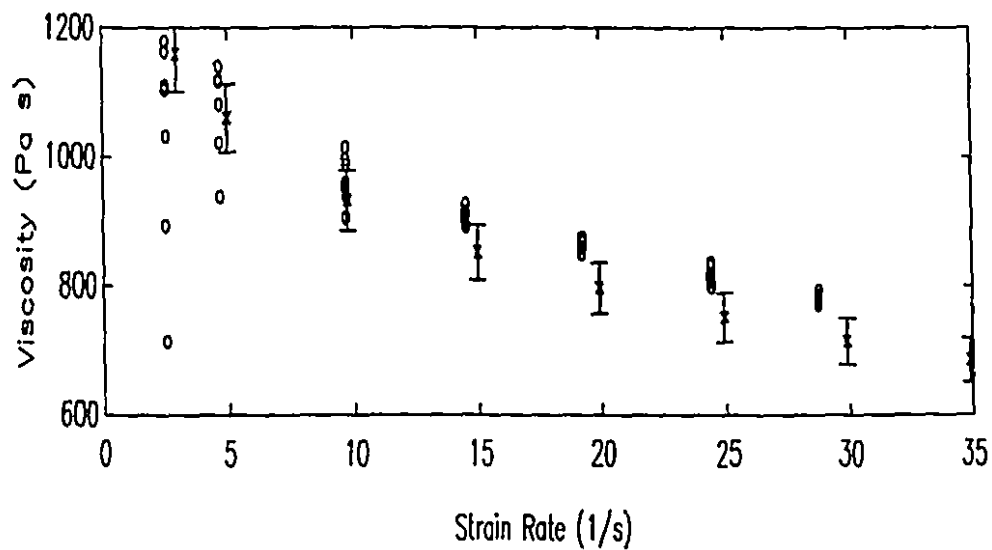
² A registered Trademark of DuPont Canada Inc.

Figure 43-1: Viscosity of Profax 6631 at 200°C

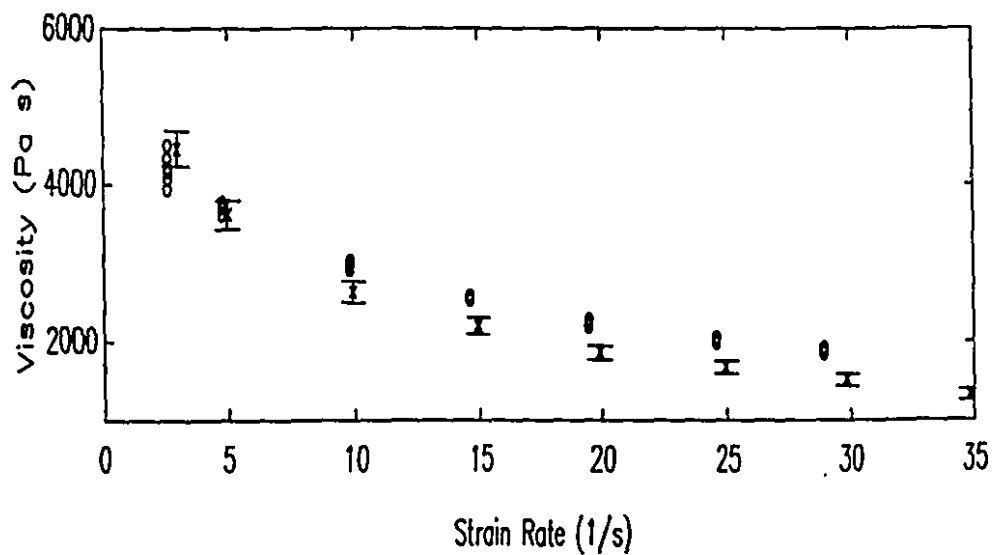
Legend: (x) SPR data at 200°C, (o) ILR data corrected to 200°C.

Figure 43-2: Viscosity of Profax 6501 at 200°C.

Legend: (x) SPR data at 200°C, (o) ILR data corrected to 200°C.

Figure 43-3: Viscosity of Sclair 2907 at 206°C.

Legend: (x) SPR data corrected to 206°C, (o) ILR data at 206°C.

Figure 43-4: Viscosity of Sclair 11L1 at 223°C.

Legend: (x) SPR data corrected to 223°C, (o) ILR data at 223°C.

because the activation energies used to adjust measurements for temperature were not specific for the materials tested but were general values for HDPE and LLDPE reported by Tanner (1985). The agreement between the rheometers is generally good, but the shapes of the curves do not match precisely. The ILR measurements suggest that the polymers are less shear-thinning than the SPR measurements show them to be. This type of mismatch may be due to the fact that the pressure drop along the shearing zone was underestimated at high strain rates. This is discussed shortly. However, the uncertainty introduced by using generic activation energies from the literature precludes a rigorous discussion of this discrepancy.

In general, the following sources of error affect measurement accuracy:

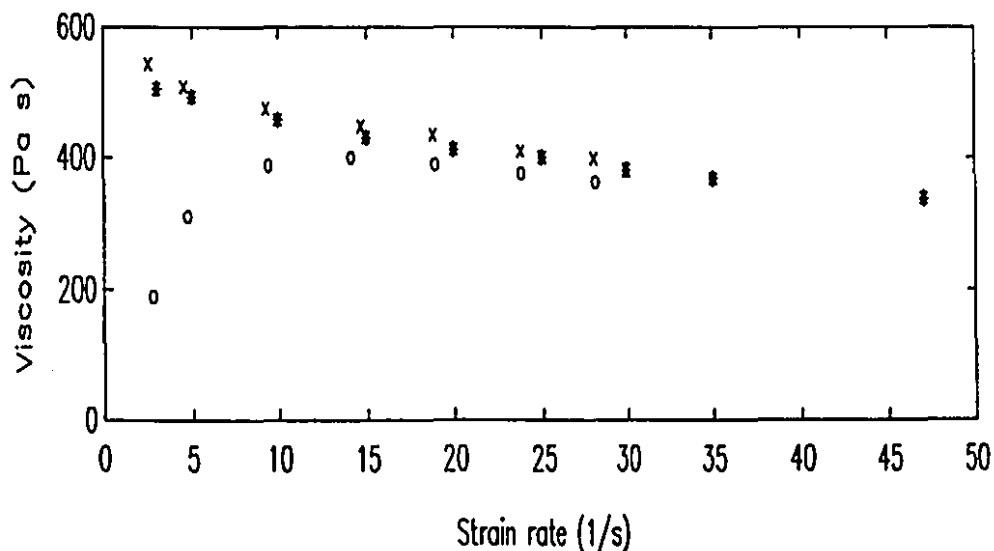
- 1) The stress measurement does not correctly account for the contribution from the pressure flow of material in the shearing zone because of the unexplained SST dynamics described in section 3.2.7. This would lead to the under-estimation of the viscosity.
- 2) Late in the project, new pressure signal amplification circuits were installed allowing direct sampling of pressure signals. It was found that the pressure drop along the shearing zone increased with drum speed. The pressure drop signal used in the measurement is sampled prior to straining and consequently does not reflect the exact value during the test. For low viscosity polymers the effect is very small. For high viscosity polymer, however, this phenomenon would lead to the over-estimation of the viscosity at high strain rates.
- 3) Experimental evidence shows that the metal surface temperatures of the rheometer gap are identical to within 1°C, but to the extent that they are not

identical, and due to the predominance of convection of heat from the main flow stream, it is likely that the temperature profile in the shearing zone is not perfectly uniform. This would have the effect of under-estimating viscosity. For example, a temperature discrepancy of 1°C would introduce a material dependent error of 1.2 to 2.5 % for the materials studied in this work.

4) As discussed in Section 2.2 and 2.3, it is likely that flow recirculation and entrance effects at the rheometer gap entrance decrease the actual pressure drop in the rheometer gap. This would lead to the under-estimation of the viscosity.

This last effect was prominent in the measurements of the viscosity of the three ionomer blends, as shown below.

Figure 43-5: Illustration of the Problem Encountered in Measuring Low Viscosity Ionomer Blends.



Legend: (o) ILR data accounting for pressure flow in the shearing zone. (x) ILR data ignoring pressure flow in the shearing zone. (*) SPR data.

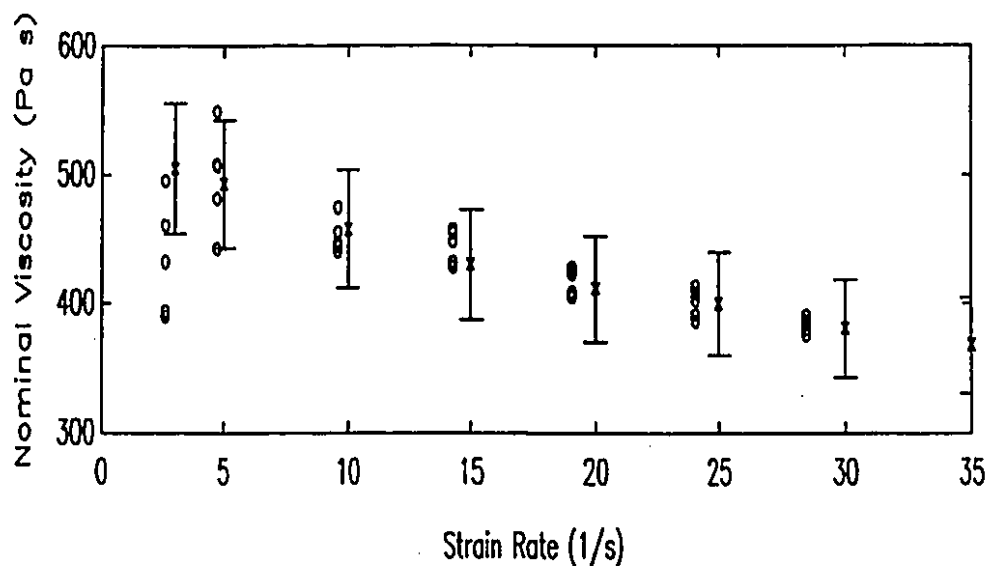
When the viscosity of the least viscous blend was first measured, the data followed the trend shown by the open circles in Figure 43-5. Consistent with the fact that the blend viscosity was very low, the pressure drop measured across the gap was very small, only 55.2 kPa. In recognition of the potential for recirculation zones at the shearing zone entrance, as well as the potential for an entrance pressure drop due to elastic forces, it is proposed that the actual pressure drop in the shearing zone could be much smaller than measured. It follows that the pressure flow contribution to the stress could be negligible. Without a pressure flow contribution, the viscosity is simply the measured stress divided by the shearing rate imposed by the rotating drum. This was defined as the "nominal viscosity". The nominal viscosity of the ionomer blend is shown with the crosses in Figure 43-5. The nominal viscosity curve has the correct shape and, in fact, agrees quite well with laboratory SPR data, which are shown as asterisks.

As the pressure drop increases with increasing viscosity, the pressure flow contribution to the measured stress will become appreciable. The point at which the pressure flow must be taken account will be material and temperature dependent, and, because of the evidence presented above, it will also depend on the shear rate. It is difficult to identify this point and correct properly for this effect. As a result, the ILR cannot accurately measure the true viscosity of low-viscosity, viscoelastic materials. Fortunately this does not preclude the application of the ILR in process monitoring and control applications. For the purposes of the current study, repeatability, reproducibility and adequate discrimination of composition using viscosity are the most important factors. The evidence presented in the following section and in Chapter 6 will show that these conditions are met.

For the reasons outlined above, nominal viscosities measured with the ILR were compared to SPR viscosity data. Viscosity curves for 15%, 22% and 29% neutralised ionomer blends are presented in Figures 43-6, 43-7 and 43-8 respectively. (Details of the ionomer blend compositions are given in Chapter 5.) The agreement between the two rheometers is good for the 15% neutralised ionomer blend. However, the ILR data for the higher viscosity blends are consistently lower than the SPR data. It is most likely that the lack of agreement between the rheometers is due to the phenomenon of moisture plasticization, which is described in Section 5.4. It is possible that the extruded ionomer samples were dried somewhat during the SPR testing procedure. Consequently, SPR viscosity measurements would be higher than ILR measurements.

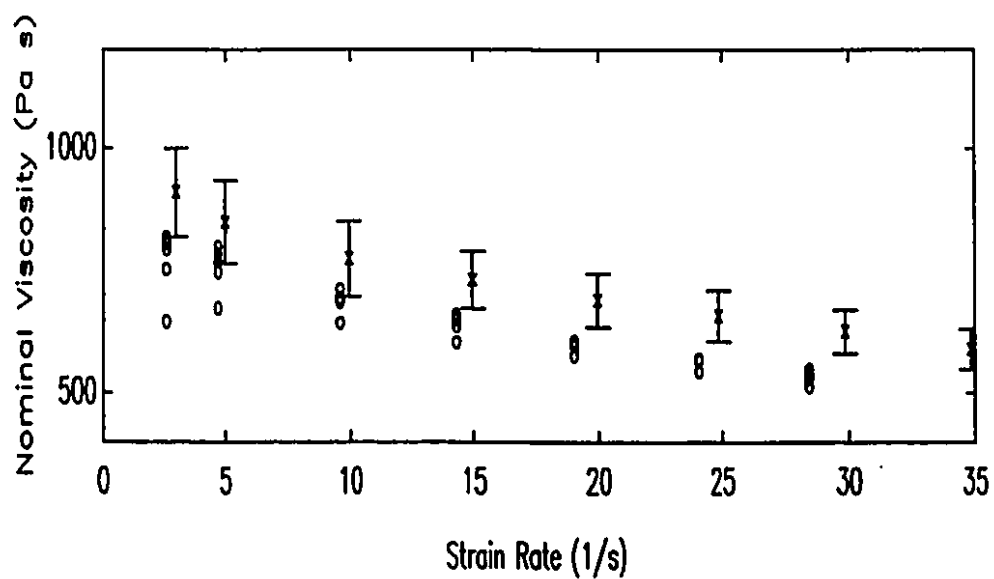
Though less likely, the phenomenon of shear modification may also contribute to the lack of agreement. Shear modification refers to a reversible change in the interaction of polymer molecules caused by intensive shearing. High molecular weight polyethylenes molecules, for example, are assumed to disentangle in strong shearing flows, resulting in a temporary decrease in viscosity. Hanson (1969) and Maxwell et al. (1982) describe this phenomenon. The same effect has been reported for ionomers by Lundberg and Phillips (1984). In the case of ionomers, it is suspected that intensive shear destroys the special ionomer melt phase morphology that is responsible for their high viscosity. Consequently, viscosities measured in-line, immediately after intensive shearing would be lower than values measured in the laboratory, where the samples have the opportunity to regain their unique morphology.

Figure 43-6: Viscosity of a 15 % Neutralised EMAA Ionomer Blend at 185°C.



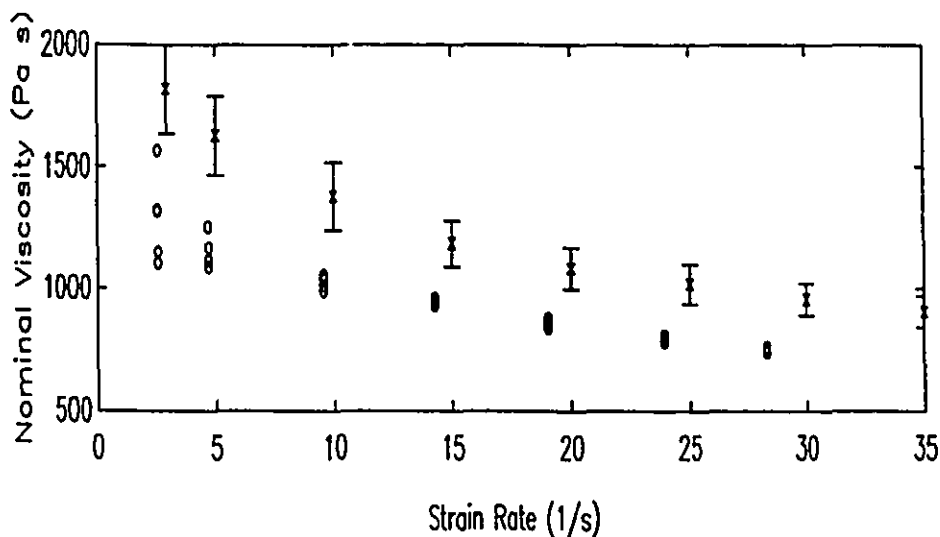
Legend: (x) SPR data at 185°C, (o) ILR data at 185°C.

Figure 43-7: Viscosity of a 22 % Neutralised EMAA Ionomer Blend at 187°C.



Legend: (x) SPR data corrected to 187°C, (o) ILR data at 187°C.

Figure 43-8: Viscosity of a 29 % Neutralised EMAA Ionomer Blend at 187°C.



Legend: (x) SPR data corrected to 187°C, (o) ILR data at 187°C.

In summary, the ILR has proven to be an accurate instrument for moderately to highly viscous polymers (1000 to 6000 Pa s). Its strong asset is that no fitted parameters are required. Calibration of the SST beam and rheometer motor are simple, material-independent procedures. To correct apparent viscosity to true viscosity, a material-dependent parameter (γ^*) must be determined a priori, but experience has shown that ILR measurement quality is insensitive to small variations in this parameter.

ILR measurements are not accurate for low viscosity materials (particularly for low viscosity, highly elastic melts). This problem is believed to be due mainly to large shearing zone entrance pressure losses, which limit the flow of polymer into the gap. Consequently, the flow in the gap approaches a pure drag flow. This situation is believed to change with increasing pressure resulting from compositional or temperature changes and with the increases in pressure

observed with increases in strain rate.

4.4 Rheometer Repeatability and Reproducibility

The term "repeatability" refers to the ability of an instrument to measure the same value of a quantity several times for a given sample or condition (Sydenham (1982)). "Reproducibility" will be used here to describe the ability of an instrument to measure the same value over a long period of time.

The repeatability of the ILR is demonstrated in the viscosity versus strain rate data plotted in Figures 43-1,2,3,4,6,7 and 8. Typically, there is a large scatter in the data obtained at low strain rate, but this decreases with increasing strain rate. At and above 20 s^{-1} , the measurement repeatability is small and approximately constant. Table 44-1 summarizes the peak to peak signal variations as a percentage of the mean for the data presented in Figures 43-1 through 43-4 and 43-6 through 43-8. Peak to peak variations more accurately represent a confidence interval for reasons that will be made clear shortly. These data show that at low strain rate, ILR viscosity measurements are repeatable only to within 20 to 40% of the mean, while at high strain rates the measurements are repeatable within 5 or 7% of the mean.

Clearly, the scatter of the ILR measurements at low strain rates is excessive. The reasons for this are as follows. As explained in Section 4.2, the ILR's ability to discriminate at low strain rate is poor. (At 3 s^{-1} , for the low viscosity ionomer, the smallest change in signal that the rheometer can discriminate is 7.5 % of full scale.) More important is the effect of the pressure fluctuations described in sections 3.2.1 and 3.2.4, which are superimposed onto the stress measurement as noise. This noise introduces a material-dependent uncertainty in the range of $\pm (600 \text{ to } 800) \text{ Pa}$. This is an absolute uncertainty

and therefore affects the small stresses measured at low strain rate more dramatically.

Table 44-1: Summary of ILR Signal Reproducibility for the Materials Tested.

Data displayed in Figure	Range of Observed Variation as a Percent of the Viscosity Mean (%) as a function of Strain Rate (1/s)						
	3	5	10	15	20	25	30
43-1	20.6	3.00	2.05	0.743	5.80	1.26	1.64
43-2	37.3	14.9	18.8	11.0	3.50	1.21	5.16
43-3	49.3	19.4	11.3	3.96	3.01	4.65	3.07
43-4	13.4	4.22	3.77	2.04	3.94	3.35	3.51
43-5	23.7	21.4	7.65	6.55	5.52	7.00	3.66
43-6	23.5	17.1	10.2	8.72	4.92	4.49	6.42
43-7	34.6	22.6	6.46	3.65	4.56	3.40	2.94

The period of these pressure fluctuations was in the range of 4 to 8 seconds. Clearly, the ILR's procedure of sampling the SST for 1 or 2 seconds and averaging cannot filter out this relatively slow variation. In future, the SST should be sampled for longer periods of time and filtered to obtain a less noisy stress signal.

Since the error introduced into the measurement in this way is deterministic, it is strictly incorrect to summarize the ILR's measurement variation with normal distribution statistics. For this reason, the full range of ILR variations (peak to peak) have been compared rather than standard deviations or confidence intervals, and raw data have been plotted here instead of means and error bars.

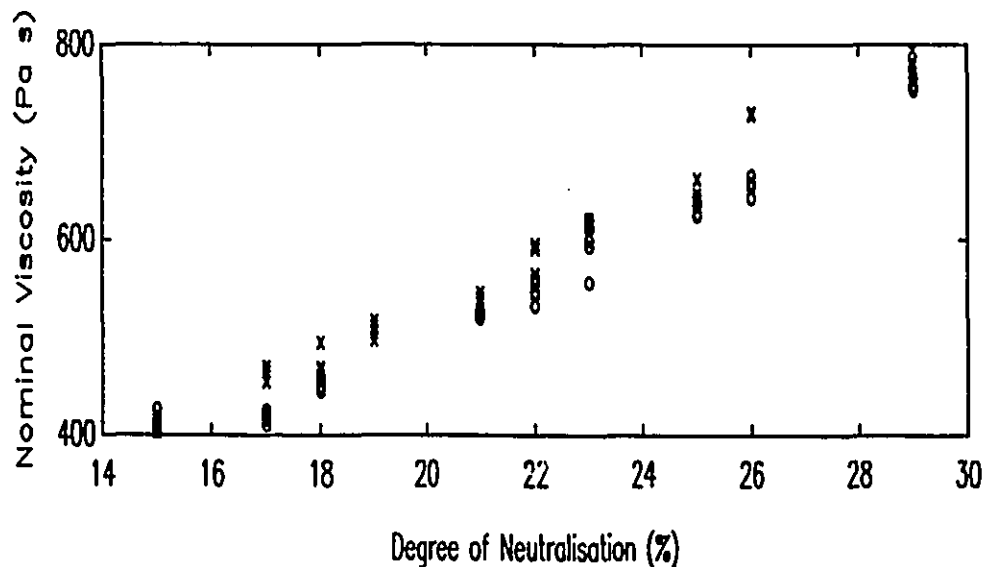
Electronic signal noise and vibration related noise

also contribute to ILR measurement variation. For the range of data collected for the ionomer blends, the noise due to these sources is approximately 50% of the pressure related signal noise.

Finally, it must be mentioned that polymer variability could affect the results of repeatability tests. The procedure of sampling 7 viscosity versus shear rate curves of 7 points each takes approximately 7 to 10 minutes. At typical operating conditions, 0.7 to 2 kg of material would be pumped through the rheometer during this time. It is conceivable that small variations in polymer material properties could occur during this interval.

Reproducibility is essential if the rheometer is to be useful as a process sensor. The rheometer's reproducibility is illustrated in Figure 44-1.

Figure 44-1: Comparison of Viscosity Data at Various Degrees of Rates Measured over a Three Week Period to a Reference Viscosity Curve Measured at the Start of the Experimental Period.



Legend: (o) Reference viscosity versus composition data,
(x) viscosity data collected over a period of three weeks.

The data plotted in Figure 44-1 are summarised in Table 44-2. Figure 44-1 shows mean viscosity values at 30 s^{-1} as a function of ionomer blend composition. The open circles represent viscosity measurements made at each composition during a single day of experiments. These data are referred to as the "reference experiments" in Figure 44-1. The crosses represent experiments at all compositions accumulated over a period of 3 weeks. The reference data appear to be consistently just lower than the accumulated data but, given the margin of error in the measurements, there is no reason to consider the two data sets to be different.

Table 44-2: Peak to Peak Variation of ILR Measurements made over a Three Week Period.

Degree of Neutral'n (%)	Reference Expt Viscosity Range		Accumulated Viscosity data	
	Minimum (Pa s)	Maximum (Pa s)	Minimum (Pa s)	Maximum (Pa s)
15	404	426	404	420
17	409	424	453	470
18	444	458	460	494
19	---	---	496	516
21	519	527	539	545
22	545	560	564	594
23	556	621	613	620
25	624	643	646	662
26	643	665	727	730
29	755	766	764	795

CHAPTER 5

REACTIVE EXTRUSION OF ETHYLENE METHACRYLIC ACID IONOMERS

5.1 Motivation for Studying the EMAA Ionomer System

Ethylene-methacrylic acid (EMAA) "ionomers" are commercially important, melt processable polymers that have a remarkable range of properties. They exhibit excellent room and low temperature toughness and are resistant to cuts and abrasion. Unlike other semi-crystalline polyolefins, EMAA ionomers are clear, and they adhere well to metals, glass and nylon as well as to epoxy and urethane finishes. These properties make them ideal for many injection moulding and coating applications. High viscosity grades of EMAA have high melt strength and high melt elasticity making them suitable for film blowing, vacuum forming and thermoforming operations.

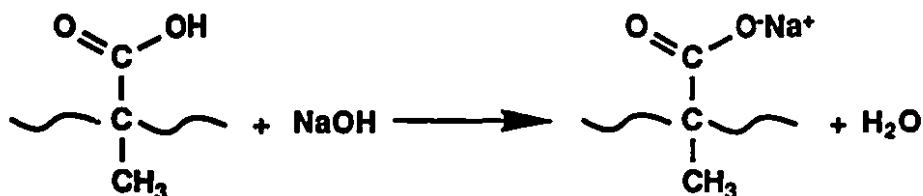
All of these useful ionomer properties are a consequence of the ionomer's unique morphology. This uniqueness extends to the molten state with the result that ionomer viscosity is very sensitive to composition. For example, the sodium neutralised EMAA ionomers studied here can exhibit a hundred fold increase in viscosity over the composition range of commercial interest. In fact, because of its link to processability, viscosity is the primary indicator of product quality used in commercial ionomer production.

The potential economic advantage offered by a process rheometer to ionomer production is obvious. Currently, ionomer product quality is controlled on the basis of periodic sampling and laboratory testing of ionomer samples. An in-line process rheometer could test product quality more frequently and much more quickly, greatly enhancing the quality control process. A closed loop control scheme employing an in-line process rheometer would further reduce product quality deviations and improve the economic return from of the process.

The ionomer production process is ideal from the point of view of testing a process rheometer. Firstly, viscosity is the parameter of interest, no primary property-viscosity correlation is needed. Secondly, because viscosity changes so dramatically with composition, the rheometer can be evaluated over a broad operating range. Also, the strong viscosity-composition relationship affords the possibility of precise control of composition by controlling viscosity.

5.2 Model Reactive Extrusion Process

Ethylene-methacrylic acid (EMAA) ionomers are polymeric salts. The material of interest in the current project is an ethylene chain with one or two (~4.1 mol%) methacrylic acid (MAA) comonomer units per chain. A fraction of the total number of acid sites are neutralised with sodium ions. The commercial ionomer production process involves the reaction of the copolymer with sodium hydroxide in a plasticating extruder. The reaction is:



It is important to emphasize the following facts about the neutralisation reaction. First, the reaction does not alter the polymer backbone in any way. The ionic bonds are labile, which means that ions can disassociate from one acid group and form a bond with another. Like all polymer melt reactions, the neutralisation reaction is diffusion controlled and relies on intensive mixing to ensure that the reaction goes to completion. These facts justify the modification of the process used in this project. Rather than using a liquid stream of concentrated sodium hydroxide, a neutralising agent "masterbatch" was used. This masterbatch was a highly

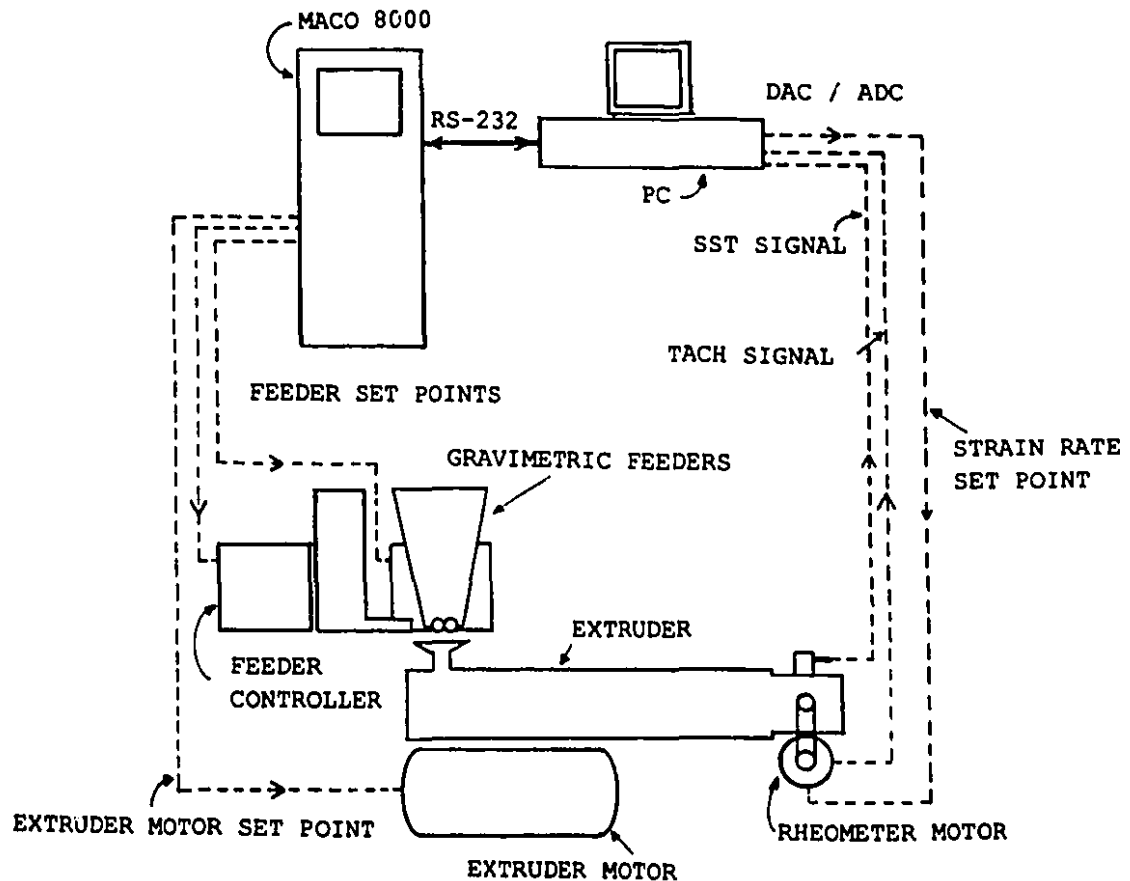
neutralised ionomer made from a copolymer identical to the one being neutralised. By blending the two materials (the highly neutralised ionomer and the un-neutralised copolymer) in a twin screw extruder, the sodium ions were re-distributed giving a product of intermediate degree of neutralisation. This model process was attractive, because it is considerably safer and much simpler to implement.

The model reactive extrusion process was carried out in the apparatus sketched in Figure 52-1. The reactants were fed in pellet form by means of two gravimetrically controlled feeders. (Control and Metering, model H0 DDSR 20-10 feeders, with Brabender Technologie Congrav C^o computer controllers.) The feeders introduced material into the feed hopper of a 30 mm Werner and Pfleiderer ZSK-30 twin-screw extruder. The extruder had a length to diameter ratio of 24:1. The screws were designed by the manufacturer for intensive mixing. The extruder was equipped with one vacuum port, and a Speedivac model 200 vacuum pump was used to withdraw volatiles, mainly water, from the reacted product.

A Barber-Coleman MACO 8000 distributed modular control system, described in Section 3.1.7, was used to control and monitor all aspects of the extruder and feeder operations. The communication pathways between the controller, the extruder, the feeders, and the supervising personal computer (PC) are also indicated in Figure 52-1. The MACO system: i) controlled temperatures in 4 extruder barrel zones by means of electric heating and water cooling, ii) monitored pressure and alarmed when limits were exceeded, iii) controlled screw speed, monitored motor torque and alarmed when torque limits were exceeded, and iv) communicated with the gravimetric feeders, transferred feedrate set points from the PC to the feeders, and monitored actual feedrates for communication back to the PC.

The rheometer was mounted on the end of the extruder. Its functional interconnections are described in Section 3.1.6.

Figure 52-1: Reactive Extrusion Process used to Neutralise EMAA Ionomer.



5.3 EMAA Ionomer System Characterisation Experiments

A series of ionomer blends were prepared on another twin screw extruder using a similar, but not identical screw design. These blends were prepared in order to verify the relationship between degree of neutralisation and blend composition, to evaluate blend homogeneity and to determine viscosity versus composition and viscosity versus temperature relationships. This information was important in the design of the shear stress transducer, for the selection of the best operating space, in the identification of the steady state

process response, and in the development of a temperature compensation algorithm.

A total of 14 blends representing 8 different compositions were prepared. The blend components were:

- 1) Nucrel® 960¹, a 4.1 mol % methacrylic acid EMAA copolymer,
- 2) Surlyn® 8920¹, a nominally 59% sodium neutralised EMAA ionomer, based on Nucrel 960 and
- 3) Irganox® B215², an organic anti-oxidant developed for molten plastics added at a level of 0.1 mass %.

The details of blend preparation, including processing conditions, are given in Appendixes A1-1 and A1-2. Because the viscosity of the blends varied greatly, the blends were processed at similar but not identical conditions. The degree of neutralisation of each blend was determined by titration as described in Appendix A1-3. Each titration was repeated once. In most cases, two samples were tested from each blend.

5.4 Degree of Neutralisation versus Ionomer Blend Composition

Measurement of the relationship between blend composition and degree of neutralisation was important in order to verify the predicted mass balance equation, and to investigate the homogeneity of the material prepared by reactive extrusion.

Nominally, Nucrel 960 and Surlyn 8920 have the same mass percentage of methacrylic acid comonomer. Assuming this to be true, a mass balance on sodium ions gives the following expression relating degree of neutralisation and mass fraction Surlyn 8920 in the blend:

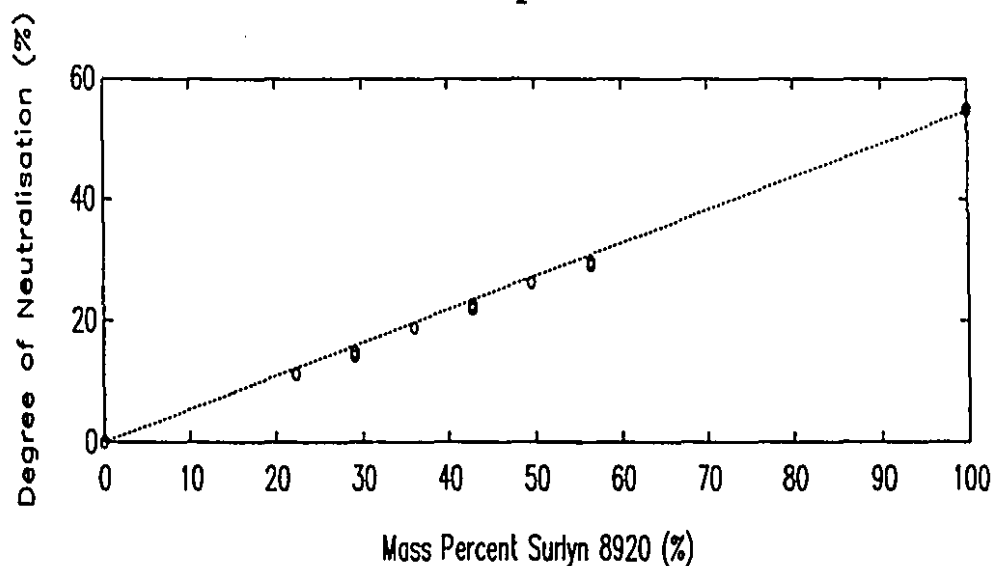
$$D_B = D_S \times m_S \quad (54-1)$$

¹ Nucrel and Surlyn are registered trademarks of the DuPont Company of Wilmington, Delaware.

² Irganox is a registered trademark of Ciba-Geigy Ltd.

where D_b is the percent degree of neutralisation of the blend, D_s is the percent degree of neutralisation of the highly neutralised ionomer (Surlyn 8920), and m_s is the mass fraction of Surlyn in the blend. This expression was used in preparing the ionomer blends. Figure 54-1 summarises the blend titration data.

Figure 54-1: Degree of Neutralisation as a Function of Ionomer Blend Composition.



Legend: (o) Titration results, (•••) expected relationship based on mass balance.

It was found that the linear model of Equation 54-1 did not fit the data adequately. An examination of the titration data revealed that the mass percentages of acid comonomer in the Nucrel and Surlyn reactants were not the same. The Nucrel had (16.7 ± 0.1) mass % methacrylic acid, while the Surlyn had (16.1 ± 0.1) mass % methacrylic acid. This caused the actual

degree of neutralisation of the blends to be lower than expected, because the number of acid sites was underestimated. It is also possible that a titration bias error, due to the difficulty in identifying the titration end point contributed to the observed deviation of the data from the linear model. In any event, a quadratic model was found to fit the data adequately.

$$D_B = 0.0005M_S^2 + 0.5019M_S - 0.1315 \quad (54-2)$$

where D_B is the degree of neutralisation (%) of the blend and M_S is the mass percent of Surlyn 8920 in the blend. This model was used throughout the balance of the research to relate degree of neutralisation to composition.

An analysis of the variances of titration, sample and blend repeats revealed that the composition of the blends varied $\pm 0.15\%$ within a compounding run. Balke (1986) attributes this type of composition inhomogeneity to the segregation of tumble blended components in an extruder's feed hopper. The analysis of variance also showed that blend repeats were marginally different. The confidence interval for blend repeatability was $\pm 0.33\%$. This was attributed to errors in blend preparation. (Titrations were found to be repeatable with $\pm 0.05\%$.)

5.5 Viscosity versus Degree of Neutralisation

Knowledge of the viscosities expected for the range of compositions of interest was necessary for designing the shear stress transducer, for defining the process operating space and for evaluating potential control problems.

The viscosities of a selected subset of the blends described in Section 5.3 were measured using a sliding plate melt rheometer (SPR). The SPR has been described in detail by Giacomini (1986). Blends with degrees of neutralisation of 0, 14.9, 22.0, 29.3 and 54.7 % were studied. The 14.9, 22.0 and

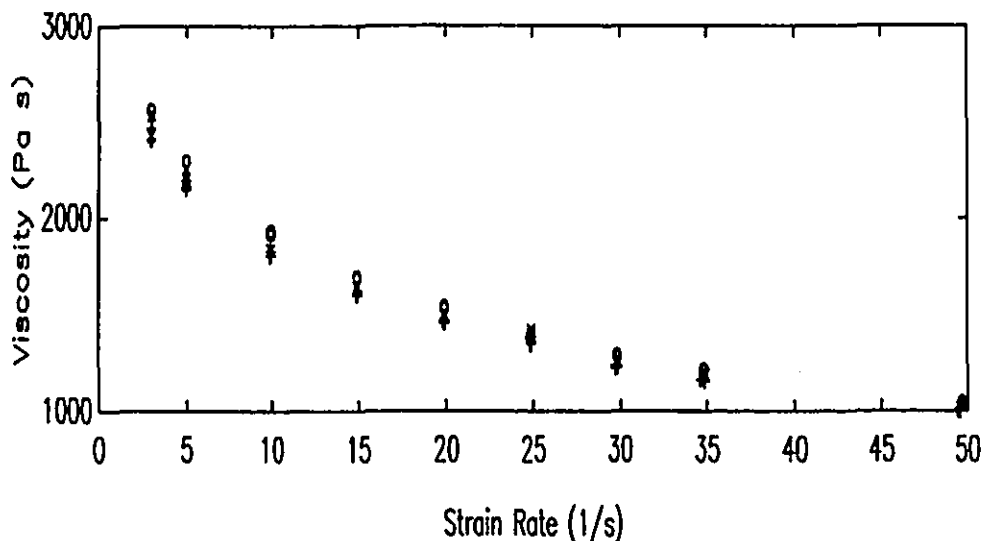
29.3 % blends were studied at 3 or 4 temperatures.

Figure 55-1 shows three replications of the viscosity versus strain rate curve for the 29.3 % neutralised ionomer blend at 175°C. The level of reproducibility illustrated in this figure is typical of all of the ionomer viscosity data. Confidence limits calculated from the means of the three tests at each strain rate are shown in Table 55-1. These confidence limits imply experimental errors ranging from 7 to 10%, expressed as a percentage of the mean. The experimental error expected with the SPR, from extensive experience with a polypropylene melt, is 3 to 5%.

The most important source of ionomer viscosity variability is moisture plasticisation. It is well known that moisture decreases the viscosity of ionomers. Figure 55-2, taken from DuPont Company product literature, shows the effect of moisture on the melt index of Surlyn 8920. This figure suggests that the viscosity of Surlyn 8920 decreases from approximately 12800 Pa s ($\sim 1.5 \text{ s}^{-1}$) at 200 ppm moisture to 5100 Pa s ($\sim 3.8 \text{ s}^{-1}$) at 5000 ppm moisture. Briefly, the ionic segments of ionomer chains associate together to form "clusters" (Eisenberg (1970)). This unique cluster morphology is responsible for the increased viscosity of ionomers. Water molecules interfere with the ionic interactions, reducing ionomer viscosity. Bazuin and Eisenberg (1981) give a succinct explanation of this phenomenon.

In recognition of this problem, the standard practice was to dry the ionomer blend sample in a vacuum oven at 62°C for 12 to 24 h prior to testing. If samples were not used immediately, they were stored in a desiccator until needed. The drying procedure was re-evaluated after persistently large experimental errors were encountered. The results of the investigation are presented in Figure 55-3. This figure shows that the viscosity of the undried sample is higher than the viscosities of the samples dried for 12 and 24 h. The dried sample viscosities agree well among themselves.

Figure 55-1: Viscosity of the 29.3 % Neutralised Ionomer Blend at 175 °C: three repeats.



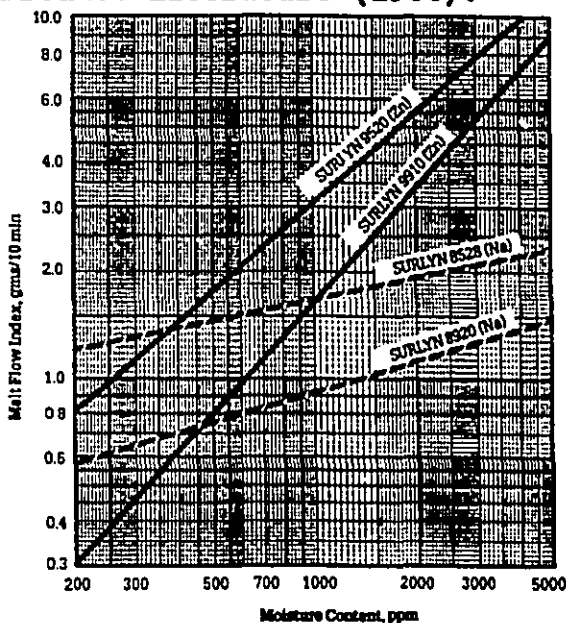
Legend: (x) 1990 April 17, (o) 1991 January 24, (+) 1991 January 29.

Table 55-1: 95% Confidence Intervals Expressed in Units of Viscosity and as a Percent of the Mean for the Data Presented in Figure 55-1.

	Strain Rate (1/s)								
	3	5	10	15	20	25	30	35	50
95% Confidence Limits (Pa s)	200	203	182	126	113	58	87	80	63
Percent Error (% of mean)	8.0	9.1	9.8	7.6	7.5	4.2	6.9	6.7	6.2

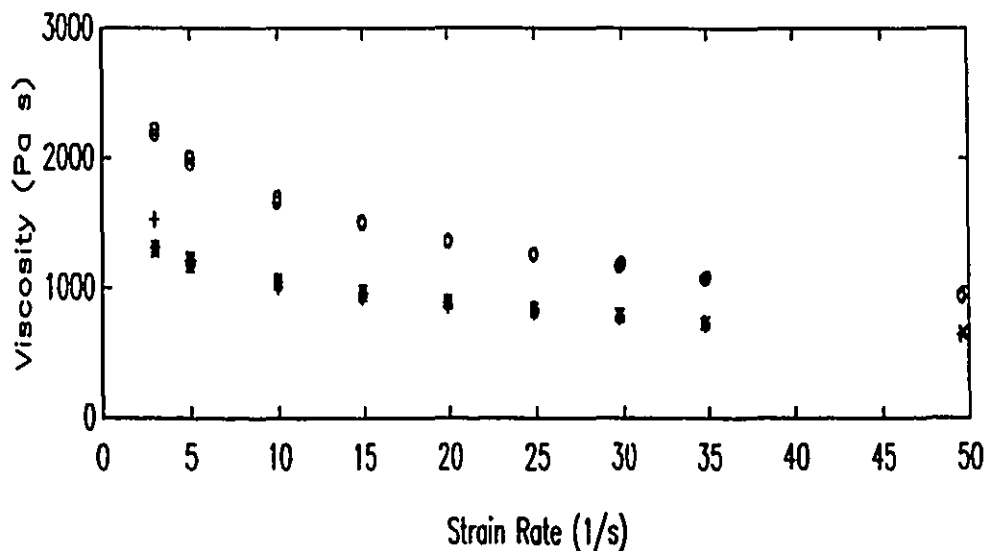
This evidence suggests that the "drying" procedure actually humidified the ionomer samples and that the samples were probably saturated with moisture after 12 h in the oven. It follows that samples dried at different times of the year, at different ambient humidities, would have different moisture levels and therefore different viscosities. Ideally, a dryer

Figure 55-2: Moisture Content versus Melt Flow Index for SURLYN® Ionomer Resins. From DuPont Company Product Literature (1986).



Legend: (-) Zinc Neutralised Ionomer, (- -) Sodium Neutralised Ionomer.

Figure 55-3: Illustration of the Effect of the "Drying" Procedure. Viscosity of a 22 % Neutralised Ionomer Blend at 180 °C.



Legend: (o) Undried sample, (x) sample dried for 12 h, (+) sample dried for 24 h.

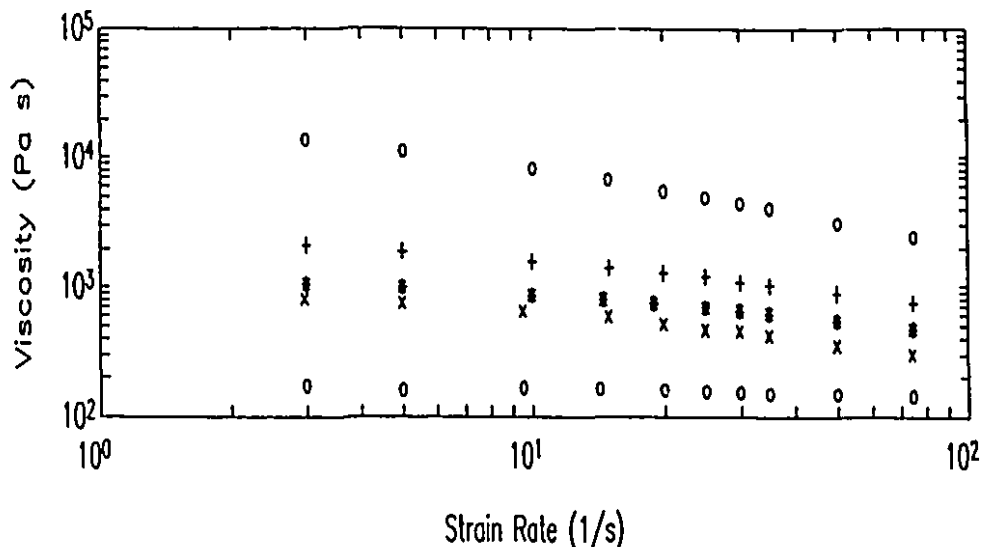
using hot, bone dry air should have been used, but one was not available. However, it was concluded that the "drying" (humidifying) method employed offered some advantage by reducing the potentially large variability of viscosity due to moisture plasticisation.

Other potential sources of experimental uncertainty in measuring ionomer viscosity were: i) small differences in composition, ii) composition inhomogeneity, iii) processing history differences, iv) thermal or oxidative degradation, and v) temperature control variability. The variability attributed to these sources was insignificant compared to the large variation attributed to the moisture effect.

Figure 55-4 shows viscosity versus strain rate curves at 180°C for 5 compositions with degrees of neutralisation of: 0, 14.9, 22.0, 29.3 and 54.7%. The data show that the copolymer has a low, almost constant viscosity, while the viscosity of the blends increases dramatically with degree of neutralisation. Also, the viscosity curves show progressively stronger shear-thinning behaviour with increasing degree of neutralisation. These data indicate that the shear stress transducer must be sensitive to as little as 500 Pa and as much as 200,000 Pa in order to measure viscosities over the whole range of compositions.

The viscosities measured at 5, 15 and 30 s⁻¹ are plotted against the degree of neutralisation in Figure 55-5a. This figure shows that at low strain rate, the viscosity can increase dramatically, especially at degrees of neutralisation higher than 30%. (The curves shown in this figure are arbitrary cubic polynomials and are shown only to highlight trends.) Controlling the degree of neutralisation over such a nonlinear operating space is very difficult. Furthermore, because the viscosity changes so dramatically, no single set of extrusion conditions will work satisfactorily for all compositions. As a result, degrees of neutralisation below 30% were studied in this work. Also, given the measurement

Figure 55-4: EMAA Ionomer Blend Viscosity for Five Blend Compositions at 180 °C.

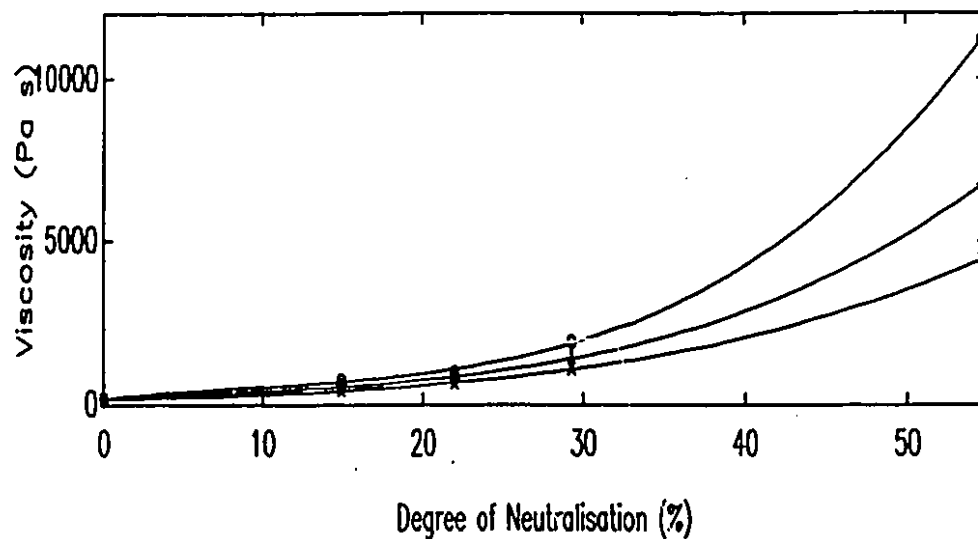


Legend: (o) Unneutralised EMAA copolymer, (x) 14.9% neutralised ionomer, (*) 22.0% neutralised ionomer, (+) 29.3% neutralised ionomer, (o) 54.7% neutralised ionomer.

repeatability limits discussed in Section 4.4, the extrusion difficulties encountered with the very low viscosity copolymer and ionomers and the problems encountered in feeding very small rates, a lower operating limit of 15% neutralisation was adopted.

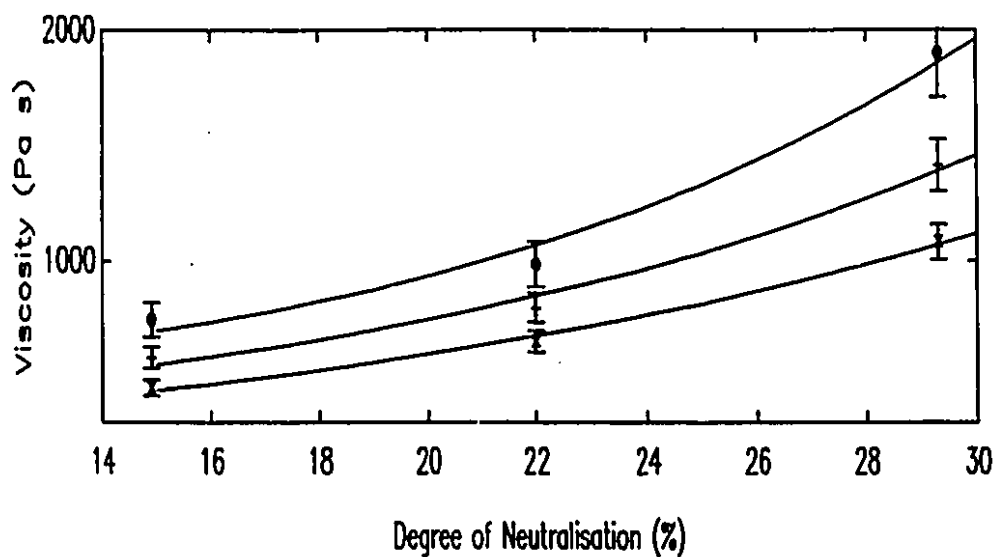
Figure 55-5b shows the viscosity versus composition curves at 5, 15 and 30 s⁻¹ for compositions within the defined 15 to 30 % neutralisation operating range. The viscosity at 5 s⁻¹ is still markedly nonlinear in this range, but the large change in viscosity with composition (or process gain) offers a greater potential for resolution of composition with viscosity measurements. On the other hand, the viscosity versus composition relationship at 30 s⁻¹ is closer to being linear, although the process gain is smaller.

Figure 55-5a: Viscosity versus Degree of Neutralisation at 5, 15 and 30 s^{-1} at 180 $^{\circ}C$.



Legend: (o) 5 s^{-1} , (+) 15 s^{-1} , (x) 30 s^{-1} , cubic polynomials were fitted to the data and plotted to highlight the trends.

Figure 55-5b: Viscosity versus Degree of Neutralisation at 5, 15 and 30 s^{-1} : Selected Composition Range

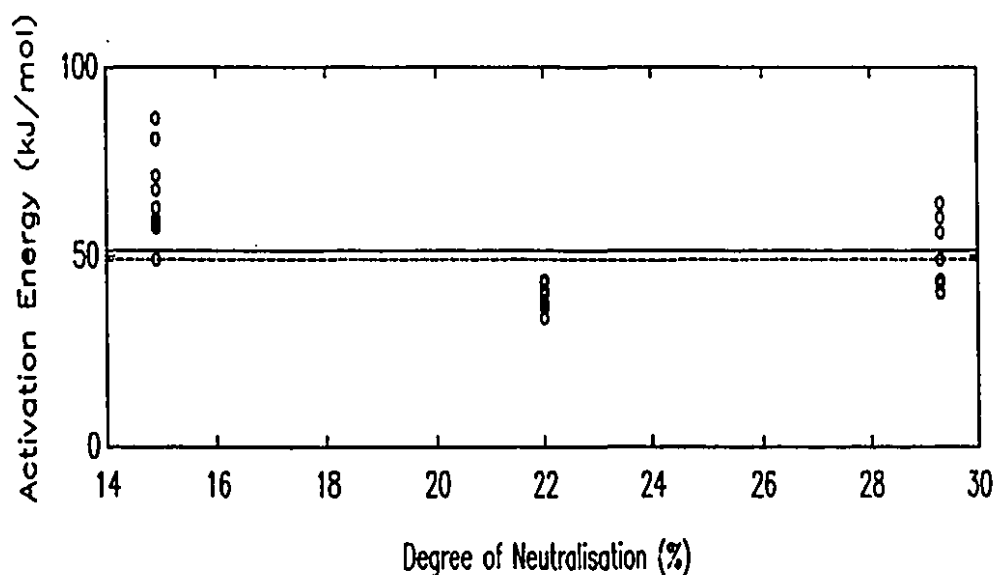


Legend: (o) 5 s^{-1} , (+) 15 s^{-1} , (x) 30 s^{-1} , cubic polynomials were fitted to the data and plotted to highlight the trends.

5.6 Viscosity versus Temperature

An Arrhenius expression for correcting ILR viscosity measurements for small deviations in temperature is presented in Section 2.4.3. An estimate of the activation energy for flow was needed in order to use this expression. The viscosities of three of the ionomer blends (14.9, 22.0 and 29.3 % neutralisation) described in Section 5.3 were measured at 4 or 5 temperatures, using the sliding plate rheometer. Flow activation energies were calculated for each blend at strain rates ranging from 3 to 50 s^{-1} . The results are plotted in Figure 56-1.

Figure 56-1: Activation Energy for Flow Calculated at Three Degrees of Neutralisation.



Legend: (o) Experimental data, (-) mean of all data points, (- -) data of Sakamoto et al. (1970)

This figure shows a broad scatter of results at each composition. This is due to the fact that the activation energy was a decreasing function of strain rate for each blend. This is expected, given that the strain rate range of

interest lies in the transition zone between the constant viscosity and power law portions of the viscosity curve. Also, the mean value of the activation energy for each composition was different, suggesting a functional relationship between activation energy and composition. Given the large uncertainty in the viscosity measurements introduced by moisture plasticisation (discussed in Section 5.4) and the effect of strain rate, a functional relationship between activation energy and strain rate or composition was not attempted. A single mean activation energy of 51,000 J/mol was used for all compositions and strain rates. This value compares favourably with the results of Sakamoto et al. (1970), who studied a very similar material over comparable conditions and reported a value of 49,400 J/mol.

CHAPTER 6

CONTROL OF ETHYLENE-METHACRYLIC ACID NEUTRALISATION

6.1 The Challenges of Ethylene-Methacrylic Acid Neutralisation Control

The goal of EMAA neutralisation control is to minimize the variation in product Melt Index (ASTM-1238). According to Ogunde (1991), an acceptable level of product MI variation is ± 10 %. Varnell (1988) has summarized the disturbances affecting the commercial production of EMMA ionomers. The most significant factors, in order of decreasing importance, are:

- 1) Changes in EMAA copolymer molecular weight. EMAA copolymers are prepared in batches. While batches are blended to minimize variation, batch related differences in molecular weight cause the largest disturbances in the EMAA ionomer process.
- 2) Changes in methacrylic acid content. The MAA content of EMAA copolymers can vary by as much as 0.5 mass %.
- 3) Changes in neutralising agent concentration.

Additional known disturbances are:

- 4) Changes in moisture content. Ionomer viscosity is affected by moisture. Variations in residual or adsorbed moisture can cause product viscosity to vary independent of a change in degree of neutralisation.
- 5) Changes in residual MAA content. EMAA copolymer may contain as much as 0.05 mass % of unreacted MAA. Free MAA reacts more readily than the bound MAA and will consequently lead to an under-neutralised copolymer. This is a small effect, and is typically masked by the aforementioned ones.

Since viscosity is the key property indicating ionomer performance, four out of five of the above disturbances will be correctly compensated by a composition change based on a viscosity measurement. However, the current experimental

apparatus has no independent measurement of ionomer moisture content and consequently, moisture disturbances cannot be controlled properly.

Evidence presented in earlier chapters offers some insight into neutralisation dynamics. The viscosity versus degree of neutralisation data presented in Section 5.5 indicate that the process gain will be nonlinear. The viscosity control work of Pabedinskas et al. (1989) suggests that the dynamics may be operating point dependent and the works of Pabedinskas et al., Curry et al. (1988) and Fritz and Stöhrer (1986) all suggest that the dynamics may be asymmetric, though the direction of the asymmetry is unclear.

6.2 Dynamic Characterisation of the Extruder plus ILR System

The response of the ILR as a viscosity sensor, the dynamics of the reactive extrusion and the dynamics of the system including the gravimetric feeders, the extruder and the rheometer are all essential pieces of information in developing a control strategy. A controller can be developed and tuned using knowledge of the combined system dynamics but, knowledge of the individual reactor and measurement dynamics is essential for developing advanced control techniques, for placing sensors in the best location and for optimizing the process design for improved control.

It is often difficult to separate process and sensor dynamics in practice. The approach taken in this work has been to identify the dynamics of the extruder plus rheometer system and to infer the individual extruder and rheometer dynamics with the aid of results of a parallel study on extrusion.

6.2.1 Viscosity Step Change Test Experiment Design

The reactive extrusion system dynamics were studied using step tests. A step change in polymer feed ratio was

introduced by the gravimetric feeders, and the viscosity response was observed with the ILR. The goal of the step tests was to provide information from which an empirical process model could be derived. Pseudo-random binary signal (PRBS) tests were not used because the viscosity signal was found to be too noisy and because the dynamics were expected (and found) to be asymmetric.

The viscosity step change tests were designed to elucidate the effects of throughput, test strain rate and ionomer composition. Throughput (or flowrate) has a significant effect on the response of the extruder. For example, the mean residence time, and consequently, the reaction time, in the extruder is a function of throughput. Also, the transportation time delay incurred by pumping polymer through the rheometer body is affected by throughput. Throughputs of 8 and 12 kg/h were chosen for study. Considered in this choice were the need to test dramatically different feed rates moderated by the compromises posed by gravimetric feeder minimum rates and maximum extruder torque limits.

In choosing the strain rate for the viscosity measurement for control, the benefits of the increased viscosity versus composition sensitivity of low strain rate tests (see Section 5.5) had to be weighed against the improved repeatability (Section 4.4) offered by high strain rate tests. Tests were performed at 5 and 30 s⁻¹ with occasional tests at 15 s⁻¹ to determine the best strain rate for measurements used in control.

Ionomer compositions giving blends with degrees of neutralisation in the range of 15 to 29% were chosen. The viscosities of blends with degrees of neutralisation greater than 30% increased very dramatically, making operation at a single set of extruder operating conditions difficult. Also, it was recognised that control would be difficult in this very nonlinear operating region. Minimum feed rate limitations

governed the lower 15% neutralisation limit. Extruder torque capacity at the chosen operating temperature and screw speed determined the upper 29% neutralisation limit. Equation 54-2 was used to related the degree of neutralisation to mass percents of the two polymer reactants. Because of the nonlinear viscosity versus composition relationship, viscosity step tests of 3, 6 and 12% neutralisation were performed. Also, both upward and downward steps were performed at each composition. This served two functions. First, it identified asymmetric responses. Second, it verified that the process returned to its initial steady state value.

A total of 43 experiments were performed using various combinations of the above parameters. This included repeats of certain experiments. Each experiment, consisting of an upward and downward step, was initiated only after the rheometer had reached thermal equilibrium at the operating conditions. The total time for an experiment was approximately 1 hour. The ILR signal was sampled every 10 s.

6.2.2 First Order plus Dead Time Model Fitting Procedure

Each viscosity step change test consisted of a step to a new composition and then a step back to the initial composition. First and second order plus dead time models were fitted to each experiment using the following procedure:

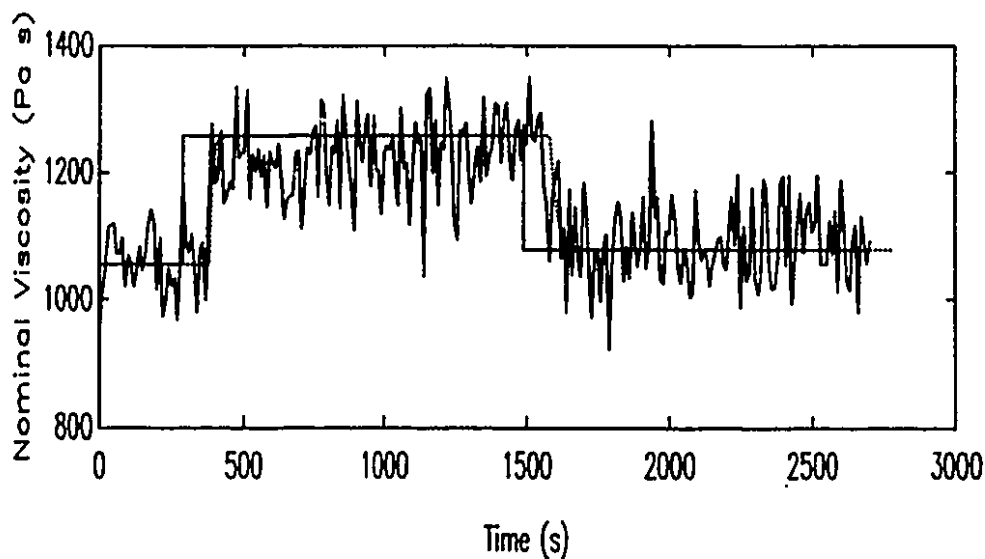
- 1) Mean viscosity values were calculated for the steady state plateaus in the data record. The viscosity data were then normalized by dividing through by the lower of the two mean values.
- 2) A range of possible dead times, in integer numbers of the sampling period, was selected by inspection.
- 3) First and second order models were fitted by nonlinear regression (function "FMINS" of Matlab(1990)).
- 4) The adequacy of the fitted models was examined by plotting the residuals and by comparing the mean squares of both first and second order models. First order plus dead time models

fit adequately to all but a few of the data sets.

The repeatability of the ILR signal limited the success of the model fitting procedure. As described in Section 4.4, repeatability of low strain rate measurements was poor. This is illustrated in Figures 62-1a, b, and c. Figure 62-1a shows the response of a 3% neutralisation step, measured at 5 s^{-1} , over the 26 to 29% neutralisation (high end) range. The solid line represents the ILR signal, the step change in composition is indicated to facilitate identification of the dead time and the dotted line represents the first order model fitted to the data. Clearly, the signal is so noisy that the dynamics of the step change is obscured. The 6 and 12% neutralisation steps shown in Figures 62-1b and c were large enough to be observed over the noise.

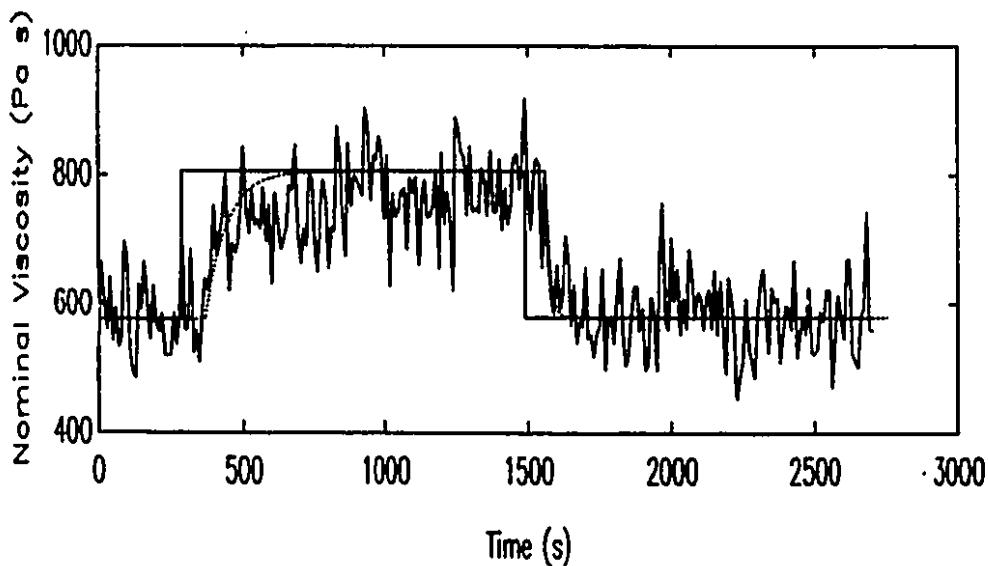
Figures 62-2a,b and c show step change responses monitored at 30 s^{-1} for 3, 6 and 12% neutralisation steps respectively. The magnitude of the ILR signal noise is considerably smaller at 30 s^{-1} and as a result, the steps were much easier to model unambiguously. Table 62-1 clearly illustrates the improvement in the rheometer's ability to discriminate a 3% neutralisation step as the test strain rate increases. The column entitled "signal" gives the change in viscosity observed for a 3% neutralisation step at the low end of the operating range. To estimate the signal noise, standard deviations of the viscosity signal were computed over steady-state periods of the step tests for each strain rate. The signal to noise ratio was calculated by dividing the viscosity change by two times the 95% confidence interval.

Figure 62-1a: Nominal Viscosity at 186°C and 5 s⁻¹ versus Time: 3% Neutralisation Steps.



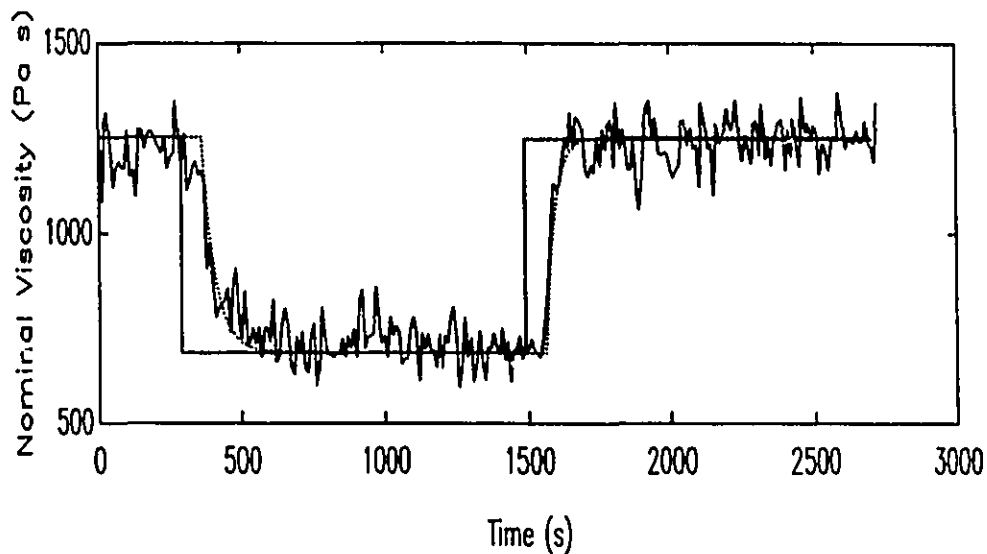
Legend: (-) ILR Signal and Composition Steps, (···) first order plus dead time model.

Figure 62-1b: Nominal Viscosity at 186 °C and 5 s⁻¹ versus Time: 6% Neutralisation Steps.



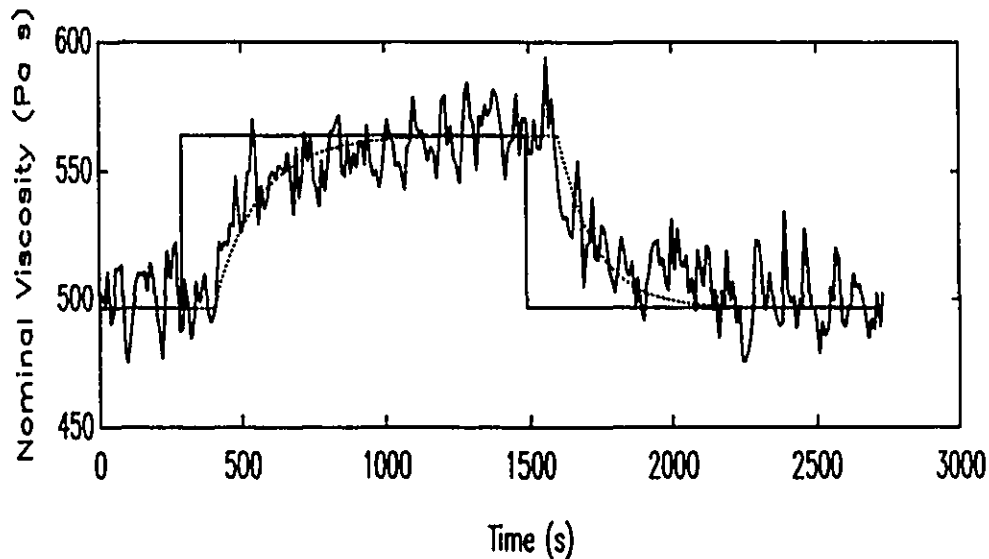
Legend: (-) ILR Signal and Composition Steps, (···) first order plus dead time model.

Figure 62-1c: Nominal Viscosity at 186°C and 5 s⁻¹ versus Time: 12% Neutralisation Steps.



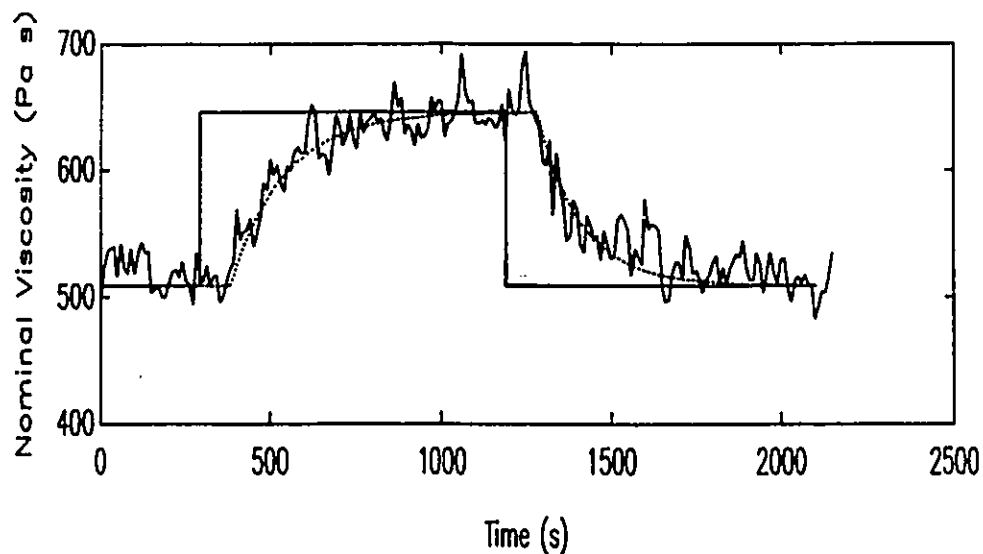
Legend: (-) ILR Signal and Composition Steps, (•••) first order plus dead time model.

Figure 62-2a: Nominal Viscosity at 186°C and 30 s⁻¹ versus Time: 3% Neutralisation Steps.



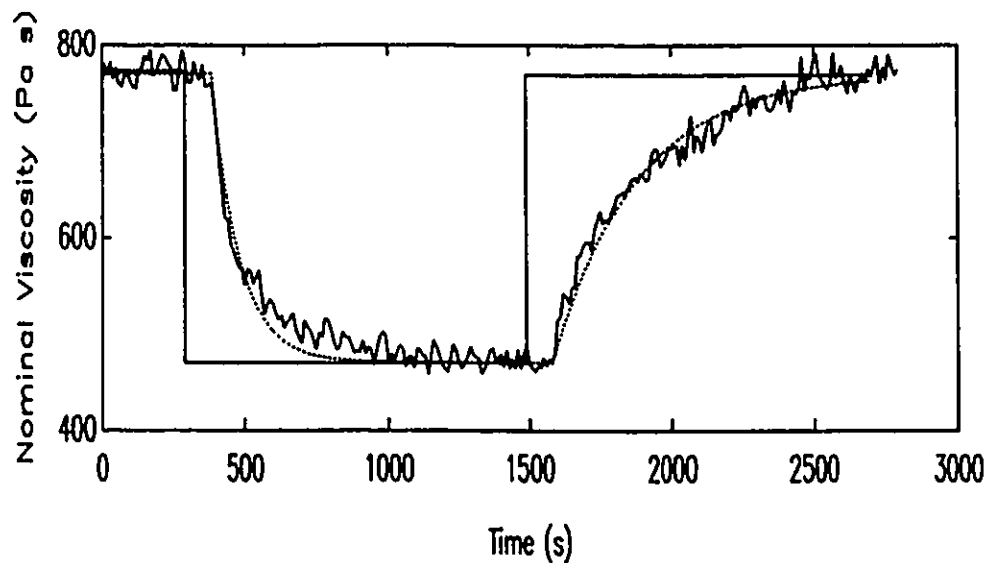
Legend: (-) ILR Signal and Composition Steps, (•••) first order plus dead time model.

Figure 62-2b: Nominal Viscosity at 186°C and 30 s⁻¹ versus Time: 6% Neutralisation Steps.



Legend: (-) ILR Signal and Composition Steps, (•••) first order plus dead time model.

Figure 62-2c: Nominal Viscosity at 186°C and 30 s⁻¹ versus Time: 12% Neutralisation Steps.



Legend: (-) ILR Signal and Composition Steps, (•••) first order plus dead time model.

Table 62-1: Summary of the Expected Change in Viscosity and the Mean ILR Signal Noise as a function of Strain Rate.

	Signal	Noise	S/N
Strain Rate [s ⁻¹]	Change in Viscosity associated with a 3% Neut. Step [Pa s]	Mean Standard Deviation of Viscosity Signal [Pa s]	Viscosity Change Divided by 2 Confidence Intervals
5	93	62	0.38
15	58	25	0.58
30	50	11.5	1.09

Two effects are illustrated in this table. The noise (signal standard deviation) clearly decreases with increasing test strain rate. However, the change in viscosity with composition, or, in other words, the ease with which a composition change can be seen by observing viscosity also decreases with increasing strain rate. Despite this effect, the 30 s⁻¹ measurements were considerably more useful in monitoring the viscosity steps because of the improved signal to noise ratio.

6.2.3 Dead Time

Table 62-2 summarises the dead times fitted to the step test data. The only significant trend observed in these data was the expected dependence of the dead time on throughput. A small decrease in dead time with increasing viscosity (see Chen (1992)) was also expected, but not observed because of signal noise. Unfortunately, it is difficult to model the dead time as a function of throughput and viscosity because the degree of fill of the extruder,

which is an essential term of such a model, is an unknown function of throughput and viscosity.

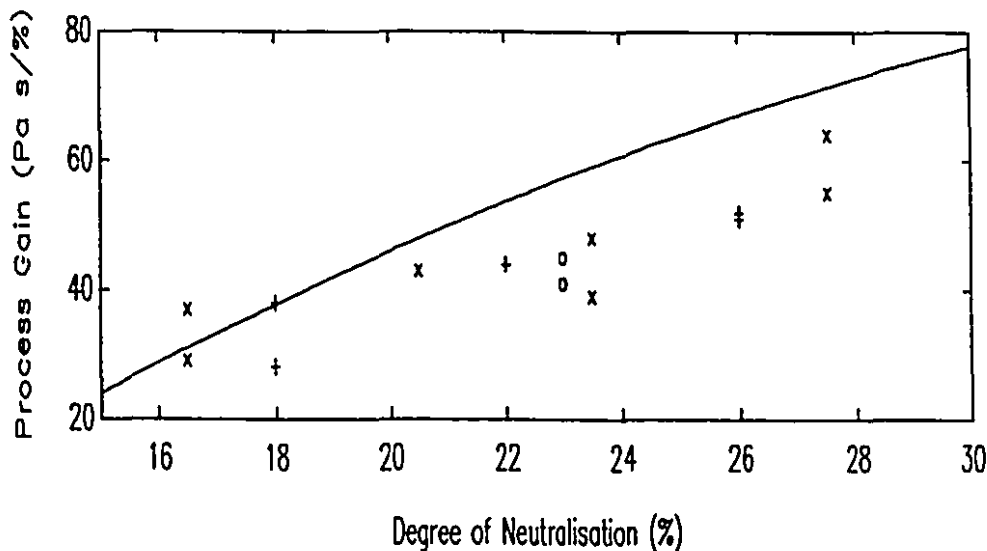
Table 62-2: Summary of Dead Times fit to Viscosity Step Change Data.

Through-put (kg/h)	Mean Dead Time (s)	Std. Dev. (s)	Range (s)	Mode (s)
8	10.22	1.78	8 to 13	10
12	8.55	1.48	7 to 12	8

6.2.4 Process Gains

The process gain represents the ultimate change in viscosity resulting from a unit change in degree of neutralisation. The process gains calculated for the viscosity step change tests are summarised in Figure 62-3 for steps monitored at 5 s^{-1} and in Figure 62-4 for steps monitored at 30 s^{-1} . Three (x), six (+) and twelve (o) percent neutralisation steps studied at 8 and 12 kg/h are summarised together. They are plotted against the mid-point of the composition range of the step. For example, the gains of the 15 to 18% neutralisation steps are plotted at 17.5% while the gains of the 17 to 29% neutralisation steps are plotted at 23%. It was recognised that plotting the data in this way introduces a bias, especially for the 12% steps but, given the scatter of the data, it was felt that this bias would not affect the interpretation of the data. The solid lines plotted in Figures 62-3 and 62-4 represent the expected process gains. These curves were derived from the SPR data of Section 5.5. The polynomial (cubic) curves fitted to the viscosity-degree of neutralisation data in Figure 55-4a were differentiated to give an approximate process gain versus composition relationship.

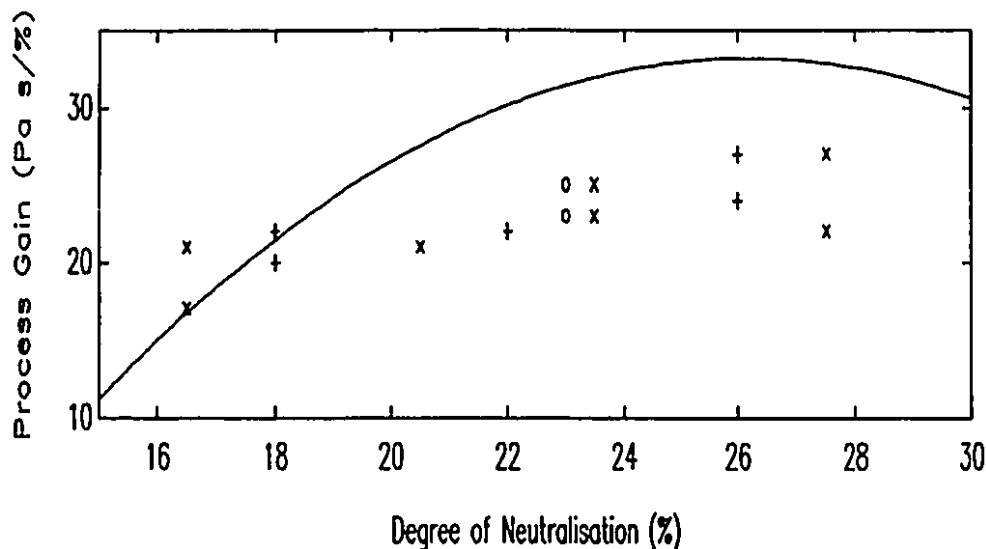
Figure 62-3: Process Gain as a Function of Degree of Neutralisation for 5 s^{-1} Viscosity Measurements.



Legend: (x) process gain estimated from 3% neutralisation steps, (+) process gain estimated from 6% neutralisation steps, (o) process gain estimated from 12% neutralisation steps, (-) differentiated viscosity data measured with SPR (see Figure 55-4a).

Prior to plotting, the process gain data were examined and found to be independent of throughput. However, Figures 62-3 and 62-4 clearly show that the gain, as measured with the ILR, is a sensitive function of operating point at 5 s^{-1} but, at 30 s^{-1} , the gain is effectively independent of operating point given the scatter in the data. (There is a hint of an increasing gain with operating point in this case, but it is insignificant.) The curves developed from the SPR data suggest that the gains should be strong functions of operating point. The ILR measured gains fall below the SPR predicted gains at both 5 and 30 s^{-1} . There is a source of error, that will be discussed shortly, that contributed to this trend, however, it is proposed that it is due mainly to the effects of moisture plasticisation and shear modification as described in Section 4.3.

Figure 62-4: Process gain as a function of degree of neutralisation for 30 s^{-1} measurements.



Legend: (x) process gain estimated from 3% neutralisation steps, (+) process gain estimated from 6% neutralisation steps, (o) process gain estimated from 12% neutralisation steps, (-) differentiated viscosity data measured with SPR (see Figure 55-4a).

These two effects reduced the nonlinear increase in viscosity with composition. This offers both an advantage and a disadvantage. From the control point of view, a "less nonlinear" viscosity-composition relationship should be easier to control. However, from the quality control point of view, the moisture plasticisation and shear modification effects will necessitate the calibration of the in-line rheological measurements with laboratory data if the ILR data are to be used to determine final product quality.

The data presented in Figures 62-3 and 62-4 exhibit more scatter than expected given the sources of error described in Sections 4.3 and 4.4. Three additional sources of uncertainty were identified that contributed to this. Some uncertainty was due to the fact that the temperature compensation algorithm was not used during the step tests.

The decision not to use the temperature compensation algorithm arose from the fact that the rheometer temperature used in the compensation was read with a precision of only 1°C. When a change in temperature was measured, the compensation algorithm introduced an artificial step of 2 or 3% in the compensated signal. This step complicated the fitting of the first order models. It was observed that the temperature usually changed by only one degree, and never more than two degrees, throughout the course of an experiment. It was reasoned that, since the temperature changed little and the measurement precision was poor, the temperature compensation was not effective. Because it introduced the undesirable 3% step it was not used at all. Without temperature compensation, the viscosity step would be generally underestimated by 3% (or perhaps 6%) of the signal, resulting in process gains that are smaller than they should be.

Accumulated evidence has suggested that ignoring the pressure flow contribution to the strain rate (as explained in Section 4.3) was not strictly correct, and that in fact, there is a pressure flow contribution at high strain rates for even the low viscosity ionomers. This approximation contributed a pressure dependent bias error to the viscosity measurement of approximately 20 Pa s and may have introduced as much as a 5 or 10 Pa s uncertainty, (1 or 2% of the signal) to the process gain calculation.

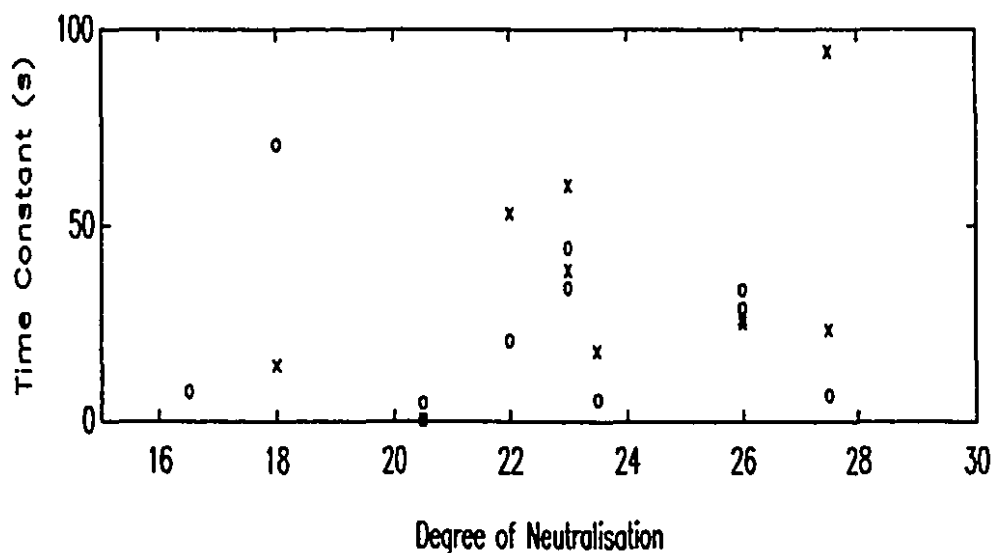
In a few cases, the composition step change was made before the viscosity was at a true steady-state. Generally, the rheometer and extruder were flushed for 15 to 25 minutes before the step, but, on these few occasions it is assumed that the shearing zone was not flushed adequately. This complicated the identification of the initial steady-state viscosity value and therefore added uncertainty to the gain.

6.2.5 First Order Time Constants

The time constants fitted to the viscosity step change tests described in Section 6.2.2 are summarised in Figure 62-5 for 5 s^{-1} viscosity measurements and in Figure 62-6 for 30 s^{-1} measurements. Time constants for 3, 6 and 12% neutralisation steps are plotted together, without differentiation. Steps to higher viscosity are represented by open circles (o); steps to lower viscosity are represented by crosses (x). As in the case of the process gain data, extruder throughput did not affect the process time constants.

Time constants could not be determined satisfactorily at 5 s^{-1} for 3% neutralisation steps because of the excessive noise. Figure 62-1a illustrates this problem. The noise amplitude is so large that it obscures the process

Figure 62-5: First Order Time Constants Determined from Step Tests at 186°C and 5 s^{-1} .

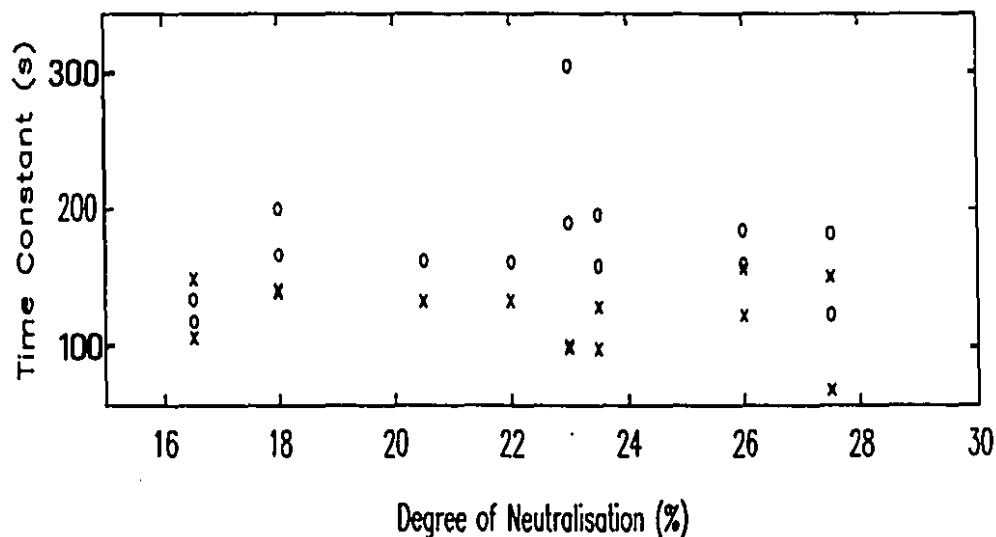


Legend: (x) time constants for steps to lower viscosities,
(o) time constants for steps to higher viscosities.

behaviour. Time constants in the range of 3 to 30 s were fitted and are clearly unreasonable given that the sampling period was 10 s. The larger percent neutralisation steps at 5 s^{-1} were fitted with more success. Time constants in the range of 40 to 60s were observed. [Examples of the models fitted to 6 and 12% neutralisation steps at 5 s^{-1} are shown with dotted lines in Figures 62-1b and 62-1c respectively.] However, because of the large experimental error, no trend with step direction, step size or composition could be identified.

The viscosity step tests monitored at 30 s^{-1} were considerably more informative. Figure 62-6 shows that 3 and 6% neutralisation steps between 15 and 29% neutralisation

Figure 62-6: First Order Time Constants Determined from Steps Tests at 186°C and 30 s^{-1} .



Legend: (x) time constants for steps to lower viscosities,
(o) time constants for steps to higher viscosities.

had time constants in the range of 120 to 190 s for steps to higher degrees of neutralisation (upward steps) while steps to lower degrees of neutralisation (downward steps) had time constants in the range of 90 to 150 s. The scatter in the

fitted time constants obscured any composition related trend. The upward 12% neutralisation steps had large time constants in the range of 200 to 300 s. Surprisingly, downward 12 % steps had time constants in the range of 90 to 100 s.

In addition to the sources of experimental uncertainty discussed up to this point, it was recognised that some uncertainty in the fitted time constants could be attributed to the deterioration of performance of the gravimetric feeders with time. This problem was controlled by periodic feeder controller recalibration.

Three conflicting trends are seen in the time constant data. First, smaller time constants were fitted to data measured at low strain rates. Ideally, of course, the time constant should be independent of strain rate but, in light of the relationship between strain rate and sample renewal in the shearing zone, one would expect that time constants would decrease with increasing shear rate. Second, upward step time constants were observed to be longer than downward step time constants. Fritz and Stöhrer (1986) explain that twin screw extruders pump highly viscous materials more effectively than low viscosity fluids. Consequently, a low viscosity fluid will be swept out more effectively by a high viscosity fluid leading to the conclusion that upward steps should be faster than downward steps. Finally, the time constant increases for 12% neutralisation upward steps, but it decreases marginally for 12% neutralisation downward steps. All of these observations suggest that the observed dynamics are representative of the viscosity measurement itself, rather than being representative of the reactive extrusion. This topic is explored in the next section.

6.2.6 Identification of Rheometer Measurement Dynamics

The data presented to this point show that the system response resembles a first order plus dead time model with

dead times in the range of 80 to 100 s, depending on extruder throughput, and a time constant in the range of 130 to 160 s for small viscosity steps at 30 s^{-1} . This response is comprised of contributions from: i) gravimetric feeder dynamics, ii) extrusion dynamics and iii) rheometer sampling and measurement dynamics. Feeder throughput responses to set point changes were studied and modelled as first order processes. Time constants in the range of 3 to 5 s were observed for set point changes of 1 to 4 kg/h, which correspond to the degree of neutralisation changes of interest in this study. The feeder response is clearly insignificant compared to the observed process response.

The feeder plus extruder dynamics can, in principle, be evaluated directly by collecting samples exiting the extruder during a viscosity transient. Viscosities could then be measured with a laboratory rheometer.

Unfortunately, the mass of sample required for laboratory analysis is too large. During a transient, a large enough sample for testing would not be homogeneous.

However, rheometer dynamics can be inferred. This is based on the assumptions that polymer neutralisation reactions are diffusion controlled and that the ionomer blends are adequately mixed in the extruder. The latter point was verified by the fact that viscosities of repeated compositions had the same viscosity when prepared at different screw speeds or at different throughputs (or residence times). Consequently, the dynamics of reaction must be equal to or less than the dynamics of mixing and therefore must be less than or equal to the residence time.

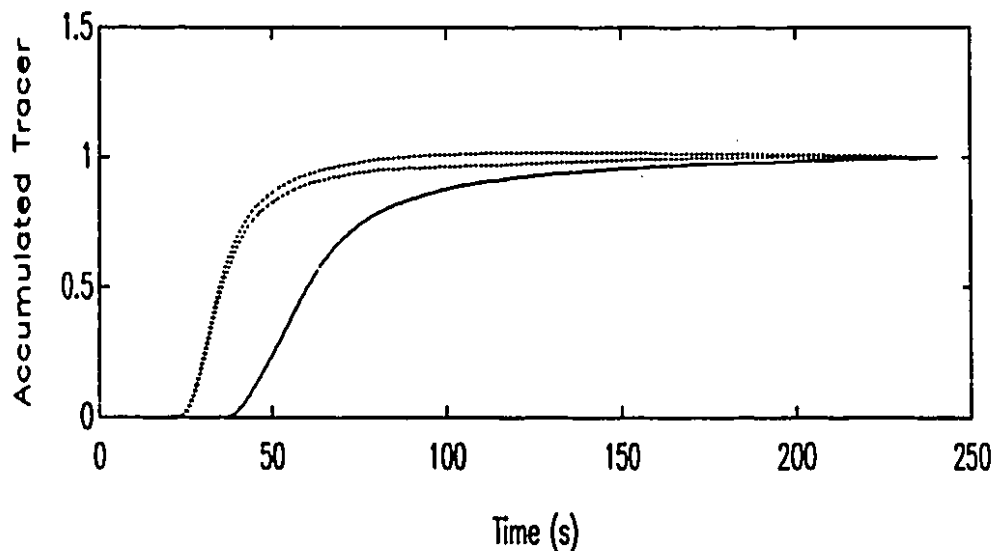
Chen (1992) has studied the residence time distribution (RTD) of the extrusion equipment used in this work. He performed RTD studies on the system with and without the ILR. Chen injected an impulse of carbon black tracer into the feed of the extruder and monitored the transmittance of laser light through the extrudate in a quartz-windowed cell.

He performed his experiments using a medium viscosity polypropylene resin and used a range of extruder screw speeds and throughputs.

There are a number of factors which limit the comparison of Chen's results with the viscosity step results of this study. First of all, changes in viscosity will affect mixing. Consequently, a constant viscosity composition change will not represent a viscosity transient exactly. Secondly, among the experimental difficulties encountered with his method, Chen (1992) found that the quartz-windowed cell contributed some measurement dynamics to his results.

Some residence time distributions (RTDs) measured by Chen, corresponding to a throughput of 12 kg/h and a screw speed of 300 rpm, are shown in Figure 62-7.

Figure 62-7: Residence Time Distributions for the Twin Screw Extruder with and without the ILR.



Legend: (-) RTD of Extruder plus ILR, (•••) RTD of Extruder alone, with repeat.

RTD curves for the system with and without the ILR are shown. Chen did not run the rheometer during his experiments. In his experiments, the rheometer acted simply as a conduit. The RTDs are plotted in cumulative form, portraying a composition step change. For comparison, the cumulative RTDs were fitted with second order plus dead time models. The results for the data of Figure 62-7, along with Chen's residence times are shown in Table 62-3.

Table 62-3: Summary of Statistics describing some Residence Time Distributions measured by Chen (1992)

Chen's Expt #	Rheometer	Mean Residence Time (s)	Dead Time (s)	Second Order Time Constants	
				T_1 (s)	T_2 (s)
DRTDF9	Removed	39.99	23.4	4.6	10.2
DRTDF10	Removed	40.47	23.4	2.8	14.0
DRTD11	Installed	70.4	37.6	6.1	26.6

These results show that, without the rheometer, the transportation delay in the extruder is approximately 23 s. The approximately 60 s difference between this result and the 80 s dead time observed during the ionomer step tests at 12 kg/h can be attributed to transportation through and sampling in the rheometer. The cumulative RTD with the rheometer indicates that flow through the ILR adds approximately 14 s of transportation delay. Keeping in mind that the drum is located mid-way along the flow in the rheometer, this suggests that a considerable delay, perhaps 50 to 55 s, is associated with sample exchange in the shearing zone and the subsequent viscosity measurement.

Table 62-3 also shows second order time constants fitted to the RTD curves. These data show that the mixing

dynamics in the extruder are very fast. Without the rheometer, the dominant time constant is in the range of 10 to 14 s. Flow through the ILR broadens the RTD and doubles the largest time constant to approximately 27 s. (The broadening of the RTD due to the flow in the ILR is also evident in the mean residence time increase from approximately 40 s to 70 s.) However, there remains a considerable difference between the cumulative RTD time constant (27 s) and the extrusion system dynamics identified by means of step tests at 30 s^{-1} (130 to 160 s). Although the viscosity change will modify the mixing in the extruder during an ionomer composition step, it is still clear that the dynamics of sampling the main stream, flushing the rheometer gap and performing the experiment dominates the system response.

Apparently the placement of the in-line rheometer has not eliminated the sampling delay problem. Some hints of the source of this delay were provided by the two dimensional, steady-state flow simulations presented in Section 2.2. These simulations showed that the material entering the shearing zone was the slow moving material flowing along the walls of the ILR channel. They also indicated large recirculation flows at the entrance and exit of the shearing zone that increased in size with increasing shearing speed. In the steady state, it is clear that the recirculation flows lengthen the flow path into the gap. It must be remembered, however, that the rotating drum is stopped during each measurement cycle in order to measure a baseline signal. Consequently, the gap entrance recirculation flows are always changing. The formation, elimination and change in size of the recirculation flows will clearly influence sampling (including shearing zone flushing) and measurement dynamics and may cause the observed response asymmetry or contribute to measurement noise. One way to confirm this hypothesis would be to

simulate the ILR flow in more detail, considering the starting and stopping of the shearing cylinder, the changes in viscosity and the complex, 3-D creeping flow situation. A more practical approach would be to eliminate the problem altogether by re-designing the rheometer. Cox and Dealy (1991) proposed a solution that involves constructing a cowl over most of the rotating drum. Only a small part of the drum at the entrance to the gap would be exposed.

It is recognized that much of the slow measurement dynamics and delay is due to the time consuming process of flushing the shearing zone by simple drag flow. This was discussed in Section 2.3. The only way to dramatically improve rheometer sampling is to flush the shearing zone positively. This is not a straightforward problem and is discussed in Section 7.1.

It is important to note that the extrusion system dynamics identified with measurements at 5 s^{-1} indicated faster responses of the same order of magnitude as suggested by the RTDs. This is not surprising in light of the results of the 2D flow simulations. They showed that the shearing zone entrance recirculation zones were smallest for low shearing rates. It is unfortunate that transducer signal noise precluded the use of viscosity measurements at 5 s^{-1} .

The evidence presented in this section demonstrates that the ILR's measurement time is probably too long to effectively monitor reactive extrusion dynamics. In fact, if Chen's extruder RTDs without the rheometer are considered like second order plus lead time step responses, it appears that the dynamics of the extruder is intrinsically difficult to control because the transportation delay in the extruder is of the same order of magnitude as the mixing dynamics.

Fortunately, the disturbances affecting EMAA neutralisation are of low frequency. A control system employing an ILR can still make an important improvement to EMAA ionomer quality by identifying and eliminating these

slow disturbances. Faster disturbances, such as those caused by poor feeder performance will not be controllable by feedback control alone.

6.3 Proportional-Integral Control of EMAA Neutralisation

A proportional-integral (PI) viscosity control scheme was studied as a first step in evaluating the performance of the in-line melt rheometer (ILR) as a control sensor. PI control is effective in eliminating the drifting (non-stationary) types of disturbances characteristic of the EMAA neutralisation process. Furthermore, because PI control is well known and because PI reactive extrusion control has been studied by other research groups, it was implemented here as a reference case. The ILR provides discrete-time viscosity measurements, consequently a digital PI algorithm was employed.

6.3.1 Description of Control System and Control Algorithm

A schematic diagram of the EMAA neutralisation process was shown in Figure 52-1. It shows the essential process elements and data pathways. The personal computer (PC) executed the control program to sample shear stress, rotational drum speed and pressure drop in the rheometer at a frequency of 32 Hz throughout the duration of the viscosity test. Prior to a viscosity test, the PC polled the MACO 8000 for the rheometer temperatures. With these essential data, the viscosity and the control action were calculated. The feed rates were actuated by a signal from the PC, through the MACO, to the gravimetric feeder controllers.

Because of its inherent "reset windup" robustness, the velocity form proportional-integral (PI) controller was used. The PI algorithm used is:

$$\Delta u_t = K_c \times [(e_t - e_{t-1}) + \frac{\Delta T_s}{T_i} \times e_t] \quad (63-1)$$

where Δu_t \equiv change in the manipulated variable, or, in other words, the required change in the degree of neutralisation,

K_c \equiv the controller gain,

e_t \equiv the deviation from set point at the current time step,

e_{t-1} \equiv the deviation from set point at the previous time step,

ΔT_s \equiv the sampling period and

T_i \equiv the controller integral time.

Changes in degree of neutralisation commanded by the controller were converted to feed rates by means of the degree of neutralisation versus blend composition correlation of Equation 54-2. Re-arranged, this expression is:

$$M_{SURLYN} = 1000 \times [\sqrt{(0.5019 + 0.002 \times (D_{OP}N + 0.1315))} - 0.5019] \quad (63-2)$$

where $D_{OP}N$ is the desired degree of neutralisation in (%) and M_{SURLYN} is the required mass percent of Surlyn 8920 (the neutralising agent) in the blend. This expression calculates the percent of the total feed that must be neutralising agent in order to achieve the desired degree of neutralisation. The total feed rate was kept constant at 12 kg/h. This rate was chosen primarily to minimize the system dead time (see Section 6.2.3). Individual feed rates were constrained to avoid poor feeder performance (or shut down) at low feed rate set points and to avoid the upper neutralising agent feed rate limit which could cause an extruder over-torque condition. No maximum limit had to be

imposed on the EMAA copolymer (Nucrel 960) feed. If a constraint was met, the actual control action was recorded.

6.3.2 Selection of Controller Parameters

The viscosity measured at 30 s^{-1} was the controlled variable in all experiments. A control period of 80 s, equal to the process dead time, was selected. Integral time absolute error (ITAE) controller parameters for set point regulation and disturbance rejection were computed for the range of plausible process parameters using the expressions summarised by Smith (1972). For the purpose of estimating controller parameters, a process dead time of 120 s (80 s dead time plus one-half of the sampling period), a process gain of 21.7 (Pa s/% neutralisation) and process time constants of 130 and 160 s were used. These parameters are summarised in Table 63-1.

Table 63-1: Digital Proportional-Integral Controller Settings using ITAE Criteria (Smith (1972))

Parameter	Units	Parameter values for steps to higher viscosity	Parameter values for steps to lower viscosity
For Set Point Changes			
Controller Gain	%/Pa s	0.035	0.029
Integral Time	s	177	148
For Disturbances			
Controller Gain	%/Pa s	0.053	0.042
Integral Time	s	195	183

N.B. Controller gain units are (% neutralisation/Pa s)

6.3.3 Set Point Tracking Experiments

A series of experiments were performed in which 60 and 120 Pa s set point changes were commanded at high and low operating points within the range of 15 to 29% neutralisation. Steps of 200 Pa s were also used, which spanned most of the operating range. The 200 Pa s changes were repeated. The smaller set point changes were repeated in adjacent operating ranges. This provided both an estimate of repeatability and allowed more of the operating range to be investigated.

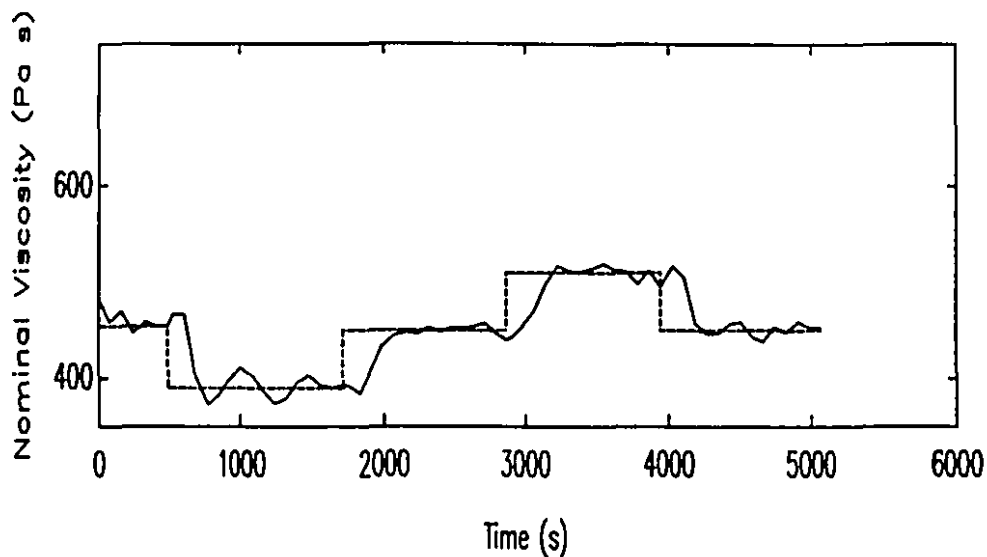
Examples of the results are plotted in Figures 63-1, 63-2 and 63-3. Figure 63-1 shows the nominal viscosity and the neutralising agent feed rate versus time for a program of 60 Pa s set point changes. Figures 63-2 and 63-3 show the nominal viscosity responses for set point changes of 120 and 200 Pa s respectively.

To quantify the performance of the PI controller, response times, defined as the minimum time required to first reach the new set point value, were calculated for each controlled response. The observed response times, summarised in Table 63-2, were found to be dependent on step direction and on step size.

Table 63-2: Summary of Observed Process Response Times with PI Control.

Viscosity Step Size [Pa s]	Response Time (s)	
	Steps to Higher Viscosity	Steps to Lower Viscosity
60	320 to 360	250 to 290
120	430 to 540	300 to 325
200	515 to 530	318 to 320

Figure 63-1a: Nominal Viscosity at 186°C and 30 s⁻¹:
60 Pa s Viscosity Set Point Changes.



Legend: (- -) viscosity set point, (-) ILR signal.

Figure 63-1b: Neutralising Agent Feed Rate versus Time:
Controller Response to Program of 60 Pa s
Viscosity Set Point Changes.

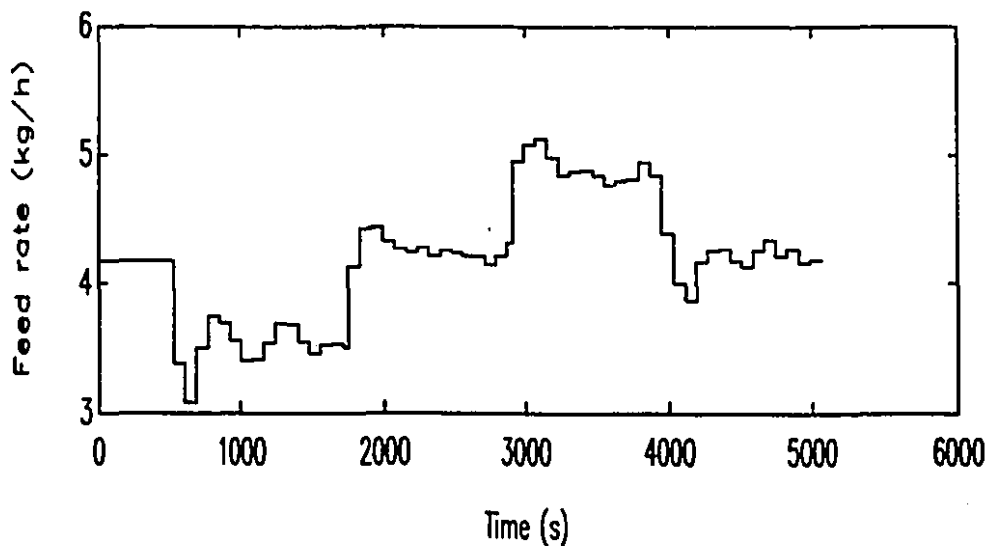
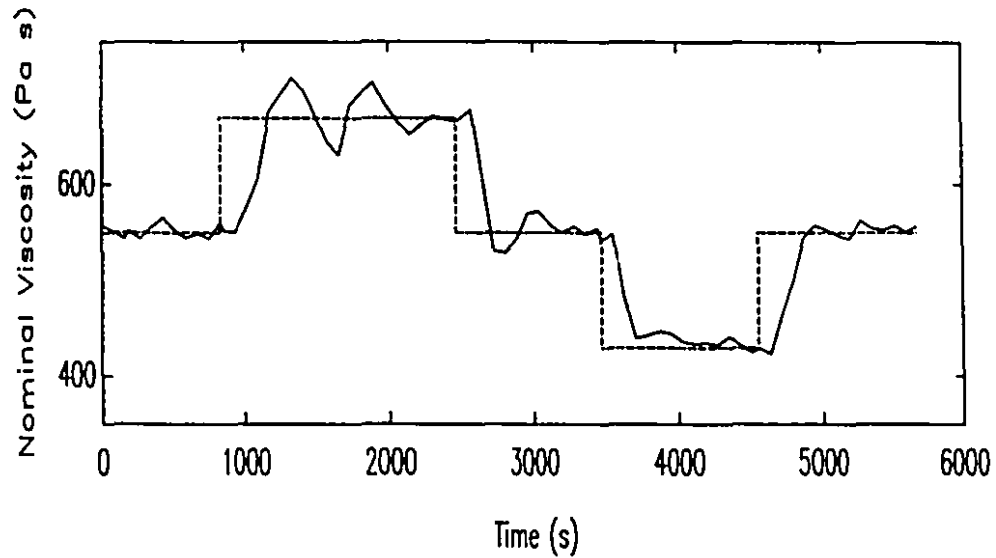
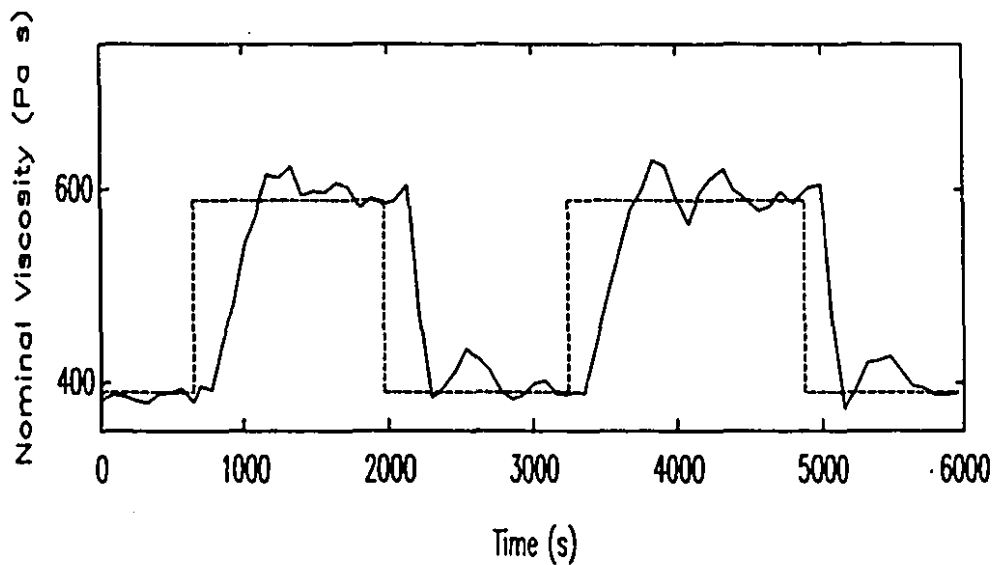


Figure 63-2: Nominal Viscosity @ 186°C and 30 s⁻¹:
120 Pa s Viscosity Set Point Changes.



Legend: (- -) viscosity set point, (-) ILR signal.

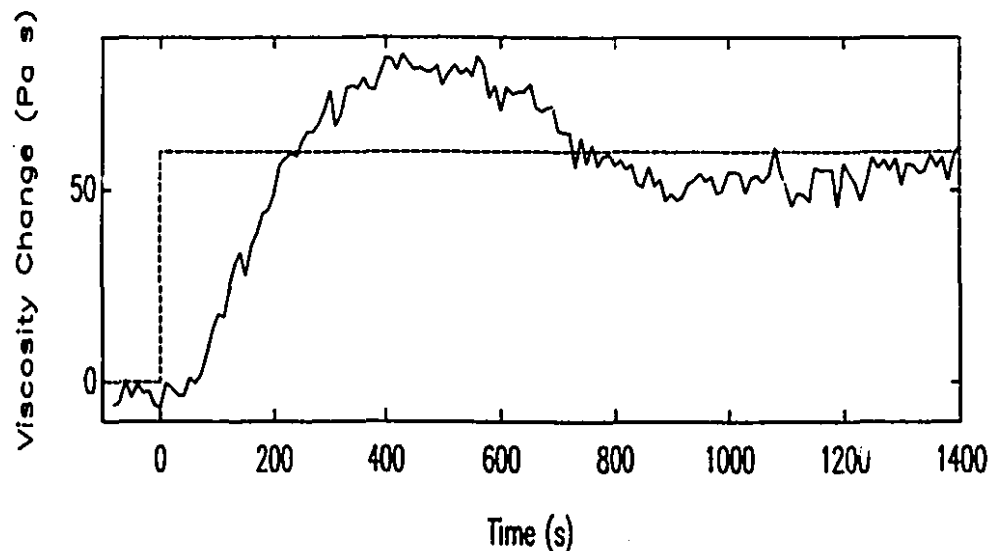
Figure 63-3: Nominal Viscosity at 186°C and 30 s⁻¹:
200 Pa s Viscosity Set Point Changes.



Legend: (- -) Viscosity Set Point, (-) ILR Signal.

To have a reference for comparison, the PI controller (Equation 63-1) and the process, as represented by the linear, discrete time model described in Section 6.4.1 (Equation 64-1), were simulated. The simulated process response to a 60 Pa s viscosity step is shown below in Figure 63-4. The simulation exhibits a response time of 255 s and an overshoot of 43%.

Figure 63-4: Simulated PI Controlled Process Response to a 60 Pa s Viscosity Set Point Change.



Legend: (- -) viscosity set point, (-) ILR signal.

The simulation agrees quite well with the response times of the experimental 60 Pa s set point steps to lower viscosity. The increase in rise time associated with the change in direction of the set point step was shown by simulation to be consistent with the 30 or 40 s increase in open loop upward step time constant. The further increase in response time observed with step size can also be attributed to increases in open loop process time constants with step size. First order time constants were fitted to the controlled responses and confirmed the response time

conclusions. They also showed that the controlled system responded considerably faster than the open loop response.

The PI controlled responses observed in this study are marginally better than the ones reported by Curry et al (1988) and are considerably better than the ones reported by Fritz and Stöhrer (1986) and Pabedinskas et al. (1989). This is attributed to the reduction of measurement delay when using the ILR.

Figures 63-1, 2 and 3 show that both damped and oscillatory responses were observed. The most dramatic oscillations were observed for set point changes at the high viscosity end of the operating range. Also, first order time constants fitted to the controlled 60 Pa s step responses at the high end of the operating range confirmed that the controller was acting much more aggressively in this region. This phenomenon may be explained by the suggested, but statistically insignificant increase in process gain at high degrees of neutralisation (Figure 62-4). This is consistent with the supposition that the controller gain, selected for a lower process gain, is too high and causes the oscillatory response.

Oscillations were also observed during steps to the lowest viscosity set point in Figure 63-1. This too is due to nonlinear process dynamics.

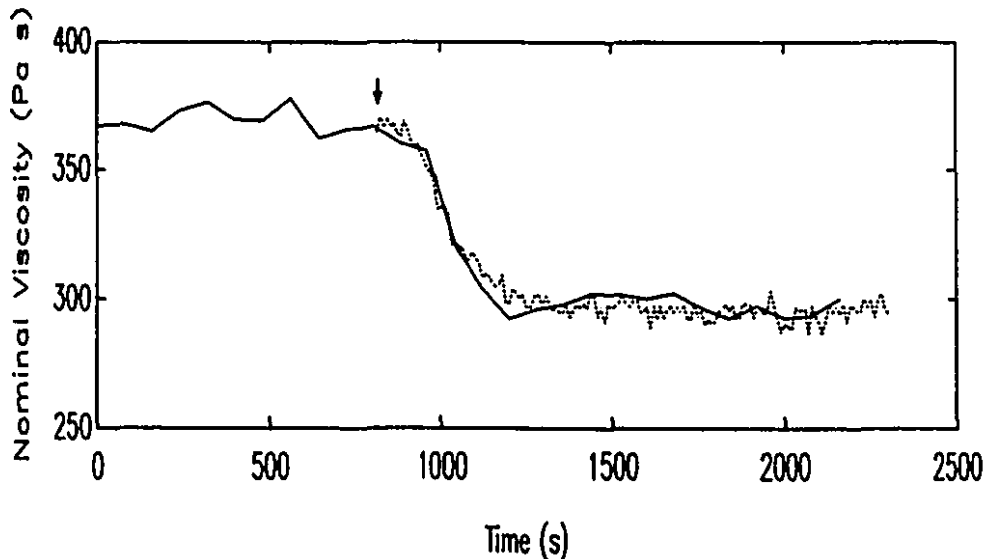
The period of the observed oscillations is difficult to quantify because of the viscosity signal noise. Periods ranging from 3 to 10 minutes were observed. These are consistent with the periods of oscillation observed during simulations of the process.

6.3.4 Disturbance Rejection Experiments

A number of different process disturbances were created to test the PI controller. The first series of tests represented a step change in neutralising agent (NA) activity. This was accomplished by blending some un-

neutralised copolymer (Nucrel 960) with the Surllyn 8920 neutralising agent (40:60 ratio by mass). The low activity NA was added to the feeder hopper after 10 or 15 minutes of controlled operation. The disturbance occurred after the feeder hopper had flushed its original charge. The solid line in Figure 63-5 illustrates the experimental open loop response. The low activity NA causes an approximate 70 Pa s drop in viscosity. The dotted line in Figure 63-5 represents a simulation of the disturbance. Because of the mixing of new NA pellets in the feed hopper with the existing higher activity ones, it was not possible to create a step disturbance. The simulated process input disturbance had to be adjusted until the simulated output matched the experimental one.

Figure 63-5: Nominal Viscosity @ 186°C and 30 s⁻¹:
Open Loop Response to a Neutralising Agent
Concentration Disturbance.



Legend: (-) Experimentally observed disturbance,
(...) simulated disturbance. Arrow indicates time
of disturbance.

The controlled response at this operating point, shown in Figure 63-6, exhibits a relatively large deviation due to the long process dead time. However, the process returned

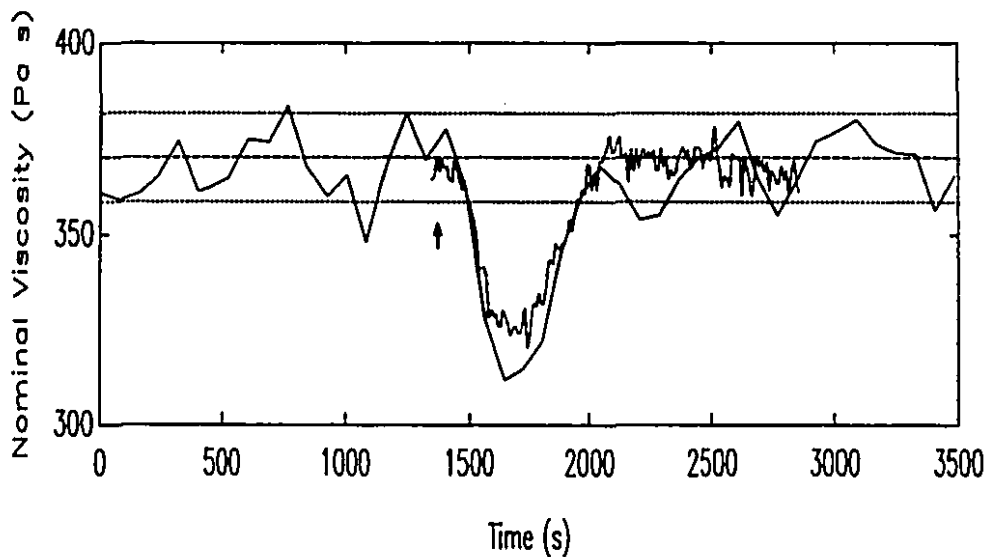
to its set point within 600 s. These experimental results are predicted reasonably well by the simulation (dotted line), confirming that the controller is operating as expected.

Figure 63-7 shows the response of the same type of disturbance at a higher viscosity operating point. Included in this figure is the response to the reciprocal disturbance; the high activity neutralising agent is re-introduced after the first disturbance is rejected. The two disturbance durations are 668 and 602 s respectively. This is in good agreement with the previous result. The second high activity NA disturbance caused a strongly oscillatory response. One reason for this is that there was a concomitant feeder error at the time of the disturbance that complicated the response. Process dynamics nonlinearity was another factor in the oscillatory response. A low activity NA disturbance forces the ionomer composition to low degrees of neutralisation. The controller reacts with the equivalent response to a set point change to higher viscosity. A high activity NA disturbance is controlled by a downward step in neutralising agent, which has been consistently observed to have the faster response.

The response times observed in this study are considerably faster than those reported by Fritz and Stöhrer (1986) and Pabedinskas et al. (1989). Again, this is attributed to the reduced measurement delay of the ILR.

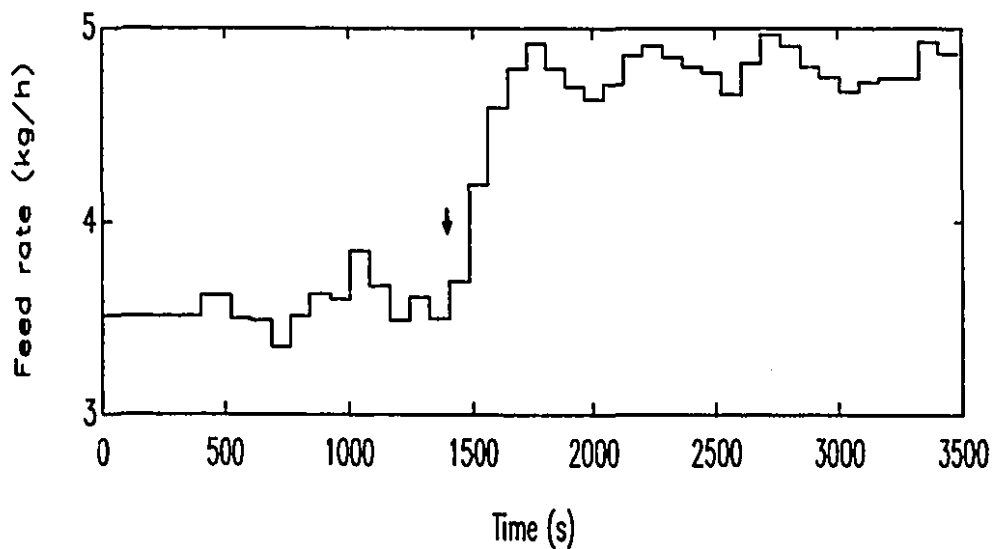
Small disturbances in neutralising agent activity and copolymer molecular weight were also studied. These disturbances were created by introducing Nucrel and Surlyn resins from a different lot. The response to these disturbances is shown in Figures 63-8. No visible perturbation to the viscosity is obvious, however proof that the ILR did sense a viscosity change is confirmed by the response of the controller in Figure 63-8b. This confirms

Figure 63-6a: Nominal Viscosity at 186°C and 30 s⁻¹:
Controlled Response to a Neutralising Agent
Disturbance. 15% Neutralisation Set Point.



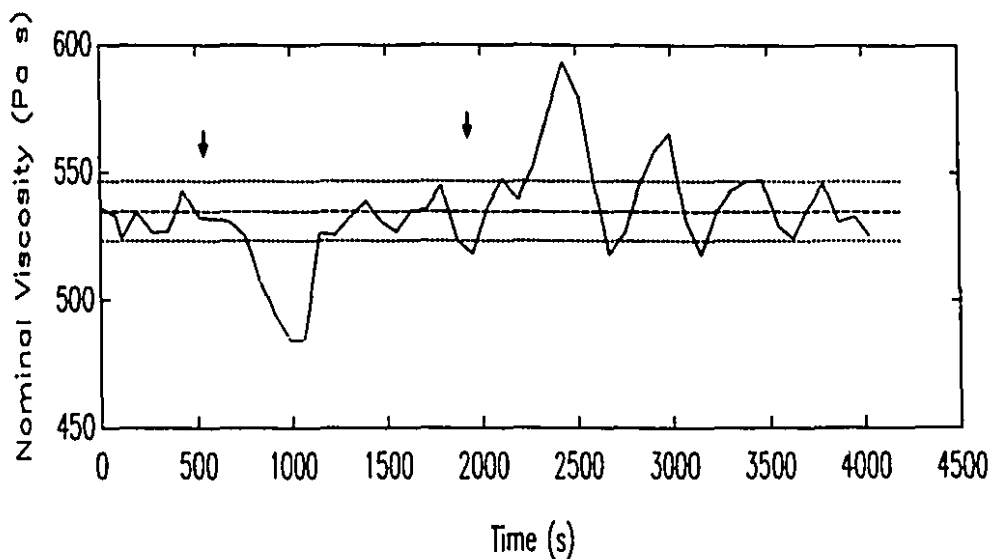
Legend: (-) Process response, (- -) set point,
(• -) simulated process response, (•••) ± 1
standard deviation.

Figure 63-6b: Neutralising Agent Feed Rate in Response to
the Neutralising Agent Concentration
Disturbance. 15% Neutralisation Set Point.



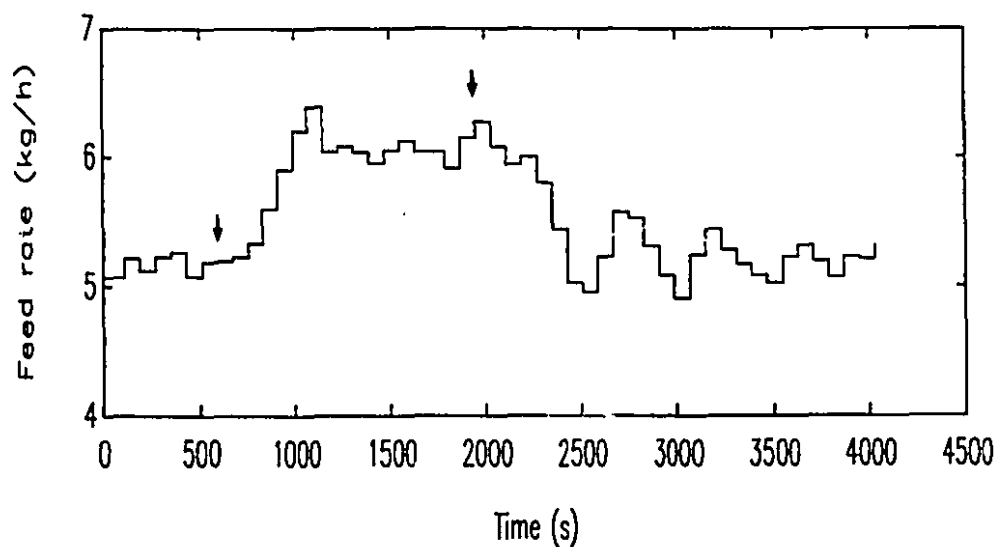
Legend: Arrow indicates time of disturbance.

Figure 64-7a: Nominal Viscosity at 186°C and 30 s⁻¹:
Controlled Response to two Neutralising Agent
Disturbances. 22% Neutralisation Set Point.



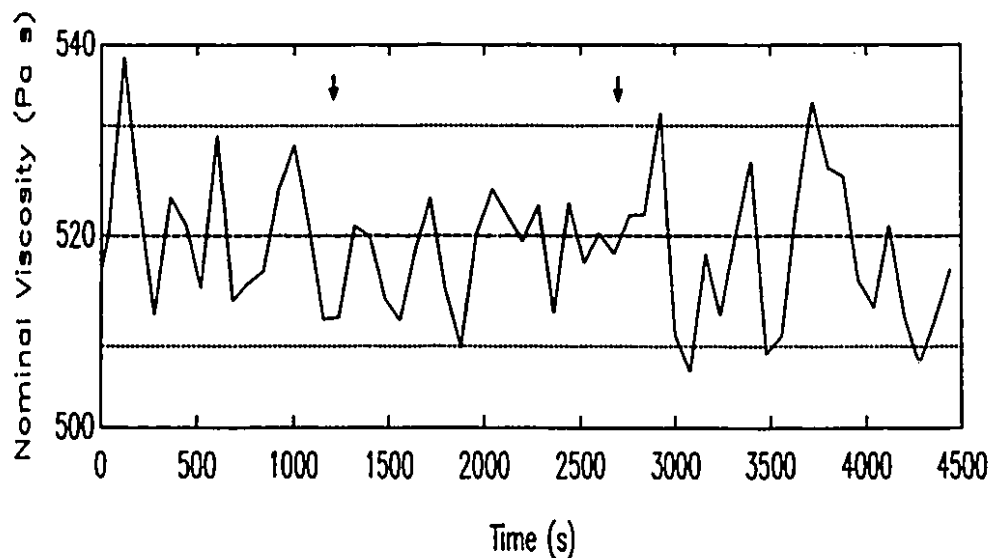
Legend: (-) Process response, (- -) set point,
(•••) ± 1 standard deviation.

Figure 63-7b: Neutralising Agent Feed Rate in Response to
the Neutralising Agent Concentration
Disturbance. 22% Neutralisation Set Point.



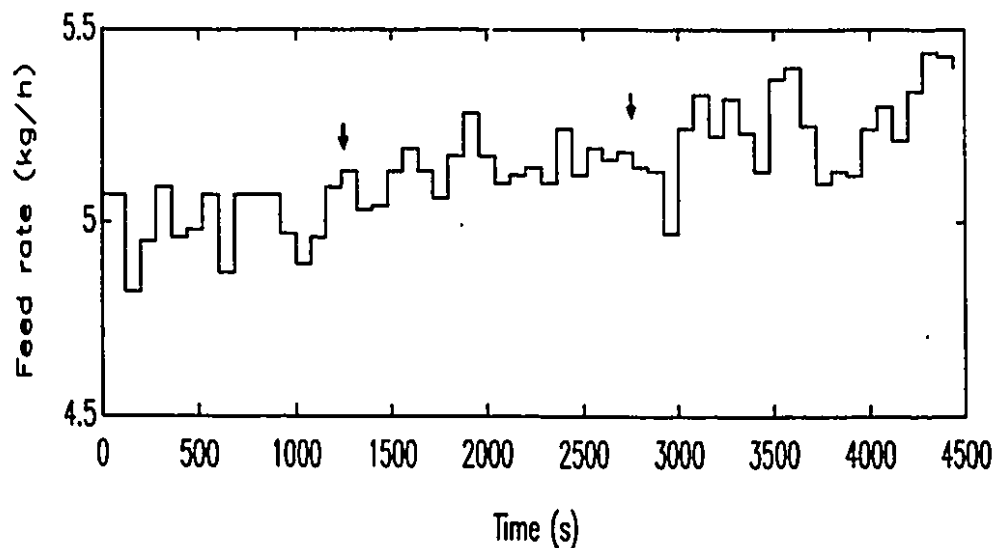
Legend: Arrows indicate times of disturbances.

Figure 63-8a: Nominal Viscosity at 186°C and 30 s^{-1} : Controlled Response to Subtle Neutralising Agent Concentration and Copolymer Molecular Weight Disturbances. 22% Neutralisation Set Point.



Legend: (-) Process response, (- -) set point, (···) ± 1 standard deviation.

Figure 63-8b: Neutralising Agent Feed Rate in Response to the Small Neutralising Agent Concentration and Copolymer Molecular Weight Disturbances.



Legend: Arrows indicate times of disturbances.

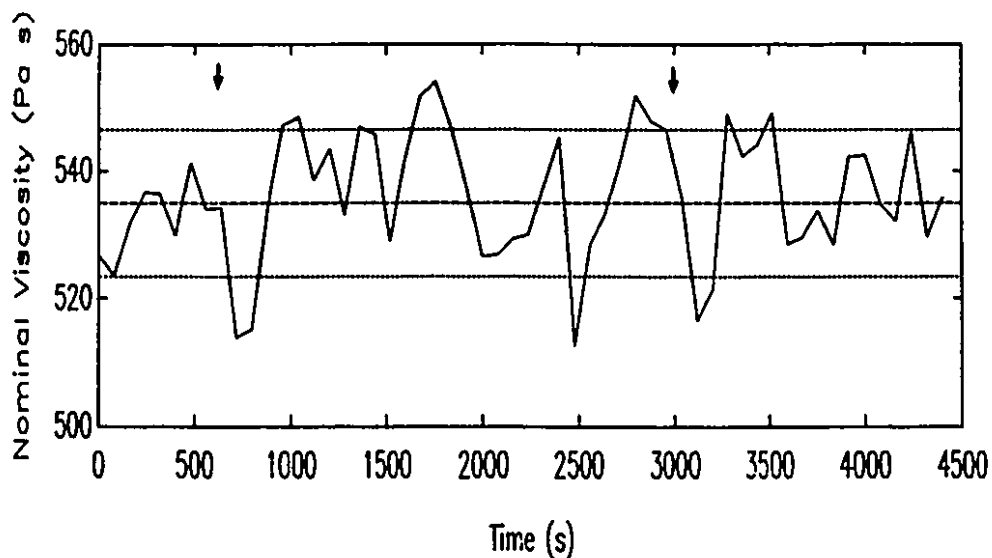
that the ILR and controller are capable of detecting and controlling small feed composition disturbances.

Finally, the PI controller was evaluated by introducing step changes in total feed rate. The purpose of these tests was to see how the controller would perform in response to the change in process dead time that accompanies a throughput change. An experiment in which the throughput was decreased from 12 to 8 kg/h, nominally increasing the process dead time from 80 to 100 s (see Section 6.2.3), is illustrated in Figures 63-9. Figure 63-9b shows the controlled neutralising agent feed rate as a function of time. The feed rate change occurs at approximately 1700 s. Figure 63-9a shows the nominal viscosity as a function of time. No perceptible deterioration in performance was observed. To test the controller, a disturbance impulse was introduced before and after the throughput change by adding a handful of copolymer to the feed hopper. The points at which the impulses were added are indicated with arrows in Figure 63-9a. The impulses and controller reactions are clearly visible in Figure 63-9b. The controller reaction appears to be no different after the throughput change. This result was predicted by the simulation results, which showed only a modest deterioration in controller performance with a process dead time increase. This experiment illustrated the controller's robustness to a disturbance that might be expected in the course of normal operation.

6.3.5 Comments on PI Control Effectiveness

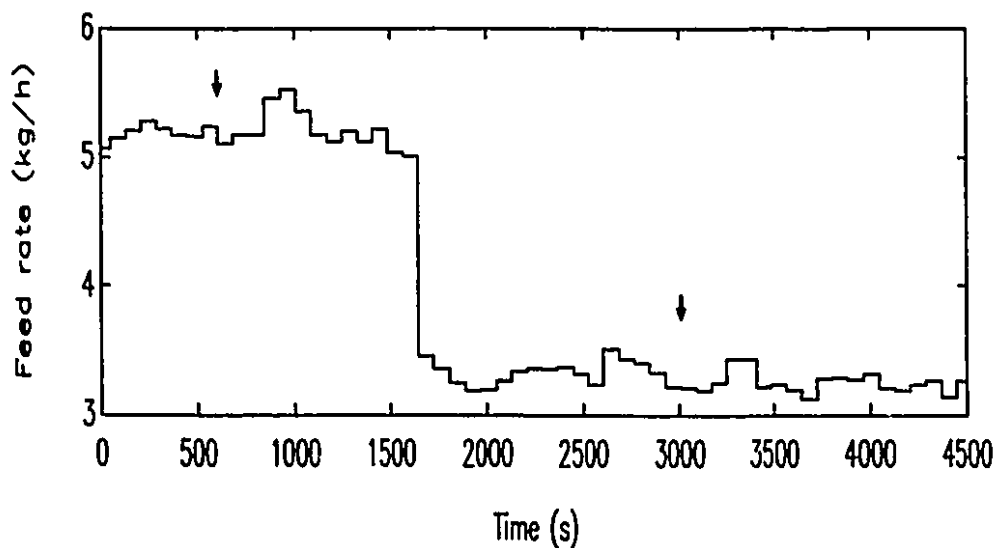
The PI controller, tuned using ITAE (Smith (1972)) criteria, performed well. Set point changes were tracked with response times in the range of 260 to 530 s. Disturbances were completely rejected in 10 to 11 minutes. This represents a considerable improvement in performance compared to the reactive extrusion studies of Fritz and

Figure 63-9a: Nominal Viscosity at 186°C and 30 s⁻¹:
Controlled Response to Impulse Disturbances
Introduced Before and After a Throughput
Change.



Legend: (-) Process response, (- -) set point,
(•••) ± 1 standard deviation.

Figure 63-9b: Neutralising Agent Feed Rate in Response to
Impulse Disturbances Introduced Before and
After a Throughput Change.



Legend: Arrows indicate times of impulse disturbances.

Stöhrer (1986) and Pabedinskas et al. (1989) and can be attributed to the favourable decrease in measurement delay.

Faster and more oscillatory responses to the downward steps at the two composition range extremes confirm that the process is nonlinear over the operating range. Gain scheduling or the use of nonlinear transformations such as those surveyed and used by Alison (1986) would address some of the nonlinear gain problems. The time constant asymmetry is believed to be due largely to rheometer sampling, as discussed in Section 6.2.6. Consequently, this issue should be addressed in the re-design of the rheometer.

6.4 Minimum Variance Control of EMAA Neutralisation

Two factors limiting the effectiveness of the PI viscosity control presented in the previous section were the long process dead time and the noise that contaminated the viscosity measurement. These problems can be addressed specifically using the stochastic control techniques developed for digital (sampled data) systems by Box and Jenkins (1976). These techniques are based on models of the process that include a noise and disturbance model. With careful selection of the noise model structure, the drifting (non-stationary) disturbances expected in the EMAA neutralisation process can be eliminated.

6.4.1 Minimum Variance Controller Structure and Parameters

MacGregor (1972, 1980) summarises the theory of minimum variance (MV) control. The objective of MV control is to minimize the variation of the process output, using knowledge of the process disturbances. The control algorithm is developed from a process model that accounts for both process dynamics and stochastic noise and disturbances. The technique described by MacGregor employs a time series model of the form described by Box and Jenkins (1976) to model the stochastic noise and disturbances.

The step test identification study presented in Section 6.2 indicated that the neutralisation process was well represented with a first order plus dead time model. To obtain a stochastic noise model, time series analyses were performed on selected step test data sets (30 s⁻¹ tests) representing small degree of neutralisation steps over the complete operating range. To remove the process dynamics and any non-stationarity (drift), the data were differenced once. Figure 64-1a shows a typical plot of the differenced data that illustrates the noise underlying the process dynamics. A plot of the autocorrelation function of the differenced data is given in Figure 64-1b. This analysis suggested that a first order moving average model (MA(1) model) describes the noise adequately. In a few of the data sets, higher order MA models were indicated and some autocorrelation plots exhibited sustained oscillations.

The step test data were collected with a sampling period of 10 s. Recognising that the controllers would operate with longer sampling periods, noise models were identified using time series with sampling periods of 20 and 30 s which were extracted from the original 10 s sampling time data. Noise models for different sampling and operating conditions are summarized in Table 64-1. These data show that a MA(1) model with parameter equal to -0.6 should represent the data adequately. These data also suggest that the MA parameter decreases in magnitude with operating point. It is also clear from the recorded model parameter standard deviations that as the sampling period increases, the model certainty decreases. This is because the number of data points decreases as the sampling period increases.

Figure 64-1a: Differenced Nominal Viscosity Signal
Illustrating the Underlying Noise

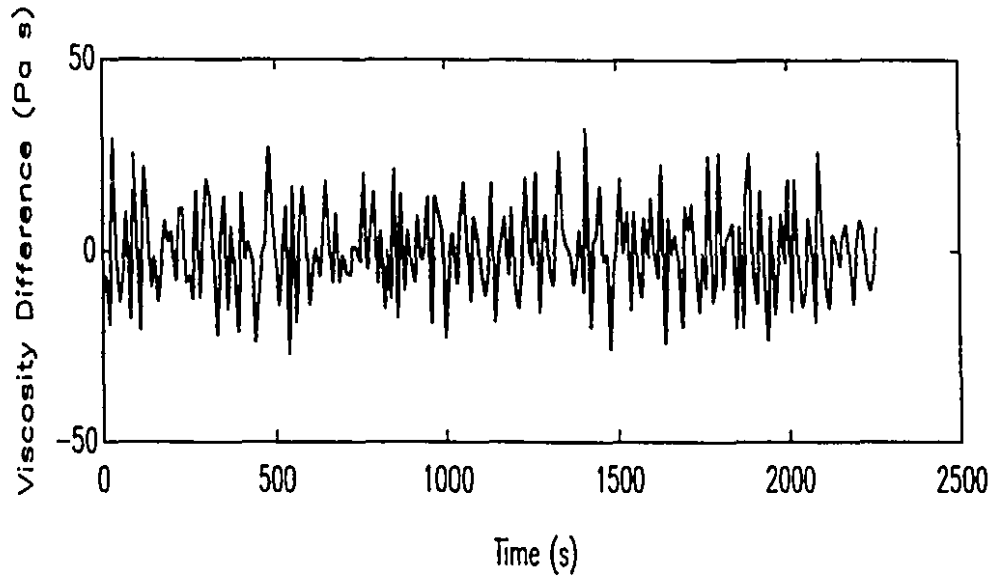
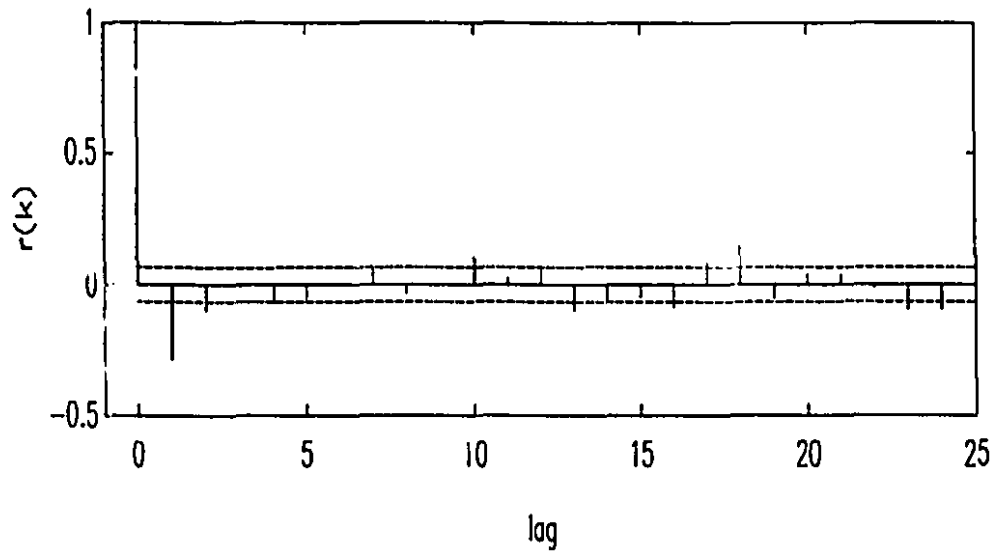


Figure 64-1b: Autocorrelations of Differenced Nominal
Viscosity Signal.



Legend: (--) ± 1 standard deviation

Table 64-1: Summary of Moving Average Noise Model Parameters

Operating Range (% to % Neutraln)	Moving Average Model Parameter					
	Ts = 10 s		Ts = 20 s		Ts = 30 s	
	θ	s	θ	s	θ	s
15 to 18	-0.6045	0.0573	-0.6535	0.0715	-0.5918	0.0921
19 to 22	-0.4090	0.0558	-0.6884	0.0614	-0.6274	0.08
22 to 25	-0.4655	0.0542	-0.5490	0.0712	-0.5266	0.0882
26 to 29	-0.4717	0.0624	-0.4515	0.0890	-0.4054	0.1106

Ultimately, the model chosen to represent the EMAA neutralisation process was a 1st order plus dead time with an integrated moving average, IMA (1), noise model. It is given in discrete form by Equation 64-1.

$$\Delta\eta = \frac{\omega_o}{(1-\delta z^{-1})} \times \Delta u_{t-d} + \frac{\theta}{(1-z^{-1})} \times a_t \quad (64-1)$$

where $\Delta\eta$ = the observed change in viscosity,

ω_o = the discrete process gain,

δ = the discrete process time constant,

Δu_{t-d} = the change in composition that was implemented d sampling times in the past,

θ = the noise model parameter,

a_t = the random number sequence with a mean of zero and a standard deviation of one, and

z^{-1} = the backward shift operator.

Minimum variance controllers derived from this specific process model are particularly useful. Palmor and Shinnar (1979) and Harris et al. (1982) have pointed out that such MV controllers are, in effect, digital PI controllers with

optimal dead time compensation and optimal signal filtering. In fact, the minimum variance controller derived from a first order, dead time plus IMA(1) noise model gives a controller that is identical to both the digital Smith predictor and the Dahlin controller formulations.

The control algorithm, taken from Palmor and Shinnar (1979) is:

$$\Delta u_t = -[1-\theta] \times \sum_{k=1}^d \Delta u_{t-k} + \left(\frac{1-\theta}{\omega_o}\right) \times (e_t - \delta e_{t-1}) \quad (64-2)$$

where Δu_t \equiv the control action, i.e. the required change in degree of neutralisation,

θ \equiv the noise model parameter [= -0.6],

Δu_{t-k} \equiv the control action at k time steps in the past,

d \equiv the number of sampling periods per dead time,

ω_o \equiv the discrete process gain (6.25),

δ \equiv the discrete process time constant (0.8),

e_t \equiv the process deviation from set point,

e_{t-1} \equiv the process deviation from set point at the previous time step.

This expression presumes that the dead time is an integer number of sampling periods. A sampling period of 30 s was adopted. This implies a 90 s process dead time. The actual dead time is 80 s plus one half of the 30 s sampling period to give 95 s. In light of the level of uncertainty, this 5s discrepancy was not considered significant. The change in degree of neutralisation computed with the control algorithm was converted to a neutralising agent flow rate using Equation 63-2.

6.4.2 Set Point Tracking Experiments

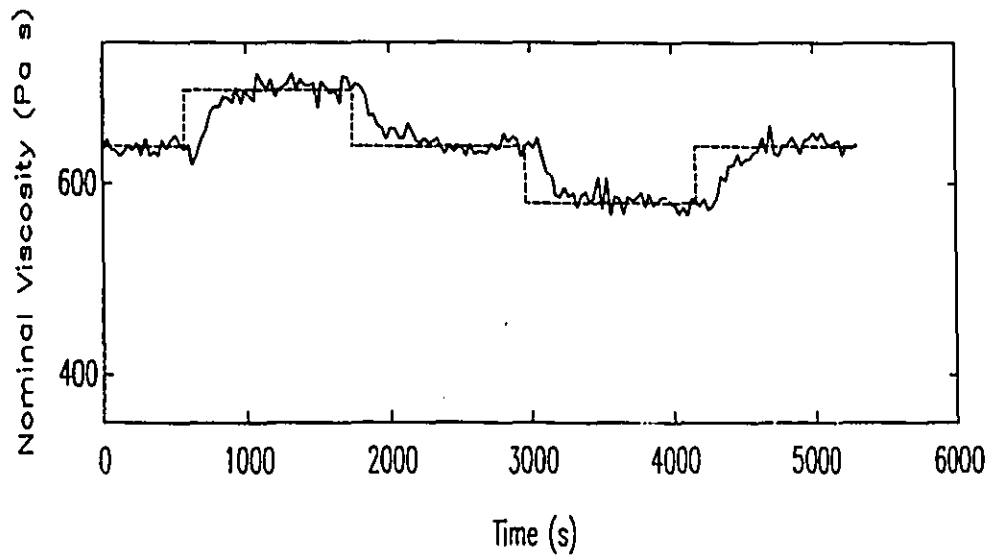
Experiments identical to those described in Section 6.3.3 were performed with MV control. Representative results of 60, 120 and 200 Pa s set point changes are shown in Figures 64-2, 64-3 and 64-4.

A preliminary check of the effectiveness of the MV controller can be made by examining the standard deviations of the uncontrolled and the controlled signals. The controlled viscosity signals shown in Figures 64-2, 64-3 and 64-4a do seem to vary within tighter limits when compared to the open loop steps shown in Figure 62-2a, 62-2b and 62-2c. This is confirmed quantitatively by the data in Figure 64-5. This figure shows the standard deviations of the open loop, closed loop PI and closed loop MV viscosity signals plotted as histograms. These standard deviations were computed at each steady state plateau of the controlled and uncontrolled experiments. The histograms confirm that the MV controller has reduced the range and mean magnitude of the observed viscosity signal standard deviations.

The MV controlled responses shown in Figures 64-2, 64-3 and 64-4a are markedly different from the PI controlled results illustrated in Figures 63-2a, 63-3 and 63-4. The MV responses are all overdamped; no oscillations are observed. An example of the manipulated variable (neutralising agent feed rates) is shown in Figure 64-4b. It too is different. The MV controlled manipulated variable makes a large initial correction, then assumes almost the required steady state level. The MV controlled manipulated variable is considerably more active or "nervous", even when one takes into account that the MV controller has a control period of 30 s, compared to the PI controller period of 80 s. These are characteristics of MV controller dead time compensation.

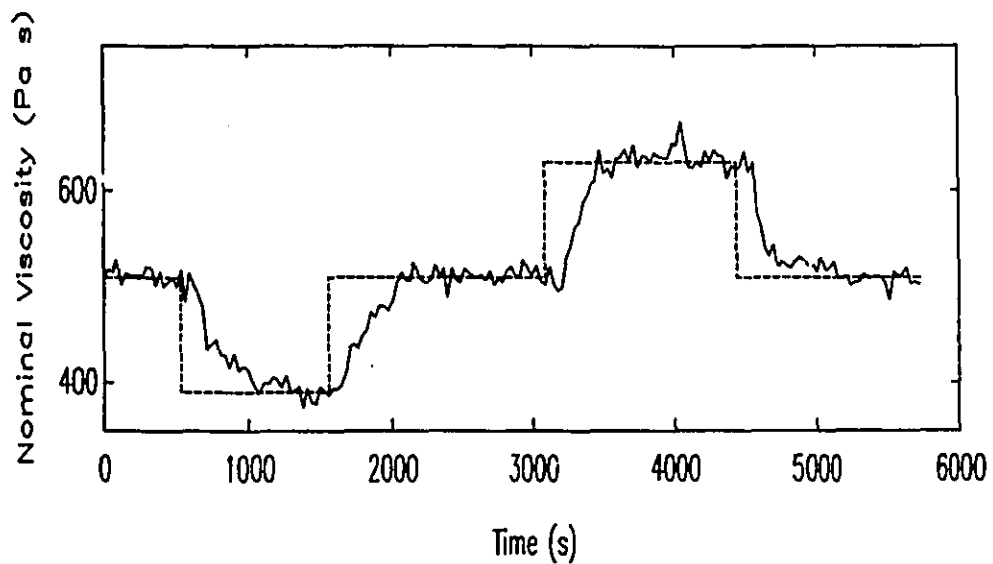
Examining the response times of the MV controlled runs showed that the MV controller was acting sluggishly compared to the PI controller. Response time statistics and first

Figure 64-2: Nominal Viscosity at 186°C and 30 s⁻¹:
MV Controlled, 60 Pa s Viscosity Set Point
Changes.



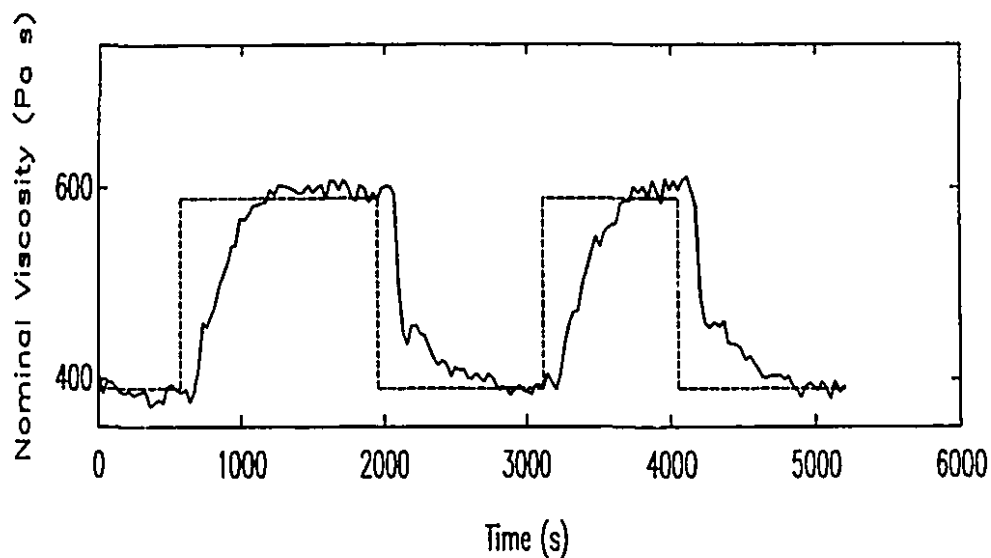
Legend: (-) Process response, (- -) set point.

Figure 64-3: Nominal Viscosity at 186°C and 30 s⁻¹:
MV Controlled, 120 Pa s Viscosity Set Point
Changes.



Legend: (-) Process response, (- -) set point.

Figure 64-4a: Nominal Viscosity at 186°C and 30 s⁻¹:
MV Controlled, 200 Pa s Viscosity Set Point
Changes.



Legend: (-) Process response, (- -) set point.

Figure 64-4b: Neutralising Agent Feed Rate Response to
200 Pa s Viscosity Set Point Changes

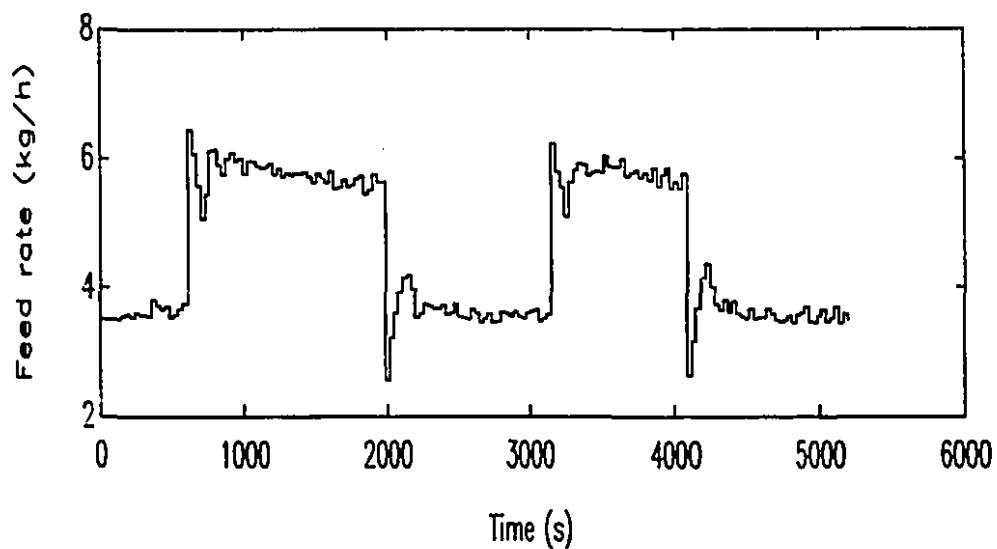


Figure 64-5a: Histogram of Standard Deviations Computed during Open Loop Operation.

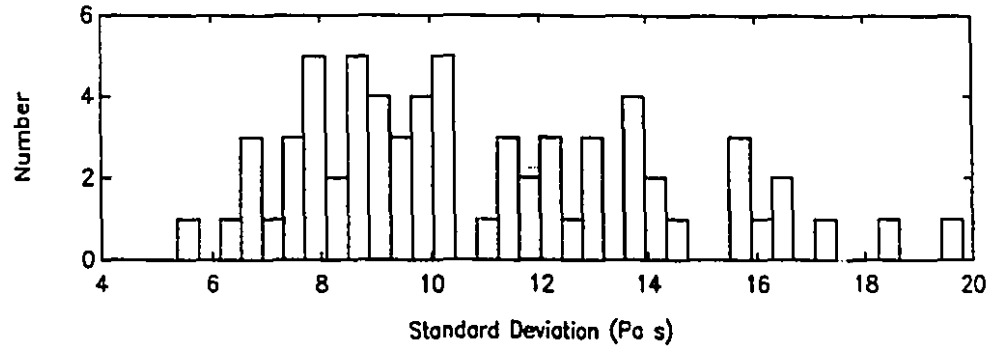


Figure 64-5b: Histogram of Standard Deviations Computed during PI Controlled Operation.

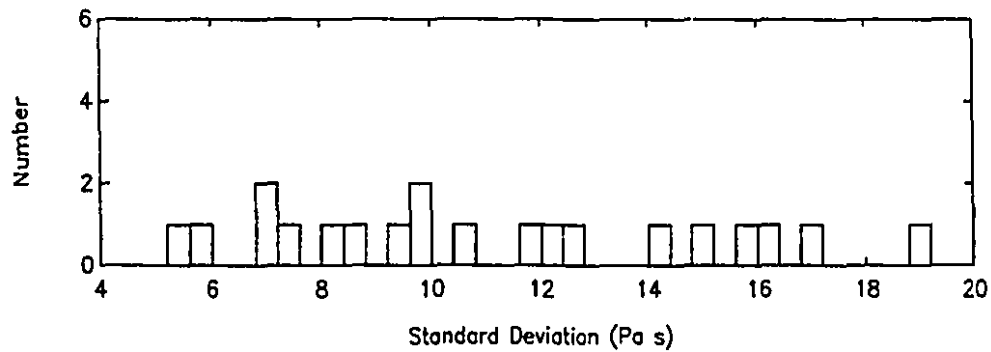
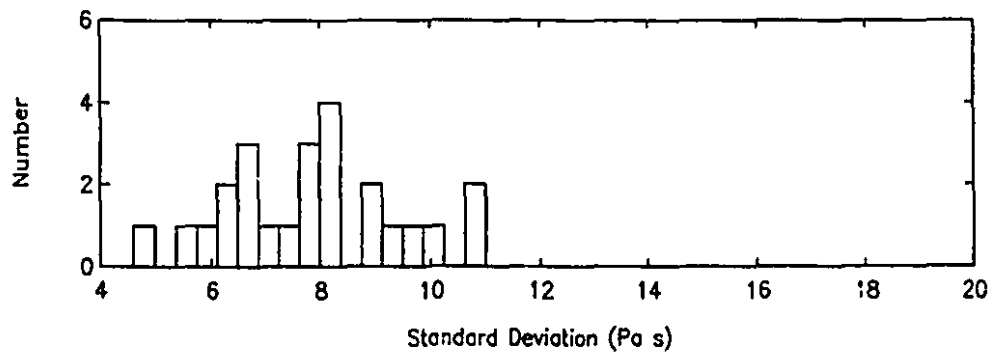


Figure 64-5c: Histogram of Standard Deviations Computed during MV Controlled Operation.



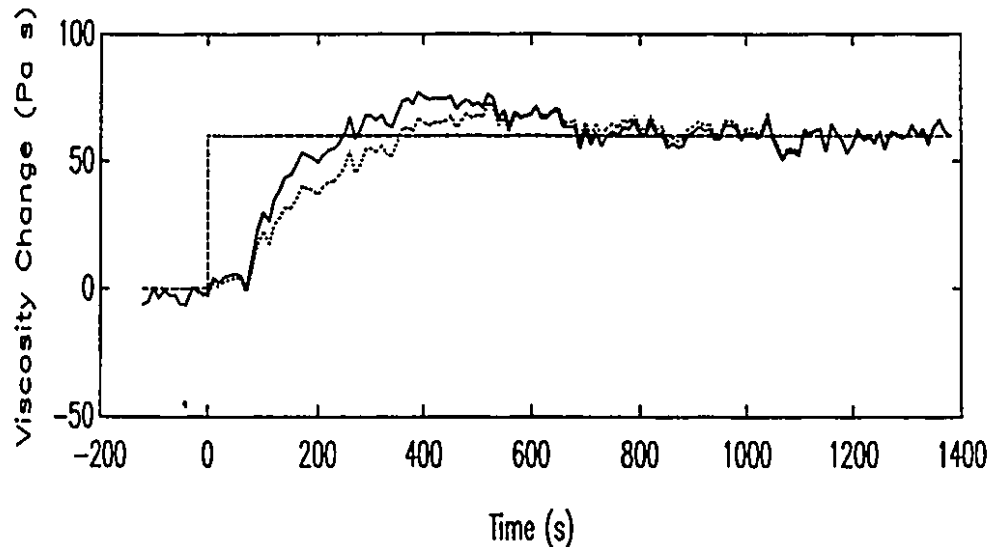
order time constants fitted to the controlled responses illustrating this point are summarised in Table 64-2. The time constant data suggest that the MV controlled response was only marginally faster than the open loop response.

Table 64-2: Summary of Observed Process Response Times with MV Control.

Viscosity Step Size [Pa s]	Response Time (s)	First Order Time Constant (s)
60	400 to 670	80 to 160
120	480 to 760	80 to 160
200	660 to 880	100 to 190

In the process of investigating this unexpected result, the MV controller parameters were re-computed and an error was discovered in the controller gain calculation. The correct value, corresponding to a gain of 22 Pa s/%, should be 4.5 rather than 6.25 (see Equation 64-2). The consequences of the use of the incorrect gain were investigated by simulation using Equations 64-1 and 64-2. The simulated MV controller response to a 60 Pa s set point step is shown in Figure 64-6. The controller response using the correct gain is shown by the solid line while that of the incorrect gain is shown by the dotted line. The simulation correctly predicts that a slower response, with a response time of 365 s, is expected if the incorrect gain is used. With the correct gain, the response time is 255 s. This is identical to the response time predicted for the PI controller but, the MV response offers the considerable advantage of greatly reducing the overshoot. This can be quantified by comparing the integrated squared error

Figure 64-6: Simulated MV Controlled Response to a 60 Pa s Viscosity Set Point Change.



Legend: (- -) Set point change, (-) correct gain, (•••) incorrect gain.

statistics for the simulated PI (60874 Pa s^2) and the simulated MV (39353 Pa s^2) controllers.

The only clear evidence of step direction asymmetry was found in ISE statistics. The asymmetry is not obvious in the rise time or time constant data.

Another reason for the MV controller's sluggishness lies in the choice of time constant used in the controller. A discrete time constant equivalent to 130 s ($T_s = 30 \text{ s}$, $\delta = 0.8$) was selected. This is at the faster end of the observed time constant range. Consequently the longer time constant responses are under-compensated by this particular controller since it is optimal only for the faster dynamics. Simulations showed that underestimating the true process dynamics lead to a slower response. To meet the objective of the fastest possible response, it would have been prudent to formulate the controller with the longest process time constant.

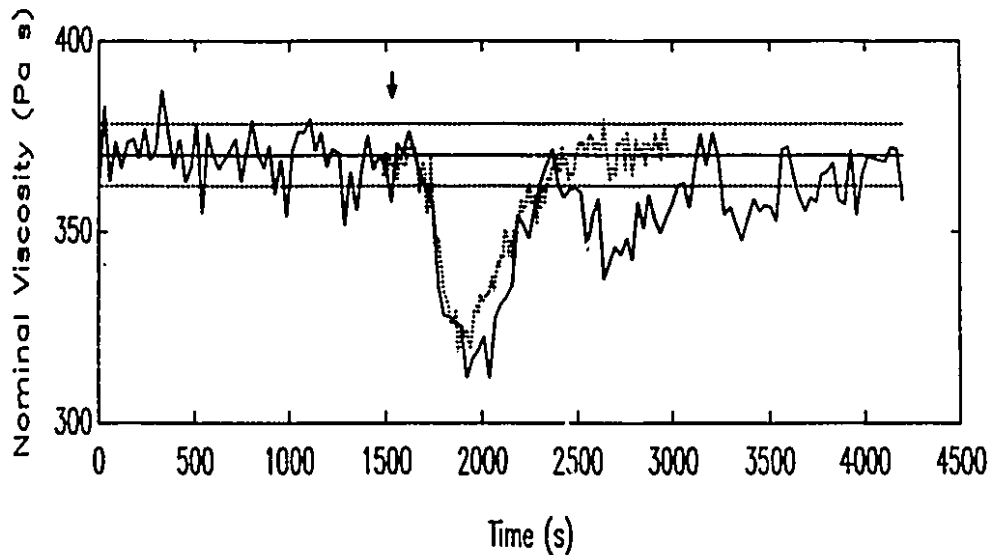
The MV controller's slow response can also be attributed to the noisy viscosity signal. It is useful to refer to the parallel between the Dahlin and MV controllers highlighted by Palmor and Shinnar (1979) and Harris et al. (1982) in discussing this point. The Dahlin controller cancels the process dynamics and imposes a first order plus dead time response on the process output. Harris et al. (1982) point out that the MV controller design method automatically selects the imposed first order time constant. Noise free processes ($MA(1) \rightarrow 0$) can be forced to react quickly, while noisy processes ($MA(1) \rightarrow 1$) can only react slowly. Inspection of Equation 64-2 makes this point clear. As the MA parameter increases, not only is the controller gain attenuated, but the contribution of the dead time compensation terms is also decreased. The results of the MV control experiments shown in Figures 64-2, 64-3 and 64-4a conform to the response of a MV controlled noisy process. An overdamped, slow response is observed in every case. This filtering action is probably also responsible for the symmetry of responses.

Thus, despite the error made in the MV controller gain specification, it is clear that an advantage can be realised with MV control. Fast responses are possible with the benefit that overshoots and oscillations are avoided. The process nonlinearities that strongly influenced the PI controlled responses are manifested as slow responses with MV control.

6.4.3 Disturbance Rejection Experiments

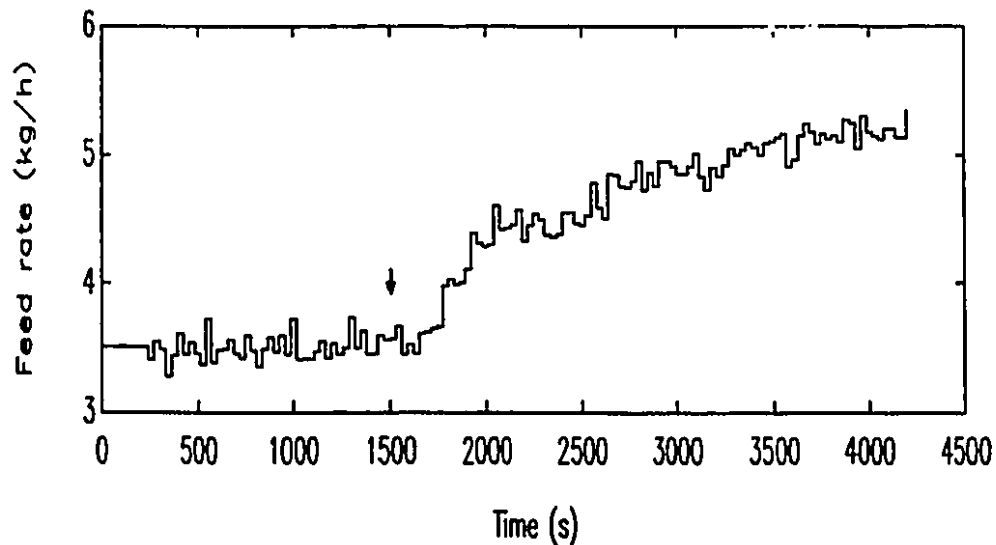
The large neutralising agent disturbances described in Section 6.3.4 were repeated to test the MV controller. The results are presented in Figures 64-7 and 64-8. The responses shown are much slower than the corresponding PI control results of Figures 63-6 and 63-7 and, as before, this can be attributed to the use of the incorrect MV

Figure 64-7a: Nominal Viscosity at 186°C and 30 s⁻¹:
MV Controlled Response to a Neutralising
Agent Concentration Disturbance. 15%
Neutralisation Set Point.



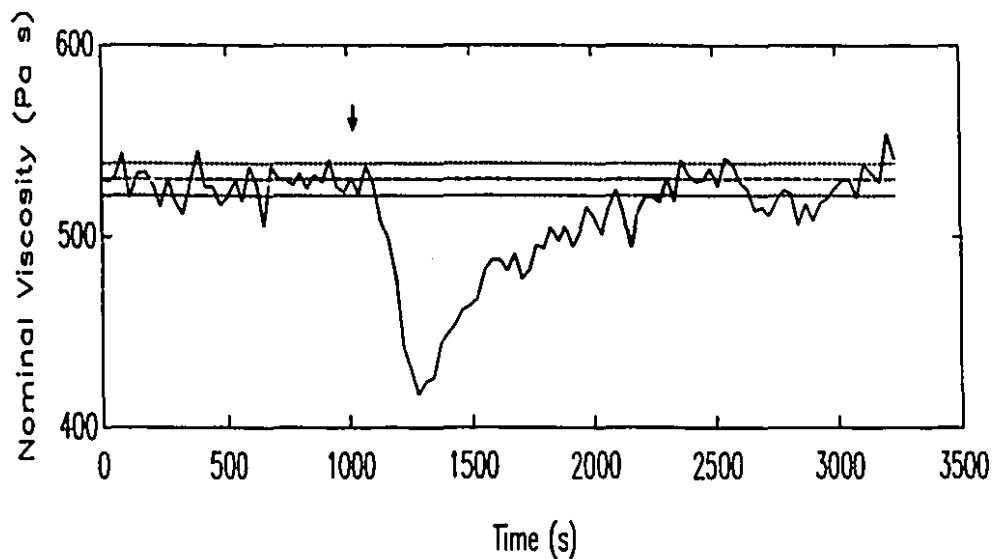
Legend: (-) Set point, (-) process response,
(- -) simulated process response,
(•••) ± 1 standard deviation.

Figure 64-7b: Neutralising Agent Feed Rate in Response to
Neutralising Agent Concentration Disturbance.



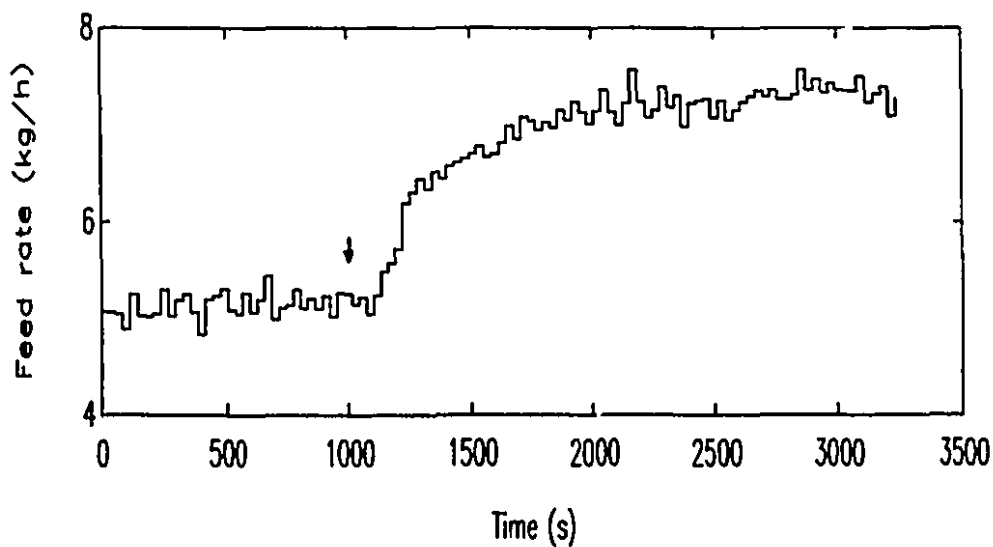
Legend: Arrow indicates time of disturbance.

Figure 64-8a: Nominal Viscosity at 186°C and 30 s⁻¹:
MV Controlled Response to a Neutralising
Agent Concentration Disturbance. 22%
Neutralisation Set Point.



Legend: (-) Set point, (-) process response,
(•••) ± 1 standard deviation.

Figure 64-8b: Neutralising Agent Feed Rate in Response to
Neutralising Agent Concentration Disturbance.



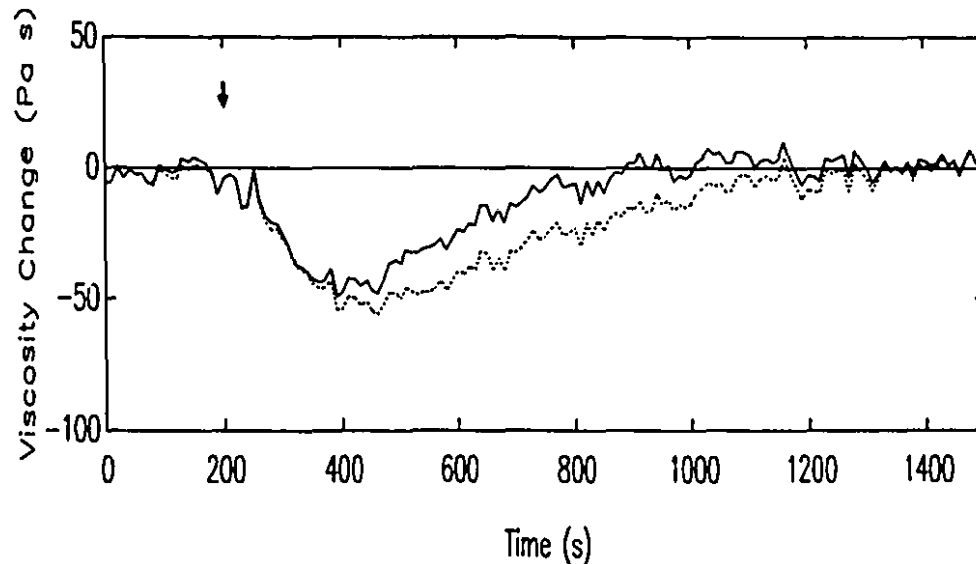
Legend: Arrow indicates time of disturbance.

controller gain. This conclusion was verified with the controller simulation. The simulated disturbance response, shown with the dotted line in Figure 64-7, employed the actual rather than the ideal controller parameters. It predicts the initial response of the experimental results quite well. The initial response time is approximately 720s. Unfortunately, the controller encountered another process disturbance after rejecting most of the first one causing the final set point to be reached only very slowly. The disturbance at the higher viscosity operating point (shown in Figure 64-8) exhibited an even more sluggish response. Its response time was 1250 s.

There are three additional factors, other than the use of the incorrect gain, that contributed to the MV controller's sluggish disturbance response. First of all, the controller was designed using a process model that describes the viscosity response to step changes (or, set point changes) in composition and consequently it is optimal only for these types of changes. Since the dynamics of disturbances are generally different from set point changes, the MV controller will not be optimal for disturbances. Also, as mentioned in the previous section, the MV controller's performance was limited by the noisy viscosity signal. This is illustrated for the case of disturbances in Figure 64-9. It shows simulated disturbance responses for controllers using two different noise (MA) model parameters, $\theta=0.4$ and $\theta=0.8$. Clearly, as θ approaches unity the disturbance response becomes progressively sluggish, adopting the shape of the response shown in Figure 64-8. Finally, it is recognised that the MV controller performance deteriorates as the process parameters change with operating point. The consequences of using an inaccurate gain or time constant in the MV controller have already been discussed. Examining Table 64-1 shows that the noise model parameter also changes with operating point; it decreases with

increasing degree of neutralisation. This suggests that the MV controller could react more aggressively at higher operating points and that the employed, fixed parameter MV controller was not operating optimally in this region.

Figure 64-9: MV Controller Simulation Illustrating the Effect of Signal Noise on Controller Performance.



Legend: (-) Set point, (-) $\theta = 0.4$, (•••) $\theta = 0.8$.

The subtle feed composition disturbances described in Section 6.3 were repeated with MV control. The results were qualitatively the same as for PI control. No drift in viscosity was seen, but a gradual change in the mean neutralising agent feed rate was observed. Unfortunately, a number of feeder errors occurred during the course of this experiment, precluding the determination of the response time to the disturbance. This again implies that the ILR is useful in sensing small viscosity changes.

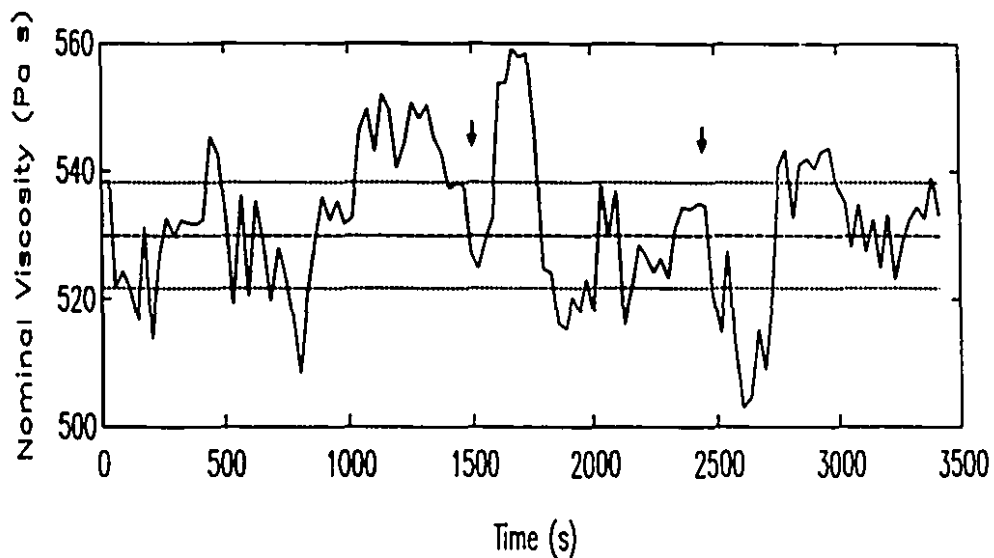
Finally, the feed rate disturbances described in Section 6.3 were repeated using the MV controller. Though MV controllers are particularly sensitive to incorrectly

specified process dead times (Palmor and Shinnar, 1979), simulations showed that the magnitude of disturbances introduced in these experiments should not destabilize the controller. To reiterate, the process was run for 15 minutes at one feed rate, then the total feed rate was changed instantaneously while maintaining the proportion of the two feed streams. Impulse disturbances were introduced to the process by adding a handful of neutralising agent, and then copolymer to the feed hopper. The purpose of these disturbances was to test the controller's performance. The results of the 12 to 8 kg/h feed rate change are shown in Figure 64-10a, b. The times of introduction of the disturbances are marked by the arrows in the figures. This figure shows that the performance of the controller was unaffected by the process dead time change. The impulse disturbances prompted only a modest controller reaction. As before, these experiments are of interest because they illustrate that the controller is robust to the typical types of disturbances it might encounter in normal operation.

6.4.4 Comments on MV Control Effectiveness

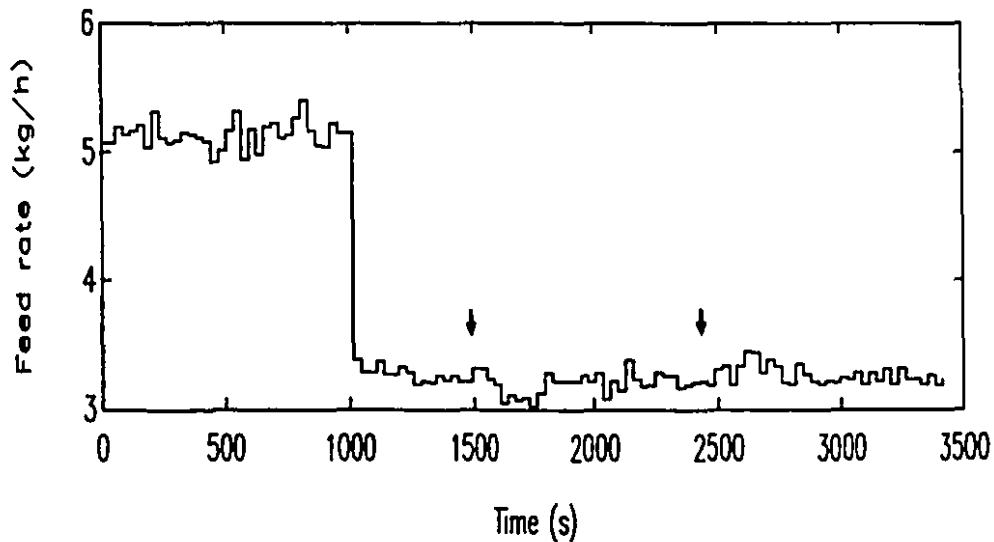
The results reported in this chapter suggest that minimum variance control can be used to advantage to control reactive extrusions. Though an incorrectly selected controller gain resulted in a sluggish response, simulations indicated that a fast process response without oscillations is possible. Eliminating oscillations would be critical if avoiding undesirable product compositions or processing condition limitations is important. The sluggish response resulting from the incorrectly specified controller gain highlighted another problem. The gain of the ionomer neutralisation process is inherently nonlinear. Clearly, if the MV controller is to operate optimally at all operating points, adaptive control techniques must be used.

Figure 64-10a: Nominal Viscosity at 186°C and 30 s⁻¹: MV Controlled Response to Two Impulse Disturbances Introduced After a Throughput Change.



Legend: (-) Process response, (- -) set point, (•••) ± 1 standard deviation.

Figure 64-10b: Neutralising Agent Feed Rate in Response to Impulse Disturbances Introduced After a Throughput Change.



Legend: Arrows indicate times of impulse disturbances.

There was also evidence of process and noise nonlinearity, which contributed to the sluggish, sub-optimal MV response. These problems are manifestations of the viscosity measurement and should be addressed in the ILR's re-design rather than by means of adaptive control.

6.5 ILR Performance as a Viscosity Sensor

The primary function of a viscosity control loop for EMAA copolymer neutralisation is to reject feed material disturbances. PI and MV controllers, using the ILR to measure viscosity, rejected both large and small feed composition disturbances. The PI controller performed best, rejecting disturbances in 10 to 11 minutes. This represents a considerable improvement over the reported performances of PI controllers using other rheological sensors controlling polypropylene visc-breaking. Using a Rheometrics[®] On-Line Rheometer¹, Fritz and Stöhrer (1986) showed that composition disturbances could be rejected in 25 minutes. Pabedinskas et al. (1989) used a pressure signal to infer viscosity. Their controller rejected composition disturbances in times greater than 30 minutes.

The minimum variance controller studied in this work did not perform to its potential because of an incorrectly selected controller gain. Experimental and simulation results showed, however, that MV control has advantages. For example, fast responses without overshoot are possible with MV control.

The improved performance obtained in this study can be attributed to the decrease in measurement delay introduced by the ILR due to its "in-line" location. This improvement is illustrated by comparing the dead times of simple first order plus dead time models fitted to the reactive extrusion

¹ Tradename of Rheometrics, Inc., Piscataway, NJ, USA

responses. In this study, dead times ranging from 80 to 100 seconds were observed. Fritz and Stöhrer (1986) reported a 180 s dead time; Pabedinskas et al.(1989) reported a 160 s dead time.

The performance of the ILR was not ideal. Experimental evidence showed that the ILR response was affected by the viscosity test strain rate and the viscosity step direction. These observations suggested that the way in which the ILR samples the polymer stream affects the speed of the response and obscures the true process dynamics. Cumulative residence time distributions for the extruder used in this study, determined by Chen (1992), showed that the process response is faster than indicated by the ILR. Simulations of the flow in the ILR (described in Chapter 2) predicted large recirculation flows at the entrance and exit of the rheometer's shearing zone. It was concluded that these recirculation flows exacerbated the measurement delay caused by the slow renewal of sample by laminar flow in the main body of the ILR and the slow laminar flow sample renewal in the rheometer's shearing zone.

CHAPTER 7

EVALUATION OF THE MCGILL IN-LINE MELT RHEOMETER

This chapter presents a detailed evaluation of the design and performance of the McGill in-line rheometer. It summarizes the key observations and conclusions of this study and presents recommendations for future rheometer development work and reactive extrusion control studies.

7.1 In-Line Rheometer Design

7.1.1 Principle of Operation

The two key features of the McGill in-line rheometer are: 1) its in-line location, intended to minimize measurement delay compared to on-line process rheometers and 2) its use of simple shear deformation, which makes possible the control of strain rate independent of process throughput.

The benefit of an in-line location was clearly demonstrated in this study. The time delay attributed to the operation of the ILR was small compared to the delays reported for on-line rheometers used in previous reactive extrusion studies using twin-screw extruders (Fritz and Stöhrer (1986) and Curry et al. (1988)). However, simulations and experimental evidence indicated that the simple action of laminar shear provided an inadequate rate of sample renewal in the shearing zone and limited the performance of the ILR. The experimental evidence shows that an appreciable measurement delay still exists. A comparison of reactive extrusion viscosity step change data with a cumulative residence time distribution for the same extruder, [determined by Chen (1992)], suggests that the rheometer itself contributes significantly to the dynamics of the observed viscosity response. Furthermore, contrary to expectations, it was observed that the viscosity step change response time increases with increasing drum speed.

A two-dimensional finite element simulation of the flow in the rheometer suggested an explanation for the observed

behaviour. The simulation showed that the only material that enters the shearing zone is the material that flows close to the wall of the main flow channel. This explains some of the observed time delay. The simulation also predicted zones of recirculating flow at the entrance and exit of the shearing zone. These recirculating flows were shown to increase in size with increasing drum speed, effectively increasing the flow path for material entering the shearing zone. It was concluded that the zones of recirculating flow are responsible for the observed dependence of the measurement dynamics on strain rate, although it was recognised that the two-dimensional simulation could not accurately predict the actual three-dimensional flow in the ILR.

Future ILR designs must employ some method of positively feeding material into the shearing zone to reduce the dependence of rheometer performance on the sampling rate. The stationary shearing zone wall and the rotating drum surface must be mechanically cleaned of material. This will undoubtedly add to the mechanical and operational complexity of the rheometer but is essential for improved performance.

The simple shear flow employed in the rheometer provided an effective control of strain rate that was independent of throughput. A small pressure flow contribution to the deformation in the shearing zone was detected experimentally. It is particularly important to take this into account for low strain rate measurements. An effective procedure for correcting for pressure flow in the shearing zone was developed, based on the work of Schümmer and Worthoff (1979).

Difficulties in measuring the pressure drop along the shearing zone and fluctuations of the pressure gradient in the shearing zone due to process pressure fluctuations, combined with the shear stress transducer's sensitivity to process pressure fluctuations, contributed to a large uncertainty for low strain rate (5 s^{-1}) measurements. High strain rate (30 s^{-1}) measurements were considerably less affected.

Consequently, high strain rate measurements were used in the control studies where a higher degree of measurement repeatability was required.

Experimental data showed that the rotation of the drum had an effect on the pressure drop in the main flow channel. This pressure drop dependence on strain rate was not recognised until late in the study. Cox and Dealy (1991) have proposed that all but a small area of the shearing drum at the gap entrance should be covered with a cowl to eliminate this problem as well as to eliminate the recirculation flows in the rheometer.

7.1.2 In-Line Rheometer Instrumentation

Experience suggests that the placement of pressure and temperature sensors in the rheometer can be improved. It is recommended that the pressure transducers be installed in the shearing zone, near the entrance and exit, to eliminate uncertainties due to entrance effects and flow geometry. It would be desirable to use combination pressure and temperature transducers in order to have two temperature measurements in the shearing zone. Unfortunately, the temperature sensors incorporated into existing, commercially available pressure transducers are not optimally designed to measure melt temperatures.

A temperature compensation algorithm based on an Arrhenius equation was used to correct stress measurements for temperature variation. This method introduced an abrupt correction of the stress because the shearing zone temperature, used in the correction, was measured with a precision of only 1°C. The abrupt corrections complicated the identification of process behaviour. It is recommended that the shearing zone melt temperature used for temperature correction be read with a precision of at least 0.1°C.

Finally, a better measurement of the shear stress transducer housing temperature must be made. The washer

thermocouple used in this research was just adequate. A thermocouple well should be machined directly into the SST housing.

7.1.3 In-Line Rheometer Temperature Control

There are two important aspects of temperature control in the ILR: the rheometer component temperatures must be uniform and insensitive to process temperature disturbances; and the temperature of the sample in the shearing zone must be uniform. The current ILR met the first requirement because the rheometer body and rotating drum were massive and had a large thermal inertia. It was observed that the rheometer body and rotating drum temperatures changed very little during experiments.

It is believed that the ILR also met the second requirement, although somewhat fortuitously. A simulation of the heat transfer in the shearing zone indicated that the convection of heat in the direction of flow could lead to a non-uniform temperature in the shearing zone. Furthermore, experimental evidence suggested that the polymer in the middle of the flow stream can be as much as 20 to 40°C hotter than the material near the rheometer body. However, a simulation of the flow in the rheometer showed that the polymer entering the shearing zone flows along the walls of the main flow channel. This polymer is thus conditioned to the rheometer temperature by virtue of its long residence time next to the rheometer wall. Though this situation is undesirable from the point of view of sample renewal, it ensured a uniform temperature distribution in the shearing zone.

The control of rheometer body and rotating drum temperatures should be improved. Both heating and cooling should be provided. To reduce the time for temperature equilibration of the sample in the shearing zone, it is recommended that a thinner shearing zone be used.

7.1.4 The Disk-Spring Shear Stress Transducer

The SST used by Nelson (1988) in an early ILR prototype employed an elastomeric seal around the SST beam tip to prevent polymer from flowing up into the housing and interfering with the capacitance probe. However, the seal interfered with the response of the transducer. The disk-spring of the SST used in the present study sealed the transducer from the incursion of polymer making an elastomeric seal unnecessary. However, a reservoir of polymer was formed below the disk spring in the lower portion of the SST housing. Initially, the polymer in the lower part of the housing was permitted to flow out of a small drain and thus purge the reservoir. This method of operation was later rejected when it was found that the purge flow had a large effect on the SST signal. Even with the drain closed, Nelson (1992) observed an effect that he attributed to minute flows of polymer in and out of the housing.

The capacitance probe clamping device was the most important refinement made to the SST during the course of this work. The clamp is described in Section 3.1.1. The key features of the clamp are that the probe is gripped over a large area and that the clamp is an integral part of the SST housing. Early, "add-on" clamp arrangements were inadequate.

The SST was also found to react to increases in pressure in the ILR. This effect was modelled empirically to correct SST measurements at high pressure. Sentmanat (1992) has recently designed a disk-spring SST that is reinforced in the axial direction to reduce its sensitivity to pressure.

Several other minor design modifications are recommended to improve the SST. First, the aluminum SST beam target is too soft. It was easily scratched during positioning of the capacitance probe and required frequent polishing. It is recommended that a material at least as hard as the stainless steel used in the construction of the capacitance probe be

used for the SST target. Also, the effective range of the SST was limited by the accuracy of alignment of the capacitance probe and the target, as explained in Section 3.1.1. It is recommended that a probe that can measure a larger maximum displacement (for example, 0.0508mm or 0.127 mm rather than 0.0254 mm) be used. The probe could then be positioned far enough away from the target so as to never touch it. Because only a fraction of the capacitance probe's measurement range would be used, its signal would have to be amplified to obtain adequate signal resolution.

The value of the SST beam calibration constant varied a little each time the SST was assembled, as mentioned in Section 3.3.2. This was attributed to the difficulty in tightening all four SST mounting bolts to the same degree. It is recommended that an alternative fastening method be developed that requires only one fastener to be tightened. This would ensure that the installation procedure would be more reproducible.

Finally, the cause of the observed but unexplained dynamics, described in Section 3.2.7., must be found and eliminated. To review, slow changes in the SST signal were observed in most experiments. These changes could not be correlated with any of the measured process variables. The observed characteristic times of the changes implied that they could have been temperature related. Eliminating this problem would improve the repeatability of rheometer measurements and would simplify the viscosity measurement procedure.

7.2 In-Line Rheometer Performance

7.2.1 ILR Accuracy and Repeatability

ILR viscosity measurements were compared to measurements made with a laboratory sliding plate rheometer (SPR). Very good agreement between the two instruments was observed for moderate to high viscosity polypropylenes, for a moderate viscosity high density polyethylene, and for a high viscosity

linear low density polyethylene. Factors contributing to ILR measurement inaccuracy were: 1) the method of estimation of the shear stress transducer baseline signal, 2) the inadequacy of the shearing zone pressure drop measurement and 3) the non-uniformity of rheometer component temperatures and of the temperature within the shearing zone.

Viscosities of three ionomer blends measured using the ILR were consistently lower than the corresponding SPR values. This discrepancy was attributed to three factors. First, the measurement of the pressure drop in the rheometer was believed to over-estimate the true pressure drop in the shearing zone. This resulted in the under-estimation of the viscosity. Second, moisture plasticises EMAA ionomers. It is likely that the samples tested with the ILR had higher moisture contents and consequently lower viscosity than the samples tested with the SPR. Finally, it is proposed that shear modification could explain part of the observed difference.

ILR viscosity measurements were repeatable to within 8 percent of the mean value at high strain rates ($30s^{-1}$). This level of repeatability is sufficient for process control applications. At low strain rates, the ILR viscosity measurements varied within 20 or 30 percent of the mean, which was unacceptable for control applications.

The principal source of rheometer measurement noise was process pressure fluctuations. A purely elastic effect of pressure on the SST beam was identified and modelled. Nelson (1992) proposes that two other phenomena, the pressure flow in the shearing zone and pressure flow in and out of the SST housing, create a complex, time-dependent SST signal response to pressure fluctuations. This complex relationship was not modelled in this study. The pressure related noise contributed an absolute error to the shear stress signal. Viscosities measured at low strain rates (small stresses) were more scattered than those measured at high strain rates (large stresses).

Mechanical vibration, the effects of cycling of the SST temperature controller, and electronic noise were also significant sources of measurement noise.

7.2.2 Dynamic Modelling of EMAA Neutralisation by Reactive Extrusion

The dynamics of the EMAA neutralisation process were investigated by means of viscosity step tests. Step changes in feed composition were generated by manipulating the gravimetric feeders, and the rheometer was used to monitor the viscosity response. The effects of composition, composition step size, step direction, process throughput and rheometer strain rate were investigated. First order plus dead time models were found to be the most appropriate and were fitted to the responses.

Process gains were found to be independent of throughput. The gain was a function of the operating point (or composition) at a low strain rate (5 s^{-1}) and was thus nonlinear. At a high strain rate (30 s^{-1}), the gain was independent of operating point within experimental error. The viscosity versus degree of neutralisation relationships (process gains) identified by the ILR were less sensitive than the viscosity versus composition relationship determined with the SPR. The mismatch was attributed to the phenomena of moisture plasticisation and shear modification.

The dead times determined from the process responses depended only on throughput. Dead times varied between 100 and 80 s for throughputs of 8 to 12 kg/h respectively.

The signal noise for viscosity measurements at 5 s^{-1} obscured the dynamics of small composition step changes. First order time constants of the larger step changes ranged from 30 to 80 s. No trends were obvious in the data.

At high strain rates (30 s^{-1}), the first order time constants found for steps to higher viscosity (upward steps) were always larger than the time constants of steps to lower

viscosity (downward steps). The time constants for downward steps ranged from 100 to 130 s, while the time constants for upward steps ranged from 160 to 190 s for small composition step changes. This trend is opposite to what was expected. The step change response was also a function of step size. For large composition step changes, the downward step time constants ranged from 90 to 100 s, while upward step time constants as high as 200 and 300 s were observed.

This strain rate and step direction dependence of the first order time constant suggested that the observed process response was heavily influenced by the measurement. This hypothesis was confirmed by comparing the measured viscosity response with the residence time distribution (RTD) of the extruder. Chen (1992) studied the RTD of the extruder used in this study and found that the extruder behaves much like a plug flow reactor, indicating that the mixing rate in the extruder is fast compared to the residence time. Since the neutralisation reaction is diffusion controlled, the mixing dynamics should represent the neutralisation dynamics fairly accurately.

Despite its significant measurement dynamics, the ILR is believed to be a useful sensor for neutralisation control, since the disturbances typical of the commercial ionomer manufacturing process either change slowly or consist of infrequent changes in feed composition or molecular structure, and can, consequently, be monitored effectively by the ILR.

7.2.3 Control of EMAA Neutralization

Proportional-integral (PI) and minimum variance (MV) control algorithms were evaluated as controllers for the neutralisation reaction. The controllers were tuned according to the models identified from the 30 s⁻¹ viscosity step change tests. Overall, the control was found to be effective. Both large and small composition disturbances were rejected. The measurement asymmetry and fundamental process nonlinearity

affected the controller performance. The PI controlled process response was overdamped over the middle of the compositional operating range, but at the operating range extremes, oscillatory responses were observed, indicating a change in process gain and/or dynamics. The PI controlled responses were asymmetric.

Minimum variance control was selected to address the problems of measurement delay and measurement noise. The MV controller gave fast process responses to set point changes without overshoot, but sluggish control of disturbances. The MV control was not as good as it could have been because of an error made in specifying the controller gain.

Future research should focus on the problems posed by signal noise, measurement delay and measurement dynamics asymmetry and strain rate dependence. These should be addressed through modification or re-design of the rheometer. Model-based control schemes, like the MV controller, are recommended, because they can address the inevitable time delay associated with rheological measurements. The problems posed by the inherently nonlinear process gain may warrant the use of adaptive control techniques.

It is proposed that the ILR must be positioned further upstream in the reactive extrusion process if closed loop control is to be dramatically improved over what is possible with the current rheometer design. A good location would be just after the devolatilisation (DV) zone of the twin screw extruder. Most of the reaction will be complete at this point in the extruder. Furthermore, the process pressure is low in this region, which would simplify the design of the shear stress transducer. It is important that devolatilisation be complete before the polymer enters the rheometer to avoid problems with gas bubbles or problems of plasticisation of the polymer by the volatile species.

CHAPTER 8 CONTRIBUTIONS TO KNOWLEDGE

This research represents a contribution to process rheometer technology. It also offers some insights into the field of viscosity control of reactive extrusion. A list of specific contributions follows.

- 1) This research identified the problems posed by the effects of pressure, temperature and polymer flow on the performance of a disk spring shear stress transducer.

- 2) A method to correct the strain rate of a simple shear flow between parallel plates for a superposed pressure flow was developed.

- 3) The McGill ILR's accuracy was verified with laboratory rheometer measurements for a number of polymers. A discrepancy between a laboratory sliding plate rheometer (SPR) and the ILR for certain polymers suggests the possibility of the phenomenon of shear modification complicating in-line rheometer measurements. It was recognised that for those specific polymers, in-line measurements are process specific and must be calibrated if they are to be used as a definitive material property measurement.

- 4) Empirical first order plus dead time models were identified for the response of ethylene-methacrylic acid (EMAA) ionomer viscosity to step changes in feed composition. It was shown, by comparing the models to residence time distribution data for the extruder, that the viscosity measurement has an appreciable dynamics. This measurement dynamics was attributed to the difficulty of sampling the main process stream. Simulations showed that only the slowest moving polymer in the main process stream was sampled, and furthermore that sampling was complicated by

recirculation flows that formed at the entrance and exit of the rheometer shearing zone.

5) The ILR was used successfully as a viscosity sensor in the closed loop control of EMAA neutralisation in a twin screw extruder. Feed composition disturbances and set point changes were controlled effectively with proportional-integral (PI) and minimum variance (MV) algorithms. The performance of the controllers was comparable, but the MV controller was shown to have the advantage of greatly reducing overshoot while maintaining a fast response.

REFERENCES

- Alison, B., (1986), Nonlinear Adaptive Control of pH Neutralization, M.Eng. Thesis, McMaster University, Hamilton, Ontario.
- ASTM 1238 (1990), "Standard Test Method for Flow Rates of Thermoplastics by Extrusion Plastometer", American Society for Testing and Materials, Volume 8.01, Phila. PA.
- Balke, S.T., (1986), Adv. Polym. Technol. 6(2), 193-201.
- Bazuin, C.G., Eisenberg, A., (1981), Ind. Eng. Chem. Prod. Res. Dev. 20, 271-286.
- Blanch, J.F., Garritano, R.F., Richards, W.D., Golba, J.C., (1989), U.S. Patent 4,817,416.
- Box, G.E.P., Jenkins, G.M., (1976), Time Series Analysis: Forecasting and Control (Revised Edition), Holden-Day Inc., San Francisco, California.
- Bubic, F.R., (1988) Process Rheometer -- Model no: 3.45, Dept of Chemical Engineering, McGill University, Montreal.
- Chen, T. (1992) An On-Line Residence Time Distribution Measurement in a ZSK Twin Screw Extruder, M.Eng. Thesis, McGill University, Montreal.
- Curry, J.E., Jackson, S., Stohrer, B., van der Veen, A., (1988), Chem. Eng. Prog., Nov, 43-46.
- Cox, R.G., Dealy, J.M., (1991), personal communication.
- Dealy, J.M., (1982a), Rheometers for Molten Plastics, Van Nostrand Reinhold, New York.
- Dealy, J.M., (1982b), Rheol. Acta, 21, 475-477.
- Dealy, J.M., (1984a), Chemical Engineering, Oct. 1, 62-70.
- Dealy, J.M., (1984b), United States Patent # 4,464,928.
- Dealy, J.M., (1986) United States Patent # 4,571,989.
- Dealy, J.M., Giacomini, A.J., Samurkas, T., (1989), Polym. Eng. Sci., 29, 499-504.
- Dealy, J.M., Wissbrun, K.F., (1990), Melt Rheology and its Role in Plastics Processing, Van Nostrand Reinhold, New York.

Dealy, J.M., Bubic, F.R., Doshi, S.R., (1992), Improved method for measuring shear stress, US Patent, claims accepted, 1991, Patent to be issued in 1992.

DuPont Company, (1985), SURLYN: Product Guide, (E-68761) Polymer Products Dept, Wilmington, DE.

DuPont Company, (1986), SURLYN: Industrial Extrusions Manual, (E-78684), Polymer Products Dept, Wilmington, DE.

Eisenberg, A. (1970), *Macromolecules*, 3, 147-154.

Elicabe, G.E., Meira, G.R., (1988), *Polym. Eng. Sci.*, 28(3), 121-135.

Ferry, J.D., (1980), Viscoelastic Properties of Polymers, Wiley and Sons, New York, Chapter 11.

FIDAP (1987) Users Manual Revision 4.0, Fluid Dynamics International, Inc., Evanston, Illinois, USA

Flumerfelt, R.W., Pierick, M.W., Cooper, S.L., Bird, R.B., (1969), *I & EC Fundamentals*, 8(2), 354-357.

Fritz, H.-G., Stohrer, B., (1986), *Intern. Polym. Proc.* 1, 31-41.

Giacomin, A.J., (1987), A Sliding Plate Melt Rheometer Incorporating a Shear Stress Transducer, Ph.D. Thesis, McGill University, Montreal.

Göttfert, A. (1986), *Kunststoffe* 76, 1200-1203.

Göttfert, A. (1991), SPE 49th ANTEC proceedings, 2299-2301.

Hanson, D.E., (1969), *Polym. Eng. Sci.*, 9(6), 405-414.

Harris, T.J., MacGregor, J.F., Wright, J.D., (1982), *Can. J. Chem. Eng.*, 60, 425-432.

Heinz, W., (1984), Proc. IX Intl. Congress on Rheology, Mexico, 85-92.

Hertlein, T., Fritz, H.-G., (1990), SPE 48th ANTEC, 1593-1598.

Lacey, T., (1991), DuPont Canada Inc., St. Clair River Site, Telephone Conversation, 1991 August 8.

Laun, H.M., (1983), *Rheol. Acta.*, 22, 171-185.

Lundberg, R.D., Phillips, R.R., (1984), *J. of Polym. Sci., Polymer Letters*, 22, 377-384.

- MacGregor, J.F., (1973), *Can. J. Chem. Engng.*, 51, 468-478.
- MacGregor, J.F., (1982), Optimal Stochastic Control Theory and Applications, Dept of Chemical Engineering, McMaster University, Hamilton, Ontario, Course notes.
- MacGregor, J.F., Penlidis, A., Hamielec, A.E., (1984), *Polym. Proc. Eng.*, 2(2&3), 179-206.
- Matlab (1990) "PC-MATLAB" for MS-DOS Personal Computers, The MathWorks, Inc., South Natick, MA
- Maxwell, B., Dormier, E.J., Smith, F.P., Tong, P.P., (1982), *Polym. Eng. Sci.*, 22(5), 280-286.
- Nelson, B.I., (1988), An Improved In-Line Process Rheometer for Use as a Process Control Sensor, M.Eng. Thesis, Dept of Chemical Engineering, McGill University, Montreal, Quebec.
- Nelson, B.I., (1992), Ph.D. Thesis, Dept of Chemical Engineering, McGill University, Montreal, Quebec.
- Ogunde, K., (1991), DuPont Company, Sabine River Site, Texas, Telephone conversation.
- Orwoll, R.D., (1983), *Adv. Polym. Technol.*, 3(1), 23-32.
- Pabedinskas, A., Cluett, W.R., Balke, S.T., (1989), *Polym. Eng. Sci.*, 29(15), 993-1003.
- Pabedinskas, A., Cluett, W.R., Balke, S.T., (1991), *Polym. Eng. Sci.*, 31(5), 365-375.
- Palmor, Z.J., Shinnar, R., (1979), *I & E C Proc. Des. Dev.*, 18(1), 8-30.
- Ross, C., Malloy, R., Chen, S., (1990), SPE 48th ANTEC, 243-248.
- Sakamoto, K., MacKnight, W.J., Porter, R.S., (1970), *J. Polym. Sci.*, Part A-2, 8, 277-287.
- Samurkas, T., (1989), Dow Canada Inc., Sarnia Division, Telephone Conversation, 1989 November 24.
- Schummer, P., Worthoff, R.H., (1978), *Chem. Eng. Sci.* 33, 759-763.
- Sentmanat, M.L., (1992), M.Eng. Thesis, Dept of Chemical Engineering, McGill University, Montreal.

- Smith, C.L., (1972), Digital Computer Process Control, Intext, Toronto.
- Springer, P.W., Brodkey, R.S., Lynn, R.E., (1975), Polym. Eng. Sci., 15(8), 583-587.
- Starita, J.M., Rohn, C.L., (1987), Plastics Compounding, Mar/Apr, 46-51.
- Sydenham, P.H., (1982), Handbook of Measurement Science Volume 1: Theoretical Fundamentals, John Wiley, U.K.
- Tadmor, Z, Klein, I, (1970), Engineering Principles of Plasticating Extrusion, Van Nostrand Reinhold Co., New York
- Tanner, R.I., (1985), Engineering Rheology, Oxford University Press, USA., pp 353.
- Tzoganakis, C., (1988), Ph.D. thesis, McMaster University, Hamilton, Ont.
- Varnell, B., (1988), The DuPont Company, Wilmington Delaware, Telephone conversation and subsequent written correspondence.
- Walters, K., (1975), Rheometry, Chapman and Hall, London.
- Wu, S., (1985), Polym. Eng. Sci., 25, 122-128.
- Zeichner, G.R., Patel, P.D., (1981), Proc. 2nd World Congr. Chem. Eng., 6, 333-337.
- Zeichner, G.R., Macosko, C.W., (1982), SPE 28th ANTEC, 79-81.

A1 APPENDIX OF EXPERIMENTAL PROCEDURES

A1-1 Typical Extrusion Conditions used to Prepare Ionomer Blends

The extrusion conditions used throughout the ionomer blend studies are summarised in the following tables:

Table A11-1: Summary of Typical Operating Temperatures Used for Ionomer Blend Preparation and Control Experiments

Extruder Temperature Control Zone	Temperature Set Points (°C)	Range of Actually Observed Temperatures (°C)
Zone 1	170	168 to 175
Zone 2	180	179 to 181
Zone 3	180	179 to 181
Zone 4	180	179 to 181
Rheometer Body	180	185 to 187
Shaft	180	185
SST	180	180
Die	180	180 to 185

Table A11-2: Summary of Typical Extruder Settings Used for Ionomer Blend Preparation and Control Experiments.

Extrusion Parameter	Units	Typical Value
Screw Speed	rpm	250
Vacuum	kPa	-92
Throughput	kg/h	8 to 12

**A1-2 Summary of Ionomer Blend Compositions used in the
Composition-Degree of Neutralisation-Viscosity Study**

The compositions of the ionomer blends described in Sections 5.3, 5.4 and 5.5 are summarised in Table A12-1.

Table A12-1: Table of Ionomer Blend Compositions Described in Section 5.3.

Blend ID	Target Degree of Neutral'n (%)	Mass of Blend Components (kg)		
		Nucrel 960	Surlyn 8920	Anti-oxidant Concentrate
1	25	6.795	5.085	0.12
2	0	11.880	0	0.12
3	17	8.422	3.458	0.12
4	59	0	11.880	0.12
5	25	6.795	5.085	0.12
6	33	5.168	6.712	0.12
7	29	5.982	5.898	0.12
8	0	11.880	0	0.12
9	25	6.795	5.085	0.12
10	21	7.609	4.271	0.12
11	59	0	11.880	0.12
12	17	8.422	3.458	0.12
13	33	5.168	6.712	0.12
14	13	9.236	2.644	0.12

N.B. The anti-oxidant concentrate was prepared by melt blending 20 mass % Irganox B215 powder in Nucrel 960.

The above compositions were tumble blended and fed with a single, volumetric pellet feeder to a Werner and Pfleiderer ZSK-30 twin screw extruder. The extrusion conditions were similar, but not identical to the conditions given in Appendix A1-1.

A1-3 Ionomer Titration Procedure

The following ionomer titration procedure was used to determine the degree of neutralisation of ionomer samples. The procedure is similar to a DuPont Company procedure communicated by Varnell (1988).

Apparatus

- 1) Erlenmeyer flasks, 500 ml, with TS24/40 joint,
- 2) Electric stirrer-hot plate, with magnetic stirring bar,
- 3) Burets, 25 ml precision,
- 4) 50, 100, 500 and 1000 ml volumetric flasks for preparing standard solutions,
- 5) Reflux condenser,
- 6) Drying tubes.

Materials

- 1) Solvent: Xylene-butanol-ethylene glycol solvent mixture in the proportions 75:25:5.
- 2) Basic titrant: 0.1 N tetramethylammonium hydroxide (TMAH) in methanol. The TMAH solution was prepared by diluting a commercially available 20 mass % TMAH-methanol solution. The 0.1 N solution was standardized with a 1 N HCl standard.
- 3) Acidic titrant: 0.1 N HCl in methanol was standardized with the 0.1 N TMAH solution. It was standardized every second day after preparation.
- 4) Thymol blue indicator in dimethyl formamide.

Titration Procedure

- 1) Weigh (1.0±0.1) g (with a precision of ±0.001g) of polymer sample into a 500 ml Erlenmeyer flask containing a magnetic stirring bar.
- 2) Add 100 ml of solvent mixture with a volumetric pipet.
- 3) Connect the flask to a reflux condenser, and place it on a hot-plate stirrer.

- 4) Reflux the sample with stirring for 30±1 minutes.
- 5) Cool the sample with stirring, until refluxing stops.
- 6) Remove the condenser and swirl to dissolve the polymer ring at the solution edge. All polymer must be in solution before performing the titration.
- 7) Fill burets with the methanolic TMAH and HCl. Insert drying tubes containing "Drierite" and "Ascarite" pellets into the top of the burets to protect the solutions from atmospheric moisture and CO₂.
- 8) Add 5 drops of thymol blue in dimethyl formamide (DMF) and titrate while hot to the pink end point with 0.1 N HCl in methanol. After end point is reached, swirl the flask so that the liquid level goes half-way up the flask. Continue titration and swirling until end point holds for at least 30 seconds.
- 9) Titrate with 0.1 N TMAH in methanol to the blue end point.
- 10) Determine reagent blanks on 200 ml of xylene-butanol-ethylene glycol with steps 2 through 5 and 8 and 9 above. It is not necessary to reflux for 30 minutes; heat only to boiling before proceeding. The reagent blanks must be determined whenever a new batch of solvent mixture is prepared or whenever there is a change in normality of the standard solutions.

Calculations

- 1) The weight percent of neutralised acid is determined using,

$$\text{Wt \% neutralised acid} = \frac{(A-B) \times N_{\text{HCl}} \times 86.1}{W \times 1000} \times 100\%$$

where **A** is the sample titer, (ml of HCl) from Step 8 above, **B** is the blank titer, (ml of HCl) from Step 10, N_{HCl} is the normality of the HCl standard and **W** is the mass of polymer, (g) from Step 1.

- 2) The total weight percent of acid is calculated using,

$$Wt\% \text{ acid} = \frac{(C-D) \times N_{TMAH} \times 86.1}{W \times 1000} \times 100 \%$$

where **C** is the sample titer, (ml of TMAH), Step 9, **D** is the blank titer, (ml of TMAH), Step 10, N_{TMAH} is the normality of the TMAH standard and **W** is the mass of polymer (g).

- 3) The degree of neutralisation (%) is calculated using,

$$D_{of}N = \frac{(A-B) \times N_{HCl}}{(C-D) \times N_{TMAH}} \times 100 \%$$

A2 APPENDIX OF SOFTWARE LISTINGS

A2-1 BASIC Program Simulating the Heat Balance in the ILR Shearing Zone

Program "DGAPTEMP.BAS", listed in the following pages, was used to solve for the steady state temperature distribution in the ILR shearing zone. It solves a finite difference approximation of a two-dimensional heat balance equation (Equation 24-1) in dimensionless form. The program prompts for boundary conditions, such as the rotating drum speed and the maximum melt temperatures, and for the parameters of the velocity profile in the shearing zone; V , the shearing rate and β , a parameter summarising the power-law behaviour of the fluid. β must be estimated ahead of time using Equations 22-7a and c or 22-8a and d, which are based on the work of Flummerfelt et al. (1969). The solution grid is initialised to 1 (temperatures are normalised by 200°C) and the equation is solved by iteration.

The program is documented with comment lines imbedded in the text.

```
'Program DGAPTEMP.BAS
```

```
DEFDBL A-Z           ' Define double precision
DIM TK(0 TO 10, 0 TO 260) ' Dimension matrices of
DIM TKM1(0 TO 10, 0 TO 260) ' present and past
DIM T(0 TO 10, 0 TO 260) ' dimensionless temperatures
                        ' and current temperature in
                        ' degrees Celcius
```

```
' Input desired output file name
```

```
CLS : PRINT "STEADY STATE RHEOMETER GAP TEMPERATURE
SIMULATION"
LOCATE 10, 15: PRINT "Input desired output filename"
LOCATE 11, 15: INPUT "format: filename.dat --> ", F$
```

```
' Input Physical Constants (Polypropylene)
```

```

k = .117          ' Thermal conductivity, [W/(m K)]
Cp = 1924.6      ' Heat capacity, [J/(kg K)]
d = 750          ' Melt density, [kg/m3]

' Finite difference computational steps

dy = .000025    ' (m)
dx = .002        ' (m)

' Shearing zone geometry

g = .001        ' Shearing zone gap (m)
L = .052        ' Shearing zone length (m)

' Iteration parameters

IMAX% = CINT(g / dy) ' gap size divided by vertical grid
                        ' unit
JMAX% = CINT(L / dx) ' gap length divided by horizontal
                        ' grid unit
ALPHA = .75        ' convergence weight

TR = 200         ' Reference temperature (C)

' Input desired boundary conditions, including: 1) rotating
' drum temperature, 2) maximum temperature of incoming melt,

CLS : LOCATE 5, 10: PRINT "Input desired rotating drum
temperature"
LOCATE 7, 12: INPUT " --> ", TSC

LOCATE 10, 10: PRINT "Input desired maximum melt
temperature"
LOCATE 12, 12: INPUT " --> ", TMM

TRB = 200        ' Rheometer body temperature

' Constants for analytical expression for velocity profile
' in the gap, use Flummerfelt et al. (1969) expression, see
' Chapter 2, section 2.2
' (bottom plate stationary, top plate moving at velocity V)

CLS : LOCATE 5, 10: PRINT "Input shearing velocity (m/s) and
appropriate"
LOCATE 6, 10: PRINT "beta factor corresponding to desired
pressure"
LOCATE 8, 12: INPUT " Velocity (m/s) --> ", V
LOCATE 9, 12: INPUT " beta (dimensionless) --> ", beta
CLS : LOCATE 12, 20: PRINT "Simulation in progress"

n = .595        ' power law exponent for Profax 6501

```

```

E = (n + 1) / n

' Definition of Fixed Dimensionless Parameters
ddx = dx / g      ' dimensionless x increment
ddy = dy / g      ' dimensionless y increment

' Initialize solution matrix to 1
FOR IX = 1 TO IMAX% - 1
  FOR JX = 1 TO JMAX% - 1
    TKM1(IX, JX) = 1
  NEXT JX
NEXT IX

ICOUNTER% = 1      ' Iteration counter

DO                ' Main iteration loop

  MAXERR = 0      ' re-set maximum error flag

  ' Boundary Conditions

  FOR I = 0 TO IMAX%      ' Temperature profile of melt
                        ' entering the shearing zone

    TKM1(I, 0) = (TRB - (TMM - TR) * 4 * ((I * ddy) ^ 2 -
(I * ddy)) + (TSC - TRB) * I * ddy) / TR

    TK(I, 0) = TKM1(I, 0)
  NEXT I

  FOR J = 1 TO JMAX%
    TKM1(0, J) = TRB / TR      ' Rheometer body temperature

    TK(0, J) = TKM1(0, J)
    TKM1(IMAX%, J) = TSC / TR  ' Rotating drum
                                ' temperature
    TK(IMAX%, J) = TKM1(IMAX%, J)
  NEXT J

  FOR I = 1 TO (IMAX% - 1)

' Expressions for velocity, UI, and shear rate DUDY in the
' gap due to superimposed pressure and drag flow

    UI = ((beta ^ E - (beta - (I * dy) / g) ^ E) / (beta
^ E - (beta - 1) ^ E))
    DUDY = E * (beta - (I * dy) / g) ^ (1 / n) / (beta ^
E - (beta - 1) ^ E)

```

```

' Define viscosity dependent dimensionless numbers
' ETA = 2980 * (DUDY * V / g) ^ .595           ' Pa s -- Power
                                                ' law model
ETA = 2000
BR = ETA * V ^ 2 / k / TR                     ' (pseudo-Brinkman
                                                ' number)
RE = d * V * g / ETA                          ' Reynolds number
PR = Cp * ETA / k                             ' Prandtl number

' Estimate temperatures at each grid point using finite '
difference approximation, CONV is the convection term,
' COND1 is the x direction conduction term, COND2 is the y '
direction conduction term, VISHEAT is the viscous heating '
term

      rOR J = 1 TO (JMAX% - 1)
          A1 = (2 / RE / PR * ((1 / (ddx ^ 2)) + (1 / (ddy
^ 2))))
          CONV = (TKM1(I, J - 1) - TKM1(I, J + 1)) / 2 /
ddx
          COND1 = (TKM1(I, J + 1) + TKM1(I, J - 1)) / (ddx
^ 2)
          COND2 = (TKM1(I + 1, J) + TKM1(I - 1, J)) / (ddy
^ 2)
          VISHEAT = BR / PR / RE * (ABS(DUDY) ^ 2)

          TK(I, J) = (1 / A1) * ((UI * CONV) + (1 / RE /
PR) * (COND1 + COND2) + (BR / RE / PR) * (ABS(DUDY) ^ 2))

          ER = ABS(TK(I, J) - TKM1(I, J))

          IF ER > MAXERR THEN                 ' Identify the grid point
              MAXERR = ER                     ' at which the temperature
              IME% = I                         ' estimate is converging
              JME% = J                         ' slowly
          END IF

' Update estimate with a weighted average of previous
' values

          TKM1(I, J) = ALPHA * TK(I, J) + (1 - ALPHA) *
TKM1(I, J)

          NEXT J

' Boundary condition: fully developed temperature profile at

```

```

' the end of the shearing zone

      FOR II = 0 TO IMAX%
        TK(II, JMAX%) = TK(II, JMAX% - 1)
        TKM1(II, JMAX%) = TK(II, JMAX%)
      NEXT II

      NEXT I
      ICOUNTER% = ICOUNTER% + 1      ' Increment iteration counter

' Terminate iteration if solution is not converging

      IF ICOUNTER% > 150 THEN
        CLS : LOCATE 15, 30: PRINT "Iteration not converging"
        GOTO theend
      END IF

      LOOP WHILE MAXERR > .00001

      OPEN "O", 1, "B:" + F$

' Convert from dimensionless temperature to degrees C
' Print data to output file

      FOR J = 0 TO JMAX%
        FOR I = 0 TO IMAX%
          T(I, J) = TK(I, J) * TR
        NEXT I
        PRINT #1, USING "####.#"; T(0, J); T(1, J); T(2, J);
        T(3, J); T(4, J); T(5, J); T(6, J); T(7, J); T(8, J); T(9,
        J); T(10, J)
      NEXT J
      CLOSE #1

      BEEP: CLS : LOCATE 12, 30: PRINT "Done!"
      theend:
      END

```

A2-2 Example of Rheometer Control Software

The program listed and documented in the following pages was used to control the reactive extrusion of EMAA ionomers with a minimum variance algorithm. It was selected for this appendix because it includes all of the key programming elements used throughout this research. These key elements are:

i) Calls to the Data Translation (DT) board (analogue to digital; digital to analogue conversion) using B.I.Nelson's subroutines to sample shear stress, rotating drum velocity, up and downstream pressure and to communicate the drum speed set point to the motor controller, ii) Calls to the MACO 8000, using B.I.Nelson's subroutines to read rheometer temperatures and actual gravimetric feedrates and to communicate gravimetric feeder set points, iii) DOS clock timer interrupts for sample timing control, iv) DT board sampling control to provide a second level of timing within the DOS interrupts, and v) viscosity and control action computations.

The BASIC program listing is documented with comprehensive comment lines interspersed throughout. The comments are preceded by a single quotation mark ('). The program structure can be reduced to the following steps.

```
INPUT: rheometer and process control parameters,  
LABEL: start of measurement cycle  
START: rheometer motor  
SAMPLE: SST, tachometer, pressures, temperatures  
COMPUTE: viscosity, control action  
SAMPLE: actual feedrates  
IMPLEMENT: control action (specify new feedrates)  
WAIT: until ON TIMER interrupt, return to start of  
measurement cycle
```

The MACO and Data Translation board sampling subroutines, written by B.I.Nelson, are included on the diskette accompanying this thesis.

Program VMVC.BAS

Program VMVC.BAS actuates the gravimetric feeders in order to control the viscosity measured by the McGill In-Line Rheometer. This version of the program considers the test time as the point at which the viscosity calculation is finally made. The MACO controller auto-start function is employed by VMVC. After the extruder is up and running, the viscosity can be monitored initially without any control action. When the operator is satisfied that the system is at steady state, the controller can be invoked by typing " U " (ie capital U), choosing selection " S " and specifying a set point. The program's function can be interrupted any time to allow selection of: i) a new set point, ii) a minor modification of the controller parameters, or iii) termination of the program.

```
'$INCLUDE: 'MACODEC.BAS'      ' Declarations for MACO
                               ' communication subroutines
'$INCLUDE: 'DT1-2DEC.BAS'    ' Declarations for Data
                               ' Translation board driver
                               ' subroutines
DECLARE SUB BOX ()           ' Declarations for graphics
DECLARE SUB HALFBX1 ()      ' box drawing subroutines
DECLARE SUB UDATEBOX ()
DIM ZERO%(1 TO 768)         ' Vector of "Zero" SST Voltages
DIM TEST%(1 TO 1500)        ' Vector of SST, Tach and
                               ' Pressure signals during the
                               ' test
DIM A!(0 TO 4)              ' Vector of strain rate/process
                               ' follower voltage calibration
                               ' equation coefficients
DIM AA!(0 TO 1)             ' Vector of coefficients for
                               ' strain rate vs tach feedback
                               ' voltage correlation
DIM APU!(1 TO 2)           ' Vector of upstream pressure/
                               ' voltage calibration constants
DIM APD!(1 TO 2)           ' Vector of downstream pressure/
                               ' voltage calibration constants
DIM U!(1 TO 10)            ' Vector of past control actions,
                               ' element 1 is the most recent
DIM E!(1 TO 3)             ' Vector of past errors, element
                               ' 1 is most recent
DIM CC!(1 TO 8)            ' Vector of controller parameters

H! = 16061                  ' SST beam calibration constant: TOB11-110
YSTAR! = .0005              ' True strain rate "interpolation" parame-
                               ' ter, See Chapter 2, section 2.2
L! = .0516                  ' Rheometer shearing zone length in (m)
GAP! = .001                 ' Rheometer gap in (m)
```

```

CF! = 6894.733      ' psi to Pa conversion factor
ALPHA! = 0!         ' SST pressure correction parameter; see
                    ' Equation 32-1
APU!(1) = 93.96    ' Upstream pressure transducer voltage-
APU!(2) = 3.16     ' pressure calibration constants
APD!(1) = 90.73    ' Downstream pressure transducer
APD!(2) = -9.93    ' voltage-pressure calibration constants
A!(0) = -.0409     ' Strain rate / process follower
A!(1) = 3.286      ' calibration constants; see Equation
A!(2) = .2458      ' 31-3
A!(3) = -.0247
A!(4) = 0!

```

```

AA!(0) = -.34755   ' Tach voltage / strain rate
AA!(1) = 3.353306 ' calibration; see Equation 31-2

```

```

' Input screen #1: Gives program description and prompts for
' output file name

```

BOX

```

LOCATE 2, 3: PRINT "Program VMVC - Updated: 91 April 10 by
TOB"
LOCATE 4, 10: PRINT "Enter experimental parameters"
LOCATE 5, 10: PRINT "After extruder initiates auto-start,
wait for 10 or 15"
LOCATE 6, 10: PRINT "minutes, then initiate rheometer and
monitor viscosity"
LOCATE 7, 10: PRINT "When ready to start control, type U,
select set point"
LOCATE 8, 10: PRINT "Program is terminated by typing U and
choosing T"
LOCATE 9, 10: PRINT "SET THE CAPS LOCK ON"
LOCATE 13, 20: PRINT "ENABLE THE EXTRUDER'S AUTOSTART
FUNCTION"
LOCATE 15, 10: PRINT "Data is saved in subdirectory E:\DATA\
with file extension '.CON'"
LOCATE 18, 26: INPUT "Enter a filename: ", FILE$

```

```

' Input screen #2: Prompts for desired feedrates

```

FEED.RATE.SELECT:

CLS

HALFBOX1

```

LOCATE 2, 5: PRINT "SPECIFY INITIAL FEEDRATES"
LOCATE 11, 5: PRINT "OVERHEAD FEEDER = NUCREL 960 : REMOTE
FEEDER = SURLYN 8920"
LOCATE 4, 10: PRINT "Enter the desired total feed rate
(kg/h)"
LOCATE 5, 20: INPUT "----> ", TFSP!
LOCATE 7, 10: PRINT "Enter the desired degree of
neutralization"
LOCATE 8, 15: PRINT "Range: 15 to 30 %"

```

```

LOCATE 9, 20: INPUT "----> ", DOFN!
      ' SURLYN is the mass percent Surlyn 8920
      ' required to achieve the desired degree
      ' of neutralization; see Equation 6??
SURLYN! = ((.251904 + .002 * (DOFN! + .1315)) ^ .5 - .5019)
* 1000
OHFSP% = INT(TFSP! * (100 - SURLYN!))      ' Overhead feedrate
RFSP% = INT(TFSP! * SURLYN!)              ' Remote feed rate
TFSP% = INT(100 * TFSP!)                  ' Total feed rate

' Input screen #3: Prompts for sampling period and test
' strain rate

STRAIN.RATE.SELECT:
CLS
HALFBOX1
LOCATE 2, 5: PRINT "SELECT NOMINAL TEST STRAIN RATE"
LOCATE 4, 10: PRINT "Enter desired nominal strain rate
(1/s)"
LOCATE 5, 15: PRINT "Range 1.5 to 31 (1/s)"
LOCATE 6, 20: INPUT "----> ", G!

VF1! = 0      ' Initial guesses for bisection method algorithm
VF2! = 10

IF G! = 0 THEN
  ADVTEST% = 0
  GOTO MACO.SET.UP
END IF

DO WHILE (ABS(VF1! - VF2!) > .005)
  VF3 = (VF1! + VF2!) / 2

  F1! = G! - (A!(4) * VF1! ^ 4 + A!(3) * VF1! ^ 3 + A!(2)
* VF1! ^ 2 + A!(1) * VF1! + A!(0))
  F2! = G! - (A!(4) * VF2! ^ 4 + A!(3) * VF2! ^ 3 + A!(2)
* VF2! ^ 2 + A!(1) * VF2! + A!(0))
  F3! = G! - (A!(4) * VF3! ^ 4 + A!(3) * VF3! ^ 3 + A!(2)
* VF3! ^ 2 + A!(1) * VF3! + A!(0))

  IF (F1! * F3!) < 0 THEN
    VF2! = VF3!
  ELSEIF (F2! * F3!) < 0 THEN
    VF1! = VF3!
  ELSE
    CLS : LOCATE 15, 30: PRINT "Problem solving for
follower voltage"
    STOP
  END IF
LOOP

```

```

ADVTEST% = INT((VF1! / 10) * 4095)      ' Calculate digital
                                         ' follower signal

BOX
LOCATE 2, 5: PRINT "VISCOSITY MINIMUM VARIANCE CONTROLLER
PARAMETERS"
LOCATE 5, 10: PRINT "Enter the sampling / control period
(s)"
LOCATE 6, 15: INPUT "----> ", SP%
LOCATE 8, 10: PRINT "Enter the process gain (Pa s/%)"
LOCATE 9, 15: INPUT "----> ", WO!
LOCATE 11, 10: PRINT "Enter the value of the discrete 1st
order time constant"
LOCATE 12, 15: INPUT "----> ", D!
LOCATE 14, 10: PRINT "Enter the value of the moving average
noise model parameter"
LOCATE 15, 15: INPUT "----> ", MA!
LOCATE 17, 10: PRINT "Enter the number of sampling periods
per dead time"
LOCATE 18, 15: INPUT "----> ", DT%

CC% = 0      ' Initially, control action is disabled
              ' with CC%=0
VSETPT! = 1  ' Initially, viscosity setpoint and
              ' corresponding temperature setpoint
TSETPT% = 1  ' are set to meaningless numbers

CLS
              ' Set MACO and DT board parameters
MACO.SET.UP:
GAIN% = 1
STCH% = 0    ' SST Signal read on channel 0, Tach read on
              ' channel 1
ENDCH% = 3   ' Upstream pressure read on channel 2,
              ' downstream pressure read on channel 3
FREQ! = 128  ' Each signal sampled at 32 Hz; 4 channels *
              ' 32 = 128 Hz
NCONVZ% = 768 ' Sample the SST Zero for 6 s @ 32 Hz
SUP% = 6      ' Allow 6 seconds for the stress signal
              ' to come to steady state after
              ' commencement of straining (ie the
              ' start-up transient)
NCONVT% = (SUP% + 2) * 128 ' Sample the SST and Tach for
              ' the duration of the expected
              ' start-up of steady shear transient and an additional
              ' 2 seconds. The data collected over the last two
              ' seconds will be used in the viscosity calculation.
              ' Four channels are sampled @ 32 Hz each for a total of
              ' SUP% + 2 seconds.

DAC.SELECT% = 1 ' Rheometer motor setpoint transmitted on
                ' DAC channel 1

```

```

MACO.INIT 1, 3, 0 ' Communication channel 1; Use 3 file
                  ' buffers for I/O
                  ' Error printing parameter = 0 to
                  ' suppress printing
DT.INIT          ' Initialize DT board

                  ' Switch on feeders at initial feedrate
MACO.OPEN
  MACO.PSET 85, 2, 1, 50, OHFSP%, OHFERR%
  MACO.SET "DRS3", RFSP%, RFERR%
  MACO.W.OPCR 2899, 1, SWERR%
  MACO.W.OPCR 2899, 0, SWERR%
MACO.CLOSE

BOX
LOCATE 12, 20: PRINT "EXTRUDER'S AUTO-START PROCEDURE
INITIATED"
LOCATE 13, 20: PRINT "WAIT 5 TO 10 MINUTES TO START
EXPERIMENT"
LOCATE 20, 35: PRINT "Press any key to start viscosity
monitor"
DO WHILE INKEY$ = ""
LOOP

CNT% = 1          ' Sample counter
                  ' Open output file
OPEN "E:\DATA\" + FILE$ + ".CON" FOR OUTPUT AS #1

' Initialize output screen
SET.UP.SCREEN:
CLS
LOCATE 2, 10: PRINT "Nominal Strain Rate "; G!; " 1/s
Viscosity Setpoint "; VSETPT!; " Pa s"
LOCATE 3, 15: PRINT "Viscosity Test Reference Temperature ";
TSETPT%; " C"
LOCATE 5, 5: PRINT "Time"; SPC(5); "OH Feed"; SPC(4); "R
Feed"; SPC(4); " Control "; SPC(4); "Delta P"; SPC(5);
"Viscosity"
LOCATE 6, 6: PRINT "(s)"; SPC(6); "(kg/h)"; SPC(3);
"(kg/h)"; SPC(6); " ( % )"; SPC(8); "(psi)"; SPC(7); "(Pa
s)"
LOCATE 7, 1: PRINT STRING$(80, 196)
LOCATE 23, 1: PRINT STRING$(80, 196)
LOCATE 24, 40: PRINT "Press 'U' to UPDATE program function"
VIEW PRINT 8 TO 21 ' Define output window

' ON TIMER INTERRUPT BASED MONITORING PROGRAM:
SAMPLE:

IF CNT% > 640 GOTO THE.END

```

```

VVSUM! = 0: VTSUM! = 0: VZSUM! = 0   ' Initiate averaging
PUSUM! = 0: PDSUM! = 0               ' sums

TIMER ON                             ' Enable TIMER interrupt
ON TIMER(SP%) GOSUB TOGGLE

DT.DAOUT DAC.SELECT%, 0              ' Stop Rheometer motor

DT.CLOCK FREQ!                       ' Set DT board clock speed
                                       ' Set up for Zero sampling
DT.SETADC GAIN%, STCH%, ENDCH%, NCONVZ%
DT.BLKADC ZERO%()                    ' Sample zero

' Poll MACO for rheometer, gap and melt temperatures

MACO.OPEN
MACO.VAL "T2V2", TSST%, ETST%        ' SST temperature
MACO.VAL "T2V6", TMELT%, ETM%        ' Upstream melt temp
MACO.VAL "T2V1", TRHEO%, ETR%        ' Rheometer body temp
' MACO.VAL "PRV1", PD1%, EPD%         ' Downstream pressure
' MACO.VAL "PRV2", PU1%, EPU%         ' Upstream pressure
                                       ' Pressure difference
' MACO.PVAL 77, 0, 0, 8, DELTAP1%, EDP%
MACO.CLOSE

DT.DAOUT DAC.SELECT%, ADVTEST%       ' Start Rheometer motor

DT.SETADC GAIN%, STCH%, ENDCH%, NCONVT% ' Set up for
                                       ' test sampling
DT.BLKADC TEST%()                    ' Sample SST, Tach and pressures

' Calculate SST signal baseline, correcting for pressure

FOR IZ% = 513 TO 768 STEP 4
  PU! = APU!(1) * (ZERO%(IZ% + 2) * 10 / 4095) + APU!(2)
  PD! = APD!(1) * (ZERO%(IZ% + 3) * 10 / 4095) + APD!(2)
  ZEROSIG! = ZERO%(IZ%) * 10 / 4095 - ALPHA * (PU! + PD!)
/ 2
  VZSUM! = VZSUM! + ZEROSIG!
NEXT IZ%

' Calculate viscosity test SST signal correcting for
' pressure

FOR IT% = (1 + SUP% * 128) TO NCONVT% STEP 4
  PU! = APU!(1) * (TEST%(IT% + 2) * 10 / 4095) + APU!(2)
  PD! = APD!(1) * (TEST%(IT% + 3) * 10 / 4095) + APD!(2)
  TESTSIG! = TEST%(IT%) * 10 / 4095 - ALPHA! * (PU! +
PD!) / 2
  VVSUM! = VVSUM! + TESTSIG!
  VTSUM! = TEST%(IT% + 1) / 4095 * 10 + VTSUM!

```

```

NEXT IT%

FOR IP% = 1 TO NCONVT% STEP 4
  PU! = APU!(1) * (TEST%(IP% + 2) * 10 / 4095) + APU!(2)
  PD! = APD!(1) * (TEST%(IP% + 3) * 10 / 4095) + APD!(2)
  PUSUM! = PUSUM! + PU!
  PDSUM! = PDSUM! + PD!
NEXT IP%

VZAVG! = VZSUM! / 64      ' Mean zero voltage
VVAVG! = VVSUM! / 64      ' Mean viscosity test voltage
VTAVG! = VTSUM! / 64      ' Mean tach signal voltage
PU! = PUSUM! / (INT(NCONVT% / 4)) ' Mean upstream pressure
PD! = PDSUM! / (INT(NCONVT% / 4)) ' Mean downstream pressure
DELTAP! = ABS(PU! - PD!)   ' Pressure drop

WSTRESS! = H! * (ABS(VVAVG! - VZAVG!)) ' Wall shear stress
                                           ' Equation 41-1
VM! = AA!(1) * VTAVG! + AA!(0)   ' Shearing velocity
                                           ' Equation 31-1

                                           ' Apparent strain rate
                                           ' Equation 41-3
APSTRNRT! = (VM! / (1000 * GAP!)) * (WSTRESS! * L! - CF! *
DELTAP! * YSTAR!) / (WSTRESS! * L! - CF! * DELTAP! * GAP! /
2)
                                           ' Apparent Viscosity
                                           ' Equation 41-5
VISCOSTY! = (WSTRESS! - (CF! * DELTAP! * GAP! / 2 / L!)) /
(VM! / (1000 * GAP!))

                                           ' Nominal Viscosity
                                           ' Equation 41-6
NOMVISC! = WSTRESS! / VM!

                                           ' Temperature Corrected
                                           ' Viscosity; Equation 24-2
'VISCOSTY! = VISCOSTY! * EXP(49450/8.314 * (1/(TRHEO%+273) + (1/473)
))

' Controller
CONTROL.LAW:

  E!(2) = E!(1) ' Update vector of past set point deviations
  E!(1) = 0
  IF CC% = 1 THEN
    E!(1) = VSETPT! - NOMVISC! ' Compute current set point
  END IF ' deviation

  FOR IU% = 10 TO 2 STEP -1
    U!(IU%) = U!(IU% - 1)
  NEXT IU%

```

```

DTSUM! = 0          ' Sum terms for the MVCs dead time
                   ' compensator
FOR IC% = 1 TO DT%
  DTSUM! = DTSUM! + (1 - MA!) * U!(IC% + 1)
NEXT IC%
                   ' Minimum variance controller algorithm

U!(1) = ((1 - MA!) / WO!) * (E!(1) - D! * E!(2)) - DTSUM!

DOFN! = DOFN! + U!(1) ' Degree of Neutralization is the
                   ' manipulated variable

                   ' Proportion of Surlyn is derived from the
                   ' degree of neutralization
SURLYN! = ((.251904 + .002 * (DOFN! + .1315)) ^ .5 - .5019)
* 1000

ACTION! = SURLYN! * TFSP! ' Control Action

' Constrain control action under following conditions:

IF (INT(ACTION!)) < 200 THEN      ' Remote feeder minimum
  RFSP% = 200
  OHFSP% = TFSP% - RFSP%
ELSEIF (INT((100 - SURLYN!) * TFSP!)) < 300 THEN ' Overhead
                                                ' feeder minimum
  OHFSP% = 300
  RFSP% = TFSP% - OHFSP%
ELSEIF (INT(ACTION!)) > 710 THEN ' Remote feeder maximum
  RFSP% = 710
  OHFSP% = TFSP% - RFSP%
ELSE
  OHFSP% = INT((100 - SURLYN!) * TFSP) ' Unconstrained
  RFSP% = INT(ACTION!)                ' control action
END IF

TT = TIMER      ' Note time that viscosity measurement was made

IF CNT% = 1 THEN ' Flag first measurement, start timing
  TSTART = TT    ' from that point on.
END IF

TESTTIME! = TT - TSTART ' Compute time of measurement

MACO.OPEN          ' Sample:
  MACO.VAL "DRV2", OHFR%, OHFRERR% ' Overhead feedrate
  MACO.VAL "DRV3", RFR%, RFRERR%  ' Remote feedrate
MACO.CLOSE

IF CC% = 1 THEN ' If controller is operational:

```

```

MACO.OPEN      ' Implement Control Actions
MACO.PSET 85, 2, 1, 50, OHFSP%, OHFERR%
MACO.SET "DRS3", RFSP%, RFERR%
MACO.CLOSE
END IF

' Output to file and to screen

PRINT #1, TESTTIME!; TSST%; TRHEO%; TMELT%; PU!; PD!;
DELTAP!; OHFR% / 100; RFR% / 100; VM!; VVAVG!; VZAVG!;
APSTRNRT!; VISCOSTY!; WSTRESS! / VM!; VSETPT!; WO!; D!; MA!;
OHFSP% / 100; RFSP% / 100

PRINT USING "    ####"; TESTTIME!; : PRINT USING "
##.##"; OHFSP% / 100; : PRINT USING "    ##.##"; RFSP% /
100; : PRINT USING "    ##.###"; U!(1); : PRINT USING "
###"; DELTAP!; : PRINT USING "    ####"; WSTRESS! /
VM!

CNT% = CNT% + 1      ' Increment
sample counter

DO
IF INKEY$ = "U" THEN GOTO UPDATE
LOOP

UPDATE:
CLS 0      ' Clear screen, including viewport definition
VIEW PRINT
TIMER OFF  ' Disable interrupt while updating set points
           ' or controller parameters

BOX
LOCATE 11, 5: PRINT "CONTROLLER UPDATE SCREEN"
LOCATE 12, 10: PRINT "Select option:"
LOCATE 13, 20: PRINT "I:  Initiate Viscosity Setpoint"
LOCATE 14, 20: PRINT "C:  Modify Controller Parameters"
LOCATE 15, 20: PRINT "T:  Terminate Control Program"
LOCATE 16, 25: INPUT "----> ", QQ$

SELECT CASE QQ$
CASE "I"      ' Update viscosity setpoint
CC% = 1
CLS : UDATEBOX
LOCATE 10, 5: PRINT "INPUT INITIAL VISCOSITY SETPOINT"
LOCATE 20, 5: PRINT "NOTE:  SYSTEM IS RUNNING OPEN
LOOP!"
LOCATE 12, 10: INPUT "Enter desired viscosity setpoint
", VSETPT!
MACO.OPEN
MACO.VAL "T2V1", TSETPT%, ETSP%
MACO.CLOSE

```

```

CASE "C"          ' Update MV controller parameters
  CLS : UDATEBOX
  LOCATE 10, 5: PRINT "CONTROLLER PARAMETER UPDATE"
  LOCATE 19, 5: PRINT "NOTE:  SYSTEM IS RUNNING OPEN
LOOP!"
  LOCATE 12, 5: PRINT "Enter new controller parameters"
  LOCATE 13, 15: INPUT "Gain (Pa s / %) ---> ", WO!
  LOCATE 16, 15: INPUT "Discrete time constant ---> ",
D!
  LOCATE 17, 15: INPUT "Moving average noise model
parameter --> ", MA!
  LOCATE 18, 15: INPUT " Integral number of dead time
periods ---> ", DT%
  CASE ELSE
    GOTO THE.END
END SELECT
CLS
GOTO SET.UP.SCREEN

THE.END:
DT.DAOUT DAC.SELECT%, 0          ' Switch off rheometer motor

TIMER OFF                        ' Switch off TIMER interrupt

MACO.OPEN                        ' Shut off feeders
  MACO.W.OPCR 2900, 1, OHFERR%
  MACO.W.OPCR 2900, 0, RFERR%
MACO.CLOSE

CLOSE #1
CLS
END

TOGGLE:
  TIMER OFF
RETURN SAMPLE

SUB BOX          ' This subroutine draws a box on the screen
  CLS
  PRINT STRING$(1, 218); STRING$(78, 196); STRING$(1, 191)
  FOR Z% = 1 TO 21
    PRINT STRING$(1, 179); SPC(78); STRING$(1, 179)
  NEXT Z%
  PRINT STRING$(1, 192); STRING$(78, 196); STRING$(1, 217)
END SUB

SUB HALFBOX1    ' This subroutine draws a half sized box
  CLS
  PRINT STRING$(1, 218); STRING$(78, 196); STRING$(1, 191)
  FOR IBOX% = 1 TO 12

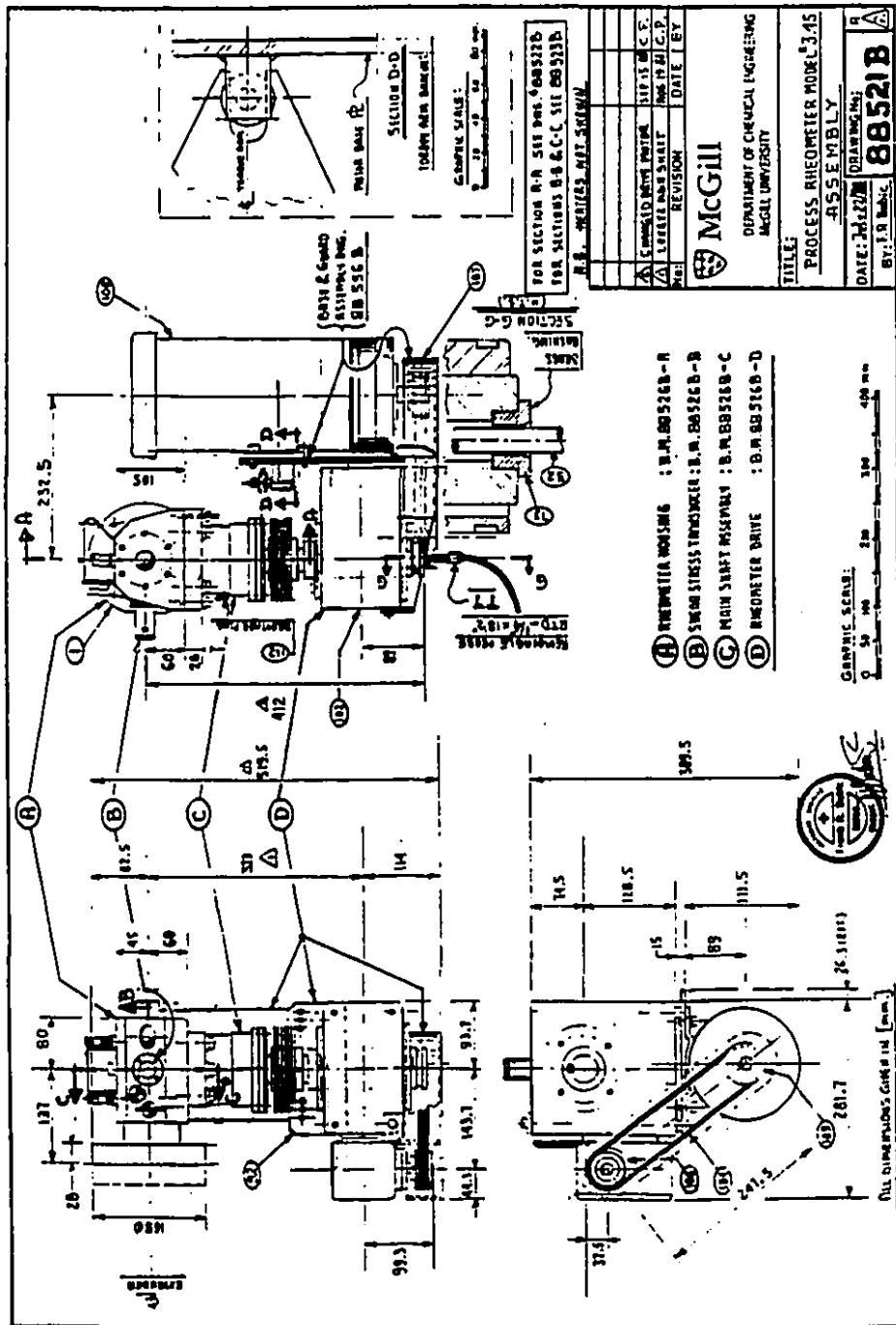
```

```
PRINT STRING$(1, 179); SPC(78); STRING$(1, 179)
NEXT IBOX%
PRINT STRING$(1, 192); STRING$(78, 196); STRING$(1, 217)
END SUB
```

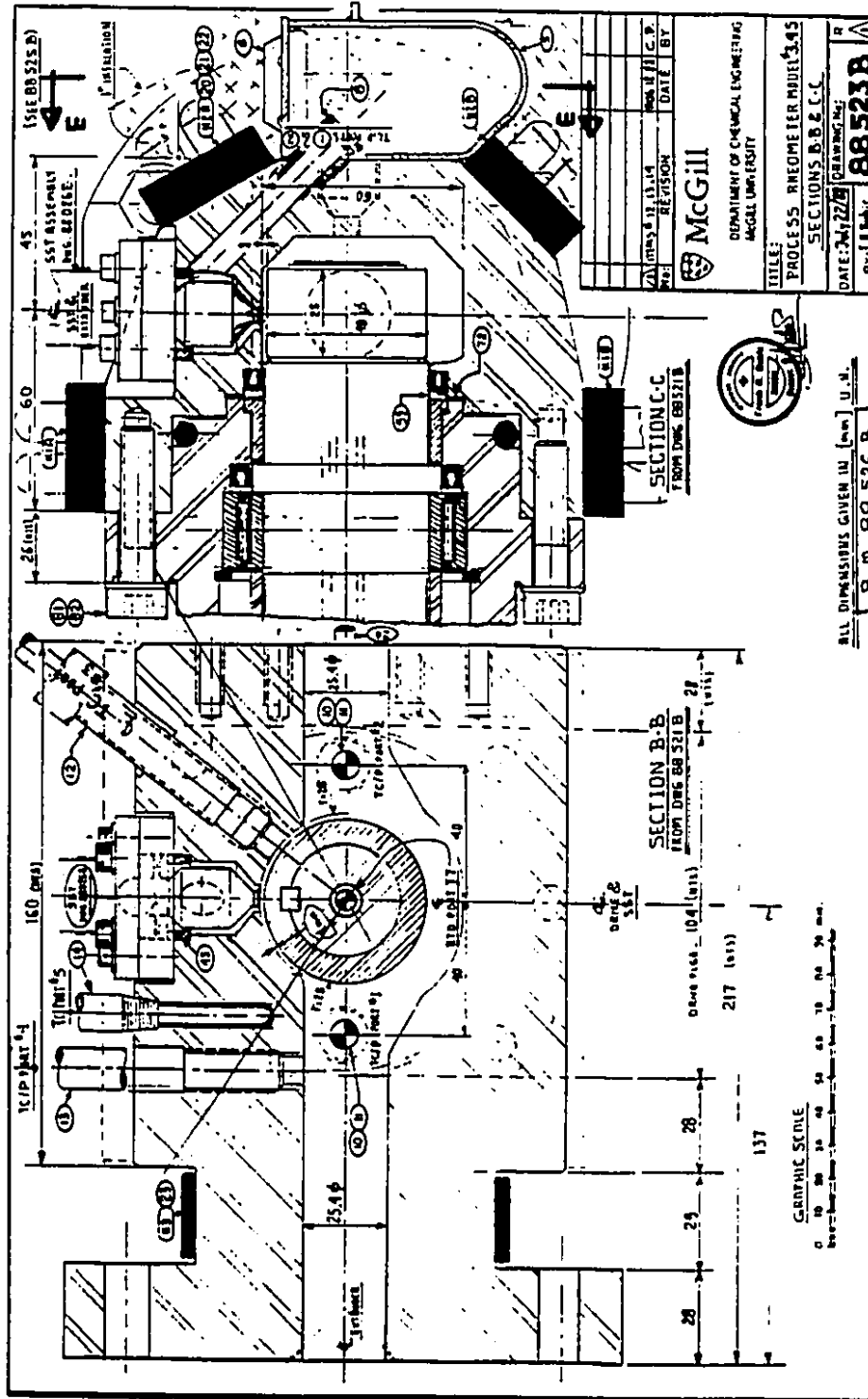
```
SUB UDATEBOX ' This subroutine draws a half sized box in
              ' the middle of the screen
LOCATE 9, 1: PRINT STRING$(1, 218); STRING$(78, 196);
STRING$(1, 191)
FOR Z% = 10 TO 19
  PRINT STRING$(1, 179); SPC(78); STRING$(1, 179)
NEXT Z%
LOCATE 20, 1: PRINT STRING$(1, 192); STRING$(78, 196);
STRING$(1, 217)
END SUB
```

A3 APPENDIX OF MECHANICAL DRAWINGS

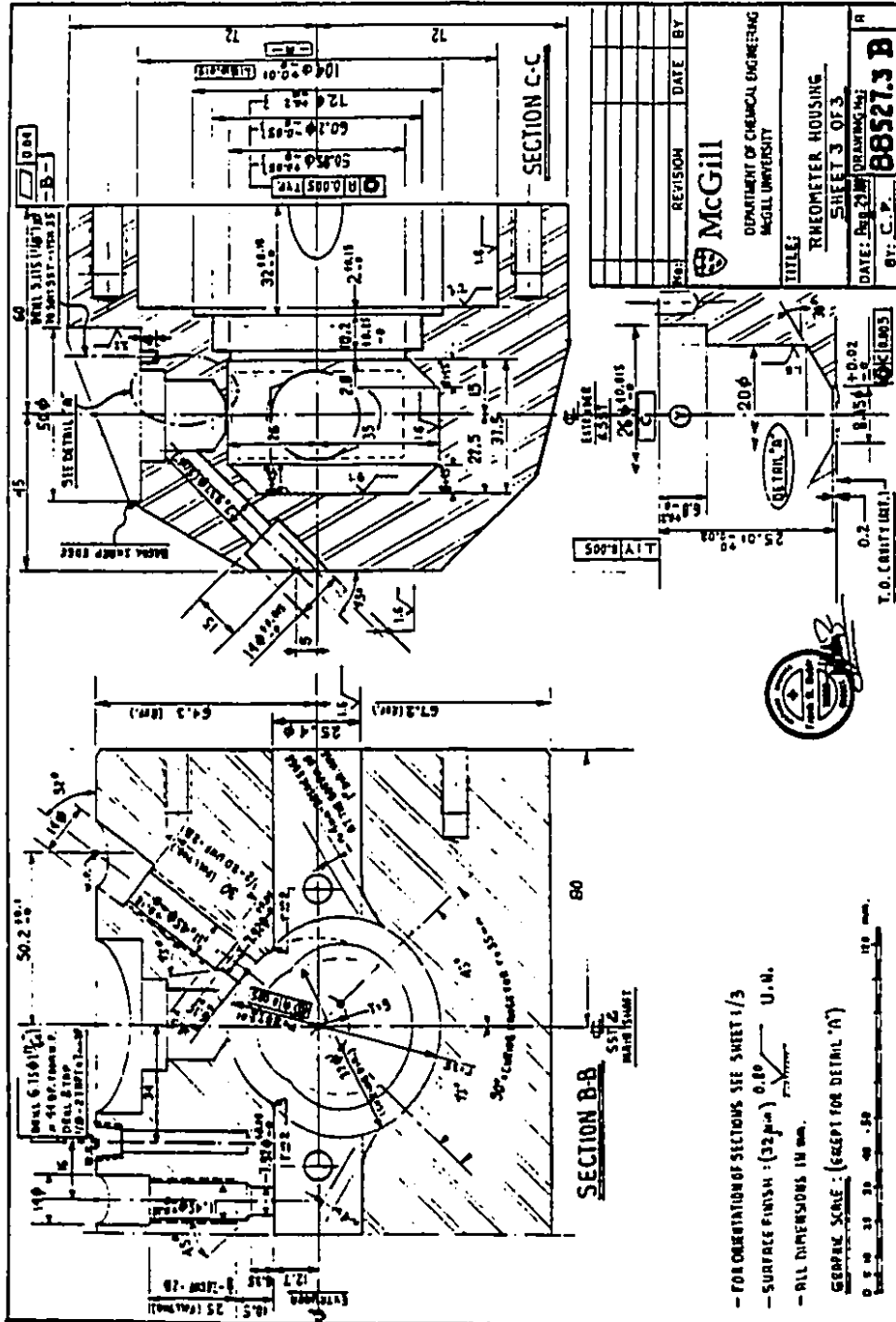
A3-1 Process Rheometer Model 3.45 - Assembly Drawing
 Prepared by F.R.Bubic



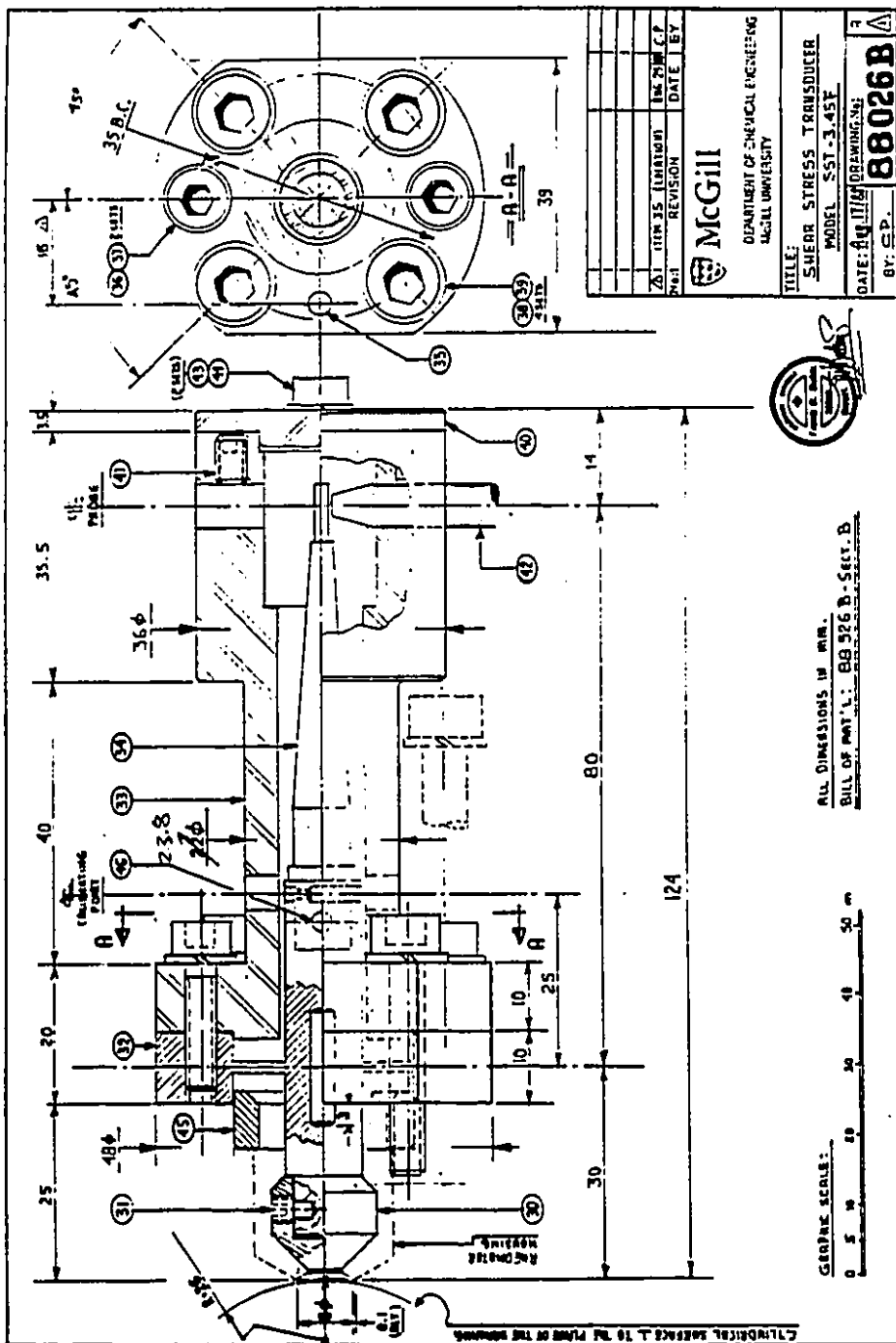
A3-2 Side and Front View Cross-Sections of the Rheometer



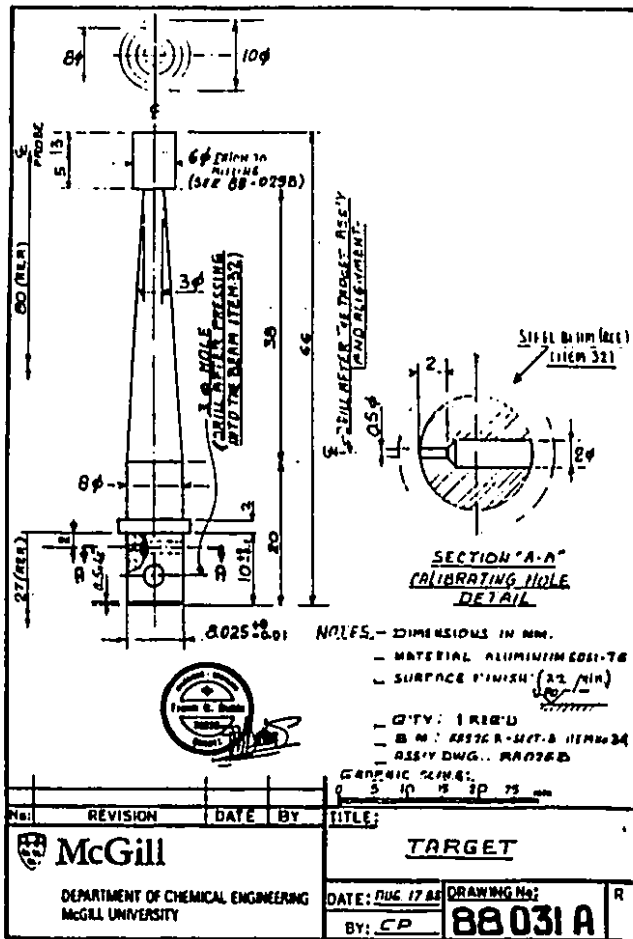
A3-3 Side and Front View Cross-Sections of the Rheometer: Detailed Dimensions



A3-7 Shear Stress Transducer - Assembly Drawing



A3-9 Shear Stress Transducer - Probe Target Detail



No.	REVISION	DATE	BY	TITLE:
				TARGET
McGill DEPARTMENT OF CHEMICAL ENGINEERING MCGILL UNIVERSITY				DATE: JUN 17 88 BY: CP DRAWING No: 88031A

**A3-11 Summary of CAD Analysis for SST Model 3.45F
by F.R.Bubic**

SUMMARY OF CAD ANALYSIS FOR SST MODEL: "SST-3.45F"

By: F.R.Bubic

Date: August 10th, 1988

1) INPUT DESIGN PARAMETERS

Active Face Dia.	DF = 8 (mm)
Disc Spring Outside Dia.	D. = 26 (mm)
Disc Spring Inside Dia.	DB = 11 (mm)
Lever Lengths: (Active Face end)	LF = 30 (mm)
(Probe End)	LP = 80 (mm)
Calibrating Port Distance	LC = 25 (mm)
Max. Measured Shear Stress	SH = 250 (kPa)
Displacement at Probe for Max. Shear	BP = 1000 (micro-in.)
Displacement at Probe for Min. Shear	BL = 7.2 (micro-in.)
Max. Operating Melt Pressure	PR = 1500 (psi)
Disc Spring Modulus of Elasticity	ME = 195 (GPa)

2) CAD ANALYSIS RESULTS:

Min. Measured Shear Stress	SL = 1.8 (kPa)
Max. Active Face Displacement	BF = 375 (micro-in)
Min. Active Face Displacement	BM = 2.7 (micro-in)
Beam Angle for Max. Shear	PH = .0003175 rad
Active Face Area	AF = .5026545 cm ²
Active Face Shear Force	FA = 12.6636 N
Spring Rate	K = 1187.373 Nm/rad
The ratio of spring disc	(ID/OD) = .423077
Spring Disc Thickness	T = .947938 (mm)

3) RESULTS OF AXIAL STRESS AND STRAIN ANALYSIS:

Melt Pressure is 1500 psi (10342.2 kPa)
 Axial Force due to 1500 psi is 519.85 (N)
 Max. Stress is 313.9 (MPa) or 45527.68 psi
 Axial Deflection is 2.188906E-02 (mm) or .861774 mils.

4) SST CONSTANTS AND MISC. CALIBRATING DATA:

Transducer Constant TC = .25 (kPa/micro-in.)
 N.B. SHEAR (kPa) = TC * DEFLECTION (micro-in.)
 Calibrating Constant CC=178.0667 (See Dwg.88 015 B)
 Calibrating Constant for EX=0 and WF (N): C1= 16.57865
 Calibrating Constant for EX=0 and W (kg): C2= 162.6366
 N.B. WF=Calibrating Force (N) of the Mass W (kg)
 Beam Section Moment of Inertia along LC: IN=7.186878E-10 (m⁴)
 Calibrating Force which would produce the Torque...
 ...corresponding to the Max. Shear: WM=15.07963
 Max Elastic Deflection fo the Beam at Probe...
 ...due to Calibrating Force WM: EM= 94.87448 (micro-in)
 Deflection Ratio (Correction Factor) DR=DT/DP= 1.094875